NUMERICAL MODELLING OF SUPERHEATED STEAM DRYING OF DISTILLERS' SPENT GRAIN PELLET-A SINGLE ELEMENT APPROACH

by

Rani Puthukulangara Ramachandran

A Thesis submitted to The Faculty of Graduate Studies of

The University of Manitoba

In partial fulfilment of the requirements for the degree of

DOCTOR OF PHILOSOPHY

Department of Biosystems Engineering

University of Manitoba

Winnipeg, Canada,

R3T 5V6

THESIS ABSTRACT

Mathematical modelling and simulation of a drying system requires a series of preliminary studies to generate strong scientific data that describe the transport phenomena, engineering properties of the product, and changes in thermodynamic properties of the drying medium. Superheated steam (SS) drying has been proven to be a suitable choice for drying biological materials especially, in the cases where the use of air as a drying medium has its limitations, such as oxidative reactions and chances of combustion. Thus, the use of SS for drying of wet byproducts from bio-processing plants is more suitable than hot air drying. Distillers spent grain (DSG), a byproduct of bio-ethanol production (from cereal grains), is generated in the form of a wet paste with high moisture of 75-80% wet basis (wb). This wet product is dried to safe storage moisture of about 10% (wb) to overcome the challenges associated with its transportation and storage. The focus of the present research is to develop a drying model for SS drying of DSG. The product of interest (i.e. DSG) has two components - coarse grain fraction and distillers' solubles. To mimic the industrial drying process, compacted cylindrical pellets of the coarse grain fraction (with and without solubles) were coated with solubles to increase the surface area for drying and then dried in SS.

Thermo-physical properties of the coarse grain fraction of DSG with various levels (0, 10, 30, and 50% w/w) of solubles concentrations and different moisture contents (25, 35, and 45% wb) were determined experimentally. The experimental values of density, thermal conductivity, and specific heat were in the range of 898.8–1136.7 kg/m^3, 0.17–0.42 W/(mK) and 1.76–3.47 kJ/(kgK), respectively. Thermal conductivity and specific heat were found to increase linearly with an increase in moisture content, soluble concentration

of the sample, and temperature of the drying medium. The regression equations for the thermo-physical properties as a function of moisture content and temperature were determined and used for simulation of SS drying. The effect of the operating parameters (SS temperatures 120, 135, 150, 165, and 180°C and velocities 0.5, 1.0, 1.5 m/s) on the effective moisture diffusivity of DSG pellets with various levels of solubles (0, 10, 30% w/w) was also determined from the experimental drying characteristics. The average effective moisture diffusivity of the solubles and DSG pellets was in the range of 3.3×10^{-10} - 3.7×10^{-9} and 4.1×10^{-9} - 4.2×10^{-8} m^2/s, respectively. The coefficients describing the effective moisture diffusivity with temperature and moisture content for all selected operating conditions of SS drying were obtained with a minimum R^2 value of ≥ 0.78 and a mean relative percentage error $\leq$10%.

The initial condensation of SS on a DSG pellet for the same set of operating conditions as selected for the diffusivity studies was modelled using the energy and mass balance at the surface of the pellet. The film condensation coefficient on the cylindrical surface was computed for each operating condition based on the pellet's surface temperature. The prediction accuracy of the film condensation on a pellet was determined. The maximum mean square error between the predicted and experimental mass condensate values was 0.20. The experimentally determined coefficients were expressed mathematically and used for simulating SS drying of two types of DSG pellets - coated with solubles and non-coated. The three-dimensional modelling of SS drying of a single DSG pellet (12.4±0.5 mm diameter and 25.5±0.5 mm length) was performed using a computational fluid dynamics (CFD) software package (ANSYS CFX Version 16.2). The simulated CFD model was validated against experimental results. Model parameters were tested for sensitivity by varying mesh

configuration and initial conditions of SS and the pellet (coated with solubles and non-coated) to yield minimum mean relative percentage error (≤10%). The model used Reynolds-Average Navier-Stokes (RANS) equations for SS flow and diffusion equations for the DSG pellet with solubles coating. The validation results show an agreement with a maximum mean relative percentage error of 9.1 and 7.8%, for the temperature and moisture predictions, respectively. Overall, the simulation model developed for SS drying of DSG pellets (with or without coating) could be used as a tool for designing and optimizing the SS drying process for high moisture solids dried with inert material in multi-layer configurations.

ACKNOWLEDGEMENTS

I sincerely thank my advisors, Dr. Jitendra Paliwal and Dr. Stefan Cenkowski for giving me the opportunity to work on this research problem. Their support, guidance and encouragement through the course of this research are greatly appreciated as it has helped me develop professionally and as a person.

I thank my committee member Dr. Scott J. Ormiston for all his support and guidance on the research especially for technical support on commercial Computational Fluid Dynamics package. I also thank Dr. Christopher B. Porth (committee member), for his support and guidance over the course of my studies.

I am appreciative of all the financial assistance I have received during my research period through Dr. Paliwal's and Dr. Cenkowski's NCERC (Natural Science and Engineering Research Council) grant, UMGF (University of Manitoba Graduate Fellowship), and GETS (Graduate Enhancement of Tricouncil Stipend). I also thank Mohawk Canada Limited, a division of Husky Oil Limited, Minnedosa, MB for supplying the Distillers' spent grain. Technical supports and advice provided by Mr. Matt McDonald, Mr. Dale Bourns, Mr. Robert lavallee, Mr. Marcel Lehmann, and Ms. Minami Maeda are appreciated. I also acknowledge the assistance of fellow post-doctoral Dr. Mohsen, Akbarzadeh, graduate student Dr. Praveen Johnson and Justin Bourassa, and undergraduate students Jennifer Pieniuta, Craig Heppner, Clifford Dueck, and Alain Jeffrey Lagasse at various stages of my research.

Finally, I would like to thank my family and friends for their constant support and encouragement and the staff of Department of Biosystems Engineering, University of Manitoba for providing a peaceful working environment.

TABLE OF CONTENTS

LIST OF TABLES

LIST OF FIGURES

LIST OF SYMBOLS AND ABBREVIATIONS

The list of symbols and abbreviations used for each chapter was added at the end of the respective chapters as each chapter is adapted from published/accepted/submitted papers. The list of the general abbreviations used is tabulated below:

CDS	Condensed Distillers' Solubles
CFD	Computational Fluid Dynamics
CVFEM	Control Volume Finite Element Method
DEM	Discrete Element Method
FEM	Finite Element Method
FVM	Finite Volume Method
EBFVM	Element Based Finite Volume Method
RANS	Reynolds-Averaged Navier-Stokes
DSG	Distillers' Spent Grain
DDGS	Dried Distillers' Grain with Solubles
DDG	Dried Distillers Grain
db	Dry Basis
SS	Superheated Steam
WDS	Wet Distillers Grain
wb	Wet Basis

PUBLICATIONS

A significant portion (Chapters 1, 2, 3, 4, 5, 6, and 7) of this thesis is based on the following published and submitted peer-reviewed journal papers. The permissions to reuse the published content are attached in Appendix A.

Published papers

1. **Ramachandran**, **R. P.**, Akbarzadeh, M., Paliwal, J. & Cenkowski, S. (2018) Computational fluid dynamics in drying process modelling - a technical review. *Food and Bioprocess Technology*, 11(2), 271-292, DOI: org/10.1007/s11947-017-2040-y.
2. **Ramachandran R. P**., Jitendra Paliwal, & Stefan Cenkowski (2018). Modelling of effective moisture diffusivity and activation energy of distillers' spent grain pellets with distillers' solubles during superheated steam drying. *Biomass and Bioenergy* 116: 39-48, DOI 10.1016/j.biombioe.2018.06.004.
3. **Ramachandran**, **R. P.**, Akbarzadeh, M., Paliwal, J. & Cenkowski, S. (2017) Three-dimensional CFD modelling of superheated steam drying of a single distillers' spent grain pellet. *Journal of Food Engineering*, 212, 121-135, DOI: 10.1016/j.jfoodeng.2017.05.025.
4. **Ramachandran**, **R. P.**, Bourassa J., Paliwal, J. & Cenkowski, S. (2017) Effect of temperature and velocity of superheated steam on initial condensation of distillers' spent grain pellets during drying. *Drying Technology* 35(2): 182-192, DOI: 10.1080/07373937.2016.1166123.
5. **Ramachandran R. P**., Paliwal, J. & Cenkowski, S. (2017) Thermo-physical properties of distillers' spent grain pellets at different moisture content and condensed distillers' soluble concentrations. *Food and Bioprocess Technology* 10: 175-185, DOI 10.1007/s11947-016-1807-x.

Submitted papers

6. **Ramachandran R. P**., Paliwal, J. & Cenkowski, S. Three-dimensional modelling of superheated steam drying of a single distillers' spent grain pellet coated with distillers' solubles. (Submitted to *Journal of Food Engineering*). Ref.No: JFOODENG-D-18-00481R2.

CHAPTER 1. THESIS OVERVIEW

1.1 Scope of research

Superheated steam (SS) drying is a complex process accompanied by heat and mass transfer, vapor-solid interaction, and turbulent flow. It has widespread applications in drying of biomass and byproducts such as wood fiber, paper, sugar beet pulp, spent grain, vegetables, lumber, fish meal, industrial waste, sludge, etc.(Chryat et al., 2017; Defo et al., 2004; Hoadley et al., 2015; Kittiworrawatt and Devahastin, 2009; McCall and Douglas, 2006; Nygaard and Hostmark, 2008; Zielinska et al., 2009). To select and optimize design parameters of drying systems, a thorough knowledge of drying kinematics including heat and mass transfer phenomena is necessary. The proposed research focuses on the utilization of SS as a drying medium for distiller's spent grain (DSG), a fiber and protein-rich byproduct from breweries, distilleries, and biofuel industries. Value addition of this byproduct from biofuel production is essential to keep the economics of biofuels cost competitive with fossil fuels in the market.

Canada is the fifth largest producer of ethanol in the world with an annual ethanol production of 1.7 billion litres (Natural Resources Canada, 2014). Husky Energy, western Canada's largest producer of ethanol, produces approximately 260,000 tonnes per year of dried distillers' grain with solubles (DDGS), which is about 35-40% of the grain input per annum. Figure 1.1 depicts the generation of DSG as a byproduct in the commercial production of bioethanol. Whole grain is mashed and goes through the fermentation process. The whole stillage after centrifugation contains thin stillage fraction and coarse grain fraction, called wet distillers' grain (WDS). The WDS has a moisture content >70% wb and a maximum shelf life of 4-5 days. Storage and

unloading of this wet material is highly challenging because of caking and bridging (Ganesan et al., 2008; Johnson et al., 2013a). Hence, WDS is dried to safe storage moisture content of about 10 to 12% wb, either by itself or by mixing it with thin solubles to prolong its shelf life and enable better transportation. Drying of WDS, with or without solubles, is generally done in large rotary drum dryers at high temperature (250-600°C). The final products obtained are dried distillers' grain (DDG) and dry distillers' spent grain with solubles (DDGS) as shown in Figure 1.1.

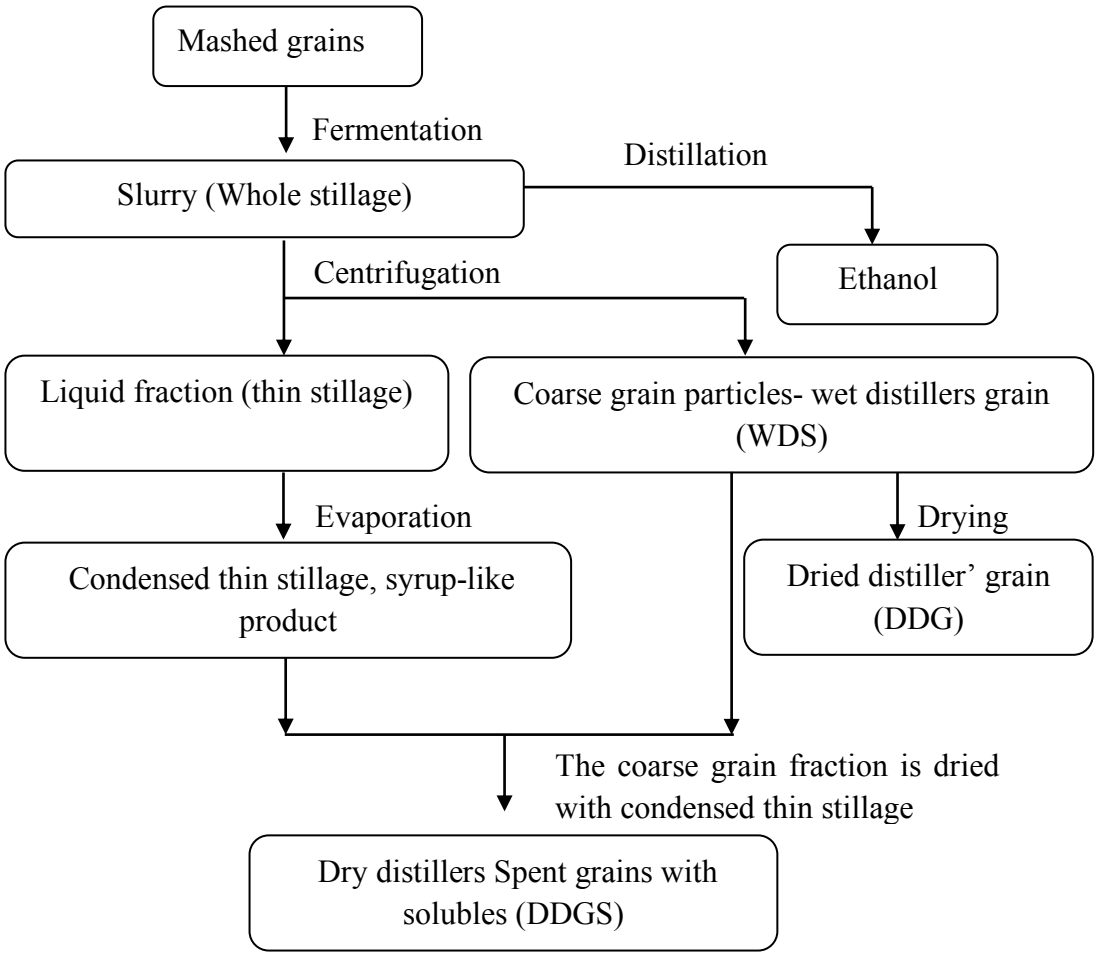

Figure 1.1 Process flow chart for the production of DDG and DDGS (modified from Bonnardeaux, 2007).

Drying of WDS in rotary drum dryers is challenging because of its paste-like consistency. It was reported by Tumuluru et al. (2010) that by increasing the bulk density of the material through densification, handling limitations could be overcome. Moreover, rotary drum drying takes place at high temperature in the presence of oxygen making the process extremely susceptible to fire and explosions. High heat also damages protein structure and causes discolouration of the product (Stroem et al., 2009). Superheated steam drying, on the other hand, takes place in the absence of oxygen, making the process safer from an operational perspective. The presence of SS in processing is known to reduce the level of mycotoxins, if present in DSG, making the product safe to consume by both animals and humans (Cenkowski et al., 2007).

Several studies have established that SS drying is advantageous than hot air drying. The SS technology has been tested successfully to dry products such as carrots, potatoes, cauliflower, celery, oat groats, shrimp, asparagus, leek, seeds, meat, herbs, spices, pork, paper, rice, noodles, soybean, brewers spent grain and distillers' spent grains (Head et al., 2011; Kittiworrawatt and Devahastin, 2009; Prachayawarakorn et al., 2006; Pronyk et al., 2008a; Taechapairoj et al., 2006; Tang and Cenkowski, 2000; Tang et al., 2005; Uengkimbuan et al., 2006; Van Deventer and Heijmans, 2001). Because of the slurry-like nature of WDS and the need to improve its drying efficiency, the industry tested extruders that produce cylindrical spent grain compacts/pellets of about 30% wb moisture content. In industry such pellets or granules are either directly introduced into a dryer as such or are coated with the wet solubles (with high moisture) first and then dried together. This forms a multi-layer configuration (particles with multiple layers of material with different moisture content and thermo-physical properties) when dealing with the heat and mass transfer phenomena. These

attempts have only been partially successful because of the lower compaction pressure and stress relaxation, and due to the steam condensation that results in the disintegration of the compacts (Johnson et al., 2015; Ramachandran et al., 2017b). In this study, the wet solubles with a moisture content of 83% wet basis (wb), which is in the form of thick paste was coated over the formed DSG pellet (25% wb) and dried in SS. To better understand the transport phenomena occurring during drying of a multi-layer product where each layer has different moisture and thermo-physical properties, a single element modelling approach was chosen. A single element refers to a single solid which is either a core pellet or a coated pellet surrounded by a fluid medium (SS). In this approach, the heat and mass transfer phenomena and the thermo-physical properties of a single solid sample which in this case is a DSG pellet or a coated DSG pellet, would be studied. The selected geometry of the element in the numerical simulations of this study resembled the geometry of feed pellets available in the market. Despite the large number of published papers in the area of SS drying, there is limited scientific data on the mathematics of superheated steam drying of such high moisture multi-layer materials. To capture the different transport processes (such as initial condensation) occurring during SS drying of multi-layer materials, advanced computational tools such as Computational Fluid Dynamics (CFD) software can be used. The presence of two arbitrary boundary layers for the coated pellets: (i) the layer between the solubles coating and the drying medium (i.e. SS); and (ii) the layer between the solubles coating and the relatively dry core, makes the computation of moisture and temperature profiles non-trivial. Simulation and modelling of such problem domains can be done using commercial CFD packages such as CFX (ANSYS software company, Pennsylvania, United States). The CFD package has necessary features for generating different geometries, meshing, initial and boundary

conditions, setting the solid (sample to be dried) and fluid (drying medium i.e. SS) domains, solving the mathematical model for heat and mass transfer of multi-layer materials, and post-processing of spatial and temporal simulation results.

1.2 Objectives

The main objective of this research was to develop a numerical model to describe the transport phenomena involved in SS drying of DSG pellets using a single element approach. This was achieved by completing the following specific objectives:

- To determine the input parameters for computational modelling of SS drying of DSG pellets under different operating conditions of SS. The important input parameters specific to the DSG pellets were:
    1. Thermo-physical properties of DSG and solubles.
    2. Effective moisture diffusivity of DSG and solubles.
- To develop a numerical model for describing the initial condensation and determine the effect of SS operating conditions on initial condensation on DSG pellets.
- To develop a three-dimensional model for describing the SS drying of a single wet DSG pellet.
- To develop a three-dimensional model for describing the SS drying of a single DSG pellet as the core material coated with distillers' solubles.

1.3 Structure of thesis

The present thesis is structured in a manuscript format, in which each chapter is based on either a published article or an article submitted to a journal as listed in the publications section of the thesis. The chapters in the thesis were arranged following the specific objectives (Section 1.2). An overview of the thesis is described in the flow chart below.

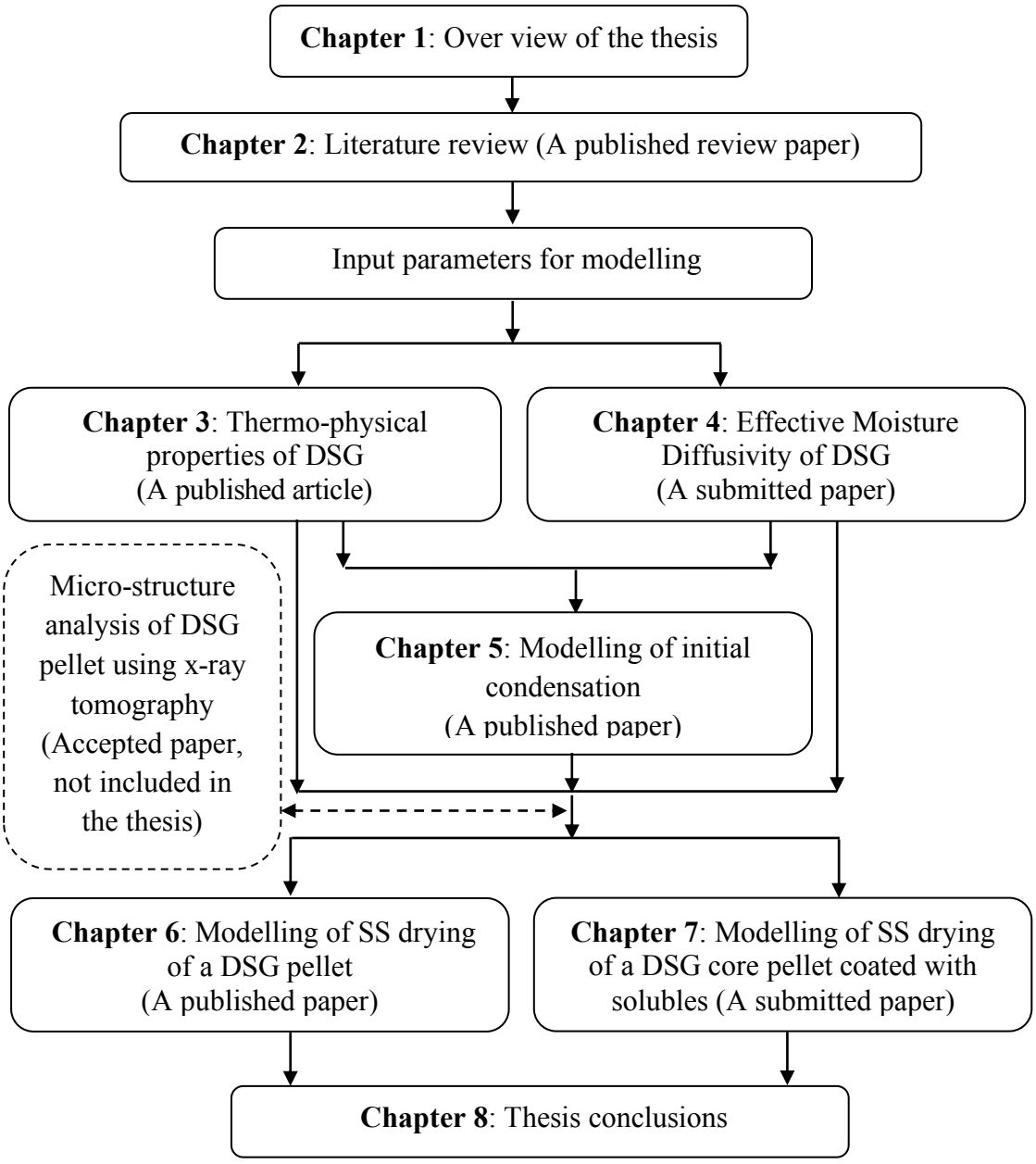

Figure 1.2 Thesis chapter flow chart.

References

1. Bonnardeaux, J., 2007. Potential uses for distillers grains, Department of Agriculture and Food, Western Australia. http://www.agric.wa.gov.au/content/AAP/DC/DFAFU. accessed on 2 August 2015.
2. Cenkowski, S., Pronyk, C., Zmidzinska, D., Muir, W.E., 2007. Decontamination of food

products with superheated steam. *Journal of Food Engineering* 83, 68–75.

3. Ganesan, V., Muthukumarappan, K., Rosentrater, K.A., 2008. Flow properties of DDGS with varying soluble and moisture contents using jenike shear testing. *Powder Technology* 187, 130–137. doi.org/10.1016/j.powtec.2008.02.003
4. Head, D., Cenkowski, S., Arntfield, S., Henderson, K., 2011. Storage stability of oat groats processed commercially and with superheated steam. LWT - *Food Science and Technology* 44, 261–268. doi.org/10.1016/j.lwt.2010.05.022
5. Johnson, P., Cenkowski, S., Paliwal, J., 2014. Analysis of the disintegration of distiller's spent grain compacts as affected by drying in superheated steam. *Drying Technology* 32, 1060–1070. doi.org/10.1080/07373937.2014.881849
6. Johnson, P., Cenkowski, S., Paliwal, J., 2013. Compaction and relaxation characteristics of single compacts produced from distiller's spent grain. *Journal of Food Engineering* 116, 260–266. doi.org/10.1016/j.jfoodeng.2012.11.025
7. Johnson, P., Cenkowski, S., Paliwal, J., 2011. Bulk Density and angle of repose of Distiller's Spent Grain under different drying methods and soluble concentrations, in: The Canadian Society of Bioengineering, CSBE/SCGAB 2011 Annual Conference. Winnipeg, Manitoba.
8. Johnson, P., Paliwal, J., Cenkowski, S., 2015. Effect of solubles on disintegration of distiller's spent grain compacts during superheated steam drying. *Drying Technology* 33, 1–13. doi.org/10.1080/07373937.2014.967403
9. Kittiworrawatt, S., Devahastin, S., 2009. Improvement of a mathematical model for low-pressure superheated steam drying of a biomaterial. *Chemical Engineering Science* 64, 2644–2650. doi.org/10.1016/j.ces.2009.02.036
10. Natural Resources Canada, Renewable energy, www.nrcan.gc.ca/energy/renewable-electricity/7295, accessed on 16 December, 2017.
11. Prachayawarakorn, S., Prachayawasin, P., Soponronnarit, S., 2006. Heating process of soybean using hot-air and superheated-steam fluidized-bed dryers. LWT - *Food Science and Technology* 39, 770–778. doi.org/10.1016/j.lwt.2005.05.013
12. Pronyk, C., Cenkowski, S., Muir, W.E., 2004. Drying Foodstuffs with Superheated Steam. *Drying Technology* 22, 899–916. doi.org/10.1081/DRT-120038571
13. Pronyk, C., Cenkowski, S., Muir, W.E., Lukow, O.M., 2008. Optimum Processing

Conditions of Instant Asian Noodles in Superheated Steam. *Drying Technology* 26, 204–210. doi.org/10.1080/07373930701831457

14. Ramachandran, R.P., Bourassa, J., Paliwal, J., Cenkowski, S., 2017. Effect of temperature and velocity of superheated steam on initial condensation of distillers ' spent grain pellets during drying. *Drying Technology* 35, 182–192. doi.org/10.1080/07373937.2016.1166123
15. Stroem, L.K., Desai, D.K., Hoadley, A.F.A., 2009. Superheated steam drying of Brewer's spent grain in a rotary drum. *Advanced Powder Technology* 20, 240–244.
16. Taechapairoj, C., Prachayawarakorn, S., Soponronnarit, S., 2006. Modelling of parboiled rice in superheated-steam fluidized bed. *Journal of Food Engineering* 76, 411–419. doi.org/10.1016/j.jfoodeng.2005.05.040
17. Tang, Z., Cenkowski, S., 2000. Dehydration dynamics of potatoes in superheated steam and hot air. *Canadian Biosystems Engineering* 42, 43–49.
18. Tang, Z., Cenkowski, S., Izydorczyk, M., 2005. Thin-layer drying of spent grains in superheated steam. *Journal of Food Engineering* 67, 457–465.
19. Tumuluru, J.S., Tabil, L., Opoku, A., Mosqueda, M.R., Fadeyi, O., 2010. Effect of process variables on the quality characteristics of pelleted wheat distiller's dried grains with solubles. *Biosystems Engineering* 105, 466–475.
20. Uengkimbuan, N., Soponronnarit, S., Prachayawarakorn, S., Nathkaranakule, A., 2006. A Comparative Study of Pork Drying Using Superheated Steam and Hot Air. *Drying Technology* 24, 1665–1672. doi.org/10.1080/07373930601031513
21. Van Deventer, H.C., Heijmans, R.M.H., 2001. Drying with superheated steam. *Drying Technology* 19, 2033–2045. doi.org/10.1081/DRT-100107287
22. Zielinska, M., Cenkowski, S., Markowski, M., 2009. Superheated steam drying of distillers' spent grains on a single inert particle. *Drying Technology* 37–41.

CHAPTER 2. LITERATURE REVIEW

This chapter is based on the review paper published by Springer Nature in *Food and Bioprocess Technology* on 18 Dec 2017, available online: www.springer.com/ [doi.org/10.1007/s11947-017-2040-y].

2.1 Abstract

Powerful computational tools such as computational fluid dynamics (CFD) have now replaced the classic method of numerical analysis of drying processes based on experimental models. Its capabilities include the adaptability to model different flow processes such as drying, with high spatial and temporal resolution facilitates and an in-depth understanding of the heat, as well as mass and momentum transfer. CFD complements the experimental and analytical approaches by simulating a range of complex flow problems. Although CFD has immense industrial applications in fluid dynamics, its use in different drying simulations is still in early stages of development. This paper presents a thorough review of the computational power of CFD packages and their application in the drying process simulation. The review also covers different mathematical approaches used in drying models, the commonly available commercial CFD codes, and the turbulence models used in simulations of drying problems. The factors contributing to the complexity and computational load of such CFD-based models are discussed. The later sections of the paper discuss various bottlenecks in the application of CFD in drying, such as the complexity of the models for convoluted geometries, and the limited description regarding the turbulent interaction between different phases.

Keywords: *Computational Fluid Dynamics, Drying models, CFD packages, Turbulence models.*

2.2 Introduction

Drying is an antiquated unit operation in the food and bio-processing industries with its history dating back to the works of pioneers such as Fourier, Fick, and Darcy (Hall 1987), who formulated mathematical expressions for heat and mass transfer in continuous media. The process of drying is governed by temperature and moisture gradients with a combined heat and mass transfer phenomenon. Even though a substantial level of research and development has been done in the drying technology, researchers are still compounding ideas and transforming the existing drying models with a detailed emphasis on fundamentals and innovative approaches to solve industrial drying bottlenecks and to further develop efficient drying techniques (Wu and Mujumdar 2008). Attempts to develop/modify a drying method, optimize drying conditions, and improve the efficiency of the drying systems are still continuing with an intention to enhance product color, minimize shrinkage, increase drying rates, improve nutritional qualities, etc. (Johnson et al. 2013).

Traditional didactic methods of experimentation and analytical modelling for solving fluid flow problems are now supplemented by new powerful simulation tools such as computational fluid dynamics (CFD). Its computing efficacy, coupled with manageable costs of CFD software packages for most engineering applications, makes it a reliable technique to provide effective and efficient design solutions (Norton and Sun 2006; Mujumdar and Wu 2008). Modelling of drying is a complex process that touches on multidisciplinary areas with a fusion of transport phenomena, material science, and fluid and solid properties. Its mathematical description is still far from being perfect and hence, needs some improvement. There is a wide range of empirical models that describe the drying process of various materials which are proven to be suitable for predicting the overall drying process. For example, more than two

dozen different drying models were reported by researchers to describe the thin layer drying of fruits and vegetables (Onwude et al. 2016; Erbay and Icier 2010). These models are only capable of describing the effective/average drying characteristics of the materials being dried and are frequently used in research. Still, such models are the basis for advanced drying models. For example, Fick's law of diffusion, which is based on the experimental moisture content, is still used for determining the effective moisture diffusivity of agricultural products, which is one of the input parameters for CFD-based drying modelling (Ramachandran et al. 2017a). But with the use of CFD, the resolution of the information on the temporal and spatial variation in transport phenomena and material properties during drying could be improved significantly. These models with appropriate input parameters (most of which are experimentally determined) and boundary conditions are capable of describing the local moisture and temperature history of the product during any stage of drying. Also, they have the versatility of application in any solid subjected to any operating condition of the dryer. For instance, if the solid exposed to a drying medium is a multilayer product where each layer has different moisture contents and thermo-physical properties as in the case of encapsulation or nucleus drying, the CFD-based models are the most suitable. A reliable CFD model could simulate the physical processes occurring during drying to any level of details, depending upon the accuracy of the physical definition of variables, selection of mathematical equations, numerical methods, boundary and initial conditions, and empirical correlations (Jamaleddine and Ray 2010). The attempts of Richardson (1910) to procure insight to the fluid motion led to the development of a powerful mathematical technique for the advanced numerical description of all types of fluid flows. His work was the pioneer accomplishment which resulted in the present widespread use of CFD techniques (Shang 2004). Later, in the 1960s, there was a wide range of developments

and applications of CFD in different aspects of fluid dynamics. However, the entry of CFD into the fields of food processing happened with an increase in demand for convenient and high-quality foods and efficient food processing techniques (Scott 1994). As CFD has the ability to deal with the complex phenomena that govern thermal, physical, and rheological properties of food materials, the technique is now widely used in modelling various food processing unit operations such as mixing, drying, cooking, sterilization, chilling, and cold storage (Xia and Sun 2002). A simulation of such flow processes with a higher spatial and temporal resolution is a more reliable tool for the industries to optimize their design parameters or to modify the existing design to accommodate versatility and efficiency in an operation rather than relying on a pure empirical (experiment-based) model.

The objective of this paper is to review and synthesize the research work done in numerical modelling of drying processes using CFD. This paper coalesces the physics behind drying of biological materials and the different ways in which various researchers used this computational technique in describing the drying process. The first half of the review focuses on the major modelling approaches for drying, and the classification of models. The second half gives more insight to the advantages of CFD, governing equations of CFD, the mathematical formulation used in CFD, commercial CFD packages, and different turbulence models used for simulation of drying processes. Additionally, factors contributing to the complexity of CFD-based modelling, applications of CFD in different drying systems, and the existing research gaps are discussed.

2.3 Major modelling approaches for drying

Generally, drying processes can be modeled using two different approaches: (i) modelling based on principles of physics and mathematics, and (ii) modelling based on an empirical

approach. The first type of modelling requires information on the material to be dried and drying media, such as its thermo-physical properties and complex interactions between the two, which is very difficult to quantify. This difficulty typically limits the relevance of such models. Hence, in most studies researchers rely on empirical or semi-empirical models as it often gives the direct relationship between the average moisture content and the drying time (Ertekin and Firat 2017). But these cannot define the underlying physical principles of drying such as the mass transfer mechanism. The physics-based models, on the other hand, generally define the heat and mass transport phenomena and thereby are used to determine the associated drying parameters (Yi et al. 2016). Empirical drying models or experiment-based drying models are comparatively easier to compute and are simpler to interpret mathematically and, therefore, worthwhile mentioning. These antiquated models form the basis for almost all currently existing drying models. The development of a simple empirical model requires an experiment in which the specific input parameters (temperature, relative humidity, and air velocity) are varied. The set of experimental data is then used to derive a mathematical relationship between variables and the drying time or moisture content of the material. Such models only consider average conditions of moisture content and temperature (Heldman and Lund 2007).

Numerous research studies have been done in the field of empirical modelling of the drying processes for different biological products using different drying media such as air (Velic et al. 2004; Baini and Langrish 2007; Rayaguru and Routray 2010), microwave (Omolola et al. 2014), and superheated steam (St. George and Cenkowski 2009; Bourassa et al. 2015). Based on various experimental trials, several empirical and semi-empirical models have been developed by individuals including Lewis (1921), Page (1949), and Newton (Hall 1975), and

their models are represented in Equations 2.1-2.3, respectively. Besides these simple empirical models, many others have been developed, for example, the logarithmic model, parabolic model, two-term exponential model, and modified Page model. The aforementioned models were developed with specific assumptions and boundary conditions (Garavand et al. 2011; Ghazanfari et al. 2006).

$$MR = \frac{M - M_e}{M_o - M_e} = \exp(-k\,t) \tag{2.1}$$

$$MR = \exp(-k\,t^n) \quad \text{where, } n \text{ is the coefficient of drying} \tag{2.2}$$

$$\frac{dM}{dt} = -k(M - M_e) \tag{2.3}$$

Besides their simplicity, these models were not successful in describing the complex drying processes. For example, the empirical model developed for drying shelled corn by Thompson et al. (1968) and Wang and Singh's model for drying rough rice (Wang and Singh 1978a; 1978b) give a function of moisture ratio and drying time but the function does not explain the drying process itself. Hence, a different view towards some robust mathematical model for drying kinetics was later considered. The new models are normally based on physical mechanisms such as the effect of air temperature, air humidity, and air velocity, and characteristics of solids (Shahari and Hibberd 2014, Shahari et al. 2014). These models are quite useful for determining the overall moisture content and drying time for different agricultural products dried using different drying systems. The results of these models have greater acceptance in the field of research and science. But, they are not capable enough for providing detailed design criteria for industrial dryer manufacturing.

As the discussion on numerical modelling of drying process proceeds in the following sections of the paper, the fluid domain refers to the drying medium and the solid domain refers to the material to be dried.

2.4 Classification of thermal process models

The existing mathematical models of various thermal processes such as sterilization, drying, refrigeration, etc. taking place in food and bio-process industry can be broadly divided into four major groups (lumped-capacitance models, diffusion models, models based on porous media theory with an equilibrium approach, and non-equilibrium models). The choice of mathematical models of drying among empirical models or lumped models, models based on heat and mass transfer, models based on porous media theory with an equilibrium approach, or non-equilibrium models, depends on the complexity of the flow problem (Shahari et al. 2014). This selection is also dependent on the level of insight required from the model which in turn is determined by the intended use of the model.

2.4.1 Lumped capacitance models

The lumped parameter models and diffusion models are collectively considered as experiment based models as they are based on empirical equations which are capable of predicting average moisture content as a function of drying time. The lumped-capacitance models are suitable for a specific product and specific processing conditions (Jurumenha and Sphaier 2011). Such models are limited and cannot be used even in a slightly different processing condition (Wang and Brennan 1992). In modelling of drying, the lumped capacitance models are used for determining the average heat transfer coefficient (Cunningham 1992; Salagnac et al., 2004; Rizzi et al., 2009). Honarvar and Mowla (2012) used the lumped capacitance model (Equation 2.4) to determine the heat transfer coefficient and an analogy of heat and mass transfer was used to define the mass transfer coefficient (Equation 2.5). They used these coefficients with the one-dimensional equation of heat and moisture diffusion in the solid to obtain the temperature and moisture distribution (Equation 2.8 and 2.9). These equations form the basis

of the second group of models (so called diffusion models) which is discussed in detail in the following section. Their computational results of heat transfer coefficient were comparable with the data published in literature.

$$\frac{(T-T_\infty)}{(T_0-T_\infty)} = \exp\left[-\frac{hA}{\rho CpV}t\right] \tag{2.4}$$

$$\frac{h}{h^*} = Cp\left[\frac{Sc}{\Pr}\right]^{\frac{2}{3}} \tag{2.5}$$

Where, T_∞ and T_0 are the ambient and initial temperature, Sc and $\Pr$ are the Schmidt and Prandtl number, respectively.

As the lumped parameter models are purely empirical, attempts were made to improve the prediction power by combining the reaction engineering approach (REA) with the lumped-capacitance approach. The REA was first proposed by Chen and Xie (1997) for modelling convective drying of agricultural materials under constant environmental conditions. In the REA, evaporation is considered as an activation process with an energy barrier. The concept of activation energy can reflect the degree of difficulty for removing water from a solid while drying (Chen 2008). Gao et al. (2016) used a combination of the lumped-capacitance approach for heat balance and the REA for mass balance equations to study the drying kinetics of green peas. They used the concept of the change in activation energy with the change in moisture content and heat balance in lumped-capacitance, which can be expressed by the following equation (Gao et al. 2016):

$$m_d \frac{dM}{dt} = -h^* A\left(C_{v,s} - C_{v,f}\right) \tag{2.6}$$

Where the surface vapour concentration, $C_{v,s} = \exp\left(-\frac{E_v}{R\,T_s}\right)C_{v,in}(T_s)$ (2.6a)

$$\frac{d\left(m_d C_p T\right)}{dt} = h\,A\left(T_f - T_s\right) + m_d \frac{dM}{dt}\lambda \tag{2.7}$$

The correlation between the activation energy and moisture content was found to have good agreement with R^2 value of 0.9 (Gao et al. 2016).

2.4.2 Diffusion models

The second group of models (diffusion models) consists of improved models that assume a conductive heat transfer phenomena for energy and a diffusive transport of moisture. These models use a transient diffusion equation where the effective diffusivity is determined experimentally. They incorporate evaporation using a surface boundary condition in the heat transfer equation while neglecting the evaporation inside the food domain. These types of models typically predict moisture content that varies with time and space (Equation 2.8), and they explain the physical transport of moisture within the material, giving a more fundamental value than pure empirical models (Shahari and Hibberd 2014). They used the diffusion model with a shrinkage effect for heat and mass balance as shown in Equations 2.8 and 2.9, respectively. However, they found that the empirical model had better predictability than the mathematical model with shrinkage. In the diffusion model, the effective diffusivity has to be determined separately, usually by using drying curves. The effective moisture diffusivity can be incorporated into the diffusion model either as a constant value or as a function of temperature. The assumption of constant diffusivity might affect the accuracy of prediction (Ramachandran et al., 2017b). Also, the shrinkage of the solid associated with drying and its corresponding effect on thermo-physical properties affects the accuracy of determination of diffusion coefficient. Whereas, the well accepted and widely used empirical models (eg: exponential models for drying) assume negligible resistance to moisture movement to the surface of the material leading to the more simplified relation between drying time and

moisture content (Aregbesola et al. 2015). A comparative study by Baini and Langrish (2007 and 2008) of the diffusion model versus the empirical model for drying bananas found that, pragmatically empirical models are simpler than the diffusion models, and they are comprehensively applied to food drying. The diffusion models rely on the effective diffusivity of the material which in turn varies with the operating condition of the dryer. These models predict the internal moisture movements in the material during drying, while empirical models describe only the change in average moisture content with time by fitting the drying curves with exponential or polynomial functions (Da-Silva et al. 2013).

$$\frac{\partial M}{\partial t} = \left[\frac{1}{L_i^2} \frac{\partial}{\partial \xi} \left(D_i^* \frac{\partial M}{\partial \xi} \right) + \frac{\xi}{L_i} \left(\frac{dL}{dt} \frac{\partial M}{\partial \xi} \right) \right] \tag{2.8}$$

$$\frac{\partial T}{\partial t} = \left[\frac{1}{L_i^2} \frac{\partial}{\partial \xi} \left(\alpha_i^* \frac{\partial T}{\partial \xi} \right) + \frac{\xi}{L_i} \left(\frac{dL}{dt} \frac{\partial T}{\partial \xi} \right) \right] \tag{2.9}$$

Where, $\frac{dL}{dt}$ is the shrinkage of the solid.

2.4.3 Models based on porous media theory with an equilibrium approach

As drying is a coupled phenomenon involving a simultaneous transfer of mass and heat in both the solid and the fluid phases (De-Bonis and Ruocco 2012), the diffusion of liquid may not be the only mechanism responsible for the moisture migration inside the solid. Cloutier et al. (1992) conducted studies on drying vegetables, employing the finite element method, and focusing on the basic aspects of the vapor and liquid water depletion and their transport. This approach evolved the third group of models (models based on porous media theory with an equilibrium approach) in thermal processing. These models are developed based on the assumption that there is a sharp moving boundary between the wet and the dry regions of the solid. Some researchers refer to these models as receding or shrinking core models (Agarwal

et al. 1986, Chen et al. 2000; Hashimoto et al. 2003; Hamawand 2013). It was experimentally proven (Thorvaldsson and Janestad 1999) that, during drying, significant water evaporation takes place inside the solid phase as well as on the external surface of a product depending on the changes in the sharp moving boundary. In a study conducted by Wang and Chen (1999), the effective diffusivity was analyzed based on the coupled effects of the moisture content and temperature on mass transfer in capillary flow, evaporation-condensation, and transition regions. They concluded that, even though the effect of the moisture concentration on the moisture diffusivity was highly significant, the temperature effect cannot be neglected especially at lower moisture concentrations. They found that the assumption of evaporation front was valid for drying of permeable materials. Shibata and Ide (2001) employed the modified receding core model for a combined superheated steam and microwave drying, where evaporation occurs not only at the receding front but also within the wet region. This was unlike the case in conventional receding front model where the drying mechanism is controlled by the surface evaporation (Equations 2.10 and 2.11) mainly occurring during constant drying rate period (Looi et al. 2002). They used equilibrium boundary conditions to determine the drying rate (Equations 2.10 and 2.11). A similar moving boundary model was also used in the study conducted by Farid (2003) with the inclusion of the shrinkage effect in drying a single droplet. The droplet size reduction occurring during evaporation period was described by Equation 2.12. Both the studies of Looi et al. (2002) and Farid (2003), where the drying curves were comparable with the experimental data, had concluded that the surface temperature can be significantly higher than that of the average temperature.

The concept of thermal equilibrium at the interface of solid and fluid has been successfully used by many researchers to account for evaporation inside the solid especially in the case of

superheated steam drying (Lu et al. 2005; Pakowski and Adamski, 2011; Ramachandran et al. 2017a). They used the thermal equilibrium approach at the interface to determine the drying rate and moisture and temperature history of the solid and concluded that the accuracy of the model is dependent on the accuracy of the computation of temperature at the interface. In the equilibrium approach, there is a relationship between the solid moisture content and the fluid phase vapour concentration which is rarely achieved during drying (Pujol et al. 2011). Putranto and Chen (2015) reported that the multiphase model with equilibrium approach is inferior to the model with the spatial reaction engineering approach. In this approach, the local evaporation or condensation rate is modelled with the non-equilibrium approach and the global drying rate is modeled with the reaction engineering approach. They also concluded that the spatial reaction engineering approach accurately modeled both convective and intermittent drying cases. Hence, another approach of modelling evaporation during drying was later developed by researchers (Zhang and Kong, 2012; Warning et al. 2015) called the distributed non- equilibrium approach which is detailed in the next section.

$$\frac{m_v}{A_{df}}\lambda = h\left(T_s - T_f\right) \text{ where, } r = r_s = r_{df} \tag{2.10}$$

$$\frac{m_v}{A_{df}}\lambda = kt\left(\frac{\partial T}{\partial r}\right]_{r\ df}\text{ where, } r = r_s \neq r_{df} \tag{2.11}$$

$$\frac{dr}{dt} = \frac{h}{\lambda\rho}\left(T_f - T_{wb}\right) \tag{2.12}$$

2.4.4 Models based on porous media theory with non-equilibrium approach

The distributed (non-equilibrium) models assume that evaporation occurs over a zone rather than at a distinct interface as opposed to sharp boundary models, where a sharp moving boundary between the dry and wet zone is assumed in drying (Yamsaengsung and Moreira

2002; Zhang et al. 2005). It is also possible that the real evaporation zone can be very narrow and close to the sharp interface. When there is a high rate of internal evaporation, a significant pressure-driven flow can be present for liquid and vapour phases throughout the material. These models are also referred as mechanistic models as they consider transport equations for each phase in porous media (Datta et al. 2007a). The model is based on the assumption that the equivalent porosity is the volume fraction occupied by gas and liquid and hence, porosity remains constant (Datta 2007b). Murugesan et al. (2001) used a conjugate model for describing drying of rectangular bricks where full Navier-Stokes formulation was used to solve the flow field considering the buoyancy term and the energy and moisture transport equations for the brick. They employed Darcy's and Fick's law of liquid mass flux and diffusion mass flux, respectively and the continuity equation for fluid and vapor phases. By comparing their simulation results with the results published by other researchers like Oliveira and Haghighi (1995) and Yang and Alturi (1984) for the same geometry, the authors concluded that the two-dimensional model is significantly different than the one-dimensional model with sharp boundary-layer approximations on the solid surface. The prediction results of flow characteristics were in agreement with that of the results obtained from Yang and Alturi (1984) and the temperature and moisture distribution were comparable with that of the Oliveira and Haghighi (1995). Murugesan et al (2001) also reported that based on temperature and moisture potential, the heat and mass transfer coefficients could act as a good representation of the transport processes in drying. This type of multiphase porous media model for drying with a non-equilibrium approach has been used in vacuum drying (Zhang and Kong, 2012) and vacuum freeze drying (Warning et al. 2015). They used the non-equilibrium approach for modelling the rate of phase change using Equation 2.13. Both the studies were comparable

with the experimental results of drying curves and temperature data and concluded that the evaporation rate constant k^* affects the model and the computation time.

$$\dot{I} = k^* \frac{W_v}{RT} \left(P_{v,sat} - P_v\right) \tag{2.13}$$

2.5 Advantages of CFD modelling

As discussed in the previous sections, the demand for a detailed study of physical phenomena involved in different types of drying techniques still exists. The addition of each phenomenon such as internal evaporation, diffusion, shrinkage, etc. increases the intricacy in solving the drying problem. The complexity of the drying process with multiphase fluid flows, and heat and mass transfer triggered the use of different CFD models which are very helpful in the optimization and the development of processing strategies. Computational Fluid Dynamics in combination with reaction engineering approach (REA) was proven to be a suitable tool to model the multiphase flow (such as in spray drying, fluidized bed drying). Also, the CFD models are a powerful tool for a dryer design with a better understanding of the drying process in comparison to experimentation. When compared to the empirical models, the numerical models for drying process simulations using CFD have numerous advantages: The heat and mass flow can be quantified throughout space and time. The sensitivity to changes in operating conditions can be easily detected without repeatability problems which are present in experimental methods. Even though there is some computational cost and time constraints in capturing random fluctuations in drying conditions such as in spray drying, there are certain numerical strategies available in CFD, to deal with such transient flows. The multi-configuration approach for such flows could simplify this job to some extent. By running a steady state simulation to establish the flow field which forms the initial solution for the transient behavior the simulation time could be reduced (Meng

2016). In the case of numerical simulation, there is no limitation for the operating conditions (eg. temperature of a dryer), as safety is not an issue. The simulations can be performed with the actual scale of the dryer which may not be feasible with the experiment-based modelling. Moreover, CFD-based models have the capability to give a deeper insight of the drying process with the 3D configuration which is not possible with drying experiments (Defraeye 2014). The versatility of CFD models with its application to any size solid being dried was utilized by many researchers to model the drying process of a single element (Ljung et al. 2011, Elgamal et al. 2014, and Ramachandran et al. 2017a). Ljung et al. 2011 studied the single element drying of an iron ore pellet using a high resolution three-dimensional CFD model. They used 3D optical scanning equipment for the meshing of the actual geometry of the solid and the moisture and temperature distribution during different stages of drying were simulated and the model was validated with the experimental data (average moisture content and solid temperature). Not only were their simulation results were in good agreement with the experimental values, but the model was also able to distinctly describe four stages of evaporation of water (evaporation at the surface, surface evaporation coexisting with internal drying, pure internal drying with complete dry surface, and pure internal evaporation at boing temperature). The hydrodynamic flow in the drying medium can be obtained with any degree of resolution in CFD, which can then be used as the boundary condition for the solid to be dried (Younsi et al. 2008). However, experiments are essential to develop mathematical models that describe physical phenomena of heat and mass transfer and to validate CFD results. Occasionally, CFD results can be validated against benchmarked analytical solutions of experiment-based models for standard conditions where they exist.

2.6 Governing equations of CFD

The development of a CFD model involves an accurate definition of the variables, a selection of mathematical equations and numerical methods, boundary and initial conditions, and applicable empirical correlations describing the process (Jamaleddine and Ray 2010). The major governing equations of fluid flow and heat transfer basically rely upon laws of conservation of mass, momentum, and energy. These equations relate the rate of change of desired flow properties with respect to external forces (Norton and Sun 2006) and are described below:

(i) The law of conservation of mass (continuity equation), which states that the mass flows entering a fluid system must balance exactly with the mass leaving the system. In other words, mass is neither created nor lost, but transferred from one point to another as explained by Eqn 14 (Norton and Sun 2006; Bernard and Wallace 2002; Erriguible et al. 2005; 2006). This flow is governed by the driving force of concentration gradients. The continuity equation/conservation of mass is given by:

$$\frac{\partial \rho}{\partial t} - \vec{\nabla} \cdot (\rho \vec{u}) = 0 \qquad (2.14)$$

Physically, $\vec{\nabla} \cdot \vec{u}$ is the time rate of change of volume of the moving fluid element per unit volume, which represents the divergence of velocity. The bar above u is a notation for the vector quantity. Simplified conceptual model equations are derived with the assumption of incompressible flow. For an incompressible fluid for which the density is constant, the aforementioned equation can be simplified as:

$$\nabla \cdot \vec{u} = 0 \qquad (2.15)$$

(ii) The law of conservation of momentum (Newton's second law of motion), which states that the sum of the external forces acting on a fluid particle is equal to its rate of change of linear

momentum. The Euler equation for fluid motion in the *x* direction (assuming the fluid is incompressible) is given by:

$$\frac{\partial(\rho\vec{u})}{\partial t} + \vec{\nabla}\cdot(\rho\vec{u}\otimes\vec{u}) = -\vec{\nabla}\cdot\left(p\vec{I}\right) + \rho\vec{g} \tag{2.16}$$

Where $\vec{u}$ is the velocity vector in all (*x, y, z*) directions. This anachronistic formulation for fluid motion has been later modified by introducing viscous transport into the equation. The resulting equation, which forms the basis for CFD (Norton and Sun 2007), is termed as Navier-Stokes equation for Newtonian fluids (Equation 2.16a).

$$\frac{\partial(\rho\vec{u})}{\partial t} + \vec{\nabla}\cdot(\rho\vec{u}\otimes\vec{u}) = \underbrace{-\vec{\nabla}\cdot\left(p\vec{I}\right)}_{1} + \underbrace{\mu\nabla^2\vec{u}}_{2} + \underbrace{\rho\vec{g}}_{3} \tag{2.16a}$$

Where, 1 refers to surface force, 2 to molecular-dependent momentum exchange (diffusion), and 3 is mass force (gravitational force).

(iii) The law of conservation of energy (the first law of thermodynamics), which states that the rate of change of energy of a fluid particle is equal to the heat addition and the work done on the particle. This energy flow is governed by the driving force of temperature gradients. The energy balance equation in the *x* direction is given by:

$$\rho C_p\frac{\partial T_f}{\partial t} + \vec{\nabla}\cdot\left(\rho C_p\vec{u}T_f\right) = \underbrace{\lambda\nabla^2 T_f}_{4} + \underbrace{S_T}_{5} \tag{2.17}$$

Where, 4 refer to heat flux (diffusion) and 5 source term for heat addition (transfer of mechanical energy to heat). For in-compressible fluids the pressure work is zero.

Besides these basic three equations, sometimes the density variation within the drying medium is also considered, which can be modeled in three different ways: (i) based on the Boussinesq approximation assuming that the density differentials in the flow are only required in the momentum equations (Ghani et al. 1991), (ii) based on the high temperature differential (Ferziger and Peric 2002), and (iii) based on the method which considers the

drying medium as an ideal gas and deriving density difference from the ideal gas equation. Likewise, the viscosity is another important fluid property which can be quantified via the mathematical correlation between the rate of deformation of the fluid and its shear stress (Norton and Sun 2007).

2.6.1 Methods of discretization of the governing differential equations of flow, heat and mass transfer

The choice of an appropriate technique for modelling the fluid continuum is of prior importance for the better analysis of numerical data, solving the flow problems, and interpreting the solution (Norton and Sun 2006). Among the different techniques, the most important ones are the finite difference method (FDM), finite element method (FEM), and finite volume method (FVM). These approaches obtain the same solution at high grid resolutions, but have a different range of applications. The finite difference method was identified as the simplest to implement, and useful in solving preliminary flow problems and for developing mathematical models. However, it was found to have limited application in real-time engineering problems due to typical geometrical complexities of the systems used in industry. This is because in finite difference method, the domain is usually meshed using structured grids and each grid node is assigned with one algebraic equation. Creating a computationally efficient structured grid for complex geometries is generally a laborious process requiring domain decomposition and other advanced techniques which if not applied proficiently, might in many cases result in massive grid nodes and subsequently extremely costly computations. Thus, any complexity in the geometry causes difficulties in creating structured grid and thereby causing convergence issues in the simulation (Bono and Awruch 2007). In contrast, the finite element and finite volume approaches employ sophisticated

meshing structures and computational techniques to deal appropriately with an arbitrary geometry with appreciable accuracy. Finite element analysis on the solution of discrete problems belongs to a function space, and the solution is strongly linked to the geometry of the domain (Dick 2009). Still, there are certain limitations for the commercial finite element packages such as the intensity of mathematics involved with no physical significances, which undoubtedly create difficulties in the programming and understanding of this technique (Ferziger and Peric 2002; Shukla et al. 2011). These difficulties are avoided through the implementation of the finite volume method. When the governing equations are expressed through finite volumes, a relation between the numerical algorithm and the principles of the conservation of mass, momentum, and energy are clearly defined within the computational domain. The numerical algorithm consists of three steps: (i) integration of the governing equations of the fluid, (ii) conversion of the integral equations to a set of algebraic equations, and then (iii) solving the algebraic equations using iteration methods (Versteeg and Malalasekera 1995). The easiness of understanding the concept, simplicity in programming, and versatility of the finite volume method has made it the most commonly used technique for modelling in food industries.

2.7 Mathematical formulations used in CFD

Usually, the motion of fluid particles in space is well represented by Navier-Stokes equation which details the change of a vector quantity in 3D space (Al Makky 2012). The simulation of the physical processes occurring during drying is done by solving Navier-Stokes equations numerically in an iterative scheme, the coupling between the velocity and pressure fields. This process encounters long computation time and divergence issues. Hence, some simplification in the domain size by introducing the concept of symmetry wherever possible is usually

performed. The governing equations are represented by different mathematical formations such as Eulerian-Eulerian or two-fluid/two-phase models (interpenetrating continuum) and Eulerian-Lagrangian or the discrete particle models as described by Jamaleddine and Ray (2010). They reported that almost all equations used in the study of fluid flows (i.e. the continuity equation, momentum equations, and the energy balance equation) are derived from Reynolds transport theory. The programmable form of these mathematical formulations for the governing equations is cast into the computational domain by discretizing the whole domain either by finite element, finite volume, or finite difference. To accomplish this, the entire problem domain is divided into cells, in which the mass balance is computed over each cell. Most of the CFD codes in the market such as ANSYS, OPENFOAM, COMSOL, STAR CCM, FLOW 3D, PHEONICS, etc. except LIGHHT CFD-DEM coupling package which is a discrete element modelling package are capable of using both Eulerian and Lagrangian Formulations (Stone et al. 2016).

2.7.1 Eulerian-Eulerian or two-fluid models

Eulerian-Eulerian formulations can handle both dense and dilute flow systems and are important in the case of handling two fluids with turbulence. In the two-fluid models (eg: fluidized bed drying), the fluid phase and the solid phase are treated as interpenetrating or interacting continua. Hence, this approach is called as a pseudo-fluid approach (Zhou 2015). Each phase is represented by the phase volume fractions and the summation of these volume fractions must be unity. The conservation laws of mass and momentum are then solved for each phase to account for the interphase interaction force called the drag force (Li et al. 2012a). The mass, energy and momentum equations for one component (a) in a

mixture of'a' and'b' (as in multiphase flow) as per Eulerian approach is given by Equations 2.18- 2.20 (Hamzehei 2011):

$$\frac{\partial}{\partial t}(V_a\rho_a) + \vec{\nabla}\cdot(V_a\rho_a\overrightarrow{u_a}) = \sum_{p=1}^{n}(m_{ba} - m_{ab}) + S_{m,a} \quad (2.18)$$

$$\frac{\partial}{\partial t}(V_a\rho_a\overrightarrow{u_a}) + \nabla(V_a\rho_a\overrightarrow{u_a}\otimes\overrightarrow{u_a}) = \vec{\nabla}\cdot\left(T_a - V_a p\vec{I}\right) + F + S_{f,a} \quad (2.19)$$

$$\frac{\partial}{\partial t}(V_a\rho_a e_a) + \nabla(V_a\rho_a e_a\overrightarrow{u_a}) = \vec{\nabla}\cdot\left(T_a\overrightarrow{u_a} - V_a p\vec{I}\right) + \vec{\nabla}\cdot(\overrightarrow{q_a}) + S_{T,a} \quad (2.20)$$

Where, m_{ba} and m_{ab} are the mass flux from component a to b (kg/(m^{3}s)), $S_{m,a}$, $S_{F,a}$, and $S_{T,a}$ are the additional source terms of component a for mass (kg/(m^{3}s)), momentum (N/ m^3), and heat (J/(m^{3}s^1)), respectively. And T_a, $\overrightarrow{u_a}$, and $\overrightarrow{q_a}$ are the temperature, velocity and Energy of dispersed phase (component a), respectively. $\bar{I}$ is the unit tensor.

The turbulence of the fluid (drying medium) plays an important role in phase distribution. Chahed et al. (2003) developed an Eulerian-Eulerian two-fluid model emphasizing the turbulence correlations associated with the added mass force. Their results proved that the two-fluid models improve the representation of the interaction between the phases. This Eulerian-Eulerian approach has been used in many drying studies such as the study of dynamics of a fluidized bed dryer (Dincer and Sahin 2004; Li and Duncan 2008; Assari et al. 2007; Assari et al. 2012; Ranjbaran and Zare 2012). The use of the kinetic theory of granular flow in conjunction with the two-fluid model helps to describe the solid particle-particle interaction in a fluidized bed (Taghipour et al. 2005; Hosseini et al. 2010). In general, the authors state that, this approach is suitable for the prediction of phase distributions which was previously limited by the inadequate modelling of the turbulence and of the interfacial forces. Additionally, the algorithm for the conveying phase can be easily modified without compromising the storage and computational time (Crowe 1991). The two-fluid (air-

droplet) formulations are not capable of representing the mass fluxes and resulting physical phenomena associated with two streams of particles moving at differential velocities at the same physical location. Hence, it has limited application in the modelling of jet impingement drying technology when compared to the discrete particle approach (Pai and Subramaniam 2006).

2.7.2 Eulerian-Lagrangian or the discrete particle models

In Eulerian-Lagrangian models, the Newtonian equations of motion are solved for each individual solid particle and an interaction model is applied to handle particle encounters. Such models were used by Huang et al. (2003) for modelling spray drying. In Eulerian-Lagrangian models, the fluid phase motion is described in an array of Cartesian coordinates forming a Cartesian grid or particle grid, which can be used for particle tracking purposes (Grace and Taghipour, 2004). Hence, such models are called trajectory models (Zhou 2015). The overall calculation time can be significantly reduced by applying the algorithms referring to particle interactions (i.e. the search algorithm for collision partners) on this grid. This approach considers fluid phase separately by solving a set of time-averaged Navier-Stokes equations and is treated using Eulerian approach. The dispersed phase is solved by tracking a large number of particles, bubbles, or droplets through the calculated flow field employing Lagrangian approach (Jamaleddine and Ray 2010). The particle trajectory is calculated by solving the equation of motion as given below (Ali et al. 2017; El-Behery et al. 2013):

$$\frac{du_p}{dt} = \underbrace{\vec{F}_D\left(\vec{u} - \overrightarrow{u_p}\right)}_{1} + \underbrace{\frac{g\left(\rho_p - \rho_g\right)}{\rho_p}}_{2} \tag{2.21}$$

Where, $\vec{u}$ and $\overrightarrow{u_p}$ are the instantaneous gas and particle velocities, 1- drag force per unit mass, 2- gravity and buoyancy force per unit mass.

The dispersed phase and the fluid phase are coupled through the fluid volume fraction and the total source term that account for heat, mass, and momentum fluxes (El-Behery et al. 2013). This approach has some unique advantages over the Eulerian-Eulerian approach, especially in describing the nonlinear dependence of interphase transfer processes on the droplet (or particle) size. Hence, it is more convenient for tracking the trajectories of particles (Pai and Subramaniam 2006; 2009). Also, the Eulerian-Lagrangian model is more suitable for simulating the fluctuations in particle velocity (Sae-Heng et al. 2011), and with a longer computation time, is more capable of giving the particle temperature history and mass change (Zhou 2015). Moreover, the phenomena prevailing at the individual particle level can be easily incorporated since the properties of each particle are described separately (Deen et al. 2007). The Lagrangian-Eulerian approach can accurately represent collisions in the presence of flow and thereby minimize numerical diffusion in dispersed-phase fields, such as volume fraction and mean velocity, when compared to the grid-based Eulerian approach (Gondret et al. 2002). However, one of the major limitations in using the Eulerian-Lagrangian approach is the lack of suitability for concentrated or dense systems with significant particle-fluid and particle-particle interaction as in the case of spouted bed drying. This is because, in the case of dense systems, there will be a high computational demand for a larger number of particles traced (Szafran and Kmiec 2004; Ali et al. 2017). In order to reduce the cost of the simulation, Fletcher et al. (2006) employed Eulerian flow representation of the spray droplets so that the particles can be modeled as a second phase. However, they lost the time history of individual particles, and could not model the interacting jets. The Eulerian-Lagrangian method was also used to model drying processes while considering the volume change by a proper structural mechanics analysis that

allowed for the determination of material shrinkage due to water evaporation. Curcio and Aversa (2010) have used an Arbitrary Lagrangian-Eulerian (ALE) method to model drying phenomena with volume changes. They used the transport and structural mechanics models to calculate the stresses developing in the solid as a result of water removal in order to simulate lateral and longitudinal shrinkage of the solid. The validation results of their model gave a maximum observed deviation less than 10% for both lateral and longitudinal shrinkage.

2.1 Commercial CFD codes

A wide variety of commercial CFD codes are available today. Over the decades, different challenges in this area have led to remarkable competition among the commercial CFD developers. These codes, with applicability in the areas of modelling non-Newtonian fluids, two-phase flows, flow dependent properties, phase change, and flow through porous media, have gained much popularity (Kopyt and Gwarek 2004). Generally, a CFD code consists of input parameters, time discretization section, space discretization section, and output section. Some of the commonly used CFD codes are shown in Table 2.1.

Table 2.1 Some of the commonly used commercial CFD codes and their important features*

Code	**Provider**	**Solver**	**TBC**	**Features/Capabilities**
CFX & FLUENT	ANSYS, Inc. www.ANSYS.com	FVM	Temperature, flux, convection, radiation, heat source	Inbuilt geometry, meshing, pre and post processing features. Enthalpy and latent heatbased phase change models available & CAD compatible.
COMSOL multiphysics	COMSOL www.comsol.com	FEM FVM, PTM	Temperature, flux, convection, radiation, electromagnetic heating	Inbuilt geometry, meshing, pre and post processing features. CAD compatible and Live link feature for MATLAB and excel.
Star-CCM Star- CD	CD adapco Group www.cd-adapco.com	FVM	Temperature, flux, convection, radiation	Inbuilt geometry, meshing, pre and post processing features. Enthalpy phase change model available & CAD compatible.
PHOENICS	CHAM Ltd. www.cham.co.uk	FEM FVM	Temperature, flux, convection, radiation	Inbuilt meshing, pre and post processing features. Both enthalpy and latent heat-based phase change models available & CAD compatible.

Code	Provider	Solver	TBC	Features/Capabilities
OpenFOAM (open source)	OpenFOAM CFD OpenFOAM.org	FVM FEM	Convection, temperature, flux, radiation, heat source	Inbuilt geometry, meshing, pre and post processing features & CAD compatible.
Flow 3D	Flow Science, Inc. www.flow3d.com	FVM	Convection, temperature, flux, radiation, heat source	Inbuilt meshing, pre and post processing features. CAD import and edit feature.
SOLIDWORKS Flow Simulation	Dassault Systèmes SOLIDWORKS Corp www.solidworks.com	FVM	Convection, temperature, flux, radiation	Inbuilt meshing, pre and post processing features. CAD import and edit feature.
CFD-DEM Coupling LIGGGHTS (open source)	CFDEM®project www.cfdem.com	DEM	Convection, temperature, flux, radiation, heat source	CAD import feature for geometry and meshing. Inbuilt pre and post processing features.

* modified from the results reported by Kopyt and Gwarek, (2004)

The commercial codes like CFX and FLUENT currently owned by ANSYS, Inc. had occupied the major share in the market with its wide range of educational and industrial applications (Xia and Sun 2002; Chen and Sun 2012; Defraeye 2014). ANSYS CFX package has high CFD solver capabilities using a unique multi grid linear solver (with essentially linear parallel CPU scalability) and access to a broad set of models that provide accurate results (Frank et al. 2012). ANSYS codes have wide applications in the design of heat exchangers, discrete phase models for multiphase flows and for numerous reaction models, and phase change models which are common in food processing (Mirade and Daudin 2006; Hosseinizadeh et al., 2012; Muhammad et al., 2015; Ali, et al. 2017). The PHOENICS codes were also reported as a powerful tool in modelling various food processes, including Newtonian and non-Newtonian fluid flow modelling (Hlawitschka et al. 2016), flow through porous media with direction-dependent resistances, and conjugate heat transfer (Norton et al. 2007; Ghani and Farid 2010). Since this package involves structured grid code, the meshing of complex geometries might involve more effort than that in the case of ANSYS (Bolot et al. 2004; Dick 2009). Also, ANSYS has a single-user interface for generating geometry; meshing; setting up the fluid properties, the initial and boundary conditions, and the numerical options; and displaying the numerical results which make it more appealing than PHEONICS.

FLOW 3D is another highly-accurate CFD software that can provide insightful information to many physical flow processes, especially for free-surface flows. It has some advanced features such as liquid-vapour and liquid-solid phase change simulations available in the latest version of FLOW 3D, and are highly useful for modelling drying and cooling processes (Lang and Todte 2011; Saravacos and Kostaropoulos 2016). STAR-CD is suitable for dealing with

unstructured meshes (which do not follow a uniform pattern) containing all cells shapes including polygons and for any hybrid unstructured meshes (combination of structured and unstructured mesh) with the arbitrary interface (Nicolai et al. 2001; Lo 2005). These codes were successfully used for modelling natural convection in solar dryers (Rigit and Low 2010). The CFD module of the COMSOL is capable of modelling different aspects of fluid flow, such as two-phase and porous media flows for the laminar and turbulent flow regimes. It has been used in defining the fluid flow in drying processes (Aversa et al. 2007; Sabarez 2012; ElGamal et al. 2014). It has a wide range of simulation applications, including fluid flows involving heat transfer, solid mechanics, and electromagnetics (Table 2.1) (Kunkelmann and Stephan 2009; Zadin et al. 2015).

2.2 Turbulence models used for simulation of drying process

Along with the selection of the appropriate commercial CFD package, the choice of a suitable turbulence model for the simulation of the flow process is also important as the type of the turbulence model has a huge effect on the CFD results. The performance of these models in terms of different response variables such as deterioration of heat transfer, wall temperature, variation in buoyancy parameter, etc. vary for different fluid conditions (Zhi et al. 2016). In dryer design, fluid conditions such as the pressure profile and velocity of the fluid (drying medium) play a key role (Kaushal and Sharma, 2012). For example, these flow models that are capable of modelling the important flow parameters such as the flow pattern, velocity, temperature, humidity profile, etc. along with the other heat, mass and momentum transfer variables had been successfully used in the design of spray dryer (Langrish and Fletcher 2001; Fletcher et al. 2006). In most engineering problems, the selection of turbulence model mainly relies on the computational cost, time, and accuracy.

The complexity of the turbulence model depends on how much information is desired from the flow field. The degree of complexity for the turbulence model is due to differences in simplifications made to Navier-Stokes equation and (i.e., whether it is nonlinear, time-dependent, three-dimensional partial differential equation, etc.). It also depends on the type of different flow phenomena (such as flow distortion, transition, convection, dissipation, etc.) occurring in the fluid domain (Wilcox 1994). When modelling turbulent flow in CFD, it is very difficult to capture every scale of motion. Therefore, a model with minimal complexity, but capable of capturing the essence of the relevant physics, should be chosen (Wilcox 1994). Based on the governing equation used in the model, the turbulence models are classified into two groups: (i) Reynolds-Averaged Navier-Stokes (RANS) Models and (ii) Computation of fluctuating quantities such as Large Eddy Simulations (LES). The two-equation turbulence models such as the k-$\mathcal{E}$ (k-epsilon) model, k-ω (k-omega) model, and wall functions in conjunction with the Reynolds-Averaged Navier-Stokes (RANS) equations, are the widely used approaches for flow studies involving drying (Defraeye et al. 2012a; Defraeye 2014).

The RANS models are highly suitable for modelling large complex systems with lesser cost than LES (Kondjoyan 2006; Jongsma et al. 2013). The two-equation turbulence models, namely the k-$\mathcal{E}$ and k-ω models are more effective for the drying processes with high Reynolds numbers (Trujillo et al. 2003). The k-$\mathcal{E}$ model solves for two variables: k, the turbulent kinetic energy, and $\mathcal{E}$, the rate of dissipation of kinetic energy. This model gives good convergence and is well suited for the flow processes which do not involve adverse pressure gradients (Launder and Spalding 1974). It also works well for external flow around complex geometries. The k-ω model solves for ω, the specific rate of

dissipation of kinetic energy, and is more difficult for converging for low Reynolds flows. However, this model is more accurate for internal flows and flows with convoluted curvatures (Wilcox 1994). Trujillo et al. (2003) tried four different turbulence models (standard k-Ɛ model, RNG (Re-Normalization Group**)** *k-ℰ* model, SST (Shear Stress Transport) *k-ω* model, and laminar models) with a standard wall function and enhanced wall treatment for modelling heat and mass transfer during evaporation of water from the circular cylinder. They reported that the RNG *k-ℰ* model with enhanced wall function has given the best fit to the experimental data while considering the radiation effect as well. The model predicted the heat transfer coefficient as well as the mass transfer coefficient with high accuracy. The SST model is another turbulence model, which is a combination of the *k-ℰ* model in the free stream and the *k-ω* model near the walls (Menter 2009). This model performs well with low Reynolds numbers (Defraeye et al. 2012b; Ramachandran et al. 2017a) and was found to be sufficiently accurate for predicting the convective heat transfer coefficient (Dixon et al. 2011) and moisture and temperature profile in single element drying (Ljung et al. 2011, Ramachandran et al. 2017a). The superior predictability of the SST models is mainly attributed to the elimination of the large free-stream dependency (Ljung et al. 2011). The difference between SST and *k-ℰ* model in defining the drying process is illustrated in Figure 2.1. The central plane moisture and temperature profile of a cylindrical pellet dried under superheated steam obtained using SST and *k-ℰ* simulation is shown in Figure 2.1. The geometry and the mesh chosen for the simulation is the same as reported by Ramachandran et al. (2017a) where the distillers' spent grain pellet was subjected to superheated steam at 120°C and 1 m/s velocity. The distribution of moisture and temperature inside the solid after 100 s of

drying (Figure 2.1) shows that the definition of the mass and heat transfer phenomena is more distinctly visible in SST model than the k-$\mathcal{E}$ model, especially near the solid fluid interface. The validation of the model with their experimental results of superheated steam drying also established that the SST had better predictability over the k-$\mathcal{E}$ model. This shows that the near boundary prediction of SST model is superior especially for low Reynolds numbers and hence, the model could be used for the simulation of single element drying

The accuracy of RANS models is still questioned when compared with the LES models. Hence, more advanced approaches such as hybrid RANS-LES techniques (Detached Eddy Simulations (DES) and Scale Adaptive Simulation (SAS)) (Fletcher and Langrish 2009; Egorov et al. 2010) were used to model drying processes with higher accuracy than a pure RANS model (Fletcher et al. 2006; Kuriakose and Anandaramakrishnan 2010).

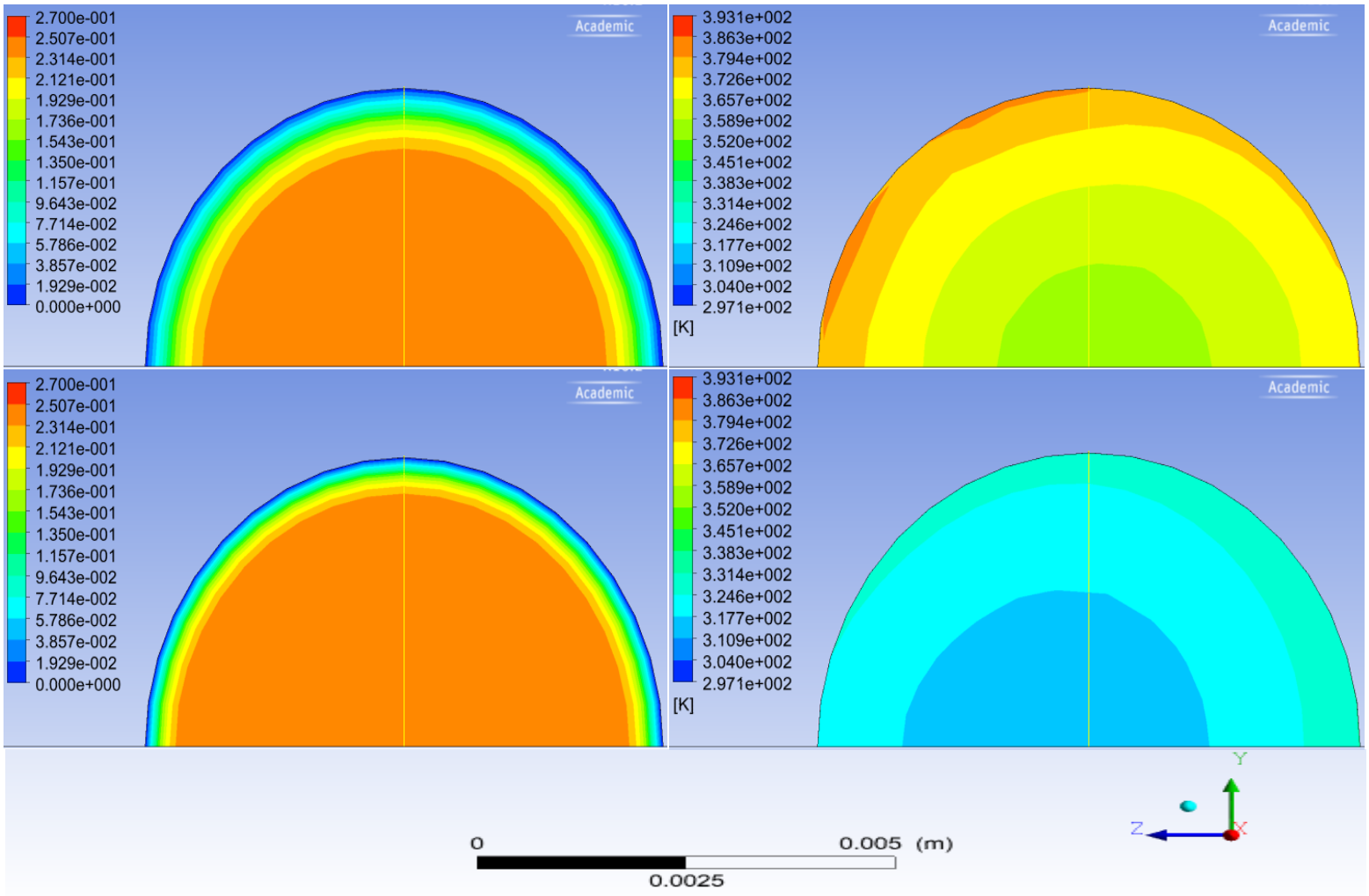

Figure 2.1 Comparison of central plane moisture and temperature profile of SST simulation (a and b) and *k-ε* simulation (c and d) of superheated steam drying of a single cylindrical Distillers' spent grain pellet, respectively.

2.3 Complexity of CFD models

In the previous section, it was mentioned that the complexity and computation load of a CFD simulation is influenced by the turbulence model chosen for defining the fluid flow. Other contributing factors worth mentioning include the geometry of the problem domain, the degree of details expected from the model, and the physics to be solved in the fluid and solid domains. The CFD package finds applications in different types of drying systems for various geometries (Table 2.2). In many cases, for the simplicity of meshing the solid geometry, it is assumed to be any standard shape (sphere, cylinder, slab or cubes) (Defraeye et al. 2012a). A rectangular geometry of the solid is most common when modelling using CFD (Table 2.2). This might be because meshing and convergence with the heat and mass transfer equations are easier in the case of rectangular geometry than other convoluted geometries such as cylinders (Kaya et al. 2006; Chandramohan and Talikdar 2010; Curcio et al. 2008). The nature of pre-requisite parameters for numerical modelling such as the thermo-physical properties of the material to be dried as well as the fluid (drying medium) defined in the model (ie. whether it is assumed to be constant with time or a function of moisture content) also affects the complexity and computational time of the model of the model (Ramachandran et al. 2017c).

In most of the cases, the granular biological material is assumed to be spherical in shape which simplifies the model equations. Such models usually consider three parameters: a surface mass transfer coefficient, dynamic equilibrium moisture content, and a drying constant (Nishiyama et al. 2006). As the shape of the modelling domain changes, the complexity of the model and the computational efforts also change. For example, the transport equations for the cylindrical shaped solids are three-dimensional while for a sphere

they are one dimensional. In cylindrical geometry, the shape effect causes a rapid change in the boundary layer conditions which in turn affects the local heat and mass transfer coefficients (Trujillo et al. 2003). However, by using different meshing options such as unstructured hybrid mesh with more defined structured mesh at the boundaries using CFD packages, the heat and mass transfer coefficients of these complex geometries can be simulated with appreciable accuracy (Jamaleddine and Ray 2010).

As the physics of the drying problem involves multiple phenomena, the computational efficiency of the CFD packages is challenged. For example, the drying of porous media which has tremendous practical applications, as most of the biological materials are considered porous (Kulasiri and Woodhead, 2005; Feng et al. 2012). A diffusion model of heat and mass transfer in moist porous solid obtained for low-intensity convection drying by Wang and Chen (1999) proved that the assumption of an evaporation front was valid for drying of very permeable materials. Later a conjugate modelling approach was used for determining the heat and mass transport in the fluid and porous solid simultaneously in a transient way. This was done by imposing convective transfer coefficients as boundary conditions at the fluid-solid interface (Defraeye et al. 2012a). The moisture transport characteristics of the porous solid determined the level of complexity of the CFD simulation for such conjugate models. Hence, a sensitivity analysis with variable meshing considering the relevance of the convective transfer coefficients is required prior to finalizing a conjugate model. In the case of a 3D conjugate problem with unsteady turbulent flow, the computational complexity of the CFD simulation will be undoubtedly higher than that for the 2D problems (Defraeye 2014).

Another phenomenon occurring during most of the drying cases is the shrinkage of the solid which add complexity and effort in mathematical modelling. Even though the phenomenon is significant in describing drying, the shrinkage behavior is less evaluated or reported in association with CFD models (Jubaer et al. 2017). The attempts to include hydro-mechanical deformation/shrinkage in the drying modelling led to the coupling of water transport and solid deformation in CFD (Katekawa and Silva 2006; Niamnuy et al. 2008; Defraeye 2014). The shrinkage of solid during drying could be modelled either by introducing an experiment based empirical model for volumetric change as a function of moisture content (Panyawong and Devahastin 2007; Kittiworrawatt and Devahastin 2009), or by solving the momentum balance of the solid (Singh et al. 2003a, 2003b; Zhu et al. 2010). The latter method involves additional modelling effort which in turn adds complexity to the drying model. Instead of modelling shrinkage for the entire drying period, a discrete approach to shrinkage modelling can be also used along with the models involving spatially resolved variables. For example, in the receding core model, the shrinkage behavior is included in the first stage of drying and was neglected in the second stage in which a dry crust is already formed (Buck et al. 2012, Mezhericher et al. 2015). A further detailed single droplet drying model proposed by Ali et al. (2017) includes a third stage in which the particle inflates because of the internal vaporization of moisture. To do that they incorporated user defined functions to the ANSYS FLUENT code. They reported that the inclusion of user defined functions increased the simulation time but, it was worth since the error in overall mass and energy balances at the end of the simulation were < 1%. Jubaer et al. (2017) compared the prediction of drying model for spray drying with perfect shrinkage and linear shrinkage models. In the linear shrinkage models, the reduction in the effective surface area is limited. In this model, shrinkage is expressed as a linear function (Patel et al. 2009) of

moisture content (Equation 2.22). In the perfect shrinkage model, the shrinkage is considered as a consistent reduction of size only owing to the moisture removal. In both the cases, the shrinkage behavior was incorporated into the CFD code by using user defined functions and the dimensional change was implemented indirectly by changing the density (Jubaer et al. 2017). They concluded that this additional phenomenon increases the intricacy of the drying model but at the same time the shrinkage cannot be neglected in the case of certain drying techniques such as spray drying and is worth for future studies.

$$\frac{r}{r_0} = \beta + (1-\beta)\frac{M}{M_0} \tag{2.22}$$

Another example of a multi-physics model for drying that involves the mechanism other than fluid flow and shrinkage are the cases of microwave drying and freeze drying. Ranjbaran and Zare (2012) introduced user-defined source terms into the FLUENT code to account for the rate of heat generation due to microwaves in their attempt to model microwave assisted fluidized bed drying. They used additional model equations for computing this heat generation based on the microwave power density and dielectric constants. In the case of freeze drying, an additional user defined function for capturing the sublimation rate for an air-water mixture and local mass fraction of generic species (nitrogen gas used in freeze dryer) may be required to accompany the transport equations (Li et al. 2007; Petitti et al. 2013; Ganguly et al. 2013). Hence, developing and running such drying models with compounded physical phenomena is challenging and computationally demanding.

Even though CFD has been widely used in modelling spray drying (Figure 2.2), the attempts to improve its application efficiency in terms of computational load and memory requirement are still going on. For example, the droplet tracking in the transient case requires significant additional memory and longer simulation time (Fletcher et al. 2006). The prediction of

agglomeration of particles is challenging especially in dense flow as it relies on the accurate prediction of the particle-particle interaction. Additional models such as stochastic collision models have to be implemented in the discrete phase model to account for such particle-particle collisions which again adds to the computation effort (Jin and Chen 2009, Jaskulski et al., 2015). Besides these factors, the existence of random fluctuations in the flow conditions (anisotropic turbulence in the spray dryer) could also add intricacy in the model. These types of flow fluctuations are generally resolved using more advanced turbulence modelling techniques such as the Large Eddy Simulation (LES) or by solving the Navier-Stokes equations for all spatial and time scales (i.e., Direct Numerical Simulation (DNS)) (Jongsma et al. 2013). These methods need extreme computational time and resources. But, by using certain hybrid turbulence models such as the detached eddy simulation (DES), the overall computational load of LES modelling could be minimized. The DES model utilizes the LES model away from the boundary layer and RANS near the wall (Gimbun et al. 2015). The capturing of random fluctuations in the flow via experimental trials is also a tedious job and requires complex test rigs and advanced experimental equipment that have high temporal and spatial resolutions (e.g., Particle Image Velocimetry, Planar Laser Induced Florescence, etc.).

Table 2.2 Overview of common solid geometries considered in modelling of drying process using CFD

Product	**Model on**	**CFD package**	**Reference**
Water droplet	Resident time distribution analysis of particle in the superheated steam spray dryer	FLUENT (FVM)	Ducept et al.2002
Circular cylinder	Heat and mass transfer during evaporation of water from cylinder	FLUENT 6.1.18	Trujillo et al. 2003
Rectangular porous solid	Interfacial transfer coupled with analysis of temperature, moisture, and pressure (superheated steam)	FLUENT (EBFVM)	Erriguible et al. 2006
Rectangular moist solid	Conjugate model of external and internal flow (pneumatic drying)	FLUENT (FVM)	Kaya et al. 2006
Wood	Heat and mass transfer of external and internal flow	ANSYS CFX	Younsi et al. 2008
Rectangular moist solid	Simultaneous heat and mass transfer during convective drying	ANSYS CFX (FVM)	Chandramohan and Talukdar. 2010
Iron ore pellet	Capillary flow of liquid moisture and internal vapour flow (convective air drying)	ANSYS CFX	Ljung et al.2011

Product	Model on	CFD package	Reference
Porous flat plate	Conjugate modelling of heat and mass transport in the air flow and the porous material	FLUENT (CVFEM)	Defraeye et al. 2012a
Rapeseed	Superheated steam fluidized bed drying	FLUENT (FVM)	Xiao et al. 2013
Rectangular potato slice	Conjugated heat/mass transfer problem during drying with impinging-jets	FLUENT (FVM)	Kurnia et al. 2013

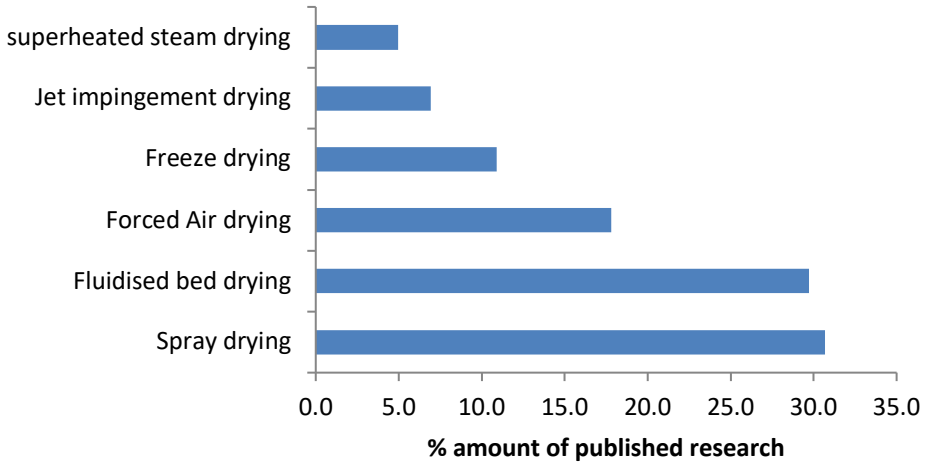

Figure 2.2 Published peer-reviewed papers on drying modelling using CFD between the year 2000 and 2017

2.4 CFD in different drying systems

The evaluation and design of commercial dryers used in food industry involve numerous experimental and computational processes. This complicated process has become convenient, reliable, and modifiable by computational tools and software based modelling techniques. As discussed in the previous sections, CFD, with its constantly evolving computational power, had a paramount role in industrial drying modelling. The high spatial and temporal resolution of CFD simulations was utilized by researchers to model the flow of drying medium in the dryer systems (Ducept et al. 2002; Smolka et al. 2010) to predict the convective transfer coefficients, predict moisture and temperature profiles in both solid and drying medium (Verboven et al. 1997; Wang and Sun 2003; Chandramohan and Talukdar 2010; Ljung et al. 2011), and to gain insight into the particle flow and its trajectories in drying systems (Chiesa et al. 2005; Zhang and Chen 2007; Jin and Chen 2010; Anandharamakrishnan et al. 2010; Defraeye 2014). Most models for convective drying used the analogy of thermal and concentration boundary layers to determine the convective mass transfer coefficient using Eqn 11 (Kaya et al. 2006; 2007; 2008; Elgamal et al. 2014; Chandramohan and Talukdar 2010). However, under conditions in which the temperature-concentration analogy is valid yet not fulfilled practically, CFD has succeeded in predicting convective transfer coefficients in pneumatic dryers with a high degree of detail and spatial resolution (Defraeye et al. 2012a). The heat transfer coefficient around the moist object can be easily determined using the local temperature profile around the object using the energy balance equation (Equation 2.23).

$$kt\frac{\partial T}{\partial x} = h\left(T_f - T_s\right) \tag{2.23}$$

$$h^* = h\left(\frac{D^* Le^b}{kt}\right) \tag{2.24}$$

Where, the Lewis number (dimensionless) represents a relative measure of the thermal and concentration boundary layer thickness. The value of *b* is assumed as 1/3 in most of the cases (Kaya et al. 2006; Chandramohan and Talukdar 2010).

Computational Fluid Dynamics has a broad range of applications in simulating heat and mass transfer phenomena for both external (drying medium) and internal (within the materials which are dried) flows. This includes various drying techniques such as spray drying (Jin and Chen 2009; Anandharamakrishnan et al. 2010; Jaskulski et al. 2015; Keshani et al. 2015), fluidized bed drying (Sae-Heng et al. 2011; Freire et al. 2012; Li et al. 2012a; Jang and Arastoopour 2014), deep bed drying (Jamaleddine and Ray 2011; Defraeye et al. 2011; Defraeye et al. 2012b; Ranjbaran et al. 2014; Elgamal et al. 2014), freeze drying (Li et al. 2007; Barresi et al. 2010; Ganguly et al. 2013; Chen et al. 2014), jet impingement drying (De-Bonis and Ruocco 2007; Liewkongsataporn et al. 2008; Jiang et al. 2012; Kurnia et al. 2013; Yahyaee et al. 2013; Taghinia et al. 2016; Xu et al. 2016), microwave drying (Ranjbaran and Zare 2012; Jin et al. 2015), solar drying (Rigit and Low 2010; Yunus and Al-Kayiem 2013) and superheated steam drying (Yang et al. 2011; Xiao et al. 2013; Adamski and Pakowski, 2013; Ramachandran et al., 2017a). All of these methods utilize the computational capability of CFD in solving the transport equations in the drying medium, which sets the boundary condition for the solid to be dried. The capability of modern CFD packages to couple the equations of fluid flow (drying medium) and existing empirical drying models for the solid had strengthened its application in drying. For example, the numerical techniques such as pore network models (Yiotis et al. 2001; Vorhauer et al. 2010), diffusion models (Erriguible et al. 2005, 2006; Elgamal et al. 2014), and macroscopic models (Nasrallah and Perre 1988; Perre 2010) were applied in the convective drying process

coupled with the CFD codes. The coupling of the porous media models with the Navier-Stokes equations in the fluid medium was performed by introducing appropriate boundary conditions at the solid-fluid interface. Such coupled models were adopted by researchers for simulating high-temperature convective drying, superheated steam drying, and vacuum drying (Erriguible 2006) where the classic boundary layer hypothesis could not be applied. The application of CFD techniques is more frequently found in some drying methods such as spray drying and spouted bed and fluidized bed drying (Figure 2.2 where there is a direct application of the equations of fluid dynamics and moisture and heat transfers (Ullum et al. 2010). These types of methods combine drying with pneumatic transport for which CFD had proven its application. The CFD-based modelling in these types of drying is mainly used for design, modification, and evaluation of the drying chamber (Defraeye 2014). It focuses primarily on the flow parameters of the drying medium and its inhomogeneity throughout the problem domain which affect the drying behavior (Barresi et al. 2010; Shokouhmand et al. 2011). In such methods where continuous solid-fluid interaction is common, the gas and the solid motion need to be modeled separately. A Discrete Element Method (DEM), which relies on Newtonian equations for particle motion or a two-fluid model (TFM) dependent on the description of interfacial forces and solid stresses, could be used to model fluidized/spouted bed drying processes (Zhou et al. 2004; Wu and Mujumdar 2008). Besides the study of the aerodynamics of the particles, Sae-Heng et al. (2011) used a combination of computational fluid dynamics CFD models and kinetic theory of granular flow for predicting gas and particle temperature profiles and heat transfer coefficients (Hoffmann et al. 2011; Tatemoto and Sawada 2012) in a two-dimensional fluidized bed. They found that the combined model had better prediction efficiency than the pure CFD model. Li et al. (2012b) employed the Eulerian-Eulerian approach of a CFD

simulation to describe fluid dynamics, drying behavior, and dust integration and used a Two-Fluid Model (TFM) to solve the drop deposition rate and the dust integration rate for a fluidized bed spray granulation drying process. They explained the spray granulation process using three different concepts, namely droplet deposition, drying, and dust integration. The growth of the solidified film of atomized liquid sprayed over a fluidized bed of solids was called droplet deposition, and the droplets which are not dried on the granular fluidized bed were considered as dust. The growth of the dust adhering to the wet granules in the fluidized bed was called dust integration (Li et al. 2013). Li et al. (2012b) concluded that the TFM could predict the mass of dust, the particle diameter evolution, and the temperature of the droplets successfully. Also, the modelling of the kinetic stress (stress developed by the collision of particles in the fluidized bed) based on the kinetic theory of granular flow is now widely accepted (Johansson et al. 2006; Taghipour et al. 2005; Van Wachem et al. 2001). The description of minute features occurring during fluidization during spouted bed drying, such as changes in the angle of internal friction and the effect of dissipation parameters (collision with other particles), were also studied and coded using commercial CFD packages (Ranjbaran and Zare 2012).

It has been proven that a full CFD model and a detailed investigation of problems associated with the chamber aerodynamics can be useful for the design modification of spray dryers (Oakley 2004). Wawrzyniak et al. (2012) used CFD packages to determine the hydrodynamics of drying air in an industrial counter-current spray dryer and studied the flow pattern in such a dryer. CFD packages have been extensively used for various parametric studies of gas flow, dryer performances (Huang et al. 2003), particle distribution (Anandharamakrishnan et al. 2010), and even the study of single droplet characteristics and droplet-droplet interaction (collision) (Mezhericher et al. 2008, 2010).

Commercial CFD software mainly used for forced air drying studies are ANSYS Fluent and ANSYS CFX (Table 2.2). Their use may be because of the availability of the powerful mesh generation package and problem equation solver with better graphical user interface than other CFD packages such as COMSOL, STAR- CD, etc. Besides the study of flow fields, the estimation of a spatial and temporal variation of the convective transfer coefficient is also important for modelling complex drying processes (Defraeye et al. 2012b). The CFD codes can also be used to study the variation in the convective heat transfer coefficient with the peak behavior at the transition of constant drying rate and falling drying rate with temporal changes (Halder and Datta 2012). CFD codes are also used for modelling the drying of wet particles or droplets with solid material inside. However, such modelling is challenging because of the multitude of physics behind the drying process (Nijdam et al. 2006).

CFD packages were also used for modelling complex drying processes involved in superheated steam (SS) drying. Eulerian-Eulerian multiphase models were used for the study of process parameters and transport phenomena in fluidized SS drying (Xiao et al. 2013). In the case of SS drying, there is no molecular density gradient between the water in the solid and the surrounding medium which is steam. Hence, the particles heated up by the convection reaches the boiling point at which the water evaporates. Frydman et al. (1998) integrated the heat required to evaporate water from the spray droplets in a spray dryer with SS as the drying medium in each computational volume of the dryer, using a standard k-ε model. Their results showed that the temperature field measured at different distances from the axis of the dryer and the mass flow rate of steam had good agreement with the experimental results. Ducept et al. (2002) had used CFD code to solve heat, momentum, and mass equations over a finite volume to describe the entire drying domain in SS spray drying. They reported an appreciable agreement with the

experimental results of residence time distribution and the simulation results. CFD modelling techniques were also used for comparing the spray drying of biological material using air and SS. The generated model was used to evaluate the important features of a spray dryer such as temperature distribution inside the chamber, the velocity of the gas, droplet trajectories, and deposits on the walls (Frydman et al. 1998). Suvarnakuta et al. (2007) had used COMSOL Multiphysics to study the heat and mass transfer phenomena of SS drying of heat sensitive materials such as carrots. The versatility of CFD codes in solving different flow problems even includes applications in mass transfer associated with chemical reactions. Rajika and Narayana (2016) had used a packed bed CFD model in conjunction with the devolatilization reaction occurring during biomass drying and combustion. The evolved version of CFD packages such as ANSYS CFX had the capability to describe gas phase chemical reactions, species transport, and devolatilization along with the turbulent fluid flow (Wang and Yan 2008). This feature of CFD packages could be utilized for the more detailed study of different drying/thermal processes involving volatilization or other chemical reactions.

2.5 Research challenges in CFD modelling in the field of drying

In spite of the immense potential of CFD in modelling drying processes, there are some computational challenges in the CFD application for drying of granular materials. The accuracy of such simulations is still questioned by researchers as the accuracy of the CFD models depends significantly on the turbulence modelling approach used for flow predictions (Defraeye 2014). The first limitation of the CFD simulation, especially in drying applications, is its inability to accurately predict transport phenomena in irregularly shaped materials. This is evident from Table 2.2 because researchers generally assume regular geometry when modelling heat and mass transfer as it simplifies the model. Drying processes usually involve solids of irregular shapes

and a broad range of size distribution, which might not be easily captured by some of these models (Massah and Oshinowo 2000). Also, for complex geometries flows incorporating a considerable amount of swirl and turbulence, the effect of some of the associated phenomena of drying such as shrinkage on the residence time will be difficult (Jubaer et al. 2017). Secondly, the Eulerian-Eulerian CFD methods rely on the kinetic theory approach to describe the constituent relations for fluid viscosity and pressure, which are based on binary collisions of smooth spherical particles and do not account for the deviation and distribution of their shape and size. Also, CFD models have very little description regarding the turbulent interaction between different phases and thus they sometimes lack the ability to present the associated drag models (models describing the drag force) for specific cases, especially when solid concentrations are high. Perhaps, it cannot be listed as a limitation, but some of the biggest marketed commercial CFD codes such as ANSYS FLUENT and CFX do not provide standardized boundary conditions that enable the definition of simultaneous heat and mass transfer processes at the interface of the solid and fluid phases. But an appropriate condition can be implemented at the interface by using suitable user defined functions which could be an additional effort in modelling (Krawczyk 2016). Above all, the CFD simulations of realistic three-dimensional geometries matching the industrial drying configurations are computationally demanding and expensive because of high computation time and processor memory. However, it is still more convenient for evaluating geometric changes as they save time and cost, compared to the greater challenges and expenses of laboratory testing.

Despite these challenges in the application of CFD simulations of drying processes, the use of CFD increased substantially in the last two decades (Jamaleddine and Ray, 2010). In order to show the popularity of CFD techniques in modelling different types of drying, a number of peer-

reviewed research papers (about 150) published in the past two decades were sorted and studied. The frequency of usage of CFD in numerical modelling of various drying techniques over this period is displayed in Figure 2.2. As shown in Figure 2.2, the use of CFD is higher in pneumatic drying methods, especially fluidized bed drying and sprays drying when compared to other drying methods. The learning effort needed for understanding the modelling features and the efficient use of CFD codes in modelling different drying processes are still challenging. However, the tremendous progress in the development of newer versions of these packages with advanced features in meshing, model equations set up, in-built features for incorporating user defined functions without the hassle of learning additional computer programming languages like FORTRAN or C, and solver constantly increases the usage of this technique in the simulation of various drying methods.

2.6 Conclusions

By synthesizing the research findings from the past, it is clear that the computational power of CFD packages provides a detailed understanding of the dynamics and physics of drying operations. The CFD-based models with appreciable prediction power aids in design and optimization of the drying processes with better qualitative and quantitative efficiency. Different mathematical approaches used in CFD have their own advantages and disadvantages and therefore have specific applications. The major bottleneck in the widespread use of CFD codes such as FLUENT, ANSYS CFX, PHOENICS, etc. is a high processing time for more complex flow problems and for finer meshes. Also, the accuracy of the prediction by any CFD software depends on the turbulence model used. Hence, an appropriate choice of turbulence models based on the validation results with the experimental data is important. Despite its complexity and criticism against the accuracy of CFD models,

the application of the CFD technique in the area of drying is increasingly growing because of its ability to predict the hydrodynamics of drying at a lower cost as compared to laboratory experimentation.

Acknowledgements

The authors acknowledge the Natural Sciences and Engineering Research Council of Canada, Graduate Enhancement of Tri-Council Stipends, and University of Manitoba Graduate Fellowship for their financial support.

List of symbols

α	Thermal diffusivity (m^2/s)
β	empirical coefficient for shrinkage
λ	Latent heat of vaporization in (J/kg^1)
μ	Dynamic viscosity of fluid (kg/(m s)
τ	Total tensor of strains (Pa)

Subscripts and superscripts

e	Equilibrium
f	fluid/Drying medium
i	direction in x, y, z axis
in	Interface layer
n	coefficient of drying
o	Initial point (t=0 s)
s	Solid

List of symbols

$\otimes$	Tensor product
ξ	Surface interface to a fixed value
ρ	Density (kg/m^3)
∇	Laplace gradient function

Subscripts and superscripts

v	water vapour
d	dry matter
a, b	Components of mixture
w	water
df	drying front
sat	saturation
wb	wet bulb

Nomenclature

A	Surface area of solid (m^2)
C	Concentration (kg/m^3)
C_p	Specific heat (J/(kg K)
D^*	Effective Moisture diffusivity (m^2/s)
DEM	Discrete Element Method
E	The activation energy (J/mol)
F	Momentum exchanged between phases in motion (N/m^3)
FEM	Finite Element Method
FVM	Finite Volume Method
$\dot{I}$	Volumetric evaporation ($kg/(m^3s)$)
kt	Thermal conductivity (W/mK)
L	Characteristic length (m)
Le	Lewis number (α/D)
M	Moisture content (kg/kg)
MR	Moisture ratio
P	Pressure (Pa)
PTM	Particle Tracing Method
Q	Energy of dispersed phase ($J/(m^3s^1)$)

Nomenclature

R	Universal gas constant ($8.316\ J/mol^1$)
S_T	Thermal sink or source (W/m^3)
T	Temperature (K)
TBC	Thermal Boundary Condition
V	volume fraction
W	Molecular weight of water
a	normal vector at the surface
h^*	Mass transfer coefficient (m/s)
h	Heat transfer coefficient (W/(m K)
g	Body force per unit mass (m/s^2)
k	Drying constant
k^*	Evaporation constant
m	Mass of solid (kg)
$\dot{m}$	Mass flux ($kg/(m^3s)$
p	Static pressure (Pa)
q	heat flux ($J/(m^3s^1)$
t	time (s)
u	Velocity of fluid (m/s)
r	Radius (m)

References

1. Adamski, R. & Pakowski, P. (2013). Identification of Effective Diffusivities in Anisotropic Material of Pine Wood during Drying with Superheated Steam. *Drying Technology,* 31(3), 264-268. Doi.org/10.1080/07373937.2012.717152.
2. Agarwal, P. K., Genetti, W. E., & Lee, Y. Y. (1986). Coupled drying and devolatilization of coal in fluidized bed. *Chemical Engineering Science, 41*(9), 2373-2383.

3. Al Makky, A. (2012). Coding Tutorials for Computational Fluid Dynamics, www2.warwick.ac.uk/fac/sci/eng/study/pg/students/esrhaw/cfdebook.pdf (accessed on 18 September 2013).
4. Ali, M., Mahmud, T., Heggs, P. J., Ghadiri, M. Bayly, A., Ahmadian, H., & de Juan, L. M. (2017). CFD modeling of pilot-scale countercurrent spray drying tower for the manufacture of detergent powder. *Drying Technology*, 35(3), 281-299.
5. Anandharamakrishnan, C., Gimbun, J., Stapley, A. G. F., & Rielly, C. D. (2010). A Study of Particle Histories during Spray Drying Using Computational Fluid Dynamic Simulations. *Drying Technology*, 28, 566–576.
6. Aregbesola, O. A., Ogunsinaa, B. S., Sofolahana, A. E., Chimeb, N. N. (2015). Mathematical modeling of thin layer drying characteristics of dika (*Irvingia gabonensis*) nuts and kernels. *Nigerian Food Journal*, 33, 83–89.
7. Assari, M. R., Tabrizi, H. B., & Najafpour, E. (2012). Energy and exergy analysis of fluidized bed dryer based on two-fluid modeling. *International Journal of Thermal Sciences*, 64, 213-219.
8. Assari, M.R., Tabrizi, H. B., & Saffar-Avval, M. (2007). Numerical simulation of fluid bed drying based on two-fluid model and experimental validation. *Applied Thermal Engineering,* 27, 422–429.
9. Aversa, M., Curcio, S., Calabro, V., & Iorio, G. (2007). An analysis of the transport phenomena occurring during food drying process. *Journal of Food engineering,* 78, 922-932.
10. Baini R. & Langrish T. A. G. (2008). An assessment of the mechanisms for diffusion in the drying of bananas. *Journal of Food Engineering,* 85, 201-214.
11. Baini, R. & Langrish, T. A. G. (2007). Choosing an appropriate drying model for intermittent and continuous drying of banana. *Journal of Food Engineering,* 79,330–343.
12. Barresi, A. A., Pisano, R., Rasetto, V., Fissore, D., & Marchisio, D. L. (2010). Model-Based Monitoring and Control of Industrial Freeze- Drying Processes, Effect of Batch Non-uniformity. *Drying Technology,* 28(5), 577-590.
13. Bernard, P. S. & Wallace, J. M. (2002). Turbulent Flow: Analysis, Measurement and Prediction, John Wiley and Sons Inc.
14. Bolot, R., Li, J., & Coddet, C. (2004). Modeling of thermal plasma jets: a comparison between PHOENICS and FLUENT. Presented in Conference: Thermal Spray Solutions:

Advances in Technology and Application (proceedings of International Thermal Spray Conference, mai 10-12 2004, Osaka, JAP), At Osaka (JAP).

15. Bono, G. & Awruch, A. M. (2007). Numerical study between structured and unstructured meshes for Euler and Navier-Stokes equations. *Mecanica Computacional,* 26, 3134-3146.
16. Bourassa, J., Ramachandran R. P., Paliwal, J., & Cenkowski, S. (2015). Drying characteristics and moisture diffusivity of distillers' spent grains dried in superheated steam. *Drying Technology*, 33(15-16), 2012-2018.
17. Buck, A., Peglow, M., Naumann, M., & Tsotsas, E. (2012). Population Balance Model for Drying of Droplets Containing Aggregating Nanoparticles. *American Institute of Chemical Engineers Journal*, 58(11), 3318–3328.
18. Chahed, J., Roig, V., and Masbernat, L. (2003). Eulerian–Eulerian two-fluid model for turbulent gas–liquid bubbly flows. *International Journal of Multiphase Flow,* 29, 23–49.
19. Chandramohan, V. P. & Talukdar, P. (2010). Three dimensional numerical modeling of simultaneous heat and moisture transfer in a moist object subjected to convective drying. *International Journal of Heat and Mass Transfer,* 53(21–22), 4638–4650.
20. Chen, C. C., Tsai, S. M., Cheng, H. P., & Chen, C. H. (2014). Analysis for heat transfer enhancement of helical and electrical heating tube heat exchangers in vacuum freeze-drying plant. *International Communications in Heat and Mass Transfer,* 58, 111–117.
21. Chen, X. D. & Sun, D-W. (2012). Modeling thermal processing using computational fluid dynamics (CFD). Ed. Sun, D-W. *Thermal Food Processing New Technologies and Quality Issues*, CRC Press, 131-151.
22. Chen, X. D. & Xie, G. Z., (1997). Fingerprints of the drying behavior of particulate or thin layer food materials established using a reaction engineering model. *Transactions of Institution of Chemical Engineers, Part C: Food and Bioproducts Processing,* 75, 213–222.
23. Chen, X. D. (2008). The basic reaction engineering approach to modeling air-drying of small droplets or thin-layer materials. *Drying Technology,* 26(6), 627-639.
24. Chen, Z., Wu, W., & Agarwal, P. K. (2000). Steam drying of coal part 1. Modeling the behavior of a single particle. *Fuel, 79*(8), 961-974.

25. Chiesa M., Mathiesen V., Melheim J. A., & Halvorsen B. (2005). Numerical simulation of particulate flow by the Eulerian–Lagrangian and the Eulerian–Eulerian approach with application to a fluidized bed. *Computer and Chemical Engineering,* 29, 291–304.
26. Cloutier, A., Fortin, Y., & Dhatt, G. (1992). A wood drying finite element model based on the water potential concept. *Drying technology,* 10(5), 1151-1181.
27. Crowe, C.T. (1991). The state-of-the-art in the numerical models for dispersed phase flows, in: Matsui, G., Serizawa, A., Tsuji, Y. (Eds.), Proceedings of the International Conference on Multiphase Flows,'91-Tsukuba, Tsukuba, Japan 3, 49-60.
28. Cunningham, M.J. (1992). Effective penetration depth and effective resistance in moisture transfer. *Building and Enviromnent,* 27(3), 379-386.
29. Curcio S. & Aversa, M. (2010). Transport phenomena and shrinkage modeling during convective drying of vegetables. Excerpt from the proceedings of the COMSOL conference 2009, Oct 8-10, Boston, MA, USA.
30. Curcio S., Aversa M., Calabro V., & Iorio G. (2008). Simulation of food drying: FEM analysis and experimental validation. *Journal of Food Engineering,* 87, 541-53.
31. Da-Silva, W. P., e-Silva, C. M. D. P. S., De-Sousa, J. A. R., & Farias, V. S. O. (2013). Empiirical and diffusion models to describe water transport into chickpea (*Cicer arietinum L.*). *International Journal of Food Science and Technology*, 48, 267-273.
32. Datta, A. K. (2007a). Porous media approaches to studying simultaneous heat and mass transfer in food processes. I: Problem formulations. *Journal of Food Engineering*, 80(1), 80-95.
33. Datta, A.K. (2007b). Porous media approaches to studying simultaneous heat and mass transfer in food processes. II: Property data and representative results. *Journal of Food Engineering*, 80(1), 96-110. doi.org/10.1016/j.jfoodeng.2006.05.012
34. De-Bonis M. V. & Ruocco, G. (2012). Computational transport phenomena in bioprocessing with the approach of the optimized source term in the governing equations. *Heat Mass Transfer,* 48, 1485-1493. Doi.org/10.1007/s00231-012-0992-z.
35. De-Bonis, M.V. & Ruocco, G. (2007). Modeling local heat and mass transfer in food slabs due to air jet impingement. *Journal of Food Engineering,* 78, 230-237.

36. Deen, N. G., Annaland, M. V. S., Van-der-Hoef, M. A., & Kuipers, J. A. M. (2007). Review of discrete particle modeling of fluidized beds. *Chemical Engineering Science,* 62, 28 – 44.
37. Defraeye, T. (2014). Advanced computational modeling for drying processes- A review. *Applied Energy,* 131, 323-344.
38. Defraeye, T., B. Blocken, & J. Carmeliet. (2011). Convective heat transfer coefficients for exterior building surfaces: Existing correlations and CFD modeling. *Energy Conversion Manage,* 52(1), 512–522.
39. Defraeye, T., B. Blocken, & J. Carmeliet. (2012a). Analysis of convective heat and mass transfer coefficients for convective drying of a porous flat plate by conjugate modeling. *International Journal of Heat Mass Transfer*, 55,112–124.
40. Defraeye, T., Herremans, E., Verboven, P., Carmeliet J., & Nicolai, B. (2012b). Convective heat and mass exchange at surfaces of horticultural products: A microscale CFD modeling approach. *Agricultural and Forest Meteorology,* 162– 163, 71– 84.
41. Dick, E. (2009). Introduction to finite element methods in computational fluid dynamics. In: Wendt, J. F. ed. *Computational Fluid Dynamics*. Springer, 235-274.
42. Dincer, I. & Sahin, A. Z. 2004. A new model for thermodynamic analysis of a drying process. *International Journal of Heat and Mass Transfer* 47, 645-652.
43. Dixon, A. G., Taskin, M. E., Nijemeisland, M., & Stitt, E. H., (2011). Systematic mesh development for 3D CFD simulation of fixed beds: single sphere study. *Computer and Chemical Engineering,* 35(7), 1171–1185.
44. Ducept, F., Sionneau, M., & Vasseur, J. (2002). Superheated steam dryer: simulations and experiments on product drying. Chemical Engineering Journal 86, 75–83.
45. Egorov, Y., Menter, F. R., Lechner, R., & Cokliat, D. (2010). The scale-adaptive simulation method for unsteady turbulent flow predictions. Part 2: application to complex flows, *Turbulence and Combustion*, 85(1), 139-165.
46. El-Behery, S. M., El-Askary, W. A., Hamed, M. H., & Ibrahim, K. A. (2013). Eulerian–Lagrangian Simulation and Experimental Validation of Pneumatic Conveying Dryer. Drying Technology, 31:12, 1374-1387

47. ElGamal, R., Ronsse, F., Radwan, S. M. & Pieters, J. G. (2014). Coupling CFD and diffusion models for analyzing the convective drying behavior of a single rice kernel. *Drying Technology,* 32(3), 311-320.
48. Erbay, Z. & Icier, F. (2010). A review of thin layer drying of foods: theory, modeling, and experimental results. *Critical Reviews in Food Science and Nutrition*, 50(5), 441-464.
49. Erriguible, A., Bernada, P., Couture, F., & Roques, M. (2005). Modeling of heat and mass transfer at the boundary between a porous medium and its surroundings. *Drying Technology,* 23(3), 455-472.
50. Erriguible, A., Bernada, P., Couture, F., & Roques, M. (2006). Simulation of Superheated Steam Drying from Coupling Models. *Drying Technology,* 24, 941–951.
51. Ertekin, C. & Firat, M. Z. (2017). A comprehensive review of thin-layer drying models used in agricultural products. *Critical reviews in Food Science and Nutrition*, 57(4), 701-717.
52. Farid, M. (2003). A New Approach to Modeling of Single Droplet Drying. *Chemical Engineering Science*, 58(13), 2985–2993.
53. Feng, H., Yin, Y., & Tang, J. (2012). Microwave Drying of Food and Agricultural Materials: Basics and Heat and Mass Transfer Modeling. *Food Engineering Reviews,* 4, 89–106.
54. Ferziger, J. F. & Peric, M. (2002). *Computational methods for fluid dynamics*. Third edition. Springers publications. New York.
55. Fletcher D. F. & Langrish T. A. G. (2009). Scale-adaptive simulation (SAS) modeling of a pilot –scale spray dryer. *Chemical Engineering Research and Design,* 87(10), 1371-1378.
56. Fletcher D. F., Guo B., Harvie D. J. E., Langrish T. A. G., Nijdam J. J., & Williams J. (2006). What is important in the simulation of spray dryer performance and how do current CFD models perform? *Applied Mathematical Modeling,* 30, 1281–1292.
57. Frank, T., Jain, S., Matyushenko, A. A., & Garbaruk, A. V. (2012). The OECD/NEA MATIS-H benchmark – CFD analysis of water flow through a 5x5 rod bundle with spacer grids using ANSYS FLUENT and ANSYS CFX, Conference on experimental validation and application of CFD and CMFD Codes in Nuclear Reactor Technology, OECD/NEA and IAEA Workshop, 10-12 September 2012, Daejeon, South Korea.

58. Freire, J. T., Freire, F. B., Ferreira, M. C., & Nascimento, B. S. (2012). A Hybrid Lumped Parameter/Neural Network Model for Spouted Bed Drying of Pastes with Inert Particles. *Drying Technology,* 30(11-12), 1342-1353.
59. Frydman, A., Vasseur, J., Moureh, J., Sionneau, M., & Tharrault, P. (1998). Comparison of superheated steam and air operated spray dryers using computational fluid dynamics. *Drying Technology*, 16(7), 1305-1338.
60. Ganguly, A., Alexeenko, A. A., Schultz, S. G., & Kim, S. G. (2013). Freeze-drying simulation framework coupling product attributes and equipment capability: Toward accelerating process by equipment modifications. *European Journal of Pharmaceutics and Biopharmaceutics,* 85, 223–235. doi.org/10.1016/j.ejpb.2013.05.013.
61. Gao, X., Wang, J., Wang, S., & Li, Z. (2016). Modeling of drying kinetics of green peas by reaction engineering approach. *Drying Technology,* 34(4), 437-442.
62. Garavand, A. T., Rafiee, S., and Keyhani, A. (2011). Study on effective moisture diffusivity, activation energy abd mathematical modeling of thin layer drying kinetics of bell pepper. *Australian Journal of Crop Science* 5(2): 128-131.
63. Ghani, J. A. & Farid, M. M. (2010). Computational fluid dynamics analysis of retort thermal sterilization in pouches. Ed. Farid, M.M. *Modeling of Food Processing*, CRC press, 181-201.
64. Ghani, J. A., Supnick, R., & Rooney, P. (1991). The Experience of Flow in Computer-Mediated and in Face-To-Face Groups. *Proceedings of the Twelfth International Conference on Information Systems*, New York, NY.
65. Ghazanfari, A., Emami, S., Tabil, L. G., & Panigrahi, S. (2006). Thin-Layer Drying of Flax Fiber: II. Modeling Drying Process Using Semi-Theoretical and Empirical Models. *Drying Technology,* 24(12), 1637-1642.
66. Gimbun, J., Muhammad, N. I. S., Law, W. P. (2015). Unsteady RANS and detached eddy simulation of the multiphase flow in a co-current spray drying. *Chinese Journal of Chemical Engineering*, 23, 1421-1428.
67. Gondret, P., Lance, M., & Petit, L. (2002). Bouncing motion of spherical particles in fluid. *Physics of Fluids,* 14(2), 643.
68. Grace, J. R. & Taghipour, F., (2004). Verification and validation of CFD models and dynamic similarity for fluidized beds. *Powder Technology,* 139, 99–110.

69. Halder, A. & Datta, A. K. (2012). Surface heat and mass transfer coefficients for multiphase porous media transport models with rapid evaporation. *Food and Bioproducts Processing* 90(3), 475–490.
70. Hall, C. W. (1987). The evolution and utilization of mathematical models for drying. *Mathematical modeling,* 8, 806-812.
71. Hall, C.W. (1975). Drying of Farm Crops; AVI Publishing Co.: Westport, CT, 1975. 17.
72. Hamawand, I. (2013). Drying Steps under Superheated Steam: A Review and Modeling. *Energy and Environment Research*, 3(2), 107-125.
73. Hamzehei, M. (2011). CFD modeling and simulation of hydrodynamics in a fluidized bed dryer with experimental validation. *International Scholarly Research Network Mechanical Engineering* 2011, 9. doi:10.5402/2011/131087.
74. Hashimoto, A., S. Stenstrom, & T. Kameoka. (2003). Simulation of convective drying of wet porous materials. *Drying Technology,* 21 (8), 1411-1431
75. Heldman, D. R. & Lund, D. B. (2007). *Handbook of Food Engineering*. CRC press.
76. Hlawitschka, M. W., Attarakih, M. M., Alzyod, S. S., & Bart, H-J. (2016). CFD based extraction column design-chances and challenges. *Chinese Journal of Chemical Engineering*, 24(2), 259-263.
77. Hoffmann, T.,Hailu Bedane, A., Peglow, M., Tsotsas, E., & Jacob, M. (2011). Particle–gas mass transfer in a spouted bed with adjustable air inlet. *Drying Technology,* 29(3), 257-265.
78. Honarvar, B. and Mowla, D. (2012). Theoretical and experimental drying of a cylindrical sample by applying hot air and infrared radiation in an inert medium fluidized bed. *Brazilian Journal of Chemical Engineering*, 29(2), 231-242.
79. Hosseini, S. H., Ahmadi, G., Rahimi, R., Zivdar, M., & Esfahany, M. N. (2010). CFD studies of solids hold-up distribution and circulation patterns in gas–solid fluidized beds. *Powder Technology,* 200, 202–215.
80. Hosseinizadeh, S. F., Darzi, A. A. R., & Tan, F. L. (2012). Numerical Investigations of Unconstrained Melting of Nano-Enhanced Phase Change Material (NEPCM) Inside a Spherical Container. *International Journal of Thermal Science,* 51, 77-83.

81. Huang, L., Kumar, K., & Mujumdar, A. S. (2003). A parametric study of the gas flow pattern and drying performance of co-current spray- dryer: results of a computational fluid dynamics study. *Drying Technology,* 21(6), 957-978.
82. Jamaleddine T. J. & Ray, M. B. (2010). Application of Computational Fluid Dynamics for Simulation of Drying Processes: A Review. *Drying Technology,* 28, 120–154
83. Jamaleddine, T. K., & Ray, M. B. (2011). Numerical simulation of pneumatic and cyclonic dryers using computational fluid dynamics. *Mass Transfer in Chemical Engineering Processes,* 5, 85-110.
84. Jang, J. & Arastoopour, H. (2014). CFD simulation of a pharmaceutical bubbling bed drying process at three different scales. *Powder Technology,* 263, 14–25.
85. Jaskulski, M., Wawrzyniak, P., & Zbiciński, I. (2015). CFD model of particle agglomeration in spray drying. *Drying Technology,* 33(15-16), 1971-1980.
86. Jiang, Y., Xu, P., Mujumdar, A. S., Qiu, S., & Jiang, Z. (2012). A Numerical Study on the Convective Heat Transfer Characteristics of Pulsed Impingement Drying. *Drying Technology,* 30(10), 1056-1061.
87. Jin, G., Zhang, M., Fang, Z., Cui, Z., & Song, C. (2015). Numerical Investigation on Effect of Food Particle Mass on Spout Elevation of a Gas–Particle Spout Fluidized Bed in a Microwave–Vacuum Dryer. *Drying Technology,* 33(5), 591-604.
88. Jin, Y. & Chen, X. D. (2010). A fundamental model of particle deposition incorporated in CFD simulation of an industrial milk spray dryer. *Drying Technology,* 28(8), 960-971.
89. Jin, Y. & Chen, Y. Z. (2009). Numerical Study of the Drying Process of Different Sized Particles in an Industrial-Scale Spray Dryer. *Drying Technology*, 27, 371–381.
90. Johansson, K., Wan- Wachem, B. G. M., & Almstedt, A. E. (2006). Experimental validation of CFD models for fluidized beds: influence of particle stress models, gas phase compressibility and air inflow models. *Chemical Engineering Science,* 61(5), 1705–1717.
91. Johnson, P., Cenkowski, S., & Paliwal, J. 2013. Superheated steam drying characteristics of single cylindrical compacts produced from wet distillers spent grain. *The Canadian Society of Bioengineering* Paper No. CSBE13-11. Written for presentation at CSBE 2013 annual conference, Saskatoon, Saskatchewan, 7-10 July 2013.

92. Jongsma, F. J., Innings, F., Olsson, M., & Carlsson, F. (2013). Large eddy simulation of unsteady turbulent flow in a semi-industrial size spray dryer. *Dairy Science and Technology,* 93, 373–386.

93. Jubaer, H., Afshar, S., Xiao, J., Chen, X. D., Selomulya, C., & Woo, M. W. (2017): On the importance of droplet shrinkage in CFD-modeling of spray drying, Drying Technology, DOI: 10.1080/07373937.2017.1349791.

94. Jurumenha, D. S. & Sphaier, L. A. (2011). Suitability analysis of lumped-capacitance formulations for adsorbed gas storage. *Applied Thermal Engineering,* 31(14), 2458-2463.

95. Katekawa, M. E. & Silva M. A. (2006). A review of drying models including shrinkage effects. *Drying Technology,* 24, 5–20.

96. Kaushal, P. and Sharma, H. K. (2012). Convective dehydration kinetics of noodles prepared from taro (*Colacasia esculenta*), rice (*Oryza sativa*) and pigeonpea (*Cajanus cajan*) flours. *Agricultural Engineering International: CIGR Journal*, 15(4), 202-212.

97. Kaya, A., Aydin, O., & Dincer, I. (2006). Numerical modeling of heat and mass transfer during force convection drying of rectangular moist objects. *Journal of Food Engineering*, 49, 3094–3103.

98. Kaya, A., Aydin, O., & Dincer, I. (2007). Numerical modeling of forced convection drying of cylindrical moist objects, *Numerical Heat Transfer,* A 51, 843–854.

99. Kaya, A., Aydin, O., & Dincer, I. (2008). Heat and mass transfer modeling of recirculating flows during air drying of moist objects for various dryer configurations. *Numerical Heat Transfer,* A 53, 18–34.

100. Keshani, S., Montazeri, M. H., Daud, W. R. W., & Nourouzi, M. M. (2015). CFD modeling of air flow on wall deposition in different spray dryer geometries. *Drying Technology,* 33(7), 784-795.

101. Kittiworrawatt, S., & Devahastin, S. (2009). Improvement of a mathematical model for low-pressure superheated steam drying of a biomaterial. *Chemical Engineering Science,* 64(11), 2644 – 2650. doi.org/10.1016/j.ces.2009.02.036.

102. Kondjoyan, A., (2006). A review on surface heat and mass transfer coefficients during air chilling and storage of food products. *International Journal of Refrigeration,* 29(6), 863–875.

103. Kopyt, P. & Gwarek, W. 2004. A comparison of commercial CFD software capable of coupling to external electromagnetic software for modeling of microwave heating process. In *Proceedings of the 6th seminar in computer modeling and microwave power engineering*, Austin, Texas, USA, 33-39.

104. Krawczyk, P. (2016). Numerical modeling of simultaneous heat and mass transfer during sewage sludge drying in solar dryer. In: IX International Conference on Computational Heat and Mass Transfer, ICCHMT 2016. *Procedia Engineering*, 157, 230-237.

105. Kulasiri, D. & Woodhead, I. (2005). On modeling the drying of porous materials: analytical solutions to coupled partial differential equations governing heat and moisture transfer. *Mathematical Problems in Engineering,* 3, 275-291.

106. Kunkelmann, C. & Stephan, P. (2009). CFD Simulation of Boiling Flows Using the Volume of-Fluid Method within OpenFOAM. *Numerical Heat Transfer, Part A: Applications*, 56(8), 631-646. doi.org/10.1080/10407780903423908.

107. Kuriakose, R. & Anandaramakrishnan C. (2010). Computational fluid dynamics (CFD) applications in spray drying of food products. *Trends in Food Science and Technology,* 21, 657-683.

108. Kurnia, J. C., Sasmito, A. P., Tong, W., & Mujumdar, A. S. (2013). Energy-efficient thermal drying using impinging-jets with time-varying heat input – A computational study. *Journal of Food Engineering,* 114(2), 269–277.

109. Lang, H. & Todte, M. (2011). Core drying simulation and validation. AFS proceedings 2011, American Foundry Society, Schaumburg, IL USA. Paper 11-028.

110. Langrish T.A.G. & Fletcher D.F. (2001). Spray drying of food ingredients and applications of CFD in spray drying. *Chemical Engineering and Processing*,40,345-54.

111. Launder, B. E. & Spalding, D. B. (1974). The numerical computation of turbulence flows. *Computer methods in applied mechanics and engineering,* 3, 269-289.

112. Lewis, W.K. (1921). The rate of drying of solid materials. *Journal of Industrial and Engineering Chemistry,* 13, 427–432.

113. Li, S., Stawczyk, J., & Zbicinski, I. (2007). CFD Model of Apple Atmospheric Freeze Drying at Low Temperature. *Drying Technology,* 25(7-8), 1331-1339.

114. Li, M. & Duncan, S. (2008). Dynamic Model Analysis of Batch Fluidized Bed Dryers. *Particle and Particle Systems Characterization,* 25(4), 328–344.

115. Li, T., Gopalakrishnan, P., Garg, R., & Shahnam, M. (2012a). CFD-DEM study of effect of bed thickness for bubbling fluidized beds. *Particuology,* 10, 532-541.

116. Li, Z., Kessel, J., Grunewald, G., & Kind, M. (2012b). CFD Simulation on Drying and Dust Integration in Fluidized Bed Spray Granulation. *Drying Technology,* 30(10), 1088-1098.

117. Li, Z., Kessel, J., Grunewald, G., & Kind, M. (2013). Coupled CFD-PBE Simulation of Nucleation in Fluidized Bed Spray Granulation. *Drying Technology,* 31(15), 1888-1896.

118. Liewkongsataporn, W., Patterson, T., & Ahrens, F. (2008). Pulsating Jet Impingement Heat Transfer Enhancement. *Drying Technology,* 26(4), 433-442.

119. Ljung, A. L., Lundstrom, T. S, Marjavaara, B. D., & Tano, K. (2011). Convective drying of an individual iron ore pellet – Analysis with CFD. *International Journal of Heat and Mass Transfer,* 54, 3882–3890.

120. Lo, S. (2005). Application of computational fluid dynamics to spray drying. *Le Lait*, INRA Editions, 85 (4-5), 353-359.

121. Looi, A. Y., Golonka, K., & Rhodes, M. (2002). Drying kinetics of single porous particles in superheated steam under pressure. Chemical Engineering Journal, 87, 329-338. doi.org/10.1016/S1385-8947(01)00244-3.

122. Lu, T., Jiang, P., & Shen, S. (2005). Numerical and experimental investigation of convective drying in unsaturated porous media with bound water. *Heat Mass Transfer*, 41, 1103–1111.

123. Massah, H. & Oshinowo, L. (2000). Advanced gas-solid multiphase flow models offer significant process improvements. Journal Articles by Fluent Software Users 2000. www.fluent.com/solutions/articles/ja112.pdf.

124. Meng, W. W. (2016). Computational fluid dynamics simulation of spray dryers. CRC press. Boca Raton.

125. Menter, F. R. (2009). Review of the shear-stress transport turbulence model experience from an industrial perspective. *International Journal of Computational Fluid Dynamics,* 23(4), 305-316

126. Mezhericher M., Levy, A., & Borde, I. (2010). Theoretical Models of Single Droplet Drying Kinetics: A Review. *Drying Technology*, 28, 278–293.

127. Mezhericher, M., Levy, A., & Borde, I. (2008). Droplet–Droplet Interactions in Spray Drying by Using 2D Computational Fluid Dynamics. *Drying Technology,* 26, 265–282.

128. Mezhericher, M., Levy, A., & Borde, I. (2015). Multi-Scale Multiphase Modeling of Transport Phenomena in Spray-Drying Processes. *Drying Technology*, 33:1, 2-23.

129. Mirade P.S. & Daudin, J.D. (2006). Computational fluid dynamics prediction and validation of gas circulation in a cheese ripening room. *International Dairy Journal,* 16,920-30.

130. Muhammad, M. D., Badr, O., & Yeung, H. (2015). Validation of a CFD Melting and Solidification Model for Phase Change in Vertical Cylinders. *Numerical Heat Transfer, Part A: Applications*, 68(5), 501-511.

131. Mujumdar, A. S., & Wu Z. H. (2008). Thermal drying technologies-Cost effective innovation aided by mathematical modeling approach. *Drying Technology,* 26(1), 145-153.

132. Murugesan, K., Suresh, H. N., Seetharamu, K. N., Aswatha Narayana, P. A., & Sundararajan, T. (2001). A theoretical model of brick drying as a conjugate problem. *International Journal of Heat and Mass Transfer,* 44, 4075–4086.

133. Nasrallah, B.S. & Perre, P. (1988). Detailed study of a model of heat and mass transfer during convective drying of porous media. *International Journal of Heat and Mass Transfer,* 31 (5), 957-967. doi.org/10.1016/0017-9310(88)90084-1.

134. Niamnuy, C., Devahastin, S., Soponronnarit, S., & Raghavan, G. S. V. (2008). Modeling coupled transport phenomena and mechanical deformation of shrimp during drying in a jet spouted bed dryer. *Chemical Engineering Science,* 63, 5503-5512.

135. Nicolai, B. M., Verboven, P., & Scheerlinck, N. (2001). Chaper 4: The modeling of heat and mass transfer. *Food process Modeling. Ed. by Tijskens, L. M. M., Hertog, M. L. A. T. M., and Nicolai, B. M. CRC press. Woodhead Publishing Ltd. England.*

136. Nijdam, J. J., Guo, B., Fletcher, D. F., & Langrish, T. A. G. (2006). Validation of the Lagrangian Approach for Predicting Turbulent Dispersion and Evaporation of Droplets within a Spray. *Drying Technology,* 24, 1373-1379.

137. Nishiyama, Y., Cao, W. Y., & Li, B. (2006). Grain intermittent drying characteristic analyzed by a simplified model. *Journal of Food Engineering,* 76, 272–279.

138. Norton, T. & Sun D. W. (2007). An overview of CFD applications in the food industry, chapter 1. In Da-Wen Sun (ed) Computational fluid dynamics in food processing. CRC Press, Boca Raton, FL, 1–43.

139. Norton, T. & Sun, D. W. (2006). Computational fluid dynamics (CFD)-an effective design and analysis tool for the food industry: a review. *Trends in Food science and Technology,* 17(11), 600-620.

140. Norton, T., Sun, D.W., Grant, J., Fallon, R., & Dodd, V. (2007). Applications of computational fluid dynamics (CFD) in the modeling and design of ventilation systems in the agricultural industry: A review. *Bioresource Technology,* 98(12), 2386-2414.

141. Oakley, D. E. (2004). Spray Dryer Modeling in Theory and Practice. *Drying Technology,* 22(6), 1371-1402.

142. Oliveira, L. S. & Haghighi, K. (1995). Conjugate/adaptive finite element analysis of convective drying problem. In: proceedings of the Ninth International Conference on Numerical Methods in Thermal Problems, 9, 80-88.

143. Omolola, A. O., Jideani, A. I. O., & Kapila, P. F. (2014). Modeling microwave drying kinetics and moisture diffusivity of Mabonde banana variety. *International Journal of Agricultural and Biological Engineering*, 7(6), 107-113.

144. Onwude, D. I., Hashim, N., Janius, R. B., Nawi, N. M., & Khalini, H. (2016). Modeling the thin-layer drying of fruits and vegetables: a review. *Comprehensive Reviews in Food Science and Food Safety*, 15, 599-618.

145. Page, G. E. (1949). Factors influencing the maximum rates of air drying shelled corn in thin layers. M.S. thesis. Department of Mechanical Engineering, Purdue University: West Lafayette, IL, 1949.

146. Pai, M. G. & Subramaniam, S. (2006). Modeling interphase turbulent kinetic energy transfer in Lagrangian-Eulerian sprays computations, Atom Sprays. *Journal of Fluid Mechanics,* 16 (7), 807–826.

147. Pai, M. G. & Subramaniam, S. (2009). A comprehensive probability density function formalism for multiphase flows. *Journal of Fluid Mechanics,* 628, 181–228.

148. Pakowski, Z. & Adamski, R. (2011). On prediction of the drying rate in superheated steam drying process. *Drying Technology,* 29, 1492–1498.

149. Panyawong, S. & Devahastin, S. (2007). Determination of deformation of a food product undergoing different drying methods and conditions via evolution of a shape factor. *Journal of Food Engineering,* 78, 151–161.

150. Patel, K. C., Chen, X. D., Lin, S. X. Q., & Adhikari, B. A. (2009). Composite Reaction Engineering Approach to Drying of Aqueous Droplets Containing Sucrose, Maltodextrin (DE6) and their Mixtures. *American Institute of Chemical Engineers Journal*, 55(1), 217–231.

151. Perre, P. (2010). Multiscale Modeling of Drying as a Powerful Extension of the Macroscopic Approach: Application to Solid Wood and Biomass Processing. *Drying Technology,* 28(8), 944-959. doi.org/10.1080/07373937.2010.497079.

152. Petitti, M., Barresi, A. A., & Marchisio, D. L. (2013). CFD modeling of condensers for freeze-drying processes. *Sadhana: Academy Proceedings in Engineering Sciences,* 38(6), 1219-1239.

153. Pujol, A., Debenest, G., Pommier, S., Quintard, M., & Chenu, D. (2011). Modeling Composting Processes with Local Equilibrium and Local Non-Equilibrium Approaches for Water Exchange Terms. *Drying Technology*, 29(16), 1941-1953.

154. Putranto, A. & Chen, X. D. (2015). An assessment on modeling drying processes: Equilibrium multiphase model and the spatial reaction engineering approach (S-REA). *Chemical Engineering Research and Design*, 94, 660–672.

155. Rajika, J. K. A. T. & Narayana, M. (2016). Modeling and simulation of wood chip combustion in a hot air generator system. *Springerplus* 5: 1166-1185

156. Ramachandran, R. P., Akbarzadeh, M. Paliwal, J., & Cenkowski, S. (2017a). Three-dimensional CFD modeling of superheated steam drying of a single distillers' spent grain pellet. *Journal of Food Engineering*, 212,121-135.

157. Ramachandran, R. P., Bourassa, J., Paliwal, J., & Cenkowski, S. (2017b). Effect of temperature and velocity of superheated steam on initial condensation of distillers' spent grain pellets during drying. *Drying Technology*, 35(2), 182-192.

158. Ramachandran, R. P., Paliwal, J., & Cenkowski, S. (2017c), Thermo-physical properties of distillers' spent grain pellets at different moisture content and condensed distillers' solubles concentration. *Food and Bioprocess Technology*, 10, 175-185.

159. Ranjbaran, M. & Zare, D. (2012). CFD Modeling of Microwave-Assisted Fluidized Bed Drying of Moist Particles Using Two-Fluid Model. *Drying Technology,* 30(4), 362-376.

160. Ranjbaran, M., Emadi, B., & Zare, D. (2014). CFD Simulation of Deep-Bed Paddy Drying Process and Performance. *Drying Technology,* 32(8), 919-934.

161. Rayaguru, K. & Routray, W. (2010). Effect of drying conditions on drying kinetics and quality of aromatic Pandanus amaryllifolius leaves. *Journal of Food Science and Technology,* 47(6), 668-673.

162. Richardson, L. F. (1910). The approximate arithmetical solution by finite differences of physical problems involving differential equations, with an application to the stresses in a masonry dam. *Philosophical Transactions of the Royal Society of London* . 210, 307-357.

163. Rigit, A. R. H. & Low, P. T. K. (2010). Heat and Mass Transfer in a Solar Dryer with Biomass Backup Burner. International Journal of Mechanical, Aerospace, Industrial, Mechatronic and Manufacturing Engineering, 4(2), 133-136.

164. Rizzi, Jr., A. C., Passos, M. L., & Freire, J. T. (2009). Modeling and simulating the drying of grass seeds (*Brachiaria brizantha*) in fluidized bed: evaluation of heat transfer coefficients. *Brazilian Journal of Chemical Engineering*, 26(3), 545-554.

165. Sabarez H. T. (2012). Computational modeling of the transport phenomena occurring during convective drying of prunes. *Journal of Food Engineering,* 111(2), 279-288.

166. Sae-Heng, S., Swasdisevi, T., & Amornkitbamrung, M. (2011). Investigation of Temperature Distribution and Heat Transfer in Fluidized Bed Using a Combined CFD-DEM Model. *Drying Technology,* 29(6), 697-708.

167. Salagnac, P., Glouannec, P., & Lecharpentier, D. (2004). Numerical modeling of heat and mass transfer in porous medium during combined hot air, infrared and microwave heating. *International Journal of Heat and Mass Transfer,* 47, 4479-4489.

168. Saravacos, G. & Kostaropoulos, A. E. (2016) Handbook of food processing equipment. Food engineering series. 2nd ed. Springer.

169. Scott, G.M. (1994). Computational fluid dynamics for the food industry. *Food Technology International Europe*, 49–51.

170. Shahari, N. & Hibberd, S. (2014). Modeling of Drying Tropical Fruits using Multiphase Model. World Scientific and Engineering Academy and Society (*WSEAS) Transactions on Mathematics,* 13, 840-851.

171. Shahari, N., Hussein, S. M., Nursabrina, M., & Hibberd, S. (2014). Mathematical modeling of cucumber (cucumis sativus) drying. *AIP Conference Proceedings,* 1605, 307. doi: 10.1063/1.4887607

172. Shang, J. S. (2004). Three decades of accomplishments in computational fluid dynamics. *Progress in Aerospace Sciences*, 40, 173-197.

173. Shibata, H. & Ide, M. (2001) Combined superheated steam and microwave drying of sintered glass beads: drying rate curves, *Drying Technology*, 19(8), 2063-2079.

174. Shokouhmand H., Abdollahi V., Hosseini S., & Vahidkhah K.(2011). Performance optimization of a brick dryer using porous simulation approach. *Drying Technology,*29,360–70.

175. Shukla, A., Singh A. K., & Singh, P. (2011). A comparative study of finite volume method and finite difference method for convective-diffusion problem. *American Journal of Computational and Applied Mathematics*, 1(2), 67-73.

176. Singh, P. P., Cushman, J. H., & Maier, D. E. (2003a). Three scale thermomechanical theory for swelling biopolymeric systems. *Chemical Engineering Science,* 58, 4017–4035.

177. Singh, P. P., Cushman, J.H., & Maier, D. E. (2003b). Multiscale fluid transport theory for swelling biopolymers. *Chemical Engineering Science,* 58, 2409–2419.

178. Smolka, J., Nowak A. J., & Rybarz D. (2010). Improved 3-D temperature uniformity in a laboratory drying oven based on experimentally validated CFD computations. *Journal of Food Engineering,* 97,373–83.

179. St. George, S. D. & Cenkowski, S. (2009). Modeling of thin-layer drying on an inert sphere. *Drying Technology*, 27(6), 770-781.

180. Stone, L. E., Wypych, P. W., Hastie, D. B., & Zigan, S. (2016). CFD-DEM modeling of powder flows and dust generation mechanisms - A review. ICBMH 2016 - 12th International Conference on Bulk Materials Storage, Handling and Transportation, Proceedings, Barton, Australia: Engineers Australia, 417-426.

181. Suvarnakuta, P. Devahastin, S., & Mujumdar. A. S. (2007). A mathematical model for low pressure superheated steam drying of biomaterial. *Chemical Engineering and Processing*, 46(7), 675-683. doi.org/10.1016/j.cep.2006.09.002.

182. Szafran, R. G. & Kmiec, A. (2004). CFD modeling of heat and mass transfer in a spouted bed dryer. *Industrial and engineering chemistry research* 43, 1113-1124.

183. Taghinia, J., Rahman, M. M., & Siikonen, T. (2016). CFD study of turbulent jet impingement on curved surface. *Chinese Journal of Chemical Engineering,* 24, 588–596.

184. Taghipour, F., Ellis, N., & Wong, C. (2005). Experimental and computational study of gas–solid fluidized bed hydrodynamics. *Chemical Engineering Science,* 60, 6857 – 6867.

185. Tatemoto, Y. & T. Sawada. (2012). Numerical Analysis of Drying Characteristics of Wet Material Immersed in Fluidized Bed of Inert Particles. *Drying Technology,* 30(9), 979-988.

186. Thompson, T. L., Peart, R. M., & Foster, G. H. (1968). Mathematical simulation of corn drying: a new model. *Transactions of ASAE,* 11(4), 582-86

187. Thorvaldsson, K. & Janestad, H. (1999). A model for simulteneous heat, water and vapour diffusion. *Journal of Food Engineering*, 40,167–172.

188. Trujillo, F. J., Lovatt, S. J., Harris, M. B., Willix, J., & Pham, Q. T. (2003). CFD modeling of the heat and mass transfer process during the evaporation of water from a circular cylinder. Third International Conference on CFD in the Minerals and Process Industries, CSIRO, Melbourne, Australia 10-12 December 2003.

189. Ullum, T., Sloth, J., Brask, A., & Wahlberg, M. (2010). Predicting Spray Dryer Deposits by CFD and an Empirical Drying Model. *Drying Technology,* 28(5), 723-729.

190. Van Wachem, B., Schouten, J. C., Van den Bleek, C.M., Krishna, R., & Sinclair, J. L. R. (2001). Comparative analysis of CFD models of dense gas–solid systems. *The American Institute of Chemical Engineers Journal* 47 (5), 1035–1051.

191. Velic, D., Planinic, M., Tomas, S., & Bilic, M. 2004. Influence of airflow velocity on kinetics of convection apple drying. *Journal of Food Engineering* 64, 97–102.

192. Verboven P, Nicolai B, Scheerlinck N, & De-Baerdemaeker J. (1997). The local surface heat transfer coefficient in thermal food process calculations: a CFD approach. *Journal of Food Engineering,* 33, 15–35.

193. Versteeg, H.K. & Malalasekera, W. (1995). *An Introduction to Computational Fluid Dynamics: The Finite Volume Method*. Addison-Wesley, Longman: New York.

194. Vorhauer, N., Metzger, T., & Tsotsas, E. (2010). Empirical macroscopic model for drying of porous media based on pore networks and scaling theory. *Drying Technology,* 28, 991-1000.

195. Wang C. Y. & Singh R. P. (1978a). Use of variable equilibrium moisture content in modeling rice drying. *Transactions of American Society of Agricultural Engineering (ASAE),* 11, 668–672.

196. Wang C. Y. & Singh R. P. (1978b). A single layer drying equation for rough rice. ASAE Paper No. 78–3001, ASAE, St Joseph, MI.

197. Wang, L. & Sun D-W. (2003). Recent developments in numerical modeling of heating and cooling processes in the food industry – a review. *Trends in Food Science and Technology,* 14, 408–23.

198. Wang, N. & Brennan, J. (1992). Effect of water binding on the drying behaviour of potato. In Drying'92, Part B, ed. A. S. Mujumdar. Elsevier, Amsterdam, New York, 1350-1359.

199. Wang, Y. & Yan, L. (2008). CFD studies on biomass thermochemical conversion. *International Journal of Molecular Sciences,* 9, 1108-1130.

200. Wang, Z. & Chen, G. H. (1999). Heat and mass transfer during intensity convection drying. *Chemical Engineering Science,* 54, 3899–3908.

201. Warning, A. D., Arquiza, J. M. R., & Datta, A. S. (2015). A multiphase porous medium transport model with distributed sublimation front to simulate vacuum freeze drying. *Food and Bioproducts processing*, 94, 637–648.

202. Wawrzyniak, P., Podyma, M., Zbicinski, I., Bartczak, Z., & Rabaeva, J. (2012). Modeling of air flow in an industrial countercurrent spray-drying tower. *Drying Technology,* 30, 217–224

203. Wilcox, D. C. (1994). Turbulence Modeling for CFD, DCW Industries, California, USA.

204. Wu, Z. H. & Mujumdar, A. S. (2008). CFD modeling of the gas-particle flow behaviour in spouted beds. *Powder Technology,* 183, 260–272.

205. Xia, B. & Sun, D. W. (2002). Applications of computational fluid dynamics (CFD) in the food industry: a review. *Computers and Electronics in Agriculture,* 34, 5-24

206. Xiao, Z. F., Zhang, F., Wu, N. X., & Liu, X. D. (2013). CFD Modeling and Simulation of Superheated Steam Fluidized Bed Drying Process. *International Federation for Information Processing AICT* 392, 141–149.

207. Xu, P., Sasmito, A. P., Qiu, S., Mujumdar, A. S., Xu, L., & Geng, L. (2016). Heat transfer and entropy generation in air jet impingement on a model rough surface. *International Communications in Heat and Mass Transfer,* 72, 48–56.

208. Yahyaee, A. A., Esmailpour, K., Hosseinalipour, M., & Mujumdar, A. S. (2013). Simulation of Drying Characteristics of Evaporation from a Wet Particle in a Turbulent Pulsed Opposing Jet Contactor. *Drying Technology,* 31(16), 1994-2006.

209. Yamsaengsung, R. & Moreira, R. (2002). Modeling the transport phenomena and structural changes during deep fat frying part ii: Model solution and validation. *Journal of Food Engineering,* 53, 11–25.

210. Yang, C. T. & Atluri, S. N. (1984). An assumed deviatoric stress-pressure-velocity mixed finite element method for unsteady, convective, incompressible viscous flow: Part II: computational studies. *International Journal for Numerical Methods in fluids*, 4, 43-69.

211. Yang, D., Wang, Z., Huang, X., Xiao, Z., & Liu, X. (2011). Numerical Simulation on Superheated Steam Fluidized Bed Drying: I. Model Construction. *Drying Technology,* 29(11), 1325-1331.

212. Yi, T., Dye, J. C., Shircliff, M. E., & Ashrafzadeh, F. (2016). A New Physics-Based Drying Model of Thin Clothes in Air-Vented Clothes Dryers. IEEE/ASME Transactions on Mechatronics, 21(2), 872-878.

213. Yiotis, A. G., Stubos, A. K., Boudouvis, A. G., & Yortsos. Y. C. (2001). A 2D pore-network model of the drying of single component liquids in porous media. *Advances in Water Resources,* 24 (3-4), 439-460

214. Younsi, R., Kocaefe, D., Poncsak, S., Kocaefe, Y., & Gastonguay, L. (2008). CFD modeling and experimental validation of heat and mass transfer in wood poles subjected to high temperatures: a conjugate approach. *Heat Mass Transfer,* 44, 1497–1509.

215. Yunus, Y. M. & Al-Kayiem, H. H. (2013). Simulation of hybrid solar dryer. IOP Conference Series: Earth and Environmental Science, 16, 012143.

216. Zadin, V., Kasemagi, H., Valdna, V., Vigonski, S., Veske, M., & Aabloo, A. (2015). Application of multiphysics and multiscale simulations to optimize industrial wood drying kilns. *Applied Mathematics and Computation,* 267, 465-475.

217. Zhang, Z. & Chen Q. (2007). Comparison of the Eulerian and Lagrangian methods for predicting particle transport in enclosed spaces. *Atmospheric Environment,* 41, 5236–48.

218. Zhang, A., Datta, A. K., & Mukherjee, S. (2005). Transport processes and large deformation during baking of bread. *American Institute of Chemical Engineers Journal,* 51(9), 2569–2580.

219. Zhang, Z. & Kong, N. (2012). Nonequilibrium thermal dynamic modeling of porous medium vacuum drying process. *Mathematical Problems in Engineering,* doi:10.1155/2012/347598.

220. Zhi, T., Zeyuan, C., Jianqin, Z., & Haiwang, L. (2016). Effect of turbulence models on predicting heat transfer to hydrocarbon fuel at supercritical pressure. *Chinese Journal of Aeronautics*, 29(2), 1247-1261. doi.org/10.1016/j.cja.2016.08.007.

221. Zhou, H., Flamant, G., & Gauthier, D. (2004). DEM - LES of coal combustion in a bubbling fluidized bed 1: gas-particle turbulent flow structure. *Chemical Engineering Science,* 59(20), 4193-4203.

222. Zhou, L. (2015). Two-phase turbulence models in Eulerian-Eulerian simulation of gas-particle flows and coal combustion. *Procedia Engineering,* 102, 1677-1696.

223. Zhu H., Dhall A., Mukherjee S., & Datta A. K. (2010). A model for flow and deformation in unsaturated swelling porous media. *Transport in Porous Media,* 84, 335–369.

CHAPTER 3. THERMO-PHYSICAL PROPERTIES OF DSG

This chapter is based on the research paper published by Springer Nature in *Food and Bioprocess Technology* on 6 Oct 2016, available online: www.springer.com/ [doi.org/10.1007/s11947-016-1807-x].

3.1 Abstract

The thermo-physical properties of distillers' spent grain (DSG) pellets are the key input parameters for the heat and mass transfer modelling of the drying process and for the design of the suitable drying and storage systems. The main thermo-physical properties like particle density, thermal conductivity, and specific heat capacity of DSG pellets were determined using standard laboratory methods. The effects of moisture content, percentage of condensed distillers' solubles (also called solubles), and temperature on these selected properties were determined. The average particle density of the DSG pellets with 0, 10, 30, and 50 % solubles was found to be in the range of 898.8–1136.7 kg/m3. It was observed that the particle density of DSG pellets increased with an increase in condensed distillers' soluble concentration and decreased with an increase in moisture content. Thermal conductivity (0.17–0.42 W/(mK)) and specific heat (1.76–3.47 kJ/(kgK)) of the DSG pellets increase linearly with an increase in moisture content, soluble concentration of the sample, and temperature of the drying medium. Three multiple linear regression equations were developed for predicting these properties as a function of moisture content, soluble concentration, and temperature with R2 value ≥0.86.

Keywords: *Distillers' spent grains, Condensed distillers' solubles, Particle density, Thermal conductivity, Specific heat*

3.2 Introduction

As per the annual report of Husky Energy, western Canada's largest producer of ethanol, approximately 260,000 tons of dried distillers' grain with solubles (DDGS) is produced each year, which is about 35-40% of the grain input per annum (Husky Energy 2016). Distillers' spent grain (DSG) is the major byproduct from ethanol plants, corresponding to about 85% of the total byproducts generated (Xiros et al. 2008). It accounts for 10-20% of the total income for ethanol industries when used as animal feed and is also a good source of fiber and protein when utilized in baked human foods(Johnson et al., 2011). Transportation and long-term storage of this wet slurry of DSG, obtained after wet milling method of ethanol production, is highly challenging because of its high initial moisture content (approximately 80% wet basis). The storage and handling of wet DSG could be improved by drying it to safe storage moisture content of 10-12% (Johnson et al. 2014; Bourassa et al. 2015). Hence, wet DSG is centrifuged to separate the coarse grain fraction and the semi-solid fraction called condensed distillers' solubles (CDS) or simply solubles (Stroem et al. 2009; Bourassa et al. 2015). The high amount of cellulose, hemicelluloses, lignin, protein and lipids (Sousa et al. 2007) make this byproduct attractive for added value by drying.

Superheated steam drying, has been proven to be suitable for drying wet DSG due to its superior heat transfer properties when compared to air and elimination of fire hazard during the drying process (Zielinska et al. 2009; Zielinska and Cenkowski 2012; Johnson et al. 2013). Generally, the wet DSG is poured over dry DSG granules and dried using rotary-drums dryers in order to provide greater surface area for heat and mass transfer. In this study, DSG at 25-35% wb moisture content is compacted to form cylindrical pellets. These pellets are then dried using superheated steam with wet DSG poured over them. The compaction process eliminates

mixing with already over-dried DSG granules while developing a substantial contact area with the drying medium and thereby improving the drying process. Various elements of the drying process like constant rate drying, falling rate drying, moisture diffusion, surface water evaporation, etc. can be studied using mathematical modelling of the heat and mass transfer phenomena occurred during drying (Hamawant 2013). Detailed information on the transport phenomena (heat and mass transfer) of drying process can be obtained with the help of advanced computer simulation techniques. Thermo-physical properties like thermal conductivity, specific heat and particle density of samples to be dried are the most important input variables required for validating the mathematical model (Yang et al. 2002; Suvarnakuta et al. 2007) and can be used in computational modelling of superheated steam drying (Erriguible et al. 2006). Also, these properties are essential for optimization of various processing techniques like drying, mixing, storage and handling (Mosqueda et al., 2014). These thermal properties vary with different factors such as moisture content, particle density, and composition of the material (Waszkielis et al. 2013, 2014).

The high heterogeneity of the compacted DSG in terms of particle size and high porosity creates many challenges in the measurement of its thermophysical properties. Johnson et al. (2015) reported that an increase in the percentage of CDS in a mixture of coarse grain fraction of wet DSG and CDS increases the overall strength of a DSG pellet. They reported that the particle size of the CDS being about 56% smaller than that of the coarse grain fraction of wet DSG improved the packing of particles during compaction. They also reported that the CDS contains 48.8% of crude protein and 5.76% of starch whereas the wet DSG contains only 29.4% crude protein and 3.77 % starch. The higher percentage of starch (about 52% more) and protein (65% more) in the CDS, when compared to wet DSG, justifies the lower porosity and

higher particle density (Tumuluru 2010) and strength of the DSG pellets with solubles (Johnson et al. 2014). Thomas et al. (1998) reported that the starch and protein can act as a binding agent in the compaction process. The higher percentage of protein and starch present in the CDS helps to improve the strength and durability of the pellet. The change in composition and density of the pellet due to the addition of different levels of solubles also affects the overall thermal conductivity of the pellet. In addition, the increase in the percentage of condensed solubles causes an increase in the moisture diffusivity during drying (Zielinska & Cenkowski 2012). Unlike hot air drying, superheated steam drying has a distinct phenomenon called initial condensation that occurs in the warming up period of drying. Due to the lower initial temperature of the sample to be dried, the superheated steam coming in contact with the sample is subjected to temporary condensation on the sample surface. This phenomenon of initial condensation is very important in the heat and mass transfer mechanism of superheated steam (SS) drying (Hamawand 2011; Johnson et al. 2013; Hamawand et al. 2014). The condensation stops when the surface temperature of the sample exceeds the saturation steam temperature. The temperature and the heat capacity of the sample influence this local condensation (Iyota et al. 2007). The sensible heat gain occurring during condensation is supplied by the latent heat of condensation of steam (Pakowski and Adamski 2011). The duration of condensation is governed by the temperature rise in the sample, which in turn is influenced by the heat capacity of the sample. Also, some amount of condensed water might be absorbed by the sample causing an increase in the moisture content of the sample and changing its thermo-physical properties (Emami et al. 2007).

Beside the use in heat and mass transfer modelling, these thermo-physical properties are also being utilized for various processing operations like stabilizing, pelletizing, freezing,

thawing, cooking, pasteurization, and sterilization and storage (Nesvadba 1982; Sreenarayanan and Chattopadhyay, 1986; Drouzas et al., 1991). Hence, a complete understanding of the major thermo-physical properties of the DSG sample like particle density, thermal conductivity, and specific heat is important in the heat and mass transfer modelling of the SS drying of DSG pellets. The precision of computational modelling of heat and mass transfer mechanism of superheated steam drying is highly influenced by the accuracy of input parameters of the sample as well as the heat transfer medium and the boundary conditions for energy and mass balance equations (Defraeye 2014). Hence, the main objective of this study is to determine the effect of moisture content and solubles concentration on the important thermo-physical properties of DSG pellets such as thermal conductivity, specific heat, and particle density as affected by different temperatures of heat transfer medium.

3.3 Materials and method

3.3.1 Sample preparation for compacting

The DSG samples used in this study were a mixture of 90% mashed corn and 10% mashed wheat obtained after bioethanol production. The whole stillage was collected from a local distillery, Mohawk Canada Limited (Minnedosa, MB). The whole stillage contained coarse grain fraction, condensed solubles, and water. The wet stillage was kept in a freezer (Eaton Viking, T.eaton company limited, Toronto, Canada) at -15°C in a sealed plastic pail (Poly-propylene pails from Pioneer Plastics) to prevent spoilage from further fermentation. Before sample preparation, a part of the sample was removed from the freezer and allowed to thaw at room temperature. The sample was then mixed thoroughly to ensure uniform thawing. Once thawed, the sample was subjected to centrifugation using a Sorvall General Purpose RC-3

laboratory centrifuge (Thermo Fisher Scientific, Waltham, MA) at 2200 rpm for 10 minutes. Approximately 750 mL of the sample was placed in each of the four centrifuge bowls for separation. The supernatant liquid (thin stillage), top layer thin grain fractions (solubles) and bottom layer of the coarse grain fraction of DSG, were then separated and weighed. Each of the fractions was stored separately in airtight containers (Poly-propylene 5, Pioneer Plastics) which were then stored at -15^{o}C until testing.

3.3.2 Composition and initial moisture content

Ten replicates of the centrifugation trials were conducted to determine the percentage composition of the raw sample in terms of coarse grain fraction, solubles, and thin stillage. The mass of the separated coarse grain fraction, solubles, and thin stillage were recorded for each trial. The percentage composition of each of the fraction with respect to the whole mass was calculated. The moisture content of the coarse grain fraction and the solubles were determined using the air-oven drying method (AACC 2000). Three replicates of each sample (2 g each) were dried in a laboratory oven (Thermo Electron Corporation, Waltham, MA) at 135^{o}C for 2 h (Johnson et al., 2013; 2014). The whole stillage used for the study contained 49.5 ±0.5, 9.5 ±0.5, 40.5 ±0.5% w/w of the coarse grain fraction, solubles, and supernatant liquid, respectively. All the moisture contents were determined in wet basis (%wb). The initial moisture content of the whole stillage was 89.2 ±0.05%. The initial moisture content of coarse grain fraction and solubles after centrifugal separation was 77.8 ±0.08% and 82.9 ±0.1%, respectively.

3.3.3 Compaction of Distillers' spent grain

Different amounts of solubles were added to a known mass of coarse grain fraction of DSG to obtain various desirable compositions of DSG with solubles. Different sets of DSG samples

were prepared with 0, 10, 30, and 50% solubles. A control sample was represented by DSG without any solubles. The moisture content of each mixture was also measured using standard air-oven drying method. Each of these samples with different solubles concentration and coarse grain fraction of DSG was gently mixed using a spatula for about 2 minutes and dried in a laboratory oven at a lower temperature (60 ±5°C). A small amount of mixed sample (about 20 g) capable of producing 4 -5 pellets where only prepared at a time to prevent excessive drying of the sample when stored for longer time. Gentle mixing with the spatula would prevent the heating of the sample. Lower temperature was used for drying the sample to ensure the properties of the samples are not altered as the stickiness of the distillers' spent grains increases with temperature (Stroem et al. 2009). A separate set of samples was then prepared at 25, 35, and 45% moisture content for each of the composition mentioned above. The prepared samples were stored in a freezer at -15°C.

For making the compacted DSG pellets, approximately 4.25 ±0.05 g of thawed raw material at a given moisture content and percent solubles were placed in a cylindrical steel mold with a diameter of 12.2 ±0.01 mm and height of 80 ±0.01 mm. The mold with the sample was then placed on the platform of a universal testing machine (Model 3366 Universal Testing Systems, Instron Corp., Norwood, MA). A cylindrical die with a diameter of 12.08 ±0.01 mm and a length of 83.65 ±0.01 mm was attached to a load cell of 10 kN on the upper jaw of the universal testing machine. Each sample of DSG was formed with a compaction load of 6820 N, the equivalent of 60.3 ±0.1MPa, at a compression rate of 50 mm/min (Mani et al., 2003; Johnson et al., 2014). After applying the compressive load, each individual pellet was held at the same load for 300 s by retaining the die inside the mold. This was done to maintain a constant pressure on the formed pellet and to reduce the spring-back effect (Tumuluru et al. 2010). After

300 s of holding time, the die was removed from the mold and the pellet was pushed out of the mold using the die.

3.3.4 Particle density of pellets

Dimensions of each DSG pellet with different moisture contents and soluble concentrations were measured using a digital Vernier caliper (Pro-point), with 0.01 mm accuracy. The mass of each pellet was also measured using an electronic weighing balance with an accuracy of 0.001 g (PGW 453e, Adam Equipment Inc., Danbury, CT). The calculated volume and average mass of the pellets were used to determine the particle density of the individual pellets. The experiments were repeated with five times for each moisture content and soluble concentration.

3.3.5 Determination of specific heat

Specific heat of the compacted DSG was determined using a modified method of mixtures (Stitt and Kennedy 1945; Mannheim et al. 1957; Mohsenin 1980; Muir and Viravanichai 1972). The apparatus used in this study consisted of two units: a cylindrical canister made of pure copper and an insulated thermos flask (calorimeter) attached to a mechanical shaker as shown in Figure 3.1. The pellet was placed in a copper canister before mixing with the heat transfer fluid (distilled water) within the 18/8 stainless steel thermos flask (Stanley, Pacific Market International, USA) to avoid moisture absorption and pellet deformation. The inner dimensions of the cylindrical canister were made in such a way that it could accommodate two DSG pellets with a diameter of 12.4 ±0.05 mm and a height of 28.9 ±0.05 mm. The copper canister consisted of a 1.4 ±0.02 mm thick wall and a lid with a slightly larger diameter than the canister. A soft silicon gasket was inserted between the lip of the canister and the top of the cap to ensure no penetration of fluid into the canister.

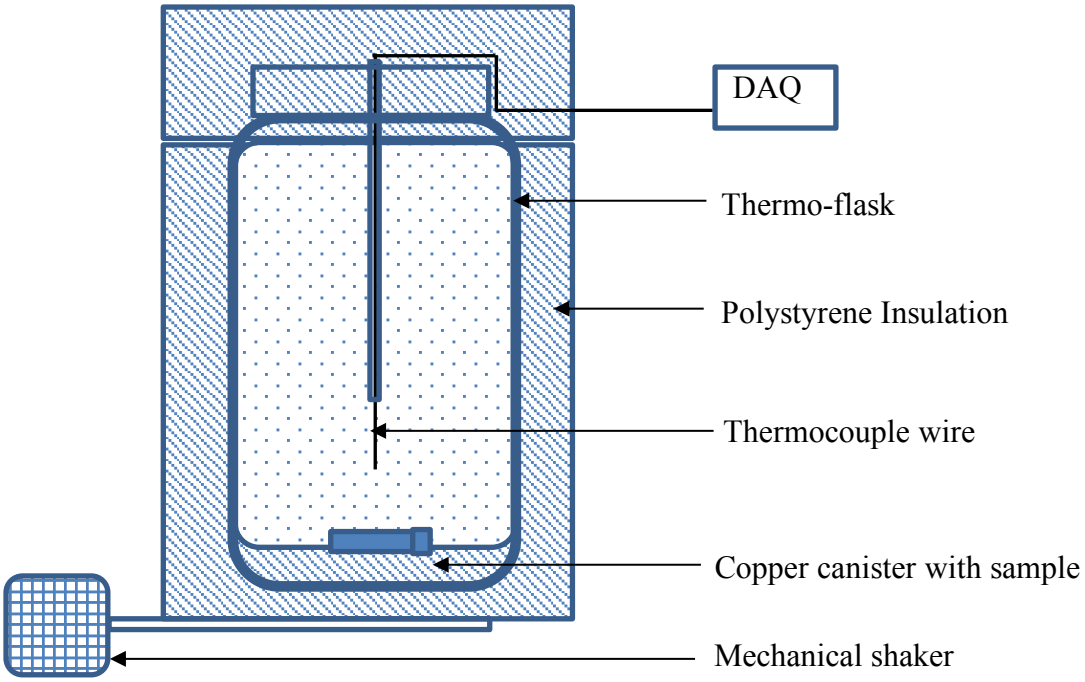

Figure 3.1 Experimental setup for measuring the specific heat of DSG pellets (modified method of mixtures).

The calorimeter was made of a double wall vacuum thermo-flask with an insulated lid. A thin plastic tube with a diameter of 0.8 ±0.05 mm was placed through a hole drilled into the lid of the thermos. A thin wire T-type thermocouple (Omega Engineering Inc. USA) with a diameter of 0.5 ±0.03 mm was placed inside the plastic tube so that the tip of the thermocouple was approximately located in the center of the heat transfer fluid within the thermo-flask. The top of the plastic tube was sealed perfectly after placing the thermocouple wire inside it ensuring the temperature sensing end of the thermocouple was only exposed to the heat transfer fluid and not the surrounding environment. Similarly, the open end of the tube on the thermos flask lid was also covered with thermal resistant tape in order to minimize the heat loss. The entire calorimeter, including the thermocouple, was then placed into a block of extruded polystyrene insulation and covered with an insulated lid. A mechanical shaker at the base of the unit ensured

that the fluid within the thermo-flask remained at a uniform temperature. The thermocouples were then connected to a Data Acquisition System (DAQ). All data obtained by the DAQ (Agilent - 34970A, USA) was then transmitted through a USB interface to a computer. By doing so, the temperature changes of the heat transfer fluid could be recorded over time.

After compaction, the pellet was carefully placed vertically inside a copper canister. The initial temperature of the pellets was checked using the thermocouple. The canister with the pellet was placed in an environmental chamber set at 25 ±1ºC. The copper canister and pellet reached equilibrium with the environmental chamber temperature after 3 to 5 minutes. Also, the resting time inside the environmental chamber allowed the pellets to slightly expand and occupy the entire volume of the canister. The temperature of the copper canister and the pellet were then checked once more before placing them into the heat transfer fluid (distilled water) to ensure that both were at the same temperature. Similarly, the polystyrene base and the lid were dismantled from the mechanical shaker and placed in an oven at 50ºC for about 5 min. This was done to minimize the heat loss during the experiment. Hot water at one of the three set temperatures was previously prepared and placed inside the calorimeter resting inside the polystyrene insulation of the mechanical shaker as shown in Figure 3.1. The water temperature was recorded 3 to 5 min prior to each experimental trial to ensure that it remained constant at the desired value. Prior to the start of each trial, the initial temperature of the canister and pellets (equal in temperature) and the hot water inside the calorimeter were recorded. The canister was then dropped into the calorimeter and the insulation lid was closed immediately. A mechanical shaker was employed to shake the assembly at a constant speed. The shaker assembly was fabricated using a rotary shaker motor (Stern Pinball motors, USA) attached to a flat platform. The temperature of the distilled water was recorded at every 1 s interval using a data acquisition

unit. The temperature of the sample canister unit and the water were allowed to reach equilibrium before stopping the experiment. Separate sets of experiments were done in triplicates for each moisture content (25, 35, and 45%), solubles concentration (0, 10, 30, and 50% w/w), and water temperature (40, 60, and 80°C). Experiments were done in triplicates for each factor (temperature, moisture content, and solubles concentration) and for every level in each factor.

To calculate the calorimeter constant of the experimental setup (water equivalent of the calorimeter and its associated parts) separate trials were conducted with a known mass of pure copper (3.5 mm diameter) and aluminum granules (1 mm diameter) with specific heat of 0.386 and 0.9 kJ/(kgK), respectively. Separate calibration tests were conducted for each heat transfer fluid temperature and corresponding calorimetric constants were determined. To estimate the canister constant, a separate set of experiments were done with the canister being empty for each temperature. Specific heat of DSG pellets was calculated using Equation 3.1, as described below, by considering the calorimetric constant at each heat transfer fluid temperature and the corresponding canister constant.

$$C_p = \frac{\left[\left(M_w - M_{th}\right)C_w\left(T_{ew} - T_{iw}\right)\right] - M_{can}C_{can}\left(T_{ew} - T_{ican}\right)}{M_{pellet}\left(T_{ew} - T_{ican}\right)} \quad (3.1)$$

where, M_{th} is the mass of water equivalent of the calorimeter (calorimetric constant) in kg, M_{pellet} is the mass of DSG pellets in kg, M_w is the mass of heat transfer fluid (water) in kg, C_w, $C_{can,}$ and C_p are the specific heat of water, copper canister, and DSG pellets, respectively, in kJ/(kgK), T_{iw}, T_{ew}, and T_{ican} are the initial temperature of water, equilibrium temperature of the water-sample mixture and initial temperature of copper canister, respectively, in K.

The temperature of the copper canister and pellet were the same before the start of the experiment. The temperature history of the water was recorded continuously at 1 s intervals using data acquisition system. All recorded data was later used for determination of specific heat of DSG pellets using Equation 3.1. The effect of thermal leakage and energy added by shaking was also considered by using the graphical method as mentioned by Stitt and Kennedy (1945). This was accomplished by calculating the temperature difference before and after mixing. A line with magnitude equal to this difference was drawn approximately through the middle of the temperature curve where a sudden deviation in temperature due to mixing was observed. The temperature corresponding to the endpoints of this line was chosen as the initial and final temperatures of the mixing fluid.

3.3.6 Determination of thermal conductivity

The thermal conductivity of cylindrical DSG pellets was determined using the modified Fitch apparatus (Fitch 1935; Dutta et al. 1988; Zuritz et al. 1989; Rahman et al. 1991), which was designed in the Department of Biosystems Engineering, University of Manitoba (Figure 3.2). It consists of a 540 mL the 18/8 stainless steel thermos flask (Stanley, Pacific Market International, USA) covered with a stopper made of extruded polystyrene foam. A copper rod of 15 mm diameter and 115 mm length was secured to a hole drilled in the center of the lid so that one end of the copper rod is exactly in line with the outer end of the polystyrene stopper. The lid-stopper assembly with the copper rod seals the thermo-flask. The top cover for the Fitch apparatus was made with polystyrene with a copper plug of the same diameter as that of the rod and 16 mm depth at its center. The copper plug in the top cover and the copper rod in the lid-stopper assembly were aligned so that a small space of 7.2 ±3 mm between the plug and rod was left for placing the test sample (DSG

pellet). Two thin T –type thermocouples were installed about 2 mm below the surface of the rod and the plug by securing them in a narrow hole drilled into the copper. In order to minimize the heat dissipation due to the air gap around the sample, the lid of the thermo-flask was covered with a Styrofoam insulation cover.

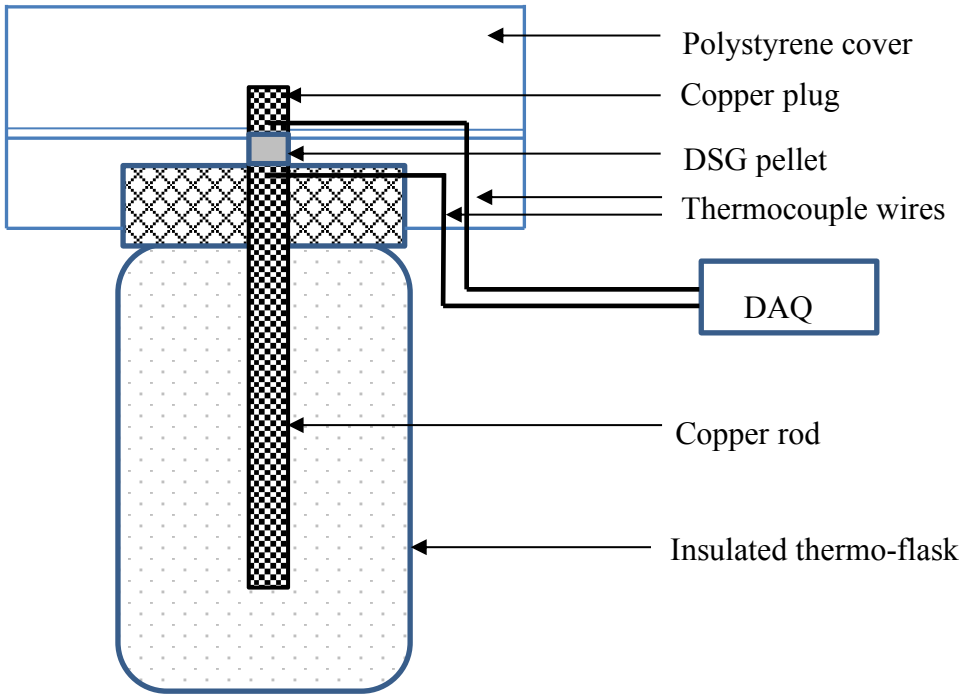

Figure 3.2 Experimental setup for measuring the thermal conductivity of DSG pellets (modified Fitch apparatus).

The thermo-flask was filled with the heat transfer fluid (distilled water and crushed ice mixture/ water with set temperature). The temperature of the heat transfer fluid inside the thermo-flask was allowed to equilibrate to a constant value for about 10 min. The thermo-flask with the heat transfer fluid was gently mixed with the help of a mechanical shaker. Compacted cylindrical pellets of approximately 12.5 ±1 mm diameter and 7.2 ±3 mm thickness were made using the universal testing machine (Model 3366 Universal Testing Systems, Instron Corp., Norwood, MA). The pellet was placed between the copper rod and plug. The temperature history of both

the top and bottom of the pellet were recorded using two thermocouples. As per the quasi-steady conduction heat transfer through the DSG pellet, the energy balance in the copper plug and its analytical solution (Mohsenin 1980) are given by equation 3.2 and 3.3:

$$\frac{Ak_p(T_{cr} - T)}{x} = m_{cp}C_{p,c}\frac{dT}{dt} \tag{3.2}$$

With initial condition: $T = T_0$, when $t = 0$.

$$\ln\frac{(T_{cr} - T_0)}{(T_{cr} - T)} = \frac{(Ak_p t)}{(x\, m_{cp}C_{p,c})} \tag{3.3}$$

where, A is the heat transfer area in m^2, k_p is the thermal conductivity of pellets in W/(mK), T, T_0, T_{cr} are the instantaneous temperature of the copper plug and sample, initial temperature of copper plug and Temperature of heat source (copper rod) in K, x is the thickness of the pellet in m, m_{cp} is the mass of the copper plug in kg, $C_{p,c}$ is the specific heat of copper in J/kg K.

The thermal conductivity of the DSG pellets was calculated from of the slope of the semi-log plot of temperature gradient versus time and by equating the slope to the lefthand side of the equation 3.3 ie. $\frac{(Ak_p t)}{(x\, m_{cp}C_{p,c})}$. The experiments were repeated five times for each moisture content, (25, 35, 45%), solubles concentration of DSG pellets (0, 10, 30, 50% w/w), and heat transfer fluid temperature (0, 40, 80°C).

3.3.7 Analysis of data

The effect of moisture content and solubles concentration on the thermo-physical properties of the DSG pellets at different temperatures were studied using Statistical software (SAS 9.4). A method of least squares to fit a general linear model (GLM procedure) and a regression analysis where conducted on the experimental data using SAS (Version 9.4, SAS Institute Inc., Cary,

NC). A regression analysis with two independent variables (solubles concentration and moisture content) and three independent variables (solubles concentration, moisture content, and temperature) were used for describing the effect of each factor on particle density, thermal conductivity, and specific heat of the DSG pellets, respectively. The predicted values were compared with the experimental values by using R-square value and mean relative percentage error (Jian et al. 2013) determined using the following equation.

$$MRP = \frac{1}{n}\sum_{i=1}^{n}\frac{|P_i - E_i|}{E_i}\times 100 \quad (3.4)$$

where, MRP is the mean relative percentage error, P_i and E_i are the instantaneous predicted and experimental values of the property tested, n is the number of data points compared.

3.4 Results and discussion

3.4.1 Density and expansion of DSG pellets

The particle density of DSG pellets with different soluble concentrations (0, 10, 30, and 50%) ranged between 898.8-1073.4, 981.4-1057.7, 995.8-1114.92, and 1039.7-1136.7 kg/m^3, respectively, for the different moisture contents (Figure 3.3). Increasing the percentage of solubles eliminated the micro-pores in the pellet A similar range of values (ie 940 – 1090 kg/m^3) were also reported by Johnson et al., (2013) for the DSG pellets compacted with different compressive pressure. They also reported that the addition of 30% solubles to the DSG sample increased the density of the pellet by about 10% even at lower compressive pressure of 60.6 MPa. At the same time their results showed that the solubles concentration didn't have an effect on pellet strength at higher compressive pressures (above 90 MPa). Statistical analysis of the experimental values using general linear model analysis shows that both the independent variables (solubles concentration and moisture content) have a significant

effect (P<0.001) on the particle density of the DSG pellets. Since there was no significant interaction between the independent variables, a simple linear regression analysis was used to predict the particle density of the DSG pellets. The prediction model for the particle density of DSG pellets as a function of solubles concentration and moisture content is shown in equation 3.5. The prediction agrees well with the experimental values with an R-square value of 0.86. The mean relative percentage error for the predicted values was 3.4%.

$$D = 213.3\,S - 45.5\,M + 1011.2 \quad (3.5)$$

Where, D is the particle density of the pellet in kg/m^3, S is the % solubles in a fraction, M is the moisture content in % wb. As shown in the Figure 3.3, the particle density of the DSG pellets increased with an increase in solubles concentration supporting the conclusions of Johnson et al. (2015). This increase in particle density with the increase in solubles concentration might be due to the superior binding properties of solubles, high amount of starch and protein, and its lower particle size as reported by Mosqueda et al. (2013) and Johnson et al. (2014). The micro-porosity of the pellet due to the small air pockets within the pellet will also affect the density of the pellet. The increase in soluble concentration in dried DSG granules lead to a decreased porosity (Mosqueda et al., 2014) because of the fact that the bulk porosity of dried solubles were about 10% lesser than that of the dried DSG powder (Zielinska 2016).

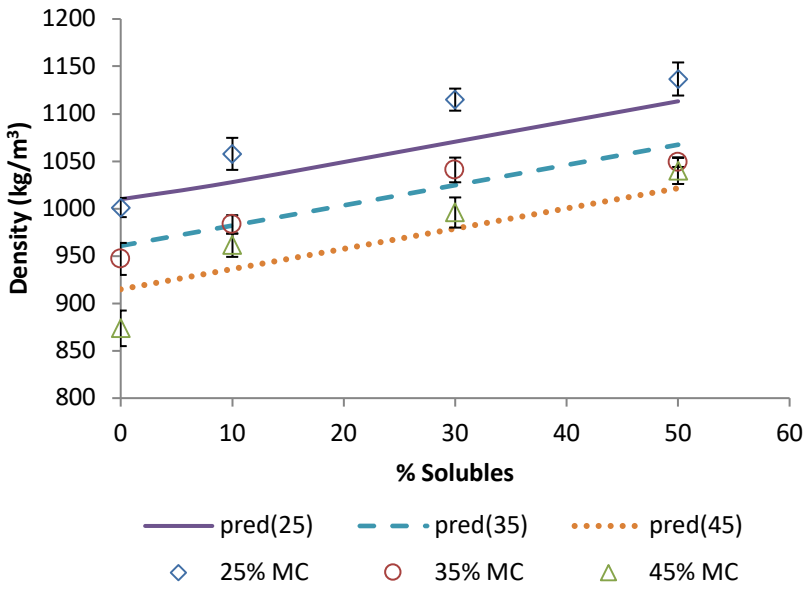

Figure 3.3 Effect of moisture content and solubles concentration on the particle density of the DSG pellets. (Where, pred(25), pred(35), and pred(45) shows the predicted density of pellets with 25, 35, and 45% moisture content, respectively)

A heterogeneous mixture of particles with different sizes has greater bonding because of the higher number of inter-particle bonds formed during compaction (Payne 1978). In contrast, the moisture content has a negative effect on the particle density of the pellets (Serrano et al. 2011; Samuelsson et al. 2012) because higher moisture content samples tend to expand quickly than the lower moisture content samples (Mohsenin and Zaske 1976). A similar negative correlation between hardness and the moisture content of the DSG pellets was reported by Johnson et al. (2015). The strength and durability of the densified products increased with increasing moisture content until an optimum is reached (Kaliyan and Morey 2009). The DSG pellets at higher moisture content (>25%) have more moisture trapped in the inter-particle spaces and these water molecules prevent the complete compression and

release of natural binders from solid particles owing to the incompressibility of water (Pickard et al. 1961).

3.4.2 Specific heat of DSG pellets

The average specific heat of DSG pellets for temperatures of 40, 60, and 80°C ranged between 1.76-2.62, 1.85-3.32, 2.67-3.47 kJ/(kgK), respectively. The specific heat values of these high moisture DSG pellets (25-45% moisture content) were found to be insignificantly higher than the dried distillers granules (1:1 ratio of wheat and corn) which were in the range of 1.7 – 2.6 kJ/(kgK) (Zielinska 2016). The higher values of specific heat were mainly attributed by the higher moisture content of DSG pellets since water has higher specific heat than dried grains. The experimental values of specific heat capacities of the DSG pellets with different percentage of solubles (0, 10, 30, 50 %) at different moisture content (25, 35, 45 %) and at three different temperatures of heat transfer fluid (40, 60, 80°C) are shown in Figure 3.4a-d. As per the results of statistical analysis, all the three independent variables (moisture content, solubles concentration, and temperature of heat transfer fluid) have a significant effect ($P<0.001$) on the dependent variable (specific heat capacity). The interaction terms between the independent variables were neglected from the model since they were insignificant at $P>0.05$. The regression model for the prediction of specific heat capacity of DSG pellets is shown in equation 3.6.

$$C_p = 0.019\,M + 0.011\,S + 0.023\,T + 0.2716 \quad (3.6)$$

where C_p is the specific heat of DSG pellets in kJ/(kgK), S is the % solubles in a fraction, M is the moisture content in % wb, and T is the temperature of the heat transfer fluid in °C.

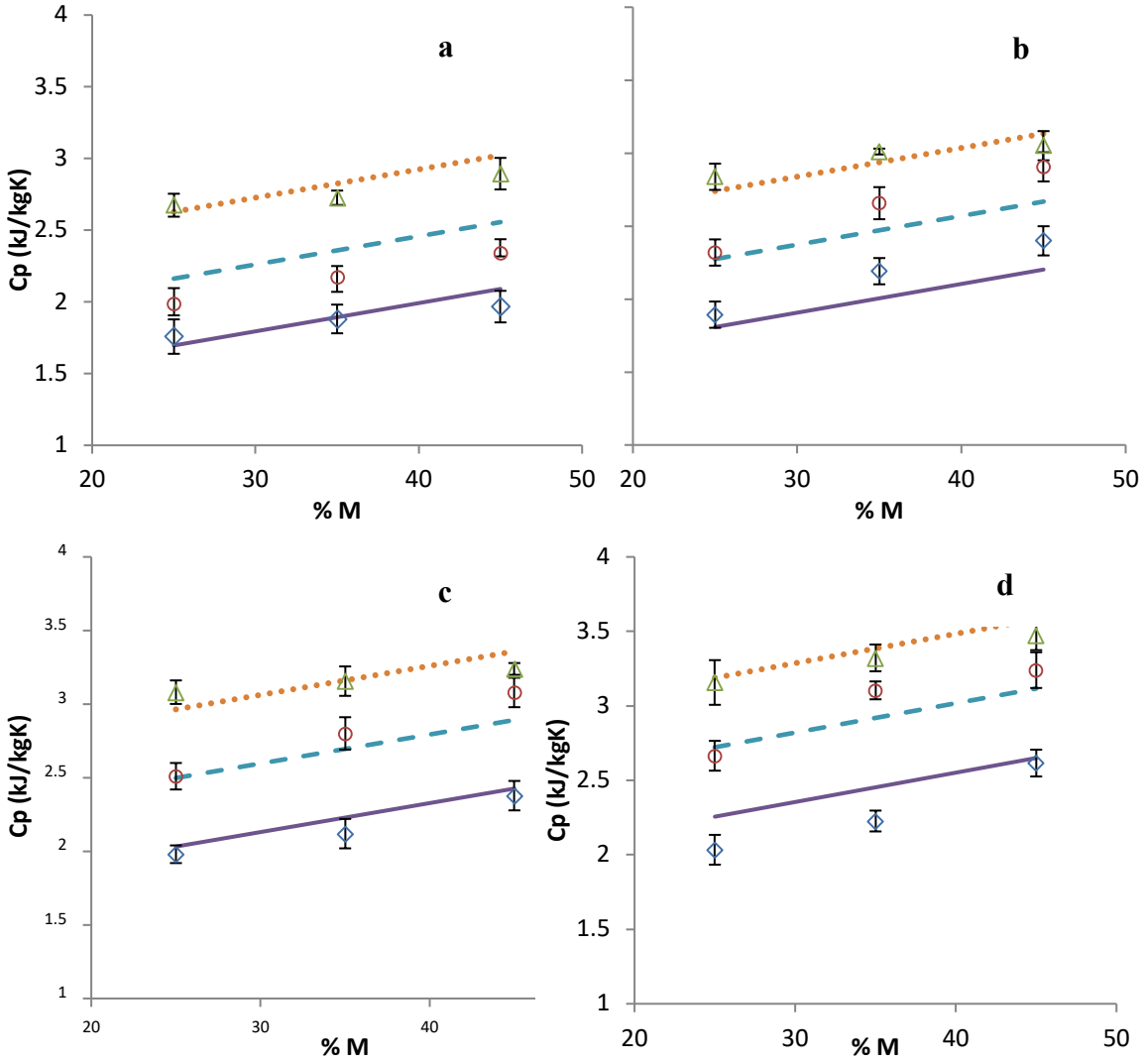

Figure 3.4 a-d Effect of moisture content (25, 35, and 45%) and temperature (40, 60, and 80oC) on the specific heat capacity of DSG pellets with different percentage of solubles (where a, b, c, and d represents the graphs for 0, 10, 30, and 50% of solubles, respectively and pred(40), pred(60), and pred(80) shows the predicted specific heat of pellets at 40, 60, and 80oC temperatures, respectively.)

The specific heat capacity of the DSG pellets increases linearly with an increase in moisture content, temperature, and solubles concentration (Figure 3.4a-d). A similar trend in the specific

heat with an increase in temperature and moisture content was also reported by Jian et al. (2013) for canola seeds and by Ashtiani et al. (2014) for sesame seeds. The mean relative percentage error and R-square value for the developed model were 5.5%, and 0.86, respectively. A comparison of predicted and experimental values of specific heat capacity of the DSG pellets shows that the general linear model as described by equation 6 has better predictability of the dependent variable (specific heat).

3.4.3 Thermal conductivity of DSG pellets

Thermal conductivity of a material depends on the structural anatomy of the sample, as well as its composition. Hence, it is highly challenging to get an accurate measurement of thermal conductivity of a sample when compared to the other thermal properties (Rahman 1991). The variation of thermal conductivity of DSG pellets at different moisture contents (25, 35, 45%) and temperature of heat transfer fluid (0, 40, 80^{o}C) for each percentage composition of solubles (0, 10, 30, 50%) is shown in Figure 3.5a-d. The value of thermal conductivity of the DSG pellets with different solubles concentration and moisture contents for the three different temperatures of heat transfer fluid (0, 40, 80^{o}C) were 0.17-0.30, 0.20-0.35, 0.22-0.42 W/(mK), respectively. These thermal conductivity values were higher than the values reported for dried DSG powder which was in the range of 0.04 - 0.05 W/(mK) (Mosquueda et al., 2014) because of the fact that the these DSG pellets were at significantly higher moisture content (ie. 25- 45% moisture content). The presently reported values were found to be closer to the thermal conductivity values of corn kernels which were reported to be in the range of 0.15 to 0.35 W/(mK) for a moisture range of 10-35% (Kustermann et al., 1981). At each moisture content and temperature, there was a gradual increase in the value of

thermal conductivity with an increase in solubles concentration up to 30%, beyond which the value seems to be approximately constant.

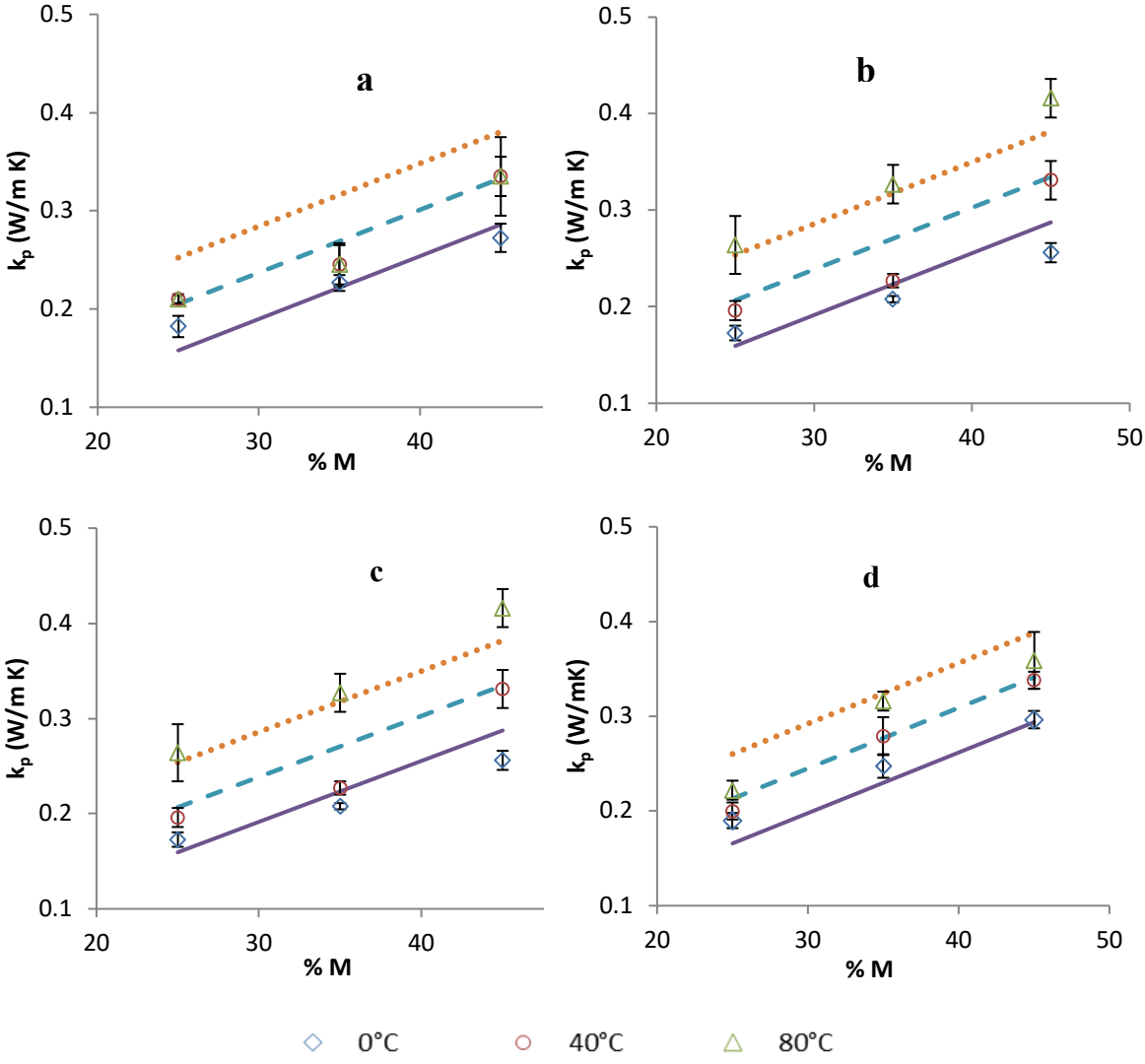

Figure 3.5 a-d Effect of moisture content (25, 35, and 45%) and temperature (0, 40, and 80°C) on the thermal conductivity of DSG pellets with different solubles concentrations (where a, b, c, and d represents the graphs for 0, 10, 30, and 50% of solubles, respectively and pred(0), pred(60), and pred(80) shows the predicted specific heat of pellets at 40, 60, and 80°C temperatures, respectively.)

All the three independent variables (moisture content, solubles concentration and temperature) have a significant effect on the dependent variable (thermal conductivity) with their P values <0.001, <0.010, and <0.001, respectively. The mathematical equation of best fit was determined with the help of multiple regression analysis avoiding the interaction terms since they were found to be insignificant. The prediction equation for thermal conductivity as a function of temperature, moisture content, and solubles concentration is given by equation 3.7.

$$k_p = 0.0012\,T + 0.016\,S + 0.0064\,M - 0.0022 \quad (3.7)$$

where, k_p is the thermal conductivity of the DSG pellet in W/(mK), S is the solubles concentration in fraction, M is the moisture content in % wb, and T is the temperature of the heat transfer fluid in ^{o}C. The thermal conductivity of the DSG pellets increases with increase in moisture content, solubles concentration, and temperature (Figure 3.5a-d). Similar results showing a positive effect of temperature (Jancazak 2013) and moisture content on the thermal conductivity of material were reported by Elansari and Hobani (2009) and Modi et al. (2014). The increase in thermal conductivity values with an increase in moisture content is attributed to the higher conductive heat transfer of water molecules (Sreenarayanan and Chattopadhyay 1986). Emami et al. (2007) reported that the thermal conductivity is greatly influenced by the atomic activity inside the material. Hence, at a higher temperature, there is a higher atomic activity which improves the ability of the material to transfer heat energy. A similar trend in thermal conductivity with increase in temperature was reported by Mahapatra et al. (2011) and Jancazak (2013). The increase in thermal conductivity values of DSG pellets with the increase in solubles concentration can be explained by the correlation between solubles concentration and particle density as mentioned in equation 7. The DSG pellets with a higher percentage of solubles have a higher density, which decreases the air pockets inside

the pellet. Since air is a poorer conductor of heat than solids, air pockets inside the material (i.e. higher porosity) lead to decreased thermal conductivity and vice versa. Hence, at constant moisture content, higher density pellets will have higher thermal conductivity. Also, the high amount of starch and protein in the solubles, increases the thermal conductivity as starch and protein have higher thermal conductivities than cellulosic fiber (Choi and Okos, 2004). The prediction equation for thermal conductivity was validated with the experimental data by using R-square value and mean relative percentage error. The value of thermal conductivity for different moisture content, temperature and solubles concentration is well predicted by the multiple regression equation (equation 3.7) with an R-square value of 0.89. The mean relative percentage error calculated for the prediction equation was 6.7%, which indicates good agreement between the experimental and predicted values of thermal conductivities.

3.5 Conclusions

Thermo-physical properties are the key input parameters required for mathematical modelling of heat and mass transfer phenomena of the drying process. Therefore, thermal conductivity, specific heat, and particle density were determined as a function of moisture content, solubles concentration, and temperature using standard laboratory methods. The particle density of DSG pellets was in the range of 898.8-1136.7 kg/m^3 for moisture content ranging from 25-45% and solubles concentration ranging from 0 -50%. The particle density of DSG pellets increased by 8.3, 10.8, and 19% with an increase in solubles concentration (0-50%) for 25, 35, and 45% moisture content, respectively. But the average particle density of the DSG pellets was found to decrease (10- 18%) with an increase in moisture content. The superior binding

properties of protein and starch and finer particle size of solubles explain the increase in density with an increase in solubles concentration.

Specific heat of the DSG pellets was positively correlated with the moisture content, solubles concentration, and temperature. The average value of the specific heat of DSG pellets ranged between 1.76-3.47 kJ/(kgK) for different moisture contents (25, 35, 45%) and solubles concentration (0,10, 30, 50%). However, at higher temperatures (80ºC) the effect of moisture content on the specific heat capacity of the DSG pellets was minimal when compared to lower temperatures (40ºC). There was an increase in the specific heat value of DSG pellets (9-20%) with an increase in solubles concentration for different temperatures of heat transfer fluid. The values of thermal conductivity also showed a positive correlation with the moisture content, temperature, and solubles concentration. The average value of thermal conductivity of DSG pellets ranged between 0.17-0.42 W/(mK) for different moisture contents (25, 35, 45%) and solubles concentration (0,10, 30, 50%). The thermal conductivity of a pellet was predominantly affected by the moisture content than other independent variables. Multiple linear regression equations for all the three properties show a good agreement with the experimental data. Hence, these equations can be used for predicting the values of these properties at any moisture content, solubles concentration, and temperature with appreciable accuracy. These equations can be used as important tools to predict thermo-physical properties of DSG pellets, as these properties are essential for the numerical modelling of heat and mass transfer mechanisms. Also, these properties will serve as essential data for optimization of different processing and storage techniques and for the design of suitable drying system for distillers spent grains.

Acknowledgement

The authors acknowledge the Natural Sciences and Engineering Research Council of Canada and University of Manitoba Graduate Fellowship for their financial support. Thanks are also due to NSERC-funded summer research assistants, Jennifer Pienuita, Clifford Dueck, and Craig Heppner, for their technical assistance.

References

1. AACC Method 44-15A. 2000. Moisture-air-oven methods. In: Approved Methods of the American Association of Cereal Chemists. St. Paul, MN.
2. Ashtiani, S., Emadi, B., Sanaeimoghadam, A., & Aghkhani, M. (2014). Effect of moisture content and temperature on thermal behaviour of sesame seed. The Annals of the University Dunarea de Jos of Galati Fascicle VI – *Food Technology*, 38(1), 87-103.
3. Bourassa, J., Ramachandran, R. P., Paliwal, J., & Cenkowski, S. (2015). Drying Characteristics and Moisture Diffusivity of Distillers' Spent Grains Dried in Superheated Steam. *Drying Technology*, 33, 2012-2018.
4. Choi, Y. and Okos, M. R. (2004) Thermal conductivity of Foods. In Heldman, D. R. (Ed.) Encyclopedia of Agricultural, Food, and Biological Engineering (pp. 1004-1010) Marcel Dekker Inc. New York, Basel.
5. Defraeye, T. (2014). Advanced computational modelling for drying processes – A review. *Applied Energy*, 131,323–344. doi.org/10.1016/j.apenergy.2014.06.027
6. Drouzas, A. E., Maroulis, Z. B., Karathanos, V. T., and Saravacos, G. D. 1991. Direct and indirect determination of the effective thermal diffusivity of granular starch. *Journal of Food Engineering.* 13(2): 91-101.
7. Dutta, K. S., Nema, V. K., & Bhardwaj, R. K. (1988). Thermal properties of gram. *Journal of Agricultural Engineering Research*, 39(4), 269-275.
8. Elansari, A. M. & Hobani, A. I. (2009). Effect of temperature and moisture content on thermal conductivity of four types of meat. *International Journal of Food Properties*, 12, 308–315.

9. Emami, S., Tabil, L.G., & Tyler, R.T. (2007). Thermal properties of chickpea flour, isolated chickpea starch, and isolated chickpea protein. *Transactions of the ASABE*, 50 (2), 597–604.
10. Erriguible, A., Bernada, P., Couture, F., & Roques, N. (2006). Simulation of superheated steam drying from coupling models. *Drying Technology*, 24, 941–951. doi:10.1080/07373930600776019
11. Fitch, A. L. (1935). A new thermal conductivity apparatus. American Physics Teacher, 3(3), 135-136.
12. Hamawand, I. (2011). Effect of colloidal particles associated with the liquid bridge in sticking during drying in superheated steam. *International Journal of Engineering*, 24(2), 119-126.
13. Hamawand, I. 2013. Drying steps under superheated steam: a review and modelling. *Journal of Energy and Environment research* 3(2): 107–125. doi:10.5539/eer.v3n2p107
14. Hamawand, I., Yusaf, T. & Bennett, J. (2014). Study and modelling drying of banana slices under superheated steam. Asia-Pacific *Journal of Chemical Engineering*, 9, 591–603.
15. http://www.huskyenergy.com/huskyproducts/canada.asp. Accessed on August 1, 2016
16. Iyota, H., Nishimura, N., Yoshida, M., & Nomura. (2007). Simulation of superheated steam drying considering initial steam condensation. *Drying Technology*, 19(7), 1425-1440. doi:10.1081/DRT-100105298
17. Jancazak, D. (2013). The effect of temperature, composition and phase of the composting process on the thermal conductivity of the substrate, *Ecological Engineering Journal*, 61, 354–357.
18. Jian, F., Jayas, D. S., & White, N. D. G. (2013). Specific heat, thermal diffusivity, and bulk density of genetically modified canola with high oil content at different moisture contents, temperatures, and storage times. *Transactions of the ASABE*, 56(3), 1077-1083.
19. Johnson, P., & Cenkowski, S. (2011). Bulk density and angle of repose of Distiller's Spent Grain under different drying methods and soluble concentrations. CSBE/SCGAB

2011 Annual Conference Inn at the Forks, Winnipeg, Manitoba 10-13 July 2011. Paper No. CSBE11-318.

20. Johnson, P., Paliwal, J., & Cenkowski, S. (2014). Analysis of the disintegration of Distiller's Spent Grain compacts as affected by drying in superheated steam. *Drying Technology,* 32, 1060–1070.
21. Johnson, P., Paliwal, J., & Cenkowski, S. (2013). Superheated Steam Drying Characteristics of Single Cylindrical Compacts Produced from Wet Distiller's Spent Grain. In proceedings of CSBE/SCGAB 2013 Annual Conference, Saskatchewan 7-10 July 2013. Paper No. CSBE13-11.
22. Johnson, P., Paliwal, J., & Cenkowski, S. (2015). Effect of solubles on disintegration of Distiller'rs Spent Grain compacts during superheated steam drying. *Drying Technology*, 33 (6), 671-683.
23. Kaliyan, N. & Morey, R.V. (2009). Factors affecting strength and durability of densified biomass products. *Biomass and Bioenergy*, 33 (3), 337–359.
24. Kustermann, M., Scherer, R., & Kutzbach, H. D. (1981). Thermal conductivity and diffusivity of shelled corn and grain. *Journal of Food Process Engineering* 4: 137-153.
25. Mahapatra, A.K., Lan, Y., & Harris, D.L. (2011). Influence of moisture content and temperature on thermal conductivity and thermal diffusivity of rice flours. *International Journal of Food Properties*, 14, 675–683.
26. Mannheim, H. C., Steinberg, M. P., Nelson, A. I., & Kendall, T. W. (1957). The heat content of bread. *Food Technology*, 11 (7), 394-388.
27. Mani, S.; Tabil, L.G.; Sokhansanj, S. (2003) An overview of compaction of biomass grinds. *Powder Handling and Processing*, 15(2), 160–168.
28. Modi, S.K., Durga P. B., & Basavaraj. M. (2014). Effect of moisture content and temperature on thermal conductivity of Psidium guajava L. by line heat source method (transient analysis). *International Journal of Heat and Mass Transfer*, 78: 354–359.
29. Mohseni, N. & Zaske, J. (1976). Stress relaxation and energy requirements in compaction of unconsolidated materials. *Journal of Agricultural Engineering Research*, 21, 193-205.
30. Mohsenin, N. N. 1980. *Thermal Properties of Foods and Agricultural Materials.* New York, N.Y.: Gordon and Breach Science Publishers.

31. Mosqueda, M.R., L.G. Tabil, and K. Muthukumarappan. 2013. Effects of condensed distillers solubles and drying temperature on the physico-chemical characteristics of laboratory-prepared wheat distillers grain with solubles. *International Journal of Agricultural and Biological Engineering* 6(2):73-85.
32. Mosqueda, M.R., L.G. Tabil, and K. Muthukumarappan. 2014. Physico-chemical characteristics of wheat distillers dried grain with solubles sourced from a Saskatchewan ethanol plant. *Canadian Biosystems Engineering* 56:3.1-3.15.
33. Muir, W. E. and Viravanichai, S. (1972). Specific heat of wheat 17, 338-342.
34. Nesvadba, P. 1982. Methods for the measurement of thermal conductivity and diffusivity of foodstuffs. *Journal of Food Engineering* 1(2):93-113.
35. Pakowski, Z., & Adamski, R. (2011). On Prediction of the Drying Rate in Superheated Steam Drying Process. *Drying Technology*, 29, 1492-1498.
36. Payne, J. D. (1978). Improving quality of pellet feeds. *Milling Feed and Fertilizer*, 162 (5), 34–41.
37. Pickard G. E., Roll W. M., & Ramser J. H. (1961). Fundamentals of hay wafering. *Transactions of ASABE*, 4 (1), 65-68.
38. Rahman, S. (1991). Evaluation of precision of the modified Fitch method for thermal conductivity measurement of foods. *Journal of Food Engineering*, 14. 71-82.
39. Samuelsson, R., Larsson, S., Thyrel, M. & Lestander, T. A. (2012). Moisture content and storage time influence the binding mechanisms in biofuel wood pellets. *Applied energy*, 99, 109-115.
40. Serrano, C., Monedero, E., Lapuerta, M., & Portero, H. (2011). Effect of moisture content, particle size and pine addition on quality parameters of barley straw pellets. *Fuel Processing Technology*, 92, 699–706.
41. Sousa, S. C. L., Silva, J. P., Ramos, A. M. M., & Simões, R. M. S. (2007). Pulping and papermaking potential of brewery's spent grain. *Cellulose Chemistry and Technology*, 41(2), 183–191.
42. Sreenarayanan, V.V. & Chattopadhyay, P.K. (1986). Thermal conductivity and diffusivity of rice bran, *Journal of Agricultural Engineering Research*. 34, 115–121.
43. Stitt, F., and E. K. Kennedy. 1945. Specific heats of dehydrated vegetables and egg powder. *Food Research International*, 10(5), 426-436.

44. Stroem, L. K., Desai, D. K., & Hoadley, A. F. A. (2009). Superheated steam drying of brewer's spent grain in a rotary drum. *Advanced Powder Technology*, 20, 240–244. doi: 10.1016/j.apt.2009.03.009
45. Suvarnakuta, P., Devahastin, S., & Mujumdar, A. S. (2007). A mathematical model for low pressure superheated steam drying of biomaterial. *Chemical Engineering and Processing*, 46(7), 675-683.
46. Sweat, V. E. (1986). Thermal properties of foods. In Engineering Properties of Foods. In M. A. Rao & S. S. H. Rizivi (Eds). Marcel Dekker, New York.
47. Thomas, M., Van-Vliet, T., & Van-der-Poel, A. F. B. (1998). Physical quality of pelleted animal feed. 3. Contribution of feedstuff components. *Animal Feed Science and Technology*, 70(1–2), 59–78.
48. Tumuluru, J. S., Tabil, L., Opoku, A., Mosqueda, M. R., Fadeyi, O., 2010. Effect of process variables on the quality characteristics of pelleted wheat distiller's dried grains with solubles. *Biosystems Engineering*, 105 (4), 466–475.
49. Unknown, (2016), http://www.huskyenergy.com/huskyproducts/canada.asp, accessed on May, 2016.
50. Waszkielis, K. M., Białobrzewski, I., Nowak, K. W., Dzadz, & Dach, J. (2014). Determination of the thermal conductivity of composted material. *Measurement: Journal of the International Measurement Confederation*, 58, 441–447.
51. Waszkielis, K. M., Wronowski, R. Chlebus, W., Bialobrzewski, I., Dach, J., Pilarski, K., & Jancazak, D. (2013). The effect of temperature, composition and phase of the composting process on the thermal conductivity of the substrate. *Ecological Engineering Journal*, 61, 354–357.
52. Xiros, C., Topakas, E., Katapodis, P., & Christakopoulos, P. (2008). Hydrolysis and fermentation of brewer's spent grain by Neurospora crassa. *Bioresource Technology*, 99(13), 5427–5435.
53. Yang, W., Sokhansanj, S., Tang, J., & Winter, P. (2002). Determination of thermal conductivity, specific heat and thermal diffusivity of borage seeds. *Biosystems Engineering*, 82 (2), 169–176.

54. Zielinska, M., & Cenkowski, S. (2012). Superheated Steam Drying Characteristic and Moisture Diffusivity of Distillers' Wet Grains and Condensed Distillers' Solubles. *Journal of Food Engineering*, 109(3), 627-634.
55. Zielinska, M., Cenkowski, S., & Markowski, M. (2009). Superheated steam drying of distillers' spent grains on a single inert particle. *Drying Technology*, 27(12), 1279 – 1285. doi: 10.1080/07373930903195065
56. Zielinska, M. 2016. Thermophysical properties of laboratory-prepared corn/wheat dried distiller's grains and dried distillers solubles dehydrated with superheated steam and hot air. *Drying Technology*, 34(10): 1147-1161. Doi.org/10.1080/07373937.2015.1099543.
57. Zuritz, C. A., Sastry, S. K., McCoy, S. C., Murakami, E. G., & Blaisdeh, J. L. (1989). A modified Fitch device for measuring the thermal conductivity of small food particles. *Transactions of ASAE*, 32(2), 711-718. doi: 10.13031/2013.31059.

CHAPTER 4. EFFECTIVE MOISTURE DIFFSUIVITY OF DSG

This chapter is based on the research paper published by Elsevier in the journal *Biomass and Bioenergy* on 14 June 2018, available online: www.sciencedirect.com/ [doi.org/10.1016/j.biombioe.2018.06.004].

4.1 Abstract

Drying is an essential unit operation needed for safe storage and handling of the wet Distillers' spent grain (DSG), a major by-product of the ethanol industry. For the simulation and modelling of the drying process, a detailed study on different pre-requisite parameters such as the thermo-physical properties and effective moisture diffusivity of the material to be dried under is required. The present study reports the effective moisture diffusivity and activation energy of the DSG pellets during superheated steam (SS) drying. Cylindrical DSG pellets at two moisture contents (25 and 35% wet basis) and three distllers' solubles concentrations (0, 10, and 30% w/w) were dried at five SS temperatures (120, 135, 150, 165, and 180°C) and three SS velocities (0.5, 1.0, and 1.5 m/s), respectively. The experiment-based effective moisture diffusivity of the DSG pellet with and without solubles was determined by using the comparison of drying characteristic and the analytical solution of Fick's law of diffusion for a finite cylinder. The results showed that the effective diffusivity increased with an increase in SS temperature and velocity and its value was in the range of 2.49×10^{-9} to 17.9×10^{-9} m^2/s. The dependency of the moisture diffusivity on temperature and moisture content was established by using Arrhenius equation and Levenberg-Marquardt optimization algorithm. The model coefficients were compared with the calculated values of instantaneous

effective moisture diffusivity with R^2 value ≥0.78 and error ≤10%. These findings could serve as a fundamental input for the numerical modelling of SS drying of DSG pellets.

Keywords: *Distillers' spent grain pellet, Distillers' solubles, Effective moisture diffusivity, Activation energy, Superheated steam drying*

4.2 Introduction

Distillers' spent grain (DSG), which contains the residue remaining after starch extraction for ethanol production, is the major by-product from the bioethanol industry. This low-value product is mainly utilized as animal feed in either processed or unprocessed form. High levels of protein and digestible fiber combined with low starch content makes this material a suitable raw material for the feed industry (Oba et al., 2010; Salim et al., 2010; Świątkiewicz and Koreleski, 2008). When converted to other useful products such as animal feed, dried distillers' grain, with or without solubles, could yield 10-20% additional income to the ethanol industry (Johnson et al., 2011a; Ramachandran et al., 2017b). The increased production of DSG in recent years has resulted in unprecedented interest to identify new value added products from this dietary fiber rich by-product. These products include fish feed (Li et al., 2011), cattle feed(Penner et al., 2009), poultry feed (Salim et al., 2010), pig feed (Lyberg et al., 2012), human food (Brochetti et al., 1991; Fiasco et al., 1990), and nutritional supplements for simultaneous saccharification and ethanol fermentation (Bi et al., 2011).

Regardless of the milling method (wet or dry milling), a by-product of the bio-ethanol industry that uses cereal grains as raw materials is the unfermented mashed grain, called wet stillage. This wet stillage is in the form of a slurry with high moisture content (about 80%) (Ramachandran et al., 2017b). Approximately, one-third of the grain used for ethanol

production ends up as wet stillage (Popp et al., 2016). Hence, drying wet stillage mitigates the inconvenience of its storage and transportation. The wet stillage is initially centrifuged to remove excess water and to separate the smaller sized particles (i.e. distillers' solubles) from coarser particles. Depending upon the requirements of the final product, the centrifuged stillage and solubles are then dried either separately or together to yield dried distillers' spent grains (DDGS) or dried distillers' spent grain with solubles (DDGSS), respectively. The quality and market value of the dried product depends on the method and operating conditions of the drying process.

The industrial drying of wet spent grains is done using rotary drum dryers at internal temperatures ranging from 250 to 600°Cs. In order to maintain the throughput of the wet stillage to dried product, the wet stillage is mixed with a batch of previously dried granules of DSG at the entrance of the rotary-drum dryer. The dried granules serve as a core (inert) material to dry the wet DSG coated over it. This approach helps to develop a desired large surface area for heat and mass exchange. But, these multiple passes of the core material through the hot dryer can lead to burning or igniting fires in such hot air. This causes either darkening of the DDGS, which affects its nutritional value, or a shutdown of the production line causing monetary losses (Ramachandran et al., 2017a). The use of superheated steam (SS) for drying such wet materials not only eliminates the risk of fire but also improves the colour and quality of the final product (Cenkowski, Pronyk, Zmidzinska, & Muir, 2007; Tang, Cenkowski, & Izydorczyk, 2005; Zielinska et al., 2009). The optimization of the antiquated drying process using SS is still under research with the aim to improve the quality of dried products; and increase the efficiency and productivity of the drying process.

The SS drying process has different stages of drying such as initial condensation, constant rate drying and falling rate drying. As opposed to air drying where the moisture content gradually decreases during the warming up period, the moisture content of the material increases in the initial stage of SS drying due to steam condensation. This phenomenon is referred to as the initial condensation or a reverse drying process (Iyota et al., 2001). The condensed water either evaporates or is adsorbed by the material depending on the properties of the material and duration of the condensation process causing an increase in the overall moisture content of the material. This increase in moisture content affects the drying rate as well as the moisture diffusivity of the material (Pakowski and Adamski, 2011a). The length and quantity of the initial condensation is dependent on the SS temperature and velocity (Ramachandran et al., 2017b). Therefore, the moisture gain due to the initial condensation is also dependent on the SS condition. Zielinska and Cenkowski (2012) reported that different factors such as the initial moisture content, fraction of distillers' solubles in the spent grain, and steam operating conditions affect the moisture diffusivity of DSG. These factors affect the heat transfer rate and thereby influence the moisture movement inside the material.

A complete understanding of the drying characteristics of the material and the dynamics of drying process are key to the design and modification of such dryers. A development of a numerical model capable of describing the drying process with a good spatial and temporal resolution is an essential step in design. To develop such model, some pre-requisite parameters such as thermo-physical properties of material (Da- Silva et al., 2014; Perussello et al., 2014; Ramachandran et al., 2017c) and the moisture diffusivity (Doymaz, 2009; Sharma and Prasad, 2004) are required. Accurate modelling of the pre-requisite

parameters at variable operating conditions of dryers will result in better predictability of results by such models. Moisture diffusivity during drying depends on many events that occur in the material such as liquid diffusion, vapour diffusion, molecular diffusion, hydrodynamic flow, capillary flow, surface diffusion, etc. (Hashemi et al., 2009) Hence, a generic term such as 'effective moisture diffusivity' could be used to describe the mechanism of moisture movement in a biological material. This movement of moisture is usually determined by incorporating Fick's law of diffusion into drying experiments (Bourassa et al., 2015a). In most drying problems, one-dimensional flow approach is used to simplify transient transfer (Li et al., 2014). The dependency of effective moisture diffusivity on moisture content (Azarpazhooh and Ramaswamy, 2012; Rizvi, 2005) and temperature (Da-Silva et al., 2012; Koukouch et al., 2017) is a contentious issue that has been studied by many researchers (Kittiworrawatt and Devahastin, 2009; Rahman and Kumar, 2011; Srikiatden and Roberts, 2006; Suvarnakuta et al., 2007). Some researchers believe that the diffusion coefficient is independent of moisture during the first falling drying rate period (Rovedo et al., 1995). This theory is based on Arrhenius type relationship of diffusivity where the temperature during drying describes the effective moisture diffusivity. The assumption of the average temperature of drying media equal to that of the material in the Arrhenius equation (Ah-hen et al., 2013; Thorat et al., 2012) has been questioned by its critics, especially in the case where a temperature gradient is present in a sample (Srikiatden and Roberts, 2006; Vaccarezza et al., 1974). In practice, it is difficult to measure the local temperature of the sample as drying progresses. Hence, it is generally assumed that the average sample temperature is equal to that of the temperature of the

drying medium. Therefore, modelling the effective diffusivity as a function temperature of the drying medium instead of the sample is apparent (Srikiatden and Roberts, 2006).

The present paper is a continuation to a previous study on determining the pre-requisite parameters for numerical modelling of SS drying of DSG pellets where a section was devoted to the thermo-physical properties of DSG pellets at variable moisture and temperature (Ramachandran et al., 2017c). The present study summarizes the results of the research on the effective moisture diffusivity and activation energy of DSG pellets at different operating conditions of SS drying. The main objective of this paper is to determine the effect of SS temperature and velocity, and distillers' soluble (CDS) concentration in the DSG on the effective moisture diffusivity and activation energy of DSG pellets. Additionally, a model is developed to predict the effective moisture diffusivity of DSG pellets during SS drying.

4.3 Materials and method

4.3.1 Sample preparation

The raw materials used for the present study was a by-product mixture of corn and wheat (9:1) stillage. The stillage was obtained from a local ethanol plant in Manitoba (Mohawk Canada Limited, a division of Husky Oil Limited, Minnedosa, MB). It was then stored in a chest freezer at -15°C in sealed plastic pails. The stillage was thawed overnight at room temperature and thereafter centrifuged at a relative centrifugal force of 790 g using a Sorvall General Purpose, RC-3 centrifuge (Thermo Scientific Co., Asheville, NC). The centrifuge was operated, with four sample bowls of 1000 mL capacity (filled approximately 75% of volume) rotating at a speed of 2200 rpm for 10 minutes. After centrifugation, the supernatant liquid (excess water with a very small amount of mashed grain soluble) was

poured out of the bowl. The semi-solid soluble fraction (distillers' solubles) and the coarse grain fraction were separated manually with a spoon. The centrifugation trials were repeated 10 times to determine the percentage composition of the raw sample in terms of coarse grain fraction, distillers' solubles, and supernatant liquid (Ramachandran et al., 2017). The mass of the separated coarse grain fraction, distillers' solubles, and liquid was recorded for each trial. The average mass fraction of the coarse grain fraction, distillers' solubles, and supernatant liquid were 49.5 ± 0.5, 9.5 ± 0.5, and 40.5 ± 0.5% w/w, respectively. The separated fractions were placed in airtight air tight polyethylene bags (2 Gauge mils thickness) of 250 g capacity of 250 g capacity and stored in a freezer at -15°C. Prior to the experimental trial, a bag was taken out of the freezer and allowed to thaw at room temperature for 2 h.

4.3.2 Pre-treatment and mixing

The initial moisture content of the coarse grain fraction and the solubles were determined using the air-oven drying method (AACC Method, 2000) using a laboratory oven (Thermo Electron Corporation, Waltham, MA) at 135°C for 2 h (Ramachandran et al., 2017a, 2017b). The average moisture content of whole stillage before centrifugation, coarse grain fraction, and distillers' solubles after centrifugation, were 89.2 ± 0.05, 77.8 ± 0.08 and 82.9 ± 0.1% wb, respectively. To prepare the different percentage mixture of distillers' solubles and coarse grain, calculated amounts of solubles were added to a known mass of coarse grain fraction of DSG. Three sets of DSG samples were prepared with 0, 10, and 30% (w/w) of distillers' solubles. The sample with 0% solubles was kept as a control sample. The moisture content of each mixture was also measured using standard air-oven drying method (AACC Method, 2000). Each of these wet mixtures was gently mixed using a spatula for about 2 -3

min. The mixed samples were dried in a laboratory oven at a low temperature (60 ± 5°C) to ensure that the properties of the samples are not altered (Stroem et al., 2009). About 20 g of mixture to produce 4–5 pellets was prepared at a time to prevent excessive drying during storage (Bourassa et al., 2015a). Each composition of the sample (with 0, 10, 30% solubles) was dried to obtain two different moisture contents (25 and 35%). The selection of moisture content was done based on the stability of compacted DSG pellets for the selected composition (Johnson et al., 2013b; Ramachandran et al., 2017a). The prepared samples were stored in a freezer at −15°C.

4.3.3 Densification

A compaction unit with a cylindrical die, a die holder and a plunger were used for producing individual pellets for the study. The compaction unit was attached to an Instron universal testing machine (Model 3366 Universal Testing Systems, Instron Corp., Norwood, MA). The DSG pellets were made by placing approximately 4.25 ± 0.05 g of thawed raw material at given moisture content and percentage solubles in a cylindrical steel die of 12.2 ± 0.01 mm and 80 ± 0.01 mm diameter and length, respectively. The cylindrical die was secured in place by using a die holder. A cylindrical plunger of 12.08 ± 0.01 mm diameter and 83.65 ± 0.01 mm length was attached to a load cell of 10 kN connected to the upper jaw of the universal testing machine. The sample was compacted at a constant load with a plunger speed of 50 mm/min until the maximum load reached 6820 N (60.3 ± 0.1 MPa). The formed pellet was then held at that constant load for 300 s by retaining the plunger inside the die to maintain a constant pressure on the formed pellet and to reduce the spring-back effect (Bourassa et al., 2015b; Ramachandran et al., 2017a; Tumuluru et al., 2010). The plunger was then released from the die and the cylindrical die was separated from its die holder. The pellet was then

pushed out of the die using the plunger. The same densification process was repeated to make pellets of different composition of distillers' solubles and moisture contents as per the experimental design.

4.3.4 Superheated steam drying unit

The SS drying unit was designed and built at the Department of Biosystems Engineering, University of Manitoba, Canada. The system consists of a water tank, boiler, superheater, drying chamber, and heat exchanger (Fig. 1). The function of each component in the system has been explained by Cenkowski et al.(2007) and Ramachandran et al.(2017b). The drying chamber walls were heated by means of strip heaters mounted on the outer wall of the drying chamber, which was further insulated by a cellular glass and an outermost layer of a steel sheet. The wall was maintained at a temperature of about 3 ± 0.5°C above the operating temperature. An array of thermocouples at different heights inside the chamber recorded SS temperature as shown in Figure 4.1. A thin perforated sample holding tray made of aluminum was hung inside the SS drying chamber using a thin metal wire of 0.5 mm diameter. The metallic wire connected to the sample holding tray was attached to the under-weighing hook of a precision weighing balance (Sartorius ENTRIS 423-1S, Sartorius, Germany) placed above the SS drying chamber (Fig. 1). The exposed portion of the wire above the SS chamber was heated with a small electric heater resting on the top of the SS chamber to avoid any condensation on the wire. The position of the holding tray was adjusted in such a way that the sample was at the center of the drying chamber.

4.3.5 Drying experiments

To avoid steam condensation on the tray and the inner walls of the drying chamber, the drying chamber with the empty holding tray was pre-heated to the desired operating temperature

(120, 150, 180°C). For safe loading and unloading of the sample, a flow diversion valve was attached to the main-steam line of the SS drying system which enabled the operator to bypass the SS from the drying chamber to the water tank (Fig. 1). It also enabled the measurement of the true mass of the sample without being affected by the upward lifting force of SS. For drying experiments, the diversion valve was set to allow steam to by-passed the drying chamber. Next, a single DSG pellet of 4.25 ± 0.05 g was placed in the preheated holding tray by opening the glass door located at the front of the drying chamber. To eliminate the steam leakage, the glass door was secured tightly with a silicon gasket of 3 mm thickness. The steam was then re-diverted to the drying chamber. The mass of the sample as well as the SS temperature inside the chamber during drying was recorded at regular intervals (3 s) with the help of a Visual Basic computer program. Each drying experiment was continued until the recorded mass of the sample reached equilibrium, i.e. when the mass change over drying time was not more than 0.01 g. At the end of the test, the final mass of the sample and the dimensions of the pellet were measured for further calculations. The change in mass of the pellet over the drying time was plotted to determine the equilibrium point for the conditions established with SS. The drying characteristic curves of the pellets were developed from the experimental data. An average of about 15-20 data points (moisture content) of the drying characteristic where the curve plateaued was used as the equilibrium moisture content (Ramachandran et al., 2017a).

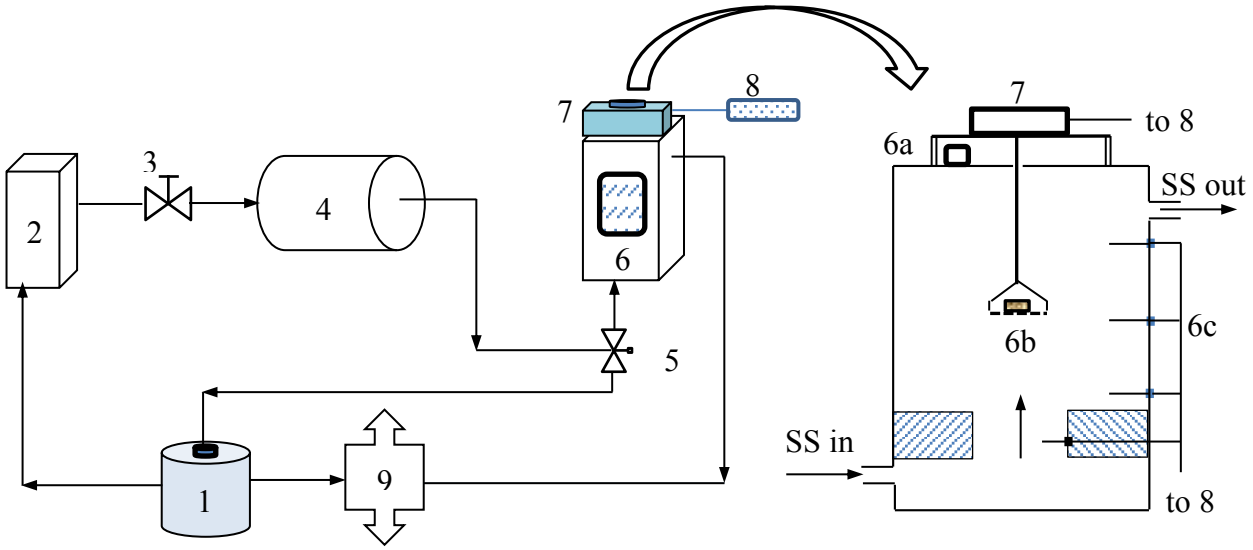

Figure 4.1 Schematic diagram of SS drying system and an enlarged cross-sectional view of the drying chamber; where, 1- Water tank, 2- Boiler, 3 and 5- Flow control valves, 4- Super-heater, 6- Drying chamber, 7- Weighing balance, 8- Data acquisition unit, 9- Heat exchanger, 6a- Heater, 6b- Sample holding tray with sample, and 6c- thermocouple assembly. (Adapted from Cenkowski et al.(2007)

The experiments were repeated in triplicate for each distillers' solubles concentration (0, 10, 30% w/w), initial moisture content (25 and 35% wb), different SS temperatures (120, 135, 150, 165 and 180°C), and SS velocities (0.5, 1.0, and 1.5 m/s) inside the chamber and at the cross-section where the sample was located. The drying experiment lasted about 1-2 h depending on the time required for the pellet to reach equilibrium moisture content, which in turn was dependent on the initial moisture content, composition of pellet, and SS operating conditions. To determine the lifting force of SS on the holding tray and the pellet, a separate set of experiments was conducted in triplicate for each operating condition selected for the drying experiments. During these experiments, SS was diverted from the drying chamber for approximately 20 s at time intervals of 2, 5, 15, 30, 45 min, and 1h and the mass of the sample without the effect of lifting force of SS was recorded. The difference in mass readings, with and without the SS, was calculated as the lifting force on the pellet and the holding tray. The lifting force values were used to determine the true mass of the pellet during actual drying experiments for developing the drying characteristics (Bourassa et al., 2015b; Pronyk et al., 2008c).

In order to compare the diffusivity of pure solubles with that of the DSG pellets with different soluble concentrations, a separate set of drying experiments was conducted with the pure distillers' soluble. These experiments were done by placing a thin layer (approximately 3 ±1 mm thickness) of wet solubles with a moisture content of 83% on a perforated sample tray. The experiments were repeated for all the SS temperatures and velocities as used for the drying trials of DSG pellets.

4.3.6 Dimensional changes

To determine the dimensional changes of the pellets when subjected to SS, a separate set of experiments was conducted with DSG pellets with different levels of distillers' solubles (0, 10, and 30% w/w) and initial moisture contents (25 and 35% wb) for all the operating conditions of the SS drying system (the same as used in the drying experiments). Each test was also done with a single pellet of known dimensions and approximately the same mass and dimension as that of the pellet used for the drying experiments. The pellet was subjected to SS drying for about 0.5, 1, 2, 5, 20, 45, and 60 min. Any pellets that disintegrated during drying were not used in further calculations for determining the volumetric change. Only freshly compacted pellets were used for each of the aforementioned SS drying time. This method prevents the alternative cooling and heating of the pellet when the same pellet is used again (Bourassa et al., 2015a). The after-treatment dimensions of the pellet were measured using Vernier calipers with an accuracy of 0.01 mm. The initial pellet dimensions for these experiments were approximately the same as that of the drying experiments (as described in section 2.5). Therefore, the final dimensions of the pellet used in the drying tests were used to determine the overall percentage volumetric change of the pellet at the end of drying time, for each operating condition.

4.3.7 Effective moisture diffusivity

The criterion for choosing the concept of a finite cylinder or an infinite cylinder for solving drying problems depends on its dimensions (Pereira and Silva, 2014). Since the pellet dimensions did not meet the criterion of infinite geometry (i.e. length to radius ratio is smaller than 5), the finite cylinder model was used for determining the effective diffusivity during drying (Erdoğdu and Turhan, 2006; Pacheco-aguirre et al., 2014). The effective

moisture diffusivity of the cylindrical pellets was hence determined by using the solution for the mass transport equation (Fick's law of diffusion) in a finite cylinder (Pabis et al., 1998). The instantaneous effective diffusivity of the DSG pellet was determined by using the optimum solution of the Fourier number Fo_m values (Crank, 1975):

$$MR(t) = \frac{M_{(t)} - M_e}{M_{(0)} - M_e} = \sum_{n=1}^{\infty}\sum_{m=1}^{\infty} \beta_n \beta_m \exp\left[-\left(\mu_n{}^2 + \mu_m{}^2 k_t{}^2\right) Fo_m\right] \quad (4.1)$$

Where, $MR_{(t)}$ is the instantaneous moisture ratio and $M_{(t)}, M_{(0)}, M_e$ are the instantaneous, initial, and equilibrium moisture content;

$$\beta_n = \frac{4}{\mu_n{}^2}, \text{ and } \beta_m = \frac{2}{\mu_m{}^2}, \quad \mu_m = (2m-1)\frac{\pi}{2}, J_0(\mu_n) = 0, \text{and} \quad k_t = \frac{r_t}{L_t}$$

Where, μ_n are the roots of the Bessel function of first kind of the order zero, and the values of μ_n are defined in Equation 4.1 for n=1 to 10 are 2.4048, 5.5201, 8.6537, 11.7915, 14.4309, 18.0711, 21.2116, 24.3525, 27.4935, 30.6346, respectively; r and L are the instantaneous radius and length of the DSG pellet;

$$D_{eff} = \frac{Fo_m r_t{}^2}{t} \quad (4.2)$$

Where, D_{eff} is the effective moisture diffusivity in m^2/s, r_t is the instantaneous radius of the DSG pellet. T is the drying time in s. As the initial condensation accompanies heat generation, the heat flux into the pellet is larger in the initial stages of SS drying when compared to air drying (Inoue et al., 2010; Kondjoyan and Portanguen, 2008; Pakowski et al., 2011). This increase in temperature might be visible throughout the drying stage, causing a shorter or negligible constant drying rate period in SS drying, especially for higher SS temperatures (Inoue et al., 2010; Iyota et al., 2008; Pakowski and Adamski,

2011a; Ramachandran et al., 2017a). The resistance to steam permeation is negligible once the condensation and restoration period is completed. Hence, the water within the pellet is taken to the evaporation front at the boiling temperature corresponding to the external pressure (Ezhil, 2010; Iyota et al., 2001). By considering the first term of Equation 4.1 with an assumption that the rest of the terms are negligible (Motevali et al., 2012; Taheri-garavand et al., 2011; Touil et al., 2014), the equation can be rewritten as:

$$MR_{(t)} = \beta_{n1}\beta_{m1}\, exp\left[-\left({\mu_{n1}}^2 + {\mu_{m1}}^2\left(\frac{r_0}{L_0}\right)^2\right)\frac{D_{eff}t}{{r_0}^2}\right] \quad (4.3)$$

The logarithmic transformation of Equation 4.3 gives a linear relation:

$$\ln\left(MR_{(t)}\right) = \ln(\beta_{n1}\beta_{m1}) - \left[\left({\mu_{n1}}^2 + {\mu_{m1}}^2\left(\frac{r_0}{L_0}\right)^2\right)\frac{D_{eff}t}{{r_0}^2}\right] \quad (4.3a)$$

The slope'*k*'of the linear plot of $\ln\left(MR_{(t)}\right)$versus drying time'*t*' is given by:

$$k = \left[\left({\mu_{n1}}^2 + {\mu_{m1}}^2\left(\frac{r_0}{L_0}\right)^2\right)\frac{D_{eff}}{{r_0}^2}\right] \quad \text{where, } \mu_{n1} = 2.4048 \text{ and } \mu_{m1} = 1.57. \quad (4.4)$$

The correlation between the temperature and the effective moisture diffusivity (from Equation 4.4) can be expressed by using Arrhenius type equation (Equation 4.3) (Babalis and Belessiotis, 2004; Chayjan et al., 2013; Chen et al., 2013; Hamawand, 2013a; Kaya et al., 2006; Koukouch et al., 2017; Sa-Adchom et al., 2011a).

$$D_{eff} = D_o\, exp\left(-\frac{Ea}{RT}\right) \quad (4.5)$$

Where, D_o is the pre-exponential factor and Ea is the activation energy in kJ/mol. The activation energy is a measure of moisture particles bonding. If the activation energy is high, then the energy required to break the moisture particle bond is also high and hence require longer time to remove moisture form the solid. The value of Ea and D_o were determined using the slope and intercept of a semi-log plot of average effective diffusivity

and inverse of corresponding drying medium temperature (Golpour et al., 2017; Mirzaee, Rafiee, Keyhani, & Emam-Djomeh, 2009; Zielinska & Cenkowski, 2012). The predicted effective diffusivity from Equation 4.3 - 4.4 was then modified to include the effect of moisture content too (Castell-Palou et al., 2012) by fitting the predicted values of the effective diffusivity (Equation 4.3) to the experimental values (Equation 4.1 and 4.2). A non-linear regression analysis for experimental values of effective diffusivities was done by using Levenberg-Marquardt optimization algorithm (Rahman and Kumar, 2011) in MatLab (R2014b, Mathworks, USA). The value of D_o and Ea obtained from Equation 4.5 was chosen as an initial guess for optimization.

$$D_{eff} = a\ exp\left[\left(-\frac{Ea^*}{RT}\right) + c\ MC_t\right] \tag{4.6}$$

Where, *a* and *c* are the model constants and Ea^* is the adjusted activation energy using Levenberg-Marquardt optimization.

4.3.8 Uncertainty analysis

The uncertainty in the calculated results (the propagated error) of the measured quantities was determined to analyze the accuracy of measurements during the experiments (Khanali et al., 2016). The combined uncertainty of measurement of a quantity can be expressed as:

$$\Delta f = \sqrt{\left(\frac{\partial f}{\partial x_1}\Delta x_1\right)^2 + \left(\frac{\partial f}{\partial x_2}\Delta x_2\right)^2 + \cdots + \left(\frac{\partial f}{\partial x_n}\Delta x_n\right)^2} \tag{4.7}$$

Where, Δf is the error of the quantity f; Δx_1, Δx_2,…, Δx_n are the error/uncertainty in the independent variables x_1, x_2,…, x_n, respectively. The derived quantities such as moisture content (M) in kg of water per kg of dry mass were determined by following equation obtained from Equation 4.7b:

$$\Delta M = \sqrt{\left(\frac{\partial M}{\partial m_w}\Delta m_w\right)^2 + \left(\frac{\partial M}{\partial m_d}\Delta m_d\right)^2} \quad (4.7a)$$

$$\Delta M = \sqrt{\left(\frac{1}{m_d}\Delta m_w\right)^2 + \left(\frac{m_w}{{m_d}^2}\Delta m_d\right)^2} \quad (4.7b)$$

Where m_w and m_d are the mass of water and dry mass in kg, respectively. The model coefficient and constant such as the activation energy, pre-exponential factor were assumed to be the maximum standard deviation obtained for the triplicate trials.

4.3.9 Statistical analysis

The effect of process parameters viz. the temperature and velocity of SS, the moisture content of the samples, and the mass fractions of distillers' solubles on shrinkage and effective moisture diffusivity were studied using statistical software (SAS version 9.4, SAS Institute Inc., Cary, NC). A factorial ANOVA and a regression analysis with multiple independent variables (temperature, velocity, moisture content, and solubles mass fractions) were conducted with data obtained from a full factorial experimental design. The model parameter was determined using Levenberg-Marquardt optimization. The quality of fit was analyzed with the help of coefficient of determination (R^2) and Root Mean Square Error (RMSE). The mean relative percentage deviation of predicted values from the experimental values was also calculated.

4.4 Results and discussion

4.4.1 Uncertainty of measured and derived values

The uncertainty of measured quantities and the combined uncertainties of the derived quantities were calculated using Equation 4.7. Since all the drying experiments were conducted in three replications, the combined uncertainties for the derived quantities such as moisture ratio, volumetric changes, effective moisture diffusivity, and activation energy were

calculated using the average values of measured independent variables. The overall combined uncertainty for these quantities is shown in Table 4.1. The uncertainty values of both measured and derived quantities were found to be less than 10%.

Table 4.1 Uncertainties of measured and derived quantities

	Parameter	Unit of measurement	Uncertainty value
Measured quantities	Temperature	°C	0.1
	Mass	g	0.01
	Velocity	m/s	0.05
	Time	s	0.02
Derived quantities	Moisture content	kg of water/kg of total mass	2.12%
	Moisture ratio	-	3.20 %
	Volumetric Change	%	2.91 %
	Effective moisture diffusivity	m^2/s	5.01 %
	Activation energy	J/mol	5.40 %

4.4.2 Dimensional changes of DSG pellet

Unlike in the case of drying agricultural materials where a volumetric shrinkage is common, the SS drying of DSG pellets experienced longitudinal and lateral expansion. The volumetric changes during drying cannot be neglected as it affects the moisture migration and in turn the effective moisture diffusivity (Hashemi et al., 2009; J. Li et al., 2014; Touil et al., 2014; Zielinska & Cenkowski, 2012). A similar result was reported by Johnson et al.(2014b). They found that the longitudinal expansion of DSG pellets over the period of SS drying was found to be greater than the lateral expansion. This was due to the relaxation of stresses stored in the pellet structure and caused by SS (Taheri-Garavand et al., 2011). The experimental results showed that the rate of expansion was about 50% more during the condensation period when compared to the later falling drying rate period. The maximum volumetric expansion noted

during initial condensation was in the range of 140-152%. This is because condensed water is adsorbed into the pellet until the evaporation front coincides with the adsorbed moisture front. This expansion of the pellet then diminishes as drying proceeds and moisture evaporation causes shrinkage.

The volumetric expansion was found to be increasing (approx. 42%) with the decrease in SS temperature and velocity irrespective of the pellet moisture content (Figure 4.2) with an R^2 value of 0.92. This is due to fact that the initial condensation decreases with SS temperature and velocity and the evaporation front develops at a faster rate due to increased heat transfer rates (Ramachandran et al., 2017b). The volumetric expansion was found to be decreasing (a maximum of 31%) with increasing soluble concentration in the pellet (Figure 4.2) which conforms to the trend reported by Johnson et al. (Johnson et al., 2015). The finer particle size and higher starch content of the distillers' solubles add more binding force between the particles in the compacted pellet. This increase in the binding force minimizes the volumetric expansion during SS drying. Ramachandran et al. (2017c) also reported that the bulk porosity of dried distillers' solubles is less than that of the coarse grain fraction of DSG. Therefore, the addition of solubles improved the packing of particles in the DSG pellet minimizing the number of larger sized pores.

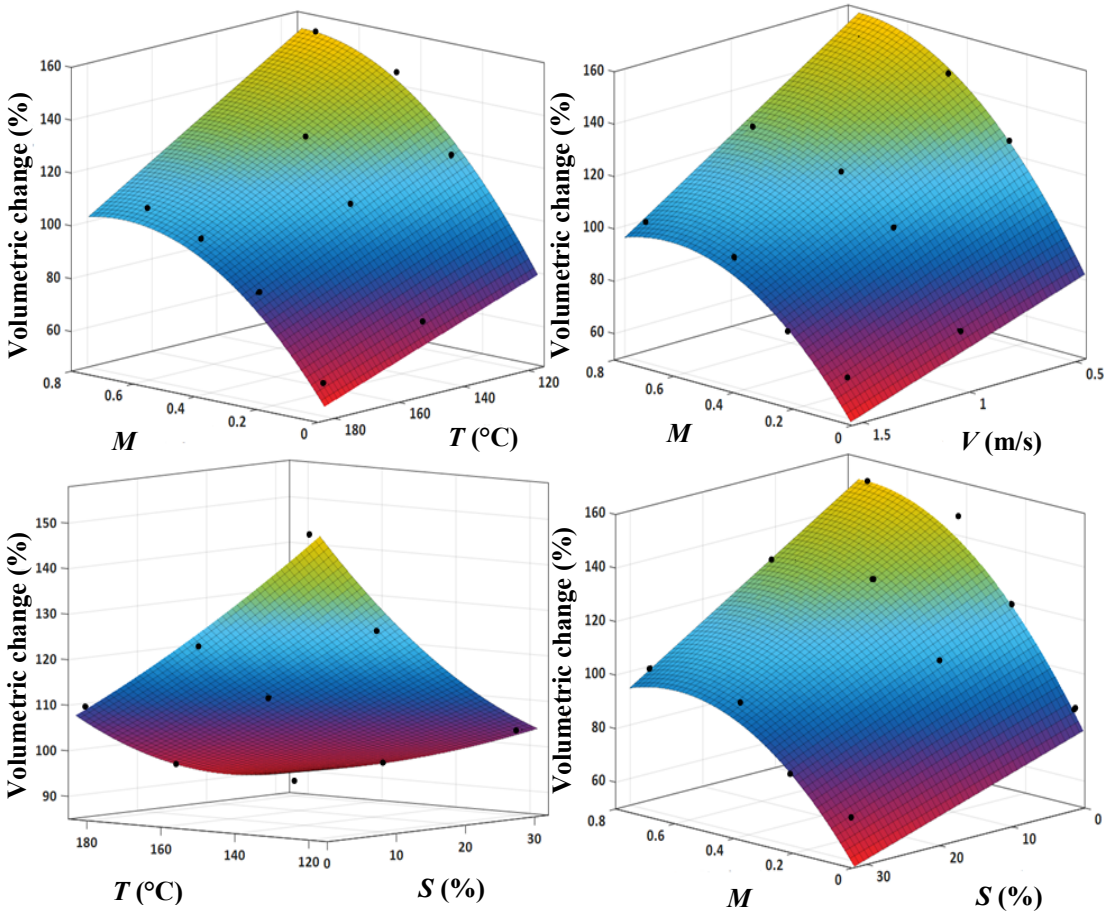

Figure 4.2 Effect of moisture content, SS temperature, SS velocity, and soluble mass fraction on percentage volumetric change of DSG pellets during SS drying; where SS - superheated steam, M-moisture content, T-SS temperature, *V* - SS velocity, and *S*- solubles concentration

4.4.3 Effective moisture diffusivity of DSG pellet

The experimental values of the effective moisture diffusivity of DSG pellets with different solubles concentration and operating conditions were in the range of $2.49 \times 10^{-9} – 17.9 \times 10^{-9}$ m^2/s. As there were no data on moisture diffusivity of DSG under hot air drying, the data on effective moisture diffusivity of wheat and corn kernels were used for a comparison. This

is because spent grain is a mixture of unfermented parts of wheat and corn kernels. The moisture diffusivities of wheat and corn under hot-air drying in a temperature range of 50-70°C were 3.89×10^{-11} to 1.78×10^{-10} and 4.87×10^{-11} to 8.6×10^{-11} m^2/s, respectively (Chayjan et al., 2011; Kahyaoglu et al., 2012). In a previous study on microwave assisted drying of wheat kernels, moisture diffusivity was observed in the range of 5.06×10^{-10} to 11.3×10^{-10} (Kahyaoglu et al., 2012). This can be attributed to the change in composition of spent grains when compared to whole grain and also a higher drying rate of SS over the other two methods. Both methods gave a lower effective moisture diffusivity range than the SS drying. The drying kinetics and the drying time of the pellets were found to be significantly affected by SS temperature and velocity with $P<0.05$ (Figure 4.3a). The effective diffusivity values calculated based on the drying kinetics (using Equation 4.1 and 4.2) also reflected the same effect. The experimental effective moisture diffusivity of DSG pellet was found to be increasing with an increase in SS temperature and velocity. A similar trend in diffusivity with temperature and velocity of drying medium was reported by other researchers (Golpour et al., 2017; Koukouch et al., 2017; Uddin et al., 2016). The effect of velocity on diffusivity was more predominant for the drying trials at higher SS temperatures (180°C) than at lower SS temperature (120°C Figure 4.3b). This might be caused by the increased heat transfer rates and decreased initial condensation with SS temperature and velocity. The experimental results showed that the value of effective moisture diffusivity during SS drying is also affected by the concentration of distillers' solubles in the DSG pellet (Figure 4. 4).

The addition of solubles minimized the volumetric expansion (Figure 4.2). The pellet undergoes a relaxation when subjected to SS due to the release of energy stored during compaction (Ramachandran et al., 2017b). This expansion was highest in the period of initial

condensation period, thereby increasing the porosity of the pellet (Bourassa et al., 2015a). Johnson et al.(Johnson et al., 2015) reported that the addition of solubles in the DSG pellet reduces the overall expansion of the pellet during initial condensation period. Since the particle-particle bonding force counteracts the relaxation process, the increase in concentration of distillers' solubles in the pellet minimizes the relaxation. At the same time, the pellet with solubles generates more micro-porosity than the coarse grain pellets. These pores hold water during the initial condensation resulting in an increase in the drying time, especially during the falling rate drying period. The experimental drying characteristics show that the increase in the concentration of solubles in the pellet increased the drying time (34-39%) and the effective moisture diffusivity (Figure 4.4). This may be attributed to the increased moisture content inside the pellet. Hence, the addition of the solubles was limited to 30%, even though a further increase in solubles concentration could improve the pellet's volumetric stability (Johnson et al., 2015). Any further increase in solubles concentration increases the drying time (≥25%) and also leads to a greater stickiness during compaction (Johnson et al., 2013a).

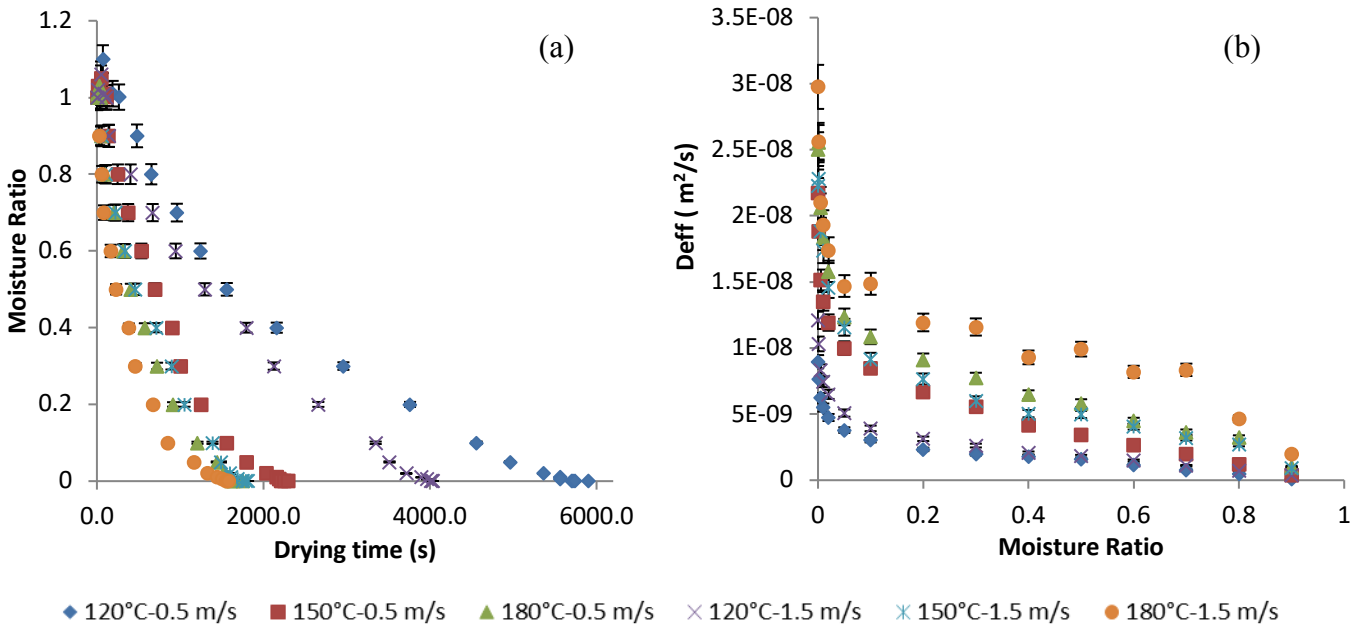

Figure 4.3 Effect of SS temperature and velocity on (a) drying kinetics and (b) instantaneous effective moisture diffusivity of DSG pellets with 0% solubles and 35% initial moisture content.

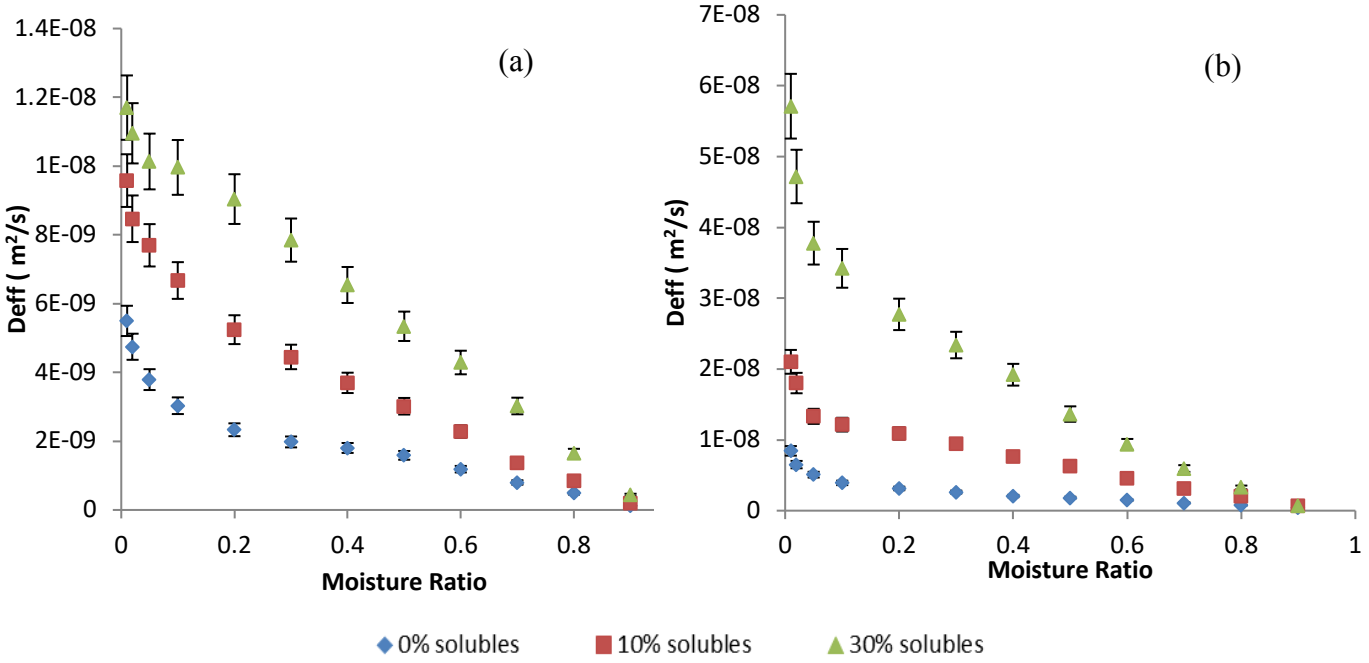

Figure 4.4 Effect of concentration of distillers' solubles on instantaneous effective moisture diffusivity of DSG pellets with 35% initial moisture content dried under SS at 180°C and (a) 0.5 m/s; (b) 1.5 m/s, respectively.

4.4.4 Prediction of effective moisture diffusivity

The coefficients of the mathematical model for effective moisture diffusivity as a function of temperature was determined first using Equation 4.5. The linear relationship between Ln(D_{eff}) and inverse SS temperature of DSG pellet with 0% solubles and 35% initial moisture is shown in Figure 4.5a. The predicted diffusivity values (Equation 4.5) were then compared with the average diffusivity values at respective SS temperatures (Figure 4.5b). These preliminary values of the coefficients (activation energy and pre-exponential factor) were used as a first approximation for the Levenberg-Marquardt optimization limits to obtain the coefficients of the model equation for effective moisture diffusivity as a function of temperature and moisture content (Equation 4.6). The modified values of activation energy and pre-exponential factor and the model coefficient for the moisture content were then compared with the calculated values of instantaneous effective moisture diffusivities (Equation 4.1 and 4.2) using R^2 and RMSE values (Table 4.2). The maximum average RMSE error of the model coefficients for the selected operating conditions was 2.27×10^{-10} (≤10%). The effect of SS temperature and velocity on the predicted effective diffusivity coefficient of DSG pellet (using Equation 4.6) was also comparable to that of the experimental effective diffusivity values (Figure 4.6b). Predicted values also showed an increasing trend with increasing SS temperature and velocity. Similarly, the predicted effective moisture diffusivity was compared with the experimental effective moisture diffusivity of randomly selected average moisture contents of the DSG pellets (Figure 4.5). The comparison shows a good agreement where the effective moisture diffusivity decreases with moisture content (Figure 4.6a). In addition, the rate of an increase in effective moisture diffusivity with decreasing moisture content was found to improve with an increase in SS temperature. The effect of

drying parameters such as SS velocity, moisture content, and concentration (% w/w) of distillers' solubles was also reflected in the values of coefficients of independent variables in the model for predicting effective moisture diffusivity (Table 4.2).

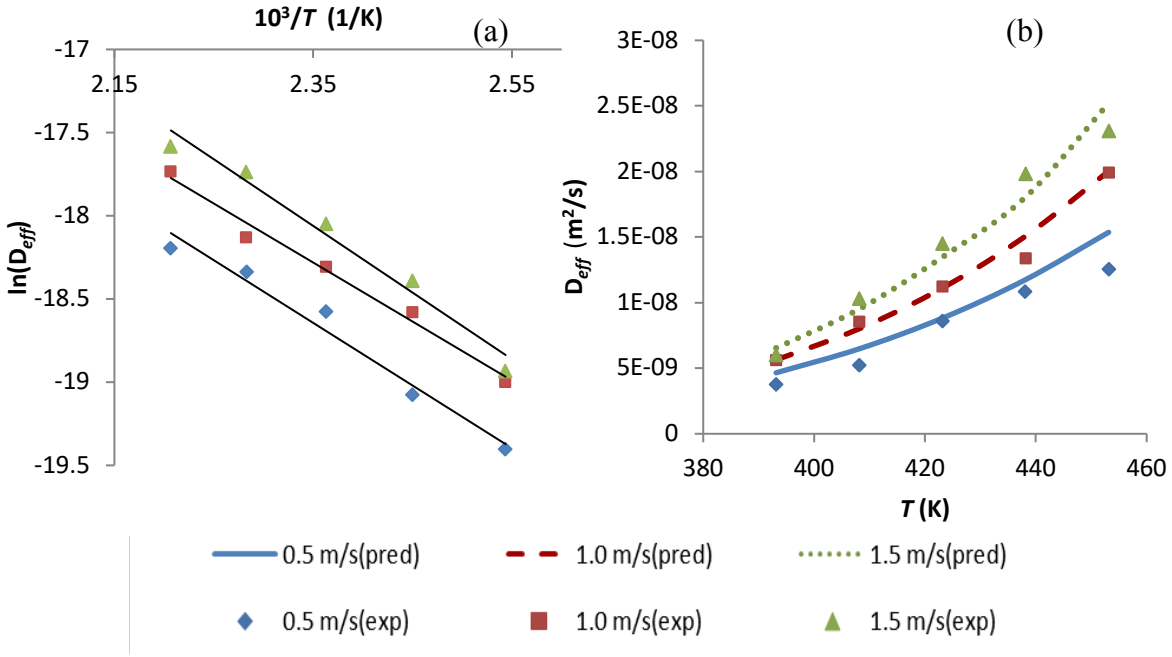

Figure 4.5 (a) Arrhenius plot of Ln(D_{eff}) versus inverse of SS temperature in K, (b) predicted and experimental effective diffusivity of DSG pellets with 0% solubles and initial moisture content of 35% wb at different SS temperature; where, D_{eff} - effective moisture diffusivity, T - temperature.

4.4.5 Activation energy

The activation energy for SS drying of DSG pellets with a different concentration of solubles and two initial moisture contents (25 and 35%) were compared for different SS velocities and different initial moisture contents (Figure 4.7). The activation energy of DSG pellets at different levels of SS velocity (0.5 – 1.5 m/s) was in the range of 20.90 - 38.52 kJ/mol. The values of activation energy obtained in the current research are comparable with those

obtained by Chayjan et al.(2011). They reported that the activation energy of the fluidized bed drying of high moisture corn when the temperature of the drying medium varied from 50 to 95°C was in the range of 18.57 - 50.74 kJ/mol. Similarly, the activation energy for hot air drying (64-75°C) of whole wheat kernels was in the range of 28.7 - 33.3 kJ/mol and 30.2 - 35.1 kJ/mol, based on the assumption of spherical and ellipsoidal shape, respectively (Kahyaoglu et al., 2012). The activation energy required for SS drying of DSG pellets showed an increasing trend with an increase in SS velocity and pellet's initial moisture content (Figure 4.7). Since the self-diffusion of moisture is a thermally agitated process, an increase in velocity of drying medium causes an increase in energy consumption (Da-Silva et al., 2013; Koukouch et al., 2017). The concentration of distillers' solubles in the pellet also showed a significant effect on the activation energy ($P<0.05$). The presence of solubles in the pellet increases the density of the pellet as solubles are finer particles than coarse distillers' spent grain causing a better inter-particle bonding (Ramachandran et al., 2017c) and micro-porosity. This justifies the increased water holding capacity of the pellet with the addition of solubles. The activation energy was also found to be increasing with an increase in the concentration of solubles since; more energy is utilized for diffusion of these water particles in the micro-pores (Figure 4.7).

Table 4.2 Estimated values of model constants of the effective moisture diffusivity function of DSG pellets with distillers' solubles (% w/w) under different superheated steam velocities. (The quantities have an uncertainty of measurement < 10%).

Initial *M* (% wb)	Solubles (% w/w)	Velocity (m/s)	a	Ea* (kJ/mol)	*c*	R^2
25	0	0.5	3.08×10^{-6}	21.00	-1.89	0.81
25	0	1.0	8.14×10^{-6}	23.11	-2.15	0.8
25	0	1.5	2.85×10^{-5}	25.4	-3.55	0.76
25	10	0.5	3.12×10^{-5}	29.92	-3.58	0.82
25	10	1.0	9.62×10^{-5}	31.83	-5.21	0.79
25	10	1.5	2.11×10^{-4}	33.42	-5.75	0.86
25	30	0.5	1.21×10^{-4}	33.53	-5.56	0.90
25	30	1.0	3.43×10^{-4}	35.02	-7.17	0.88
25	30	1.5	9.90×10^{-4}	37.26	-8.13	0.77
35	0	0.5	2.77×10^{-5}	29.61	-6.14	0.84
35	0	1.0	3.01×10^{-4}	31.94	-7.04	0.86
35	0	1.5	8.93×10^{-4}	33.23	-7.48	0.87
35	10	0.5	4.82×10^{-5}	31.81	-7.01	0.80
35	10	1.0	8.23×10^{-4}	32.96	-9.11	0.83
35	10	1.5	2.55×10^{-3}	34.52	-9.24	0.89
35	30	0.5	6.89×10^{-5}	34.43	-7.94	0.76
35	30	1.0	8.16×10^{-4}	36.18	-9.15	0.78
35	30	1.5	3.85×10^{-3}	38.55	-10.37	0.75
83	100	0.5	1.12×10^{-3}	42.01	-1.4	0.82
83	100	1.0	9.21×10^{-3}	43.35	-1.66	0.90
83	100	1.5	5.80×10^{-2}	44.05	-1.86	0.90

- *a* and *c* are the model constants, *M* is the moisture content, and Ea^* is the adjusted activation energy, R^2 is the coefficient of determination.

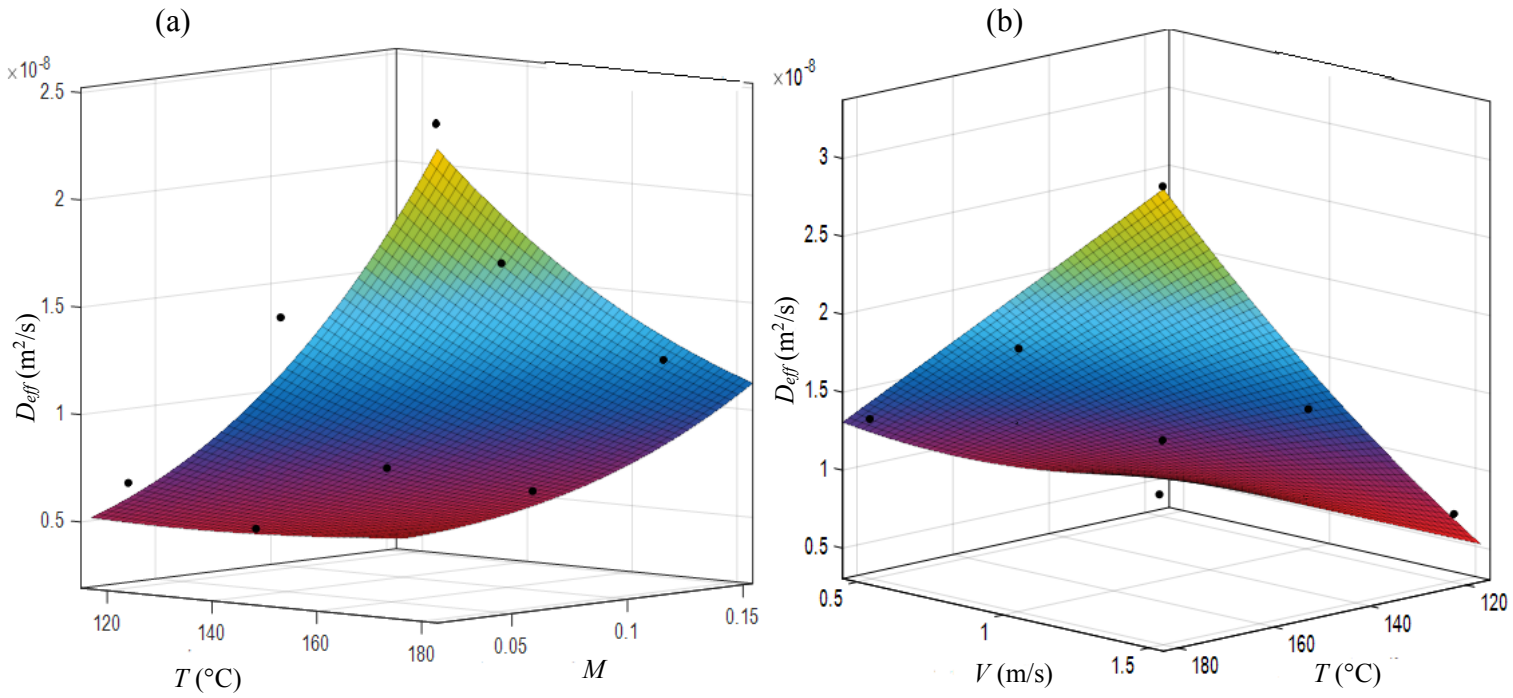

Figure 4.6 The predicted effective moisture diffusivity of DSG pellets (with 30% solubles) at various moisture contents and at different SS velocity and temperature; where, D_{eff} is the effective moisture diffusivity, T and M, are the temperature and moisture content of the pellet, respectively.

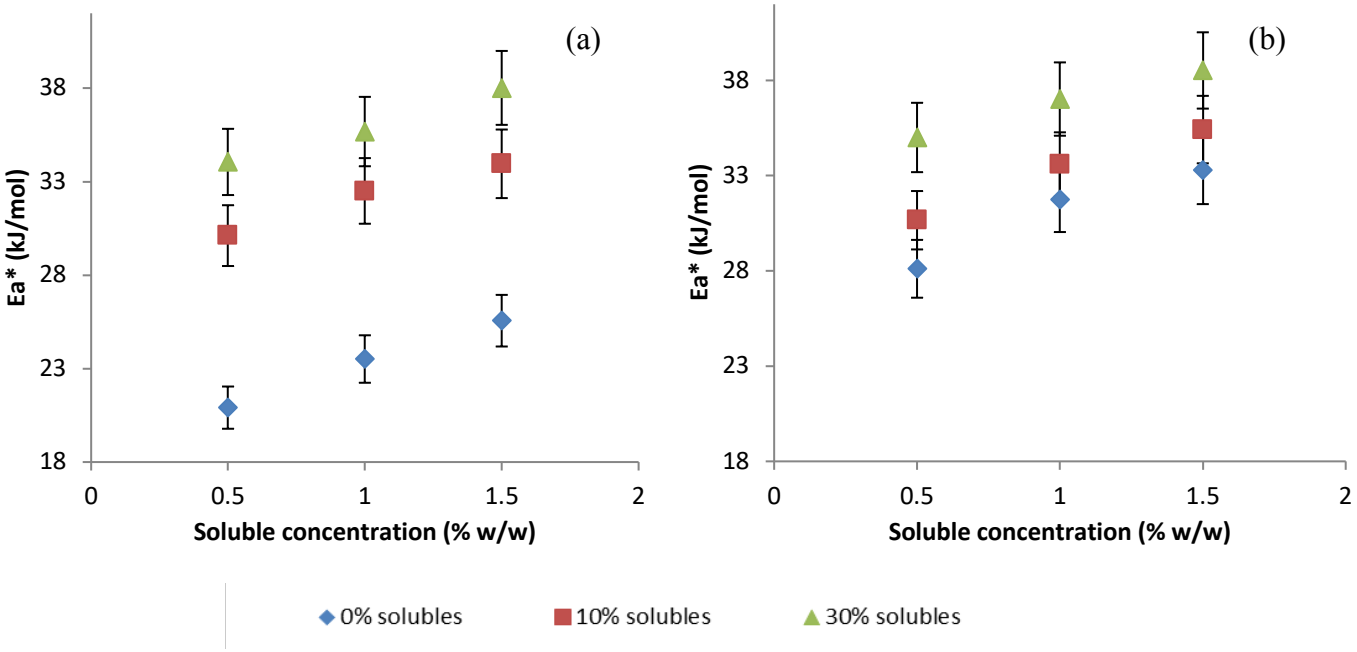

Figure 4.7 Effect of SS velocity on activation energy of DSG pellets with various soluble concentrations at (a) 25% and (b) 35% initial moisture content; where, Ea* is the adjusted activation energy using Levenberg-Marquardt optimization.

4.5 Conclusions

This work presents a mathematical model to estimate the effective moisture diffusivity of distillers' spent grain pellets with different mass fractions (0-30%) of distillers' solubles, dried using SS. The prediction results showed good agreement (RMSE 2.27×10^{-10} and MRP deviation ≤10%) with the experimental values of effective moisture diffusivity. The volumetric expansion of DSG pellets was found to decrease with an increase in solubles mass fractions. The major conclusions of the study conducted at different SS operating conditions (SS temperatures of 120, 135, 150, 165, and 180°C and SS velocities of 0.5, 1.0, and 1.5 m/s) are as follows:

- Unlike other biological materials, the compacted DSG pellets experienced volumetric expansion during SS drying. Maximum volumetric expansion (140-152%) happened in the initial condensation period and it decreased with drying time.
- The addition of distillers' solubles to the DSG reduced the percentage volumetric expansion (up to 32%) irrespective of the SS temperature and velocity.
- The temperature and velocity of the SS had a significant effect ($P<0.05$) on the moisture diffusivity and activation energy of DSG pellets of different initial moisture contents (25 and 35% wb) and soluble concentrations (0 - 30% w/w). The activation energy for DSG pellets at different SS velocities (0.5 – 1.5 m/s) was in the range between 20.90 - 38.52 kJ/mol. It increased with an increase in SS temperature, SS velocity and concentration of solubles.
- Although the addition of solubles to the DSG improves the stability of the pellet, it is not recommended to add solubles beyond 30% as it increases the drying time more than 25%.

Acknowledgements

The authors acknowledge the Natural Sciences and Engineering Research Council of Canada, Graduate Enhancement of Tri-Council Stipends, and University of Manitoba Graduate Fellowship for their financial support. The authors are also thanking the NSERC-funded summer research assistants, Jennifer Pienuita and Alain Jeffrey Lagasse.

References

1. AACC Method, 44-15A. (2000). Moisture-air-oven methods. St. Paul: Approved Methods of the American Association of Cereal Chemists.
2. Ah-hen, K., Zambra, C. E., Aguëro, J. E., Vega-gálvez, A., & Lemus-mondaca, R. (2013). Moisture diffusivity coefficient and convective drying modelling of murta (ugni molinae turcz): influence of temperature and vacuum on drying kinetics. *Food and Bioprocess Technology*, *6*, 919–930. doi.org/10.1007/s11947-011-0758-5
3. Azarpazhooh, E., & Ramaswamy, H. S. (2012). Modeling and optimization of microwave osmotic dehydration of apple cylinders under continuous-flow spray mode processing conditions. *Food and Bioprocess Technology*, *5*, 1486–1501. doi.org/10.1007/s11947-010-0471-9
4. Babalis, S. J., & Belessiotis, V. G. (2004). Influence of the drying conditions on the drying constants and moisture diffusivity during the thin-layer drying of figs. *Journal of Food Engineering*, *65*, 449–458. doi.org/10.1016/j.jfoodeng.2004.02.005
5. Bi, D., Chu, D., Zhu, P., Lu, C., Fan, C., Zhang, J., & Bao, J. (2011). Utilization of dry distiller'sgrain and solubles as nutrient supplement in the simultaneous saccharification and ethanol fermentation at high solids loading of corn stover. *Biotechnology Letters*, *33*, 273–276. doi.org/10.1007/s10529-010-0429-z
6. Bourassa, J., Ramachandran, R. P., Paliwal, J., & Cenkowski, S. (2015a). Drying characteristics and moisture diffusivity of distillers' spent grains dried in superheated steam. *Drying Technology*, *33*, 2012–2018. doi.org/10.1080/07373937.2015.1040883

7. Bourassa, J., Ramachandran, R. P., Paliwal, J., & Cenkowski, S. (2015b). Initial condensation during superheated steam drying and the effect of orientation of dsg pellets during the drying process. In *The canadian society of Bioengineering*. Retrieved from Paper No. CSBE15-054%0AInitial
8. Brochetti, D., Penfield, M. P., & Heim-edelman, M. F. (1991). Yeast bread containing distillers' dried grain dough development and bread quality. *Journal of Food Quality*, *14*, 331–344.
9. Castell-Palou, A., Váquiro, H. A., Cárcel, J. A., Rosselló, C., Femenia, A., & Simal, S. (2012). Mathematical modeling of moisture distribution and kinetics in cheese drying. *Drying Technology*, *30*(11–12), 1247–1255. doi.org/10.1080/07373937.2012.704465
10. Cenkowski, S., Pronyk, C., Zmidzinska, D., & Muir, W. E. (2007). Decontamination of food products with superheated steam. *Journal of Food Engineering*, *83*(1), 68–75. doi.org/10.1016/j.jfoodeng.2006.12.002
11. Chayjan, R. A., Parian, J. A., & Esna-Ashari, M. (2011). Modeling of moisture diffusivity, activation energy and specific energy consumption of high moisture corn in a fixed and fluidized bed convective dryer. *Spanish Journal of Agricultural Research*, *9*(1), 28–40.
12. Chayjan, R. A., Salari, K., Abedi, Q., & Sabziparvar, A. A. (2013). Modeling moisture diffusivity, activation energy and specific energy consumption of squash seeds in a semi fluidized and fluidized bed drying. *Journal of Food Science and Technology*, *50*(4), 667–677. doi.org/10.1007/s13197-011-0399-8
13. Chen, D., Liu, X., & Zhu, X. (2013). A one-step non-isothermal method for the determination of effective moisture diffusivity in powdered biomass. *Biomass and Bioenergy*, *50*, 81–86.
14. Crank, J. (1975). *The mathematics of diffusion*. *Clarendon Press* (2nd ed.) Bristol, England.
15. da- Silva, W. P., E-Silva, C. M. D. P. S., & Gama, F. J. A. (2014). Estimation of thermo-physical properties of products with cylindrical shape during drying : The coupling between mass and heat. *Journal of Food Engineering*, *141*, 65–73. doi.org/10.1016/j.jfoodeng.2014.05.010
16. Da-Silva, W. P., Farias, de O. V. S., Neves, G. de A., & De-Lima, A. G. B. (2012).

Modeling of water transport in roof tiles by removal of moisture at isothermal conditions. *Heat and Mass Transfer*, *48*, 809–821.

17. Da-Silva, W. P., e Silva, C. M. D. P. S., & Gomes, J. P. (2013). Drying description of cylindrical pieces of bananas in different temperatures using diffusion models. *Journal of Food Engineering*, *117*(3), 417–424. doi.org/10.1016/j.jfoodeng.2013.03.030
18. Doymaz, İ. (2009). An experimental study on drying of green apples. *Drying Technology*, *27*(October 2014), 478–485. doi.org/10.1080/07373930802686065
19. Erdoğdu, F., & Turhan, M. (2006). Analysis of dimensional ratios of regular geometries for infinite geometry assumptions in conduction heat transfer problems. *Journal of Food Engineering*, *77*(4), 818–824. doi.org/10.1016/j.jfoodeng.2005.08.008
20. Ezhil, C. (2010). Superheated steam drying of foods - A review. *World Journal of Dairy & Food Sciences*.
21. Fiasco, B. A., Rubenthaler, G., Borhan, M., & Dong, F. M. (1990). Baking properties of bread and cookies incorporating distillers' or brewer'sgrain from wheat or barley. *Journal of Food Science*, *55*(2), 424–429.
22. Golpour, I., Nejad, Z. M., Chayjan, R. A., Nikbakht, A. M., Guine, R. P. F., & Dowlati, M. (2017). Investigating shrinkage and moisture diffusivity of melon seed in a microwave assisted thin layer fluidized bed dryer. *Food Measure*, *11*, 1–11. doi.org/10.1007/s11694-016-9365-5
23. Hamawand, I. (2013). Drying steps under superheated steam: A review and modeling. *Energy and Environment Research*, *3*(2), 107–125. doi.org/10.5539/eer.v3n2p107
24. Hashemi, G., Mowla, D., & Kazemeini, M. (2009). Moisture diffusivity and shrinkage of broad beans during bulk drying in an inert medium fluidized bed dryer assisted by dielectric heating. *Journal of Food Engineering*, *92*(3), 331–338. doi.org/10.1016/j.jfoodeng.2008.12.004
25. Inoue, T., Iyota, H., & Nishimura, N. (2010). Prediction method for drying time of wet porous material in humid hot air and superheated steam. *Drying Technology*, *28*(5), 608–614. doi.org/10.1080/07373931003788650
26. Iyota, H., Inoue, T., Yamagata, J., & Nishimura, N. (2008). Effect of time-dependent humidity profiles from air to superheated steam on drying of a wetted starch sphere. *Drying Technology*, *26*(2), 211–221. doi.org/10.1080/07373930701831598

27. Iyota, H., Nishimura, N., Yoshida, M., & Nomura, T. (2001). Simulation of superheated steam drying considering initial steam condensation. *Drying Technology*, *19*(7), 1425–1440. doi.org/10.1081/DRT-100105298
28. Johnson, P., Cenkowski, S., & Paliwal, J. (2011). Bulk Density and angle of repose of Distiller's Spent Grain under different drying methods and soluble concentrations. In *The canadian society of Bioengineering, CSBE/SCGAB 2011 Annual Conference*. Winnipeg, Manitoba.
29. Johnson, P., Cenkowski, S., & Paliwal, J. (2013a). Compaction and relaxation characteristics of single compacts produced from distiller's spent grain. *Journal of Food Engineering*, *116*(2), 260–266. doi.org/10.1016/j.jfoodeng.2012.11.025
30. Johnson, P., Cenkowski, S., & Paliwal, J. (2013b). Superheated steam drying characteristics of single cylindrical compacts produced from wet distiller's spent grain. In *The canadian society of Bioengineering*. Retrieved from www.csbe-scgab.ca/docs/meetings/2013/CSBE13011.pdf
31. Johnson, P., Cenkowski, S., & Paliwal, J. (2014a). Analysis of the disintegration of distiller's spent grain compacts as affected by drying in superheated steam. *Drying Technology*, *32*(9), 1060–1070. doi.org/10.1080/07373937.2014.881849
32. Johnson, P., Cenkowski, S., & Paliwal, J. (2014b). Drying Technology: An International Journal Analysis of the Disintegration of Distiller's Spent Grain Compacts as Affected by Drying in Superheated Steam. *An International Journal*, *32*(9), 1060–1070. doi.org/10.1080/07373937.2014.881849
33. Johnson, P., Paliwal, J., & Cenkowski, S. (2015). Effect of solubles on disintegration of distiller's spent grain compacts during superheated steam drying. *Drying Technology*, *33*, 1–13. doi.org/10.1080/07373937.2014.967403
34. Kahyaoglu, L.N., Sahin, S., Sumnu, G., 2012. Spouted bed and microwave-assisted spouted bed drying of parboiled wheat. Food Bioprod. Process. 90, 301–308. https://doi.org/10.1016/j.fbp.2011.06.003
35. Kaya, A., Aydin, O., & Dincer, I. (2006). Numerical modeling of heat and mass transfer during forced convection drying of rectangular moist objects. *International Journal of Heat and Mass Transfer*, *49*(17–18), 3094–3103.
36. Khanali, M., Banisharif, A., & Rafiee, S. (2016). Modeling of moisture diffusivity,

activation energy and energy consumption in fluidized bed drying of rough rice. *Heat and Mass Transfer/Waerme- Und Stoffuebertragung*, *52*(11), 2541–2549. doi.org/10.1007/s00231-016-1763-z

37. Kittiworrawatt, S., & Devahastin, S. (2009). Improvement of a mathematical model for low-pressure superheated steam drying of a biomaterial. *Chemical Engineering Science*, *64*(11), 2644–2650. doi.org/10.1016/j.ces.2009.02.036
38. Kondjoyan, A., & Portanguen, S. (2008). Prediction of surface and "under surface" temperatures on poultry muscles and poultry skins subjected to jets of superheated steam. *Food Research International*, *41*(1), 16–30. doi.org/10.1016/j.foodres.2007.07.006
39. Koukouch, A., Idlimam, A., Asbik, M., Sarh, B., Bah, A., Ansari, O., & Zegaoui, O. (2017). Experimental determination of the effective moisture diffusivity and activation energy during convective solar drying of olive pomace waste. *Renewable Energy*, *101*, 565–574. doi.org/10.1016/j.renene.2016.09.006
40. Li, E., Lim, C., Cai, C., & Klesius, P. H. (2011). Growth response and resistance to streptococcus iniae of Nile Tilapia, Oreochromis niloticus, Fed Diets containing distiller'sdried grains with solubles. *Animal Feed Science and Technology*, *170*, 246–255. Retrieved from 10.1016/j.anifeedsci.2011.09.002
41. Li, J., Bennamoun, L., Fraikin, L., Salmon, T., Toye, D., Schreinemachers, R., & Léonard, A. (2014). Analysis of the shrinkage effect on mass transfer during convective drying of sawdust / sludge mixtures. *Drying Technology*, *32*(14), 1706–1717. doi.org/10.1080/07373937.2014.924136
42. Lyberg, K., Borling, J., & Lindberg, J. E. (2012). Ileal and total tract digestibility of wet and dried wheat distillers grain products in growing pigs. *Journal of Animal Science*, *90*, 131–133. doi.org/10.2527/jas53797
43. Mirzaee, E., Rafiee, S., Keyhani, A., & Emam-Djomeh, Z. (2009). Determining of moisture diffusivity and activation energy in drying of apricots. *Research in Agricultural Engineering*, *3*, 114–120.
44. Motevali, A., Abbaszadeh, A., Minaei, S., Khoshtaghaza, M. H., & Ghobadian, B. (2012). Effective moisture diffusivity, activation energy and energy consumption in thin-layer drying of Jujube (Zizyphus jujube Mill). *Journal of Agricultural Science and Technology*, *14*, 523–532.

45. Oba, M., Penner, G. B., Whyte, T. D., & Wierenga, K. (2010). Effects of feeding triticale dried distillers grains plus solubles as a nitrogen source on productivity of lactating dairy cows. *Journal of Dairy Science*, *93*, 2044–2052.
46. Pacheco-aguirre, F. M., Ladrón-gonzález, A., Ruiz-espinosa, H., García-alvarado, M. A., & Ruiz-lópez, I. I. (2014). A method to estimate anisotropic diffusion coefficients for cylindrical solids : Application to the drying of carrot. *Journal of Food Engineering*, *125*, 24–33. doi.org/10.1016/j.jfoodeng.2013.10.015
47. Pakowski, Z., & Adamski, R. (2011). On prediction of the drying rate in superheated steam drying process. *Drying Technology*, *29*(13), 1492–1498. doi.org/10.1080/07373937.2011.576320
48. Pakowski, Z., Adamski, R., & Kwapisz, S. (2011). Effective diffusivity of moisture in low rank coal during superheated steam drying at atmospheric pressure. *Chemical and Process Engineering - Inzynieria Chemiczna I Procesowa*, *33*(1), 43–51. doi.org/10.2478/v10176-012-0004-3
49. Penner, G. B., Yu, P., & Christensen, D. A. (2009). Effect of replacing forage or concentrate with wet or dry distillers' grains on the productivity and chewing activity of dairy cattle. *Animal Feed Science and Technology*, *153*, 1–10. doi.org/10.1016/j.anifeedsci.2009.05.006
50. Pereira, W., & Silva, C. M. D. P. S. (2014). Calculation of the convective heat transfer coefficient and thermal diffusivity of cucumbers using numerical simulation and the inverse method, *51*(9), 1750–1761. doi.org/10.1007/s13197-012-0738-4
51. Perussello, C. A., Mariani, V. C., & Amarante, Á. C. C. do. (2014). Thermophysical properties of okara during drying. *International Journal of Food Properties*, *17*(4), 891–907. doi.org/10.1080/10942912.2011.628430
52. Pronyk, C., Cenkowski, S., Muir, W. E., Lukow, O. M., Wyatt, J., & Nicholson, D. (2008). Effects of dough resting time and saturated steam pre-treatment on the textural properties of superheated steam processed instant asian noodles. *Canadian Biosystems Engineering / Le Genie Des Biosystems Au Canada*.
53. Popp, J., Harangi-Rákos, M., Gabnai, Z., Balogh, P., Antal, G., Bai, A., 2016. Biofuels and their co-products as livestock feed: Global economic and environmental implications. Molecules 21, 1–26. https://doi.org/10.3390/molecules21030285

54. Rahman, N., & Kumar, S. (2011). Evaluation of moisture diffusion coefficient of cylindrical bodies considering shrinkage during natural convection drying. *International Journal of Food Engineering*, *7*(1), 1–18. doi.org/10.2202/1556-3758.1352
55. Ramachandran, R. P., Akbarzadeh, M., Paliwal, J., & Cenkowski, S. (2017a). Three-dimensional CFD modelling of superheated steam drying of a single distillers' spent grain pellet. *Journal of Food Engineering*, *212*, 121–135. doi.org/10.1016/j.jfoodeng.2017.05.025
56. Ramachandran, R. P., Bourassa, J., Paliwal, J., & Cenkowski, S. (2017b). Effect of temperature and velocity of superheated steam on initial condensation of distillers' spent grain pellets during drying. *Drying Technology*, *35*(2), 182–192. doi.org/10.1080/07373937.2016.1166123
57. Ramachandran, R. P., Paliwal, J., & Cenkowski, S. (2017c). Thermo-physical properties of distillers' spent grain pellets at different moisture contents and condensed distillers' soluble concentrations. *Food and Bioprocess Technology*, *10*, 175–185. doi.org/10.1007/s11947-016-1807-x
58. Rizvi, S. S. H. (2005). Thermodynamic properties of foods in dehydration. In A. K. . D. and J. A. M. . A. . R. Syed S . H . Rizvi (Ed.), *Engineering Properties of Foods* (3rd ed., pp. 133–214). New York: Marcel Dekker: CRC press. doi.org/10.1201/9781420028805.ch7
59. Rovedo, C. O., Suarez, C., & Viollaz, P. E. (1995). Drying of foods: Evaluation of a drying model. *Journal of Food Engineering*, *26*, 1–12. doi.org/10.1016/0260-8774(94)00037-A
60. Sa-Adchom, P., Swasdisevi, T., Nathakaranakule, A., & Soponronnarit, S. (2011). Mathematical model of pork slice drying using superheated steam. *Journal of Food Engineering*, *104*(4), 499–507. doi.org/10.1016/j.jfoodeng.2010.12.025
61. Salim, H. M., Kruk, Z. A., & Lee, B. D. (2010). Nutritive value of corn distillers dried grains with solubles as an ingredient of poultry diets : A review. *World's Poultry Science Journal*, *66*(9), 411–433. doi.org/10.1017/S0043933910000504
62. Sharma, G. P., & Prasad, S. (2004). Effective moisture diffusivity of garlic cloves undergoing microwave-convective drying. *Journal of Food Engineering*, *65*(4), 609–

617. doi.org/10.1016/j.jfoodeng.2004.02.027

63. Srikiatden, J., & Roberts, J. S. (2006). Measuring moisture diffusivity of potato and carrot (core and cortex) during convective hot air and isothermal drying, *74*, 143–152. doi.org/10.1016/j.jfoodeng.2005.02.026
64. Pabis, S., Digvir S., J., Stefan, C., 1998. Grain Drying: Theory and Practice, 5th ed. John Wiley and Sons, New York, USA.
65. Stroem, L. K., Desai, D. K., & Hoadley, A. F. A. (2009). Superheated steam drying of Brewer's spent grain in a rotary drum. *Advanced Powder Technology*, *20*(3), 240–244. doi.org/10.1016/j.apt.2009.03.009
66. Suvarnakuta, P., Devahastin, S., & Mujumdar, A. S. (2007). A mathematical model for low-pressure superheated steam drying of a biomaterial. *Chemical Engineering and Processing*, *46*, 675–683. doi.org/10.1016/j.cep.2006.09.002
67. Świątkiewicz, S., & Koreleski, J. (2008). The use of distillers dried grains with solubles (DDGS) in poultry nutrition. *World's Poultry Science Journal*, *64*(2), 257–266.
68. Taheri-garavand, A., Rafiee, S., & Keyhani, A. (2011). Study on effective moisture diffusivity, activation energy and mathematical modeling of thin layer drying kinetics of bell pepper. *Australian Journal of Crop Science*, *5*(2), 128–131.
69. Taheri-Garavand, A., Rafiee, S., & Keyhani, A. (2011). Study on effective moisture diffusivity, activation energy and mathematical modeling of thin layer drying kinetics of bell pepper. *Australian Journal of Crop Science*, *5*(2), 128–131.
70. Tang, Z., Cenkowski, S., & Izydorczyk, M. (2005). Thin-layer drying of spent grains in superheated steam. *Journal of Food Engineering*, *67*(4), 457–465.
71. Thorat, I. D., Mohapatra, D., Sutar, R. . F., Kapdi, S. S., & Jagtap, D. D. (2012). Mathematical modeling and experimental study on thin-layer vacuum drying of ginger (Zingiber Officinale R.) slices,. *Food and Bioprocess Technology*, *5*, 1379–1383. doi.org/10.1007/s11947-010-0429-y
72. Touil, A., Chemkhi, S., & Zagrouba, F. (2014). Moisture diffusivity and shrinkage of fruit and cladode of Opuntia ficus-indica during infrared drying. *Journal of Food Processing*, 1–9. doi.org/10.1155/2014/175402
73. Tumuluru, J. S., Tabil, L., Opoku, A., Mosqueda, M. R., & Fadeyi, O. (2010). Effect of process variables on the quality characteristics of pelleted wheat distiller's dried

grains with solubles. *Biosystems Engineering*, *105*(4), 466–475. doi.org/10.1016/j.biosystemseng.2010.01.005

74. Uddin, Z., Suppakul, P., & Boonsupthip, W. (2016). Effect of air temperature and velocity on moisture diffusivity in relation to physical and sensory quality of dried pumpkin seeds. *Drying Technology*, *34*(12), 1423–1433.
75. Vaccarezza, L. M., Lombardi, J. L., & Chirife, J. (1974). Kinetics of moisture movement during air drying of sugar beet root. *International Journal of Food Science and Technology*, *9*(3), 317–327. doi.org/10.1111/j.1365-2621.1974.tb01779.x
76. Waszkielis, K. M., Białobrzewski, I., Nowak, K. W., Dzadz, & Dach, J. (2014). Determination of the thermal conductivity of composted material. *Measurement: Journal of the International Measurement Confederation*, *58*, 441–447. doi.org/10.1016/j.measurement.2014.09.006
77. Xiros, C., Topakas, E., Katapodis, P., & Christakopoulos, P. (2008). Hydrolysis and fermentation of brewer's spent grain by Neurospora crassa. *Bioresource Technology*, *99*(13), 5427–5435. doi.org/10.1016/j.biortech.2007.11.010
78. Yang, W., Sokhansanj, S., Tang, J., & Winter, P. (2002). PH—Postharvest Technology. *Biosystems Engineering*, *83*(4), 449–462. doi.org/10.1006/bioe.2002.0135
79. Zielinska, M., & Cenkowski, S. (2012). Superheated steam drying characteristic and moisture diffusivity of distillers' wet grains and condensed distillers' solubles. *Journal of Food Engineering*, *109*(3), 627–634. doi.org/10.1016/j.jfoodeng.2011.06.017
80. Zielinska, M., Cenkowski, S., & Markowski, M. (2009). Superheated steam drying of Distillers' Spent Grains on a single inert particle. *Drying Technology*, *27*(12), 1279–1285.doi.org/10.1080/07373930903195065.

CHAPTER 5. MODELLING OF INITIAL CONDENSATION

This chapter is based on an Accepted Manuscript of an article published by Taylor & Francis in the journal *Drying Technology* on 25 Jan 2017 available online: www.tandfonline.com/ [doi.org/10.1080/07373937.2016.1166123].

5.1 Abstract

Initial condensation on the sample surface during superheated steam (SS) drying leads to increased sample moisture affecting its mechanical and thermal properties. A study was conducted to understand the effect of temperature and velocity of SS on the amount of initial condensation on distillers' spent grain pellets with an initial moisture content of 25% (wet basis). These pellets were dried using SS at 120, 150, and 180^{o}C with velocities 0.5, 1.0, 1.2, and 1.4 m/s. Separate experiments were conducted for recording mass and surface temperature of the pellets during SS drying. Mass recorded over the drying period was then compared with the predicted mass obtained by solving the standard heat balance and film condensation equations. The predicted values of mass flux due to initial condensation were in close agreement with directly measured values with a maximum mean square error of 0.20. There was a 60-64% decrease in the amount of initial condensation as the temperature of SS was increased from 120 to 180^{o}C. The results indicate that the initial condensation can be minimal when the temperature of SS is equal to or above 180^{o}C with SS velocity equal to or above 1m/s using a preheated drying chamber.

Keywords: *Distillers' spent grain, Superheated steam, Initial condensation*

5.2 Introduction

The search for more efficient alternatives to conventional drying has led to new research in the area of drying using media such as superheated steam (SS). The popularity of SS drying can be attributed to the convenience of recycling SS in industrial drying systems with lower energy loss when compared to air-drying. The method excels over traditional hot air drying because of its higher energy efficiency, higher drying rates, zero risk of fire or explosion, lowered pollution, and potentially better physical and nutritional quality of the dried product (Tang and Cenkowski, 2000). On the other hand, SS has its own set of limitations including the increased chance of qualitative degradation of temperature sensitive materials and the requirement of complex equipment when compared to hot air drying (Erdesz and Kudra, 1990; Kumar and Mujumdar, 1990; Shibata et al., 1988). Unlike conventional air-drying, the heat and mass transfer phenomena during SS drying involves many steps. Superheated steam drying process has an initial condensation phase during which the steam at higher temperature condenses on the surface of the material to be dried, which is at a lower temperature. This local condensation on the surface of the sample is followed by diffusion of the initially condensed vapor toward the interior of the material, slightly increasing the overall moisture content of the sample. Later when the sample surface temperature reaches the steam saturation temperature, the additional energy supplied by the SS is utilized to evaporate the condensed vapor. Finally, drying of the material takes place following a receding core model (Hamawand, 2013a). The receding core model relies on the assumption that moisture is removed from a porous material by forming a dry-wet interface. As drying proceeds, this interface moves toward the center of the material (i.e. the wet zone gets depleted as the dry zone expands) (Chen et al., 2000; Khan et al., 1991). However, this model

does not consider a distinguishable initial condensation period and the constant drying rate period. Soponronnarit (2006) used a model to describe SS drying that accounts for the initial condensation period and the increase in moisture content of the material. The model was formulated for thin-layer drying and did not use the receding core model. The thin-layer drying model uses Fick's unsteady state equation to describe the drying rate (Babalis et al., 2006; Prachayawarakorn et al., 2007; Pronyk et al., 2004; Soponronnarit et al., 2006; Suvarnakuta et al., 2007).

There have been many studies done in the past to investigate the effect of SS on the drying dynamics of different biological materials such as potato, wood, oat groats, carrots, banana, and rice (Hamawand, 2013a; Head et al., 2010; Nimmol et al., 2007; Pang, 1997; Suvarnakuta et al., 2007; Taechapairoj et al., 2006; Tang and Cenkowski, 2000). Tang and Cenkowski (2000) compared SS and hot air drying of potato samples and concluded that the temperature of drying media had a significant effect on the drying rate and overall moisture diffusivity in the case of SS drying when compared to hot air drying. They also studied the inversion temperature that exists in the constant drying rate period above which the drying rate is higher in SS than in hot air, and below which the drying rate is lower than in hot air. An inversion temperature in the range of 145 to 165°C and 125 to 145°C was noticed for the first and last dehydration stages, respectively. They also reported that the constant drying rate period was more prominent during SS drying as compared to hot air drying where it was negligible. They also discussed the phenomena of initial condensation and the moisture gain associated with it, which diminished with an increase in SS temperature. Contrary to these results, Taechapairoj et al., (2003) reported that the moisture gain due to initial condensation was same, irrespective of the SS temperature and grain

depth during their experiments on paddy kernels dried in SS. They reported that the contradiction is due to the high superficial steam velocity of 3.1 m/s they used which is higher than the minimum fluidizing velocity of 2.6 m/s for paddy in SS flow. This high velocity created a fluidized condition so that larger amount of condensed water on the kernels evaporated quickly before it could be absorbed by the kernels.

As initial condensation is a reverse phenomenon of evaporation occurring at the drying stage, Iyota et al. (2001) referred it as a reverse process. They also reported that it has a greater influence on material quality since initial condensation is considered to be the reverse of the evaporation process occurring in the later stages of SS drying (Taechapairoj et al., 2003). Iyota et al. (2001) had attempted to simulate SS drying considering the increase in moisture content of the product during the initial condensation period. They reported a sudden increase in internal temperature of the sample with the increase in condensation heat transfer and a rise in surface moisture content. They also explained the fact that the condensed moisture on the surface migrates towards the center of the sample creating a wet core with higher moisture content than the surface even in the constant drying rate period. They noticed that the mass change curves for different moisture diffusion coefficients appeared to be similar; hence, they concluded that the drying rate in SS is affected more by heat transfer than by mass transfer. Hamawand (2011) reported that the initial condensation of vapour on the surface of particles may cause the particles to stick to the hot surfaces of a dryer. When the high temperature of SS increases the sample temperature, a liquid bridge is formed between the particles and the surface of the dryer. During this phase the sample and may go through a glass transition phase and become more amorphous in nature. This increases the adhesion of particles to the dryer surface, which

are then dried by the high-temperature SS forming darkened deposits on the dryer surface (Hamawand, 2011).

Even though initial condensation causes certain disadvantages during the SS drying process, like an increase in overall moisture content of the sample and increase in drying time (Inoue et al., 2010), there are certain applications of SS processing where the phenomena of initial condensation are beneficial. The process of condensation of steam on the sample surface during the SS blanching has some advantages unlike as in drying. The condensation of steam on the sample surface transfers a large quantum of latent heat to the material which increases the heat transfer rate (Rico et al., 2008; Xiao et al., 2014). The high-temperature steam condensation on the sample during SS impingement blanching was found to have positive effects on the sample drying time after blanching and the overall quality of the blanched samples like lettuce (Rico et al., 2008), seedless grapes (Bai et al., 2013), yam slices (Xiao et al., 2012), etc.

The current study is a part of a research on the heat and mass transfer modelling of SS drying of Distillers' spent grains (DSG) obtained after the wet milling process of the ethanol production. The Distillers' spent grains are the major by-product of ethanol industry which is a rich source of fiber and protein (Johnson et al., 2011b). The lower starch content and higher protein and fiber of DSG help to replace the canola meal and soy meal as the cattle feed (Oba et al., 2010). The process form of this by-product is also finding it way in the market as poultry feed (Pettersson et al., 1987), and even in human diet (Liu et al., 2011). The current method of rotary drying used for DSG drying has many disadvantages like darkened deposits on the drum reducing the product quality, and also the risk of catching fire due to the high fiber content of

the sample. This issue was addressed by Tang et al. (2005) and they recommended SS drying as a suitable drying method for drying DSG.

Another study by Zielinska and Cenkowski (2012) postulated that a portion of the SS energy is used as sensible heat to warm up the material to be dried to a temperature above the steam saturation temperature. This causes a loss in temperature of the steam, resulting in local condensation on the material. They also reported that the amount of condensate depends on the SS temperature as more condensation was observed at a lower SS temperature (110 °C) than at a higher SS temperature (160 °C). Johnson et al. (2013) reported that there was a 2.3 to 5.2% increase in the wet basis (wb) moisture content of distillers' spent grain (DSG) after 5 s of exposure to SS at 110 °C; whereas for 130 °C, there was a 1.7 -3.4% wb increase in moisture depending on steam velocities. An increase in the volume of DSG compacts, when subjected to SS drying, was reported in the study conducted by Johnson et al. (2014). They reported that volumetric expansion of DSG pellets was higher during initial warm up and condensation period due to immediate relaxation of stress occurring after placing the compact in the drying medium. During this period, the initial condensation of steam along with the rapid increase in temperature of the compacts accelerated the relaxation of stresses in the compacts. Hence, the phenomena of temporary condensation occurring for a short interval of SS drying has an influence on the heat and mass transfer processes as well as the physical properties of the material.

Even though some of the researchers consider the effect of initial condensation, there are limited studies detailing the factors affecting the phenomena. It is important to study this phenomenon especially when mathematical modelling of SS drying is considered and for the optimization of operating parameters for the SS drying process. As mentioned in the

research conducted by Johnson et al. (2015, 2014, 2013b), the process of initial condensation affects the stability of the DSG compacts or pellets thereby leading to greater disintegration. The current research focuses on the effect of various operating parameters of SS drying system on the initial condensation of SS on DSG pellets keeping the sample parameters like sample temperature and pellet size constant. Therefore, the objectives of this study were to (i) determine the effect of SS temperature and velocity on the initial condensation period of DSG compacts, and (ii) compare the amount of condensation occurring on the DSG compacts by direct mass measurements to the condensation based on the surface temperature history analysis.

5.3 Materials and method

5.3.1 Superheated steam dryer

The SS processing system has previously been described in detail by Cenkowski et al. (2007) and Zielinska et al. (2009). The system consists of a water reservoir that supplies water to an electric boiler. The boiler generates saturated steam which is passed through a pressure reducing valve creating SS and then transferred to a superheater, increasing the temperature of the steam beyond 100°C. The temperature of the superheater is regulated using an external control panel. The SS is then passed through the highly insulated drying chamber which holds the sample. The flow of SS to the drying chamber can be diverted back to the water tank with the use of a 3-way manual valve. SS is always diverted to the tank before opening the drying chamber. An electronic balance is located above the drying chamber and a fan is used to divert any SS away from the underfloor weighing hole. Figure 5.1 shows a schematic diagram of the setup used for continuous mass measurement.

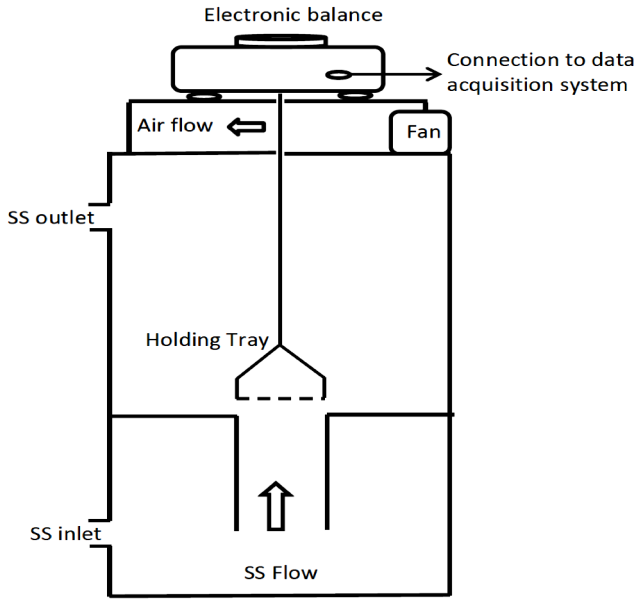

Figure 5.1 Cross section showing the SS drying chamber, location of holding tray, and location of electronic balance.

5.3.2 DSG sample preparation

The raw material used in this study was a mixture of 90% corn and 10% wheat whole stillage obtained from a distillery (Mohawk Canada Limited, a division of Husky Oil Limited, Minnedosa, MB). The raw material was stored in a freezer at -15°C in a sealed plastic pail with a 40 L capacity. Before sample preparation, the sealed plastic pail was taken out of the freezer and allowed to thaw to room temperature. The whole stillage was then centrifuged using a Sorvall General Purpose, RC-3 centrifuge (Thermo Scientific Co., Asheville, NC). The centrifuge operated at a relative centrifugal force of 790 × g, with four 1000 mL sample containers (filled approximately 75%) rotating at a speed of 2200 rpm for 10 minutes. The supernatant liquid was poured out and discarded. The semi-solid solubles fraction was scooped out in thin layers using a spatula leaving the coarse grain fraction

which was removed next. The solubles and coarse grain fractions were placed in separate airtight plastic bags and stored in a freezer at -15°C.

5.3.3 Initial moisture content

The initial moisture content of the coarse grain fraction was 78.9 ± 0.6% wb. Moisture content was determined by the air-oven drying method (AACC, 2000) by drying 2 g of wet sample at 135°C for 2 hours in a laboratory oven (Thermo Electron Corporation, Waltham, MA). Using the same method, the initial moisture content of the semi-solid solubles fraction was determined to be 84.2±0.8% wb. This procedure was conducted in triplicate.

5.3.4 Initial condensation experiments

In the present study initial condensation occurring of compacted DSG pellets were quantified using two different methods: by direct mass measurement which is considered as case 1, and by measuring the surface temperature history of the pellets which is considered as case 2, respectively. This was done because of the fact that the recording of initial condensation by direct mass measurement is highly challenging especially at high temperatures and velocities of SS. Hence a comparison of two methods helps to determine the initial condensation at higher temperatures and velocities of SS with appreciable accuracy. A detailed description of the both the cases are described in sections below.

5.3.5 Initial condensation by direct mass measurement (case 1)

5.3.5.1 DSG pellet preparation (Case1)

For initial condensation experiments based on direct mass measurement, an airtight bag of coarse grain was removed from the freezer and allowed to thaw for 2 h. The appropriate amount of sample was removed from the bag and dried in an air oven to a moisture content of 25% wb at a lower temperature (50°C). The sample was then removed from the air-oven

and placed in a cylindrical steel mold. Approximately 2.1 ±0.05 g of sample was used to make a pellet. A cylindrical die with a diameter of 12.02 mm attached to a 10 kN load cell on a universal testing machine (Model 3366 Universal Testing Systems, Instron Corp., Norwood, MA) was used to make the compacted pellets by applying a load of 6820 N to the sample (equivalent to a pressure of 60.3 MPa) at a rate of 50 mm/min. After the desired load had been reached, the die was held inside the mold for 5 minutes in order to maintain constant pressure and prevent relaxation. The pellet was then removed from the mold and a Vernier caliper with an accuracy of 0.01 mm was used to measure the length of the sample. An electronic balance with an accuracy of 0.001 g (Adventurer Pro AV313, Ohaus Corporation, Pine Brook, NJ) was used to measure the mass of the pellet. The difference in mass before and after pelletizing was assumed to be caused by the expulsion of water at high pressure.

5.3.5.2 Drying experiments (Case 1)

The following procedure was carried out to determine the maximum condensation, condensation time, and restoration time when drying DSG at 120, 150, and 180°C with SS of velocities 0.5, 1.0, 1.2, and 1.4 m/s. In each individual experimental setting, temperature and velocity fluctuations were within 2.0°C and 0.05 m/s range, respectively.

Four pellets were prepared for each experiment. The length of each pellet was measured using a Vernier caliper. Each pellet was immediately placed inside an airtight bag until all four pellets had been made to prevent moisture loss. After making the fourth pellet, all pellets were removed from the airtight bags and the length of the first pellet was recorded again. The maximum percentage of relaxation in the axial direction was calculated before drying the pellets in SS. The average percentage increase in the length of the first pellet,

while the remaining three pellets were made, was 17.7±5.3%. Any trials where the first pellet experienced axial relaxation in excess of 25% were discarded. All four short pellets were placed horizontally on a holding tray without touching each other and held in place by two steel pins each. The holding tray was attached to a thin steel rod, which was connected to an electronic balance with an accuracy of 0.001 g (PGW 453e, Adam Equipment Inc., Danbury, CT), located on top of the SS drying chamber. The pellets were then subjected to SS drying for a total of 300 s while continuously recording the mass of the samples and holding tray. Lifting force of the steam on the sample and holding tray was measured by diverting the steam to the tank using a manual flow diverting valve. Experiments for each treatment (SS temperature and velocity combinations) were conducted in triplicate.

5.3.5.3 Analysis of data (Case 1)

After plotting mass versus time, the first data point was deleted and replaced by the mass of the holding tray and the pellets measured at the starting point. Any subsequent points that were abnormally lower than the initial point were deleted due to them being affected by an increased lifting force caused by an increased chamber pressure when switching over the manual valve. On average, this resulted in the removal of the first 10 s of data. The lifting force was calculated by subtracting the average mass of the tray and sample during the last few seconds of drying from the mass of the tray and samples after drying without SS flow (Bourassa et al., 2015a; Zielinska, 2015). The tray mass was deducted and the lifting force was added to the raw data values to obtain the sample mass. A fourth power polynomial regression equation was applied. The mass values based on the regression equation were calculated for every time value present in the raw data and then plotted

against the original regression equation to ensure accuracy. The maximum amount of condensation was calculated by taking the maximum value obtained in the regression equation and subtracting the initial sample mass. The time value associated with the maximum mass value was considered the condensation time. The time taken for the mass from the regression equation to return back to the original sample mass from the maximum condensation point was considered the restoration time.

5.3.6 Initial condensation predictions based on surface temperature (Case 2)

5.3.6.1 DSG pellet preparation (Case 2)

For initial condensation experiments based on recorded surface temperature history, the same preparation method of the pellet was used but the material was slightly altered by mixing 30% solubles to the coarse grain fraction. This was done in order to avoid the disintegration of pellets as the thermocouples were placed inside the pellets. The mixing of solubles to the coarse grain fraction was done based on the assumption that initial condensation would not be significantly affected by a slight variation in the material composition. Before drying the material in the air-oven to 25% wb, a mixture of 70% coarse grains and 30% solubles (by mass) was produced with an initial moisture content of 79.2 ± 2.0 % wb. The dried mixture was made into pellets using the same procedure as in case 1.

5.3.6.2 Drying experiments (Case 2)

For these experiments, a single pellet was used per trial with the mixed material (70% coarse grains and 30% solubles). A thin needle was inserted into one end of the pellet (in the axial direction) and was pushed through the entire length until the tip just came out of the other end. The needle was then removed and a T-type thermocouple was inserted

axially into the hole left behind until the tip was approximately 1 mm from the other end of the cylindrical pellet as can be seen in Figure 5.2. The pellet was placed horizontally inside the holding tray, which was positioned inside the SS drying chamber. A second T-type thermocouple was placed on the holding tray making sure that its tip was not touching the pellet or the tray in order to record the SS temperature. The temperature experiments were run at 120, 150, and 180 ±2.0 °C for a total of 40 min. For each temperature, the target velocities were 0.5, 1.0, 1.2, and 1.4 ±0.05 m/s. Each treatment was done in triplicate and the average temperature history was taken.

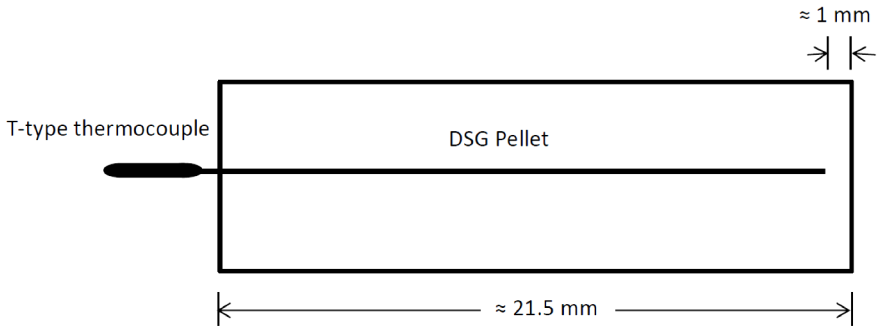

Figure 5.2 Cross section of a DSG pellet showing the location of the thermocouple (inside pellet) for recording surface temperature

5.3.6.3 Analysis of data (Case 2)

In order to predict the heat and mass transfer phenomena occurring during the initial condensation period of SS drying of DSG pellets, the sample was assumed to be homogeneous and isotropic, the initial temperature and moisture content of the samples were uniform, the drying unit is adiabatic, negligible heat convection during initial condensation since the energy from SS condensation is very high when compared to heat due to convection, and negligible radiation effect. The governing equations for energy balance and

mass balance within the solid medium (the pellet) for entire SS drying (Chandra Mohan and Talukdar, 2010; Kittiworrawatt and Devahastin, 2009) is as follows:

$$\frac{\partial T_p}{\partial t} = \frac{k_s}{\rho_s c_{ps}} \frac{\partial^2 T_p}{\partial x_j^2} \tag{5.1}$$

$$\frac{\partial M_p}{\partial t} = D_e \frac{\partial^2 M_p}{\partial x_j^2} \tag{5.2}$$

Where,T_p (°C) pellet temperature in K, k_s is the thermal conductivity of the pellet in W/(m K), c_{ps} the specific heat capacity J/(kg K) and ρ_s the density of the pellet in kg/m^3 and M is the moisture concentration in kg/kg dry basis within the pellet.

During initial condensation, the condensed water is assumed to form a layer which is uniformly distributed over the pellet surface and there is no temperature gradient through the particle in the pellet during this period (Hamawand, 2013a). Hence, the conductive heat transfer is not considered in the energy balance equation for the initial condensation period. Also, the lower Biot number (0.3) obtained for the cylindrical pellet subjected to superheated steam during initial condensation period shows that the internal resistance to heat transfer is much less than the external resistance. Thus, the effect of conductive heat transfer can be neglected (Pakowski and Adamski, 2011b). Therefore, the conductive heat flux is negligible when the surface temperature of the DSG pellet is lower than the temperature of the SS drying medium. The steam condensation occurring on the pellet surface follows the concept of film condensation (Christensen and Adler-Nissen, 2015; Kittiworrawatt and Devahastin, 2009; Messai et al., 2015) and is given by Equation 5.3:

$$m_{con} = \frac{h_f \left(T_{st} - T_p\right)}{L} \tag{3}$$

Where T_p is the surface temperature of the pellet in K, T_{St} is the saturation steam temperature at the corresponding operating pressure in K, h_f is the film condensation heat transfer coefficient in W/(m^2 K), m_{con} is the mass flux during the condensation period in kg/(m^2 s), and L is the latent heat of condensation or vaporization of steam at the corresponding operating pressure of the SS dryer in J/ kg. Since the latent heat generated during the initial condensation is very high when compared to the heat flux due to the convection, the film condensation heat transfer plays the major role in the heat flux occurring during this period (Iyota et al., 2001).The film condensation heat transfer coefficient of superheated steam where water vapour is condensed on a cylindrical pellet surface is given by Eq. (4) (Holman, 2001):

$$\mathrm{h}_f = 0.725 \left(\frac{\rho_f (\rho_{f-} \rho_v) g L k_f^3}{d \mu_f (Tst - Tp)} \right)^{\frac{1}{4}} \quad (4)$$

where, ρ_f and ρ_v are the density of water and steam in kg/m^3, respectively at the corresponding operating pressure, μ_f is the viscosity of water under operating parameters in m^2/ s, and d is the diameter of the pellet in m.

During the condensation period, the liquid water condensed on the surface of the pellet begins to evaporate as the temperature of the condensed film increases and reaches to the saturation steam temperature. The amount of water evaporated from the sample surface was determined using the kinetic theory of gases as shown in Equation 5.5 (Maa, 1969).

$$E = e \sqrt{\frac{M_w}{2\pi R}} \left(\frac{P_p}{\sqrt{T_p}} - \frac{P_{vap}}{\sqrt{T_{st}}} \right) \quad (5.5)$$

where E is the mass flux during evaporation in kg/(m^2 s), 'e' is the evaporation coefficient which is considered to be 8.5×10^{-2} in this case based on a comparison with previous experimental data as obtained from SS drying (section 5.3.5.1), P_p and T_p are the vapour

pressure (Pa) and temperature (K) on the surface of the pellet, respectively, M_w is the molecular weight of water in kg/mol, R is the universal gas constant (8.314 kJ/(kmol K)) and ρ_w is the density of water in kg/m^3. This evaporation is governed by the heat transfer between the condensed water and the SS (Hamawand, 2013a). Therefore, the effective mass flux during the condensation period can be calculated using Equation 5.6 (Hamawand, 2013a; Kittiworrawatt and Devahastin, 2009).

$$m_{flux} = e\sqrt{\frac{M_w}{2\pi R}}\left(\frac{P_p}{\sqrt{T_p}} - \frac{P_{vap}}{\sqrt{T_{st}}}\right) - m_{con} \quad (5.6)$$

Where, T_p and T_{st} are the temperature of the pellet and the saturation steam temperature, respectively. The saturation vapour pressure of condensed water at the surface of the pellet is given by Antoine's equation as described below (Hamawand, 2013a):

$$\ln\left(\overrightarrow{P_p}\right) = 16.387 - \frac{3885.7}{\left(T_p + 230.17\right)} \quad (5.7)$$

The estimated values (case 2) were compared with the experimental values (case 1) for different temperatures and velocities of SS using statistical software (SAS 9.3).

5.4 Results and discussion

5.4.1 Effect of SS temperature on initial condensation

The increase in mass of the DSG pellets obtained from direct mass measurement during SS drying is shown in Table 1. The maximum condensation time and restoration time for the DSG pellets subjected to SS are significantly different with SS temperature and velocity. Least significant difference (LSD) analysis for the increase in moisture content of the pellet due to initial condensation also showed a significant difference with SS temperature and velocity. The average increase in moisture content of DSG pellets during

the initial condensation period ranged from 3.8 to 7.2 ± 0.2%, 3.2 to 6.0 ± 0.2%, and 1.3 to 2.6 ± 0.2% wb for 120, 150, and 180ºC, respectively. ANOVA results obtained using SAS 9.3 showed that both temperature and velocity had a significant effect on the percentage increase in moisture content with $P<0.0001$. The magnitude of moisture content increase caused by initial condensation of SS decreased with an increase in SS temperature or steam velocity (Figure 5.3) which is in agreement with the results of Johnson et al. (2013a). The figure shows that the increase in moisture content of the pellet due to initial condensation was more prominent for the lower SS temperatures when compared to the higher SS temperatures. Also, at higher SS temperatures the velocity of SS flow had a negligible effect on initial condensation. The experimental results showed no measurable condensation for the highest SS temperature (180ºC) at higher SS velocities (1.2 and 1.4 m/s). The initial condensation period for these treatments were very short (< 10 s) and it was impractical to record the mass changes caused by condensation.

A comparative study of initial condensation on DSG pellets by conducting temperature profile experiments also gave reasonable agreement with the experimental data from direct mass measurement in terms of the cumulative mass flux. The higher difference in values of predicted mass flux and the experimental mass flux as shown in Figure 5.4 may be due to the limitation of the mathematical model. Since the major assumption of the model is that the condensed steam is forming a water layer on the sample surface and there is no heat flux inside the sample, the predicted mass flux gives slightly exaggerated value than the actual. This discrepancy is due to the fact that a portion of the condensed water is absorbed by the pellet because of its high porosity (Christensen and Adler-Nissen, 2015) which agrees with the studies conducted by Johnson et al. (2015). The mathematical model

used for predicting mass flux during initial condensation from the temperature history of the pellet did not account for the moisture adsorption and conductive heat flux in the pellet. But some of the heat flux due to the exothermic moisture adsorption (Kaya and Kahyaoglu, 2006; Liébanes et al., 2006) might be counteracted by the heat flux due to conduction inside the solid (pellet).

Table 5.1 Maximum mass of condensate and time of initial condensation at different SS temperatures and velocities.

SS temperature (°C)	SS velocity (m/s)	Maximum condensation time ± 3 (s)	Restoration time ± 3 (s)	Increase in M ±0.5 (% wb)*
120	0.5	45	75	7.2[a]
120	1.0	39	61	6.5 [b]
120	1.2	29	58	5.3 [c]
120	1.4	17	24	3.8 [e]
150	0.5	33	39	6.0 [b]
150	1.0	26	28	5.2 [c]
150	1.2	23	26	4.3 [d]
150	1.4	16	21	3.2 [e]
180	0.5	21	30	2.6 [f]
180	1.0	15	25	1.3 [g]

*Means with the same letter are not significantly different and M is the moisture content.

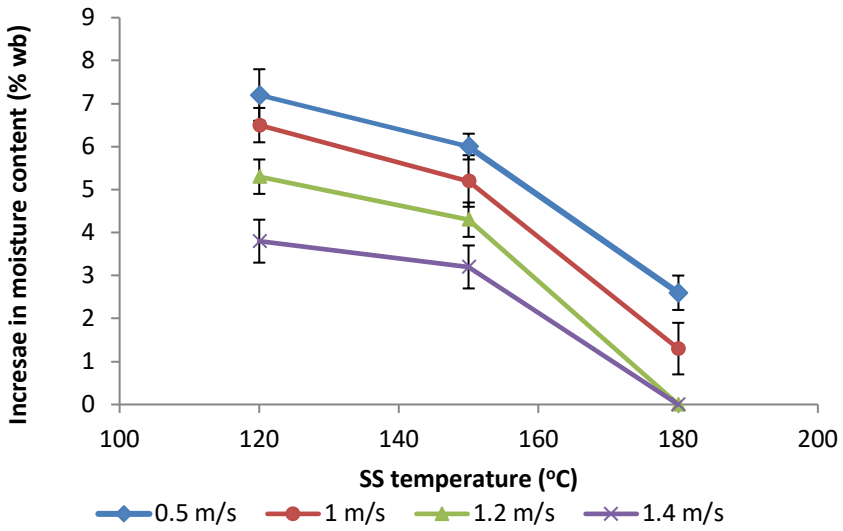

Figure 5.3 Comparison of moisture gain of DSG pellets subjected to different SS temperatures and velocities during the initial condensation period. Vertical bars indicate standard deviation based on n =3.

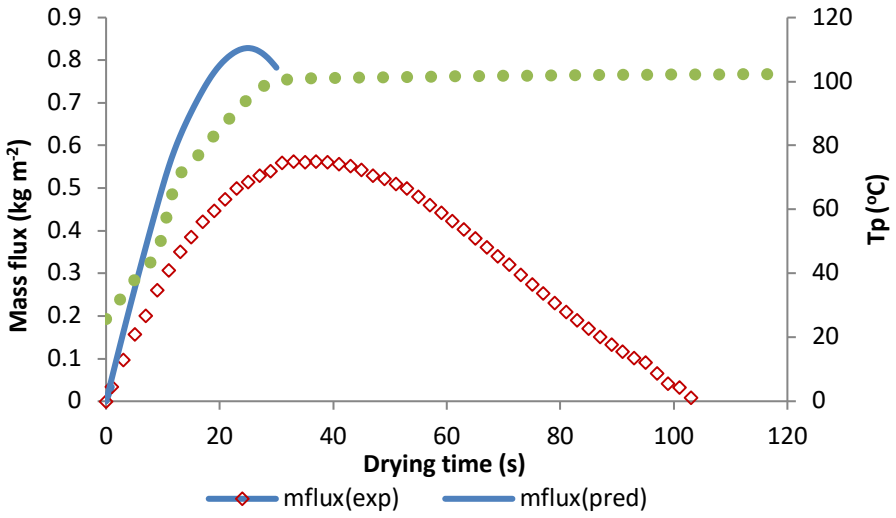

Figure 5.4 Initial condensation period and restoration period for a DSG pellet subjected to SS drying at 120°C with a velocity of 1.0 m/s, where mflux(exp)- experimentally determined mass flux, flux(pred)- predicted mass flux based on temperature history, *T*p- measured surface temperature history of DSG pellet.

Table 5.2 Experimental and predicted values of mass flux during the initial condensation period at different SS temperatures and velocities.

SS temperature (^oC)	SS velocity ($m^{-1}s$)	Cumulative mass flux (exp^*) (kg m^{-2})	Cumulative mass flux ($pred^*$) (kg m^{-2})	MSE
120	0.5	0.68	0.96	0.23
120	1.0	0.56	0.78	0.20
120	1.2	0.3	0.44	0.12
120	1.4	0.31	0.34	0.04
150	0.5	0.48	0.60	0.13
150	1.0	0.37	0.47	0.15
150	1.2	0.36	0.39	0.12
150	1.4	0.27	0.32	0.08
180	0.5	0.26	0.38	0.1
180	1.0	0.22	0.28	0.07

exp^*- Experimental value of initial condensation determined based on direct mass measurements as mentioned in case 1. $Pred^*$- Predicted values of initial condensation determined based on temperature history as mentioned in case 2.

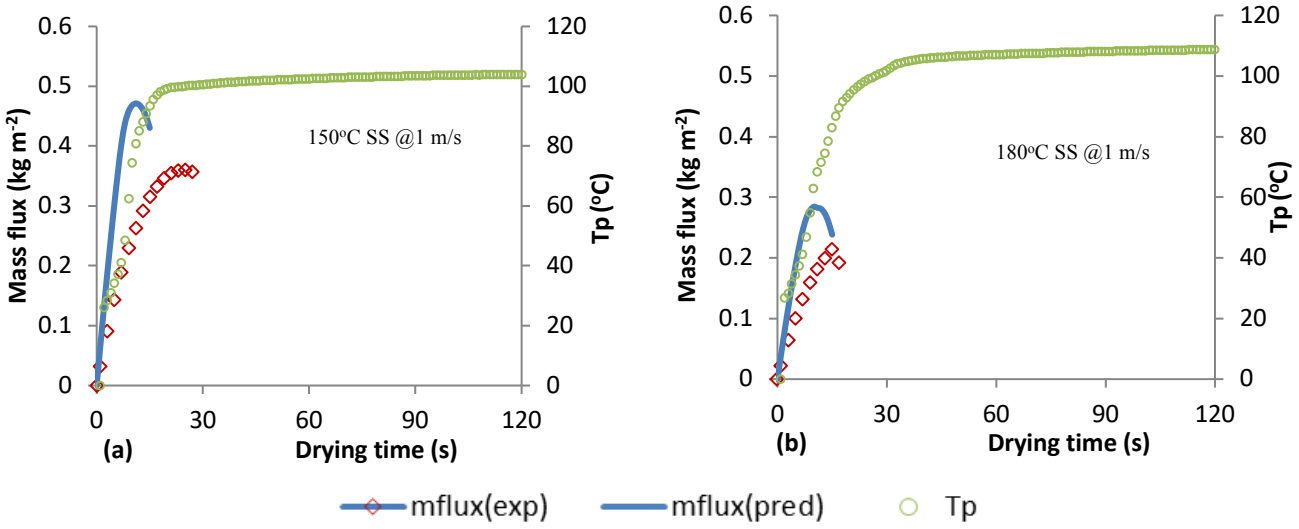

Figure 5.5 Predicted and experimental values of mass flux due to initial condensation of SS on the DSG pellet at different operating conditions, where mflux(exp)- experimentally determined mass flux, mflux(pred)-predicted mass flux based on temperature history, *T*p- measured surface temperature history of DSG pellet.

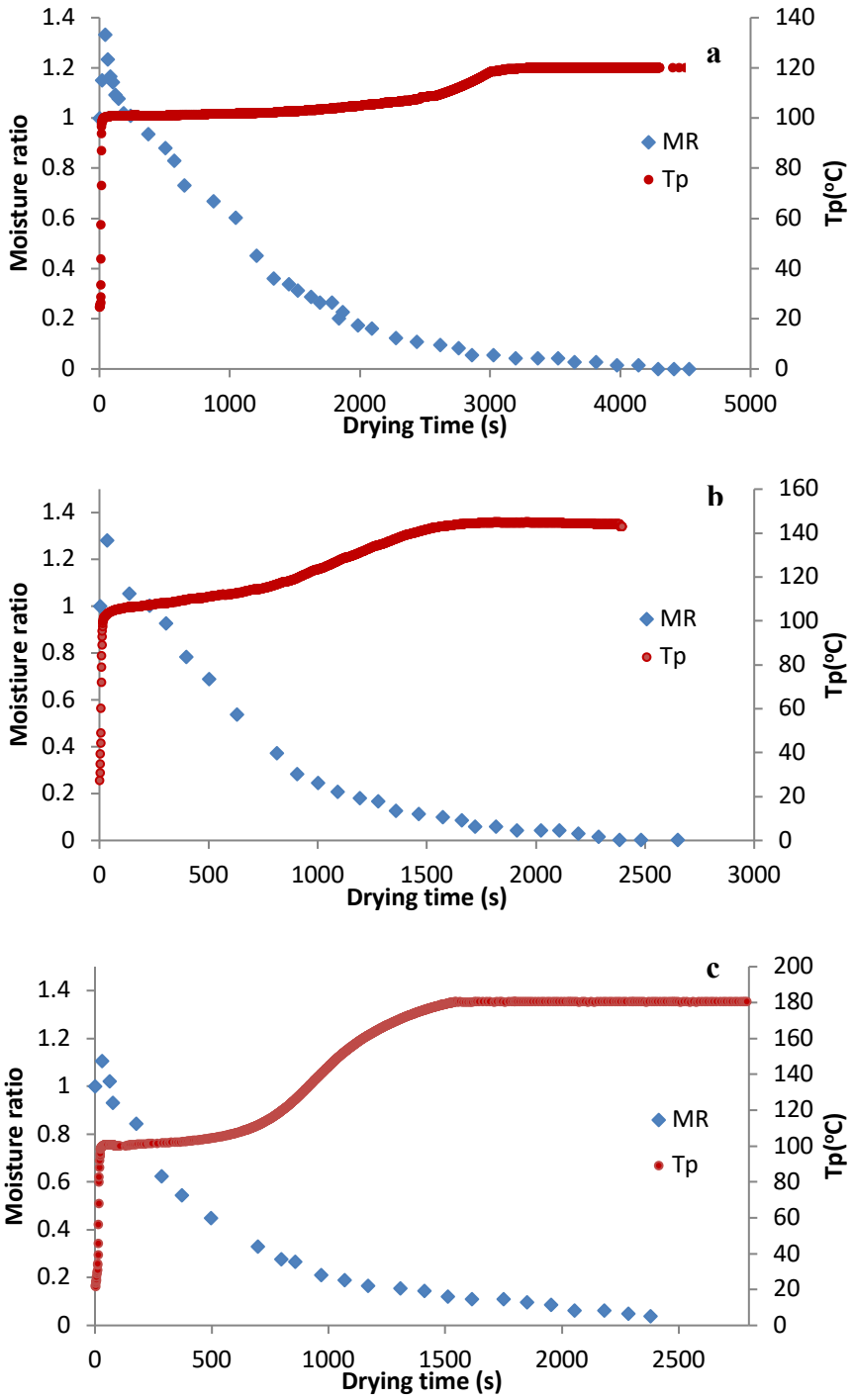

Figure 5.6 Comparison of temperature profile and moisture ratio of DSG pellets dried in various SS temperatures [(a) 120°C, (b) 150°C, (c) 180°C] at one steam velocity of 0.5 m/s.

The change in moisture ratio and temperature of the DSG pellets subjected to different SS temperature at 0.5 m/s steam velocity is shown in Figures 5.5a and 5.5b. The temperature profile of DSG pellet during SS drying shows a sudden increase in the initial warm-up period during which the condensation occurs. This increase in temperature is due to the high amount of latent heat energy rendered by SS to the sample (Chungcharoen et al., 2014). As shown in Figures 5.5a and 5.5b when the temperature of the DSG pellet reaches the saturation steam temperature the moisture ratio curve tends to take a negative slope. The decline of moisture curve indicates the evaporation of condensed water from the sample. The higher diffusion of moisture towards the exterior of the pellet due to the evaporation limits the sorption of moisture by the pellet as the temperature of the pellet increases (Christensen and Adler-Nissen, 2015).This justifies the minimal condensation reported for higher temperature (180^{o}C) and velocities (≥1 m/s) of SS. The temperature history of the DSG pellet at different SS temperature (Figures 5.5a and 5.5b), shows that the constant temperature period during SS drying is decreasing with the increase in SS temperature. The longer constant temperature period indicates a longer constant drying rate period which is also visible in Figures 5.5a and 5.5b (Erriguible et al., 2006). The comparison of cumulative mass flux during condensation obtained from the predicted and experimental data are shown in Table 5.2 with the mean square error (MSE) values for each treatment. The low MSE values for each treatment indicate that the predicted values agree well with the experimental data. The increase in velocity showed a significant effect on condensation mass flux when the SS temperature was 120, and 150^{o}C, whereas the condensation mass flux didn't vary with velocity for the higher temperature of SS i.e. 180^{o}C. There was no initial condensation recorded when the SS was at 180^{o}C at 1.2 and

1.4m/s. This is due to the fact that high temperature and high velocity of SS flow had hastened the heat transfer and the boundary layer of the pellet reached the steam saturation temperature within seconds. This sudden heating of the surface of the pellet causes little condensation on the pellet surface which is immediately evaporated with the help of high temperature and high-velocity SS. Hence, there is negligible change in overall moisture content of the pellet for a few seconds of drying where the condensation and evaporation phenomena overlap with each other leaving no time for the condensed moisture to migrate towards the center.

The condensation process stopped once the surface temperature of the pellets reached the saturation temperature of the SS. It was then followed by the restoration period where the evaporation of condensed vapour occurs as shown in Figures 5.6a-c The duration of the condensation and restoration periods is dependent on the SS temperature and steam velocity (Table 5.1). There was a noticeable decrease in initial condensation with an increase of SS temperature i.e. there was a 60-64% decrease in the cumulative mass flux due to initial condensation as the temperature of SS was increased from 120 to 180^{o}C. A comparison of mass flux values obtained from direct mass measurement and temperature profile based prediction are shown in Figure 5.4 and Figures 5.6a-c for an SS temperature of 150 and 180^{o}C at 1m/s. There was a better agreement between the experimental values and predicted values for the higher steam velocities irrespective of the SS temperature as shown in Table 5.2. For each treatment both the predicted and the experimental values reach maximum mass flux at approximately the same time when the surface temperature of the pellet reaches the saturation temperature of steam agreeing with the results reported by Kittiworrawatt and Devahastin (2009).

5.5 Conclusions

Superheated steam temperature and velocity both had a significant effect on the amount of initial condensation that occurred on the surface of DSG pellets during the initial warming up period of drying. The average increase in moisture content during the initial condensation period ranged from 1.3 to 7.2 ± 0.2% wb when the SS temperature increased from 120 to 180^{o}C with the lowest velocity of 0.5 m/s. Similarly, the average increase in moisture content ranged from 7.2 to 3.8 ± 0.2% wb when the SS temperature was at 120^{o}C and the velocity was changed from 0.5 to 1.4 m/s. Using temperature profile analysis the predicted values for cumulative mass flux due to condensation on the surface of DSG pellets were in very close agreement with the values obtained from direct mass measurement with a maximum MSE of 0.20. Mass transfer rate during the initial condensation period of SS drying can be estimated with appreciable accuracy by using the analogy of heat transfer of the sample with appropriate initial and boundary conditions. Even though the combination of instantaneous film condensation mass flux at lower sample surface temperatures and evaporation mass flux at higher temperatures gives a fair prediction of the condensation, a small deviation in the condensation values is noticed towards the later phase of prediction. This is because of the temperature fluctuations occurring in the fluid region around the pellet which causes the difference in heat and mass transfer. Also, the higher rate of increase in the predicted mass flux when compared to the experimental mass flux with the progress of time during the initial condensation period can be justified by the limitation of the prediction equation considered which does not accommodate the exothermic heat flux due to moisture adsorption and the conductive heat flux in the pellet. The experimental results also indicate that the initial condensation on the

DSG pellets can be minimized by increasing the SS temperature (≥180°C) and velocity (≥1m/s) provided the drying chamber is preheated to the set temperature.

Acknowledgements

The authors thank the Natural Sciences and Engineering Research Council of Canada for their financial support and University of Manitoba Graduate Fellowships.

References

1. AACC Method, 44-15A. (2000). Moisture-air-oven methods. St. Paul: Approved Methods of the American Association of Cereal Chemists.
2. Babalis, S. J., Papanicolaou, E., Kyriakis, N., & Belessiotis, V. G. (2006). Evaluation of thin-layer drying models for describing drying kinetics of figs (Ficus carica). *Journal of Food Engineering*, *75*(2), 205–214. doi.org/10.1016/j.jfoodeng.2005.04.008
3. Bai, J. W., Sun, D. W., Xiao, H. W., Mujumdar, A. S., & Gao, Z. J. (2013). Novel high-humidity hot air impingement blanching (HHAIB) pretreatment enhances drying kinetics and color attributes of seedless grapes. *Innovative Food Science and Emerging Technologies*, *20*, 230–237. doi.org/10.1016/j.ifset.2013.08.011
4. Bourassa, J., Ramachandran, R. P., Paliwal, J., & Cenkowski, S. (2015). Drying characteristics and moisture diffusivity of distillers' spent grains dried in superheated steam. *Drying Technology*, *33*, 2012–2018.
5. Cenkowski, S., Pronyk, C., Zmidzinska, D., & Muir, W. E. (2007). Decontamination of food products with superheated steam. *Journal of Food Engineering*, *83*(1), 68–75. doi.org/10.1016/j.jfoodeng.2006.12.002
6. Chandra Mohan, V. P., & Talukdar, P. (2010). Three dimensional numerical modeling of simultaneous heat and moisture transfer in a moist object subjected to convective drying. *International Journal of Heat and Mass Transfer*, *53*(21–22), 4638–4650.
7. Chen, Z., Wu, W., & Agarwal, P. K. (2000). Steam-drying of coal. Part 1. Modeling the behavior of a single particle. *Fuel*, *79*(8), 961–973.
8. Christensen, M. G., & Adler-Nissen, J. (2015). Proposing a normalized Biot number:

For simpler determination of Fourier exponents and for evaluating the sensitivity of the Biot number. *Applied Thermal Engineering*, *86*, 214–221.

9. Chungcharoen, T., Prachayawarakorn, S., Tungtrakul, P., & Soponronnarit, S. (2014). Quality Attributes of Germinated High Amylose and Waxy Rice in Superheated Steam and Hot Air Drying. *Drying Technology*, *3937*(March 2015), 141220085707004. doi.org/10.1080/07373937.2014.995304
10. Erdesz, K., & Kudra, T. (1990). Superheated-steam drying Book review. *Drying Technology*, *8*(4), 891–893. doi.org/doi.org/10.1080/07373939008959925
11. Erriguible, A., Bernada, P., Couture, F., & Roques, M. (2006). Simulation of Superheated Steam Drying from Coupling Models. *Drying Technology*, *24*(8), 941–951. doi.org/10.1080/07373930600776019
12. Hamawand, I. (2011). Effect of colloidal particles associated with the liquid bridge in sticking during drying in superheated steam. *International Journal of Engineering, Transactions B: Applications*, *24*(2), 119–126.
13. Hamawand, I. (2013). Drying steps under superheated steam: A review and modeling. *Energy and Environment Research*, *3*(2), 107–125. doi.org/10.5539/eer.v3n2p107
14. Head, D. S., Cenkowski, S., Arntfield, S., & Henderson, K. (2010). Superheated steam processing of oat groats. *LWT - Food Science and Technology*, *43*(4), 690–694. doi.org/10.1016/j.lwt.2009.12.002
15. Holman, J. (2001). *Heat transfer* (Tenth Ed). Boston, MA: McGraw – Hill.
16. Inoue, T., Iyota, H., & Nishimura, N. (2010). Prediction method for drying time of wet porous material in humid hot air and superheated steam. *Drying Technology*, *28*(5), 608–614. doi.org/10.1080/07373931003788650
17. Iyota, H., Nishimura, N., Yoshida, M., & Nomura, T. (2001). Simulation of superheated steam drying considering initial steam condensation. *Drying Technology*, *19*(7), 1425–1440. doi.org/10.1081/DRT-100105298
18. Johnson, P., Cenkowski, S., & Paliwal, J. (2013a). Compaction and relaxation characteristics of single compacts produced from distiller's spent grain. *Journal of Food Engineering*, *116*(2), 260–266. doi.org/10.1016/j.jfoodeng.2012.11.025
19. Johnson, P., Cenkowski, S., & Paliwal, J. (2013b). Superheated steam drying characteristics of single cylindrical compacts produced from wet distiller's spent grain.

In *The canadian society of Bioengineering*. Retrieved from www.csbe-scgab.ca/docs/meetings/2013/CSBE13011.pdf

20. Johnson, P., Cenkowski, S., & Paliwal, J. (2014). Analysis of the disintegration of distiller's spent grain compacts as affected by drying in superheated steam. *Drying Technology*, *32*(9), 1060–1070. doi.org/10.1080/07373937.2014.881849
21. Johnson, P., Paliwal, J., & Cenkowski, S. (2011). Current and potential applications of distiller ' s spent grain. In *The canadian society of Bioengineering* (pp. 1–11).
22. Johnson, P., Paliwal, J., & Cenkowski, S. (2015). Effect of solubles on disintegration of distiller's spent grain compacts during superheated steam drying. *Drying Technology*, *33*, 1–13. doi.org/10.1080/07373937.2014.967403
23. Kaya, S., & Kahyaoglu, T. (2006). Influence of dehulling and roasting process on the thermodynamics of moisture adsorption in sesame seed. *Journal of Food Engineering*, *76*(2), 139–147. doi.org/10.1016/j.jfoodeng.2005.04.042
24. Khan, J. A., Beasley, D. E., & Alatas, B. (1991). Evaporation from a packed bed of porous particles into superheated vapor. *International Journal of Heat and Mass Transfer*, *34*(1), 267–280.
25. Kittiworrawatt, S., & Devahastin, S. (2009). Improvement of a mathematical model for low-pressure superheated steam drying of a biomaterial. *Chemical Engineering Science*, *64*(11), 2644–2650. doi.org/10.1016/j.ces.2009.02.036
26. Kumar, P., & Mujumdar, A. S. (1990). Superheated-steam drying: A bibliography. *Drying Technology*, *8*(1), 195–205.
27. Liébanes, M. D., Aragón, J. M., Palancar, M. C., Arévalo, G., & Jiménez, D. (2006). Equilibrium moisture isotherms of two-phase solid olive oil by-products: Adsorption process thermodynamics. *Colloids and Surfaces A: Physicochemical and Engineering Aspects*, *282–283*, 298–306.
28. Liu, S. X., Singh, M., & Inglett, G. (2011). Effect of incorporation of distillers' dried grain with solubles (DDGS) on quality of cornbread. *LWT - Food Science and Technology*, *44*(3), 713–718. doi.org/10.1016/j.lwt.2010.10.001
29. Maa, J. R. (1969). Condensation studies with jet steam tensimeter. *Industrial and Engineering Chemistry Fundamentals*, *8*(1), 564–570. doi.org/10.1021/i160031a032
30. Messai, S., Sghaier, J., Ganaoui, M. El, Chrusciel, L., & Gabsi, S. (2015). Low Pressure

Superheated Steam Drying of a Porous Media--Part I. *Drying Technology*, 33(1),103-115. Doi.org/10.1080/07373937.2014.933843.

31. Nimmol, C., Devahastin, S., Swasdisevi, T., & Soponronnarit, S. (2007). Drying of banana slices using combined low-pressure superheated steam and far-infrared radiation. *Journal of Food Engineering*, *81*(3), 624–633.
32. Oba, M., Penner, G. B., Whyte, T. D., & Wierenga, K. (2010). Effects of feeding triticale dried distillers grains plus solubles as a nitrogen source on productivity of lactating dairy cows. *Journal of Dairy Science*, *93*, 2044–2052.
33. Pakowski, Z., & Adamski, R. (2011). On Prediction of the Drying Rate in Superheated Steam Drying Process. *Drying Technology*, *29*(13), 1492–1498.
34. Pang, S. (1997). Some considerations in simulation of superheated steam drying of softwood lumber. *Drying Technology*, *15*(2), 651–670.
35. Pettersson, D., Hesselman, K., & Åman, P. (1987). Nutritional value for chickens of dried distillers-spent-grain from barley and dehulled barley. *Animal Feed Science and Technology*, *17*(2), 145–156. doi.org/10.1016/0377-8401(87)90010-1
36. Prachayawarakorn, S., Soponronnarit, S., Wetchacama, S., & Jaisut, D. (2007). Desorption Isotherms and Drying Characteristics of Shrimp in Superheated Steam and Hot Air. *Drying Technology*, *20*(3), 669–684. doi.org/10.1081/DRT-120002823
37. Pronyk, C., Cenkowski, S., & Muir, W. E. (2004). Drying Foodstuffs with Superheated Steam. *Drying Technology*, *22*(5), 899–916. doi.org/10.1081/DRT-120038571
38. Rico, D., Martín-Diana, A. B., Barry-Ryan, C., Frías, J. M., Henehan, G. T. M., & Barat, J. M. (2008). Optimisation of steamer jet-injection to extend the shelflife of fresh-cut lettuce. *Postharvest Biology and Technology*, *48*(3), 431–442.
39. Shibata, H., Mada, J., & Shinohara, H. (1988). Drying mechanism of sintered spheres of glass beads in superheated steam. *Industrial & Engineering Chemistry Research*, *27*(12), 2353–2362.
40. Soponronnarit, S., Prachayawarakorn, S., Rordprapat, W., Nathakaranakule, A., & Tia, W. (2006). A superheated-steam fluidized-bed dryer for parboiled rice: Testing of a pilot-scale and mathematical model development. *Drying Technology*, *24*(11), 1457–1467. doi.org/10.1080/07373930600952800
41. Suvarnakuta, P., Devahastin, S., & Mujumdar, A. S. (2007). A mathematical model for

low-pressure superheated steam drying of a biomaterial. *Chemical Engineering and Processing*, *46*, 675–683. doi.org/10.1016/j.cep.2006.09.002

42. Taechapairoj, C., Dhuchakallaya, I., Soponronnarit, S., Wetchacama, S., & Prachayawarakorn, S. (2003). Superheated steam fluidised bed paddy drying. *Journal of Food Engineering*, *58*(1), 67–73. doi.org/10.1016/S0260-8774(02)00335-7
43. Taechapairoj, C., Prachayawarakorn, S., & Soponronnarit, S. (2006). Modelling of parboiled rice in superheated-steam fluidized bed. *Journal of Food Engineering*, *76*(3), 411–419. doi.org/10.1016/j.jfoodeng.2005.05.040
44. Tang, Z., & Cenkowski, S. (2000). Dehydration dynamics of potatoes in superheated steam and hot air. *Canadian Biosystems Engineering / Le Genie Des Biosystems Au Canada*, *42*(1), 43–49.
45. Tang, Z., Cenkowski, S., & Izydorczyk, M. (2005). Thin-layer drying of spent grains in superheated steam. *Journal of Food Engineering*, *67*(4), 457–465.
46. Xiao, H. W., Bai, J. W., Sun, D. W., & Gao, Z. J. (2014). The application of superheated steam impingement blanching (SSIB) in agricultural products processing - A review. *Journal of Food Engineering*, *132*, 39–47.
47. Xiao, H. W., Yao, X. D., Lin, H., Yang, W. X., Meng, J. S., & Gao, Z. J. (2012). Effect of SSB (Superheated Steam Blanching) time and drying temperature on hot air impingement drying kinetics and quality attributes of yam slices. *Journal of Food Process Engineering*, *35*(3), 370–390. doi.org/10.1111/j.1745-4530.2010.00594.x
48. Zielinska, M. (2015). Drying Kinetics and Physicochemical Characteristics of Laboratory-Prepared Corn/Wheat Distillers Grains and Solubles Dried with Superheated Steam and Hot Air. *Drying Technology*, *33*(7), 831–846.
49. Zielinska, M., & Cenkowski, S. (2012). Superheated steam drying characteristic and moisture diffusivity of distillers' wet grains and condensed distillers' solubles. *Journal of Food Engineering*, *109*, 627–634.
50. Zielinska, M., Cenkowski, S., & Markowski, M. (2009). Superheated steam drying of distillers' spent grains on a single inert particle. *Drying Technology*, 27(12), 37–41.doi.org/10.1080/07373930903195065.

CHAPTER 6. MODELLING OF SS DRYING OF A SINGLE DSG PELLET

This chapter is based on the research paper published by Elsevier in *journal of Food Engineering* on 29 May 2017, available online: www.sciencedirect.com/ [doi.org/10.1016/j.jfoodeng.2017.05.025].

6.1 Abstract

The classic method of modelling drying processes using the transfer coefficients can be replaced by a method of solving Reynolds-Averaged Navier-Stokes equations applicable to the drying medium. This specifically applies to superheated steam (SS) as the drying medium, where the mass transfer coefficient cannot be defined by the heat transfer and mass analogy. In this study, the heat and mass transfer phenomena of SS drying of distillers' spent grain (DSG) pellets were numerically studied using a commercial Computational Fluid Dynamics (CFD) package by combining the drying models related to the moist cylinder with the model describing the external flow of SS. A three-dimensional (3D) model of the DSG pellet and the drying chamber was created. The governing differential equations for mass and energy balance of the pellet and steam-flow around it were solved using the finite volume method and SIMPLE algorithm within the CFD package (ANSYS CFX). The validation of the numerical model with experimental observations showed a good agreement with a mean relative percentage error less than or equal to 10%. The obtained mathematical model could serve as a basic tool for optimization and design of large-scale SS dryers for DSG.

Keywords: *Distillers' spent grain, Superheated steam drying, Heat and mass transfer, Numerical model*

6.2 Introduction

Canada is the fifth largest producer of ethanol in the world with around 23 leading ethanol plants in the country. In 2015, Canadian ethanol industries had a current production capacity of around 240 million litres per annum, while the world total ethanol productions hit about 75 billion litres per year (Canadian Renewable Fuels Association report, 2011). Distillers' spent grain is the major by-product (85% of the total by-product) of the ethanol industry, consisting of the solid residue remaining after mashing and lautering (Awolu and Ibileke, 2011; Xiros et al., 2008). It is considered the second largest source of income from the plant next to ethanol contributing to about 10-20% of the income. The by-product is mainly used as animal feed and as a good source of fiber and protein in baked human foods (Johnson et al., 2011). The wet distillers spent grain (WDS) obtained after the centrifugation of the whole stillage has a moisture content of over 70% wb and a maximum shelf life of 4-5 days. Also, the transportation of this WDS is highly challenging because of caking and bridging issues (Ganesan et al., 2008; Johnson et al., 2013). Hence, WDS needs to be dried to 10 to 15% moisture content to enhance its shelf life and enable better handling and transportation (Bourassa et al., 2015). Currently, wet distiller's spent grains (DSG) are dried using large rotary-drum dryers at high temperature to produce protein and fibre-rich animal feed (Stroem et al., 2009). One major issue with rotary-drum drying of such materials is the risk of fire and explosion as this fibre-rich product is dried at a high temperature in the presence of oxygen (Zielinska et al., 2009). Also, the heat damage to the protein can cause discolouration of the product and affect the quality of the feed causing economic and physical losses (Johnson et al. 2011).

This study is a part of a comprehensive research on modelling of SS drying of DSG. Currently, in industrial practice, DSG slurry is mixed with previously dried granules of DSG at the entrance to the rotary-drum dryer. The dried granules serve as a core (inert) material to dry the wet DSG coated over it. This approach helps to develop a desired large surface area for heat and mass exchange, but the problem is that the core material goes through the dryer multiple times with temperatures in the range of 550°C and can burn or even catch fire when dried in such hot air. Superheated steam drying (SS) is a suitable alternative drying method for DSG as the process is anaerobic, which eliminates the risk of fire (Cenkowski et al., 2007; Tang et al., 2005; Zielinska et al., 2009). The method also has additional advantages in preserving the colour and nutritional quality of the dried products (Taechapairoj et al., 2003; Moreira, 2011; Xiao et al., 2014). Attempts to generate sufficient surface area for the DSG slurry by industry have led to the development of extruders that produce cylindrical compacts of about 30% wb moisture. Such compacts are either directly introduced into the SS dryer or are coated with the wet solubles and then dried together. These attempts have only been partially successful because of the lower compaction pressure and stress relaxation and due to the steam condensation that results in the disintegration of the compacts (Johnson et al., 2014).

The present study covers the modelling of superheated steam drying of a cylindrical DSG pellet, which can be further used as a core material for drying the wet solubles. In addition, wet solubles can serve as a binder for the compacts increasing the strength of the wet pellets. This approach mimics the industrial research and development innovations on drying in SS with inert material. As the DSG pellets are made first to produce the core material for drying wet solubles over it, the drying dynamic of the core pellet is important because it affects the

drying of wet solubles poured over it during the drying. Generally, based on the demands of consumers, either the core pellet by itself or the coated pellets are produced and sold. Hence, this study focuses on the SS drying of such core pellet as a single element to develop a model that is capable of predicting the temporal and spatial variation in temperature and moisture concentration in the pellet. As, the drying kinetic of the bulk material is affected by the local temperature and concentration of moisture, the transport phenomena occurring in a single element are of considerable interest for developing a drying model (Pabis and Henderson 1962; Baini and Langrish, 2008; Da-Silva et al., 2013; Elgamal et al., 2014; Ljung et al., 2011a; Ljung et al., 2011b). Superheated steam drying (SS) is a suitable alternative drying method for DSG as the process is anaerobic, which eliminates the risk of fire (Cenkowski et al., 2007; Tang et al., 2005; Zielinska et al., 2009). The results of these transport phenomena and interactions are difficult to quantify precisely using the experiment based empirical models. To optimize the design parameters of such a system, a thorough knowledge of drying dynamics and change in thermal and physical properties of both, the material and the drying medium is necessary. Daurelle et al. (1998) conducted a finite element analysis of SS drying of a single element and reported that the changing boundary conditions and the transfer coefficient have to be considered in the simulation to avoid errors in predicting the drying variables. In the case of SS drying, the prediction of external mass transfer is difficult because of the lack of a definite mass boundary layer and also due to the fact that the evaporation is solely governed by the heat transfer at the media interface (Johansson et al., 1997; Pang, 2007). Also, when the temperature gradient in the solid decreases, the evaporation front may move from the surface to the center as described in receding core models (Khan et al., 1991; Chen et al., 2000,). Therefore, an accurate prediction of the mass transfer coefficient from

the analogy to heat transfer is not possible for SS drying. In such a case, the solution of the Reynolds-Averaged Navier-Stokes (RANS) equations for the conservation of mass and momentum together with the energy equation in the drying medium could be used to generate information about the boundary conditions associated with the transport equations in the solid (Erriguible et al., 2005; 2006).

Computational Fluid Dynamics (CFD) packages and their computational power for solving RANS and energy equations for the fluid medium have been proven to be an effective tool for modelling the detailed process parameters of complex drying systems including SS drying (Jamaleddine and Ray, 2010; Xiao et al. 2013). The reliability of the computational modelling of the heat and mass transfer mechanisms of SS drying is highly influenced by the accuracy of input parameters, the heat transfer medium, and the boundary conditions for energy and mass balance equations (Defraeye, 2014). Also, the capability to give greater insight to the drying process with 3D configuration with respect to time and space in shorter time when compared to experimental drying makes CFD modelling a suitable choice for the simulation of SS drying (Ducept et al., 2002; Iyota et al., 2001; Defraeye 2012a; 2012b).

In this study, a combination of the drying model associated with a moist cylinder and the model describing the external flow of SS was used. A finite volume method with varying boundary conditions depending on the stages of drying and with appropriate input parameters like thermo-physical properties and effective moisture diffusivity of the sample as a function of temperature and moisture content was used to solve the transport equations. The main objective of this study is to develop a numerical model for describing SS drying of a single

DSG pellet at selected operating conditions using the commercial CFD software (ANSYS CFX) and validate the derived model using experimental results.

6.3 Materials and method

6.3.1 Sample preparation

The raw material used in this study was a whole stillage mixture of corn and wheat in the ratio of 9:1 collected from a local distillery (Mohawk Canada Limited, a division of Husky Oil Limited, Minnedosa, MB). The whole stillage mixture was a thick paste with high moisture content in the range of 84-86% wb. The bulk raw material was kept in a freezer at -15°C in a sealed plastic pail. The frozen sample was taken out of the freezer and allowed to thaw at room temperature before the experimental trials. The thawed whole stillage was mixed thoroughly and then centrifuged using a Sorvall General Purpose, RC-3 centrifuge (Thermo Scientific Co., Asheville, NC) at a relative centrifugal force of 790g at a speed of 2200 rpm for 10 minutes (Erickson et al., 2005; Johnson et al., 2013). The centrifugation was done to separate and remove the excess amount of moisture from the whole stillage and to separate fine particles of mashed grains. The supernatant liquid, the top layer of the thin grain fraction (wet solubles), and the bottom layer of the coarse grain fraction of DSG, were then separated and weighed. Each fraction was stored separately in airtight containers at -15°C until testing. Before the experimental trials, the samples were thawed for 1 h at room temperature. The centrifuged whole stillage contained 49.5 ±0.5, 9.5 ±0.5, and 40.5 ±0.5% w/w of coarse grain fraction, distillers' solubles, and supernatant liquid, respectively. Initial moisture content of the coarse fraction and solubles was determined using the air-oven drying method (AACC, 2000).

6.3.2 Compaction of sample

The current study focuses on drying the major fraction of whole stillage i.e. the coarse grain fraction. This fraction with an initial moisture content of 77.8±0.1% was dried to the final moisture of 25% wb using a laboratory oven at 60±5^{o}C.This final moisture was chosen to eliminate clogging and sticking to the surface of a compaction mold (Johnson et al., 2014). The low-temperature drying (60±5°C) ensured minimum changes in material physical properties (Stroem et al. 2009). About 4.3 g of coarse grain fraction of DSG at 25% wb moisture content was placed in a cylindrical steel mold with a diameter of 12.2 ±0.01 mm and height of 80 mm. The sample inside the mold was compressed using a cylindrical die of 12.08 ±0.01 mm diameter and 84 mm length attached to a load cell of 10 kN of a universal testing machine (Model 3366, Universal testing Systems, Instron Corp., Norwood, MA). The pellet was formed with a compaction load of 6820 N (equivalent to 60.3 MPa) at a compression rate of 50 mm/min (Johnson et al., 2014; Bourassa et al., 2015) and was held at the same pressure for 300 s to reduce the spring-back effect (Tumulura et al., 2010).

6.3.3 Thermo-physical properties

The important thermo-physical properties like thermal conductivity, specific heat, and density of DSG pellets at varying moisture contents and temperatures were also determined using standard methods. The mass and dimensions of each DSG pellet were measured using an electronic balance with an accuracy of 0.001 g (PGW 453e, Adam Equipment Inc., Danbury, CT) and a digital Vernier caliper of 0.01 mm accuracy, respectively. The calculated volume and average mass of the pellets were used to determine the particle density of each pellet. The thermal conductivity of the prepared pellets was determined using the

modified Fitch method (Fitch, 1935; Rahman et al., 1991). The specific heat of the DSG pellets was determined using the method of mixtures. Ramachandran et al., (2016) describe in detail the experimental setup and procedure. Two pellets were placed inside a copper canister with the inside diameter equal to the diameter of the pellets. The sealed canister with the pellets was placed in water at different temperatures and change in the water temperature was measured while mixing (Mohsenin, 1980; Ramachandran et al., 2016). The effect of the independent variables (moisture content and temperature) on the dependent variables (thermal conductivity, density, and specific heat) was analyzed using a statistical software package (SAS 9.4).

6.3.4 Mass changes and effective diffusivity

The superheated steam drying system described by Zielinska et al. (2009) and Pronyk et al. (2010) was used in this study with some modifications regarding improving the heat insulation of the system. The SS drying system consisted of a water reservoir that supplies water to an electric boiler, pressure reducing valves, superheater, and a drying chamber. The data recording and monitoring of the operating conditions were done with the help of an in-house developed Visual Basic computer program. A thin perforated aluminum holding tray was hung inside the SS drying chamber with a thin metal wire of 0.3 mm diameter. The metal wire holding tray assembly was attached to a precision weighing balance (Sartorius ENTRIS 423-1S, Sartorius, Germany) placed above the SS drying chamber (Figure 6.1). The empty holding tray and the drying chamber were pre-heated to the desired operating temperature (120, 150, 180°C) to avoid steam condensation on the tray and inner walls of the drying chamber. The wall temperature was maintained at 3±0.5°C with respect to the operating temperature by means of strip heaters mounted on

the outer wall of the drying chamber, which was further insulated by a cellular glass and an outermost layer of a steel sheet. The SS drying system had the capability to bypass the chamber using a flow diversion valve (Figure 6.1). This diversion enabled safe loading/unloading of the sample. It also enabled measurement of true mass changes of the sample when the SS was not exerting an upward force on the sample. A single DSG pellet of 4.3±0.05 g and 25% wb initial moisture content was placed in the holding tray by opening the glass door located at the front of the drying chamber. The glass door was secured tightly with a 3 mm thick silicon gasket. The SS was re-diverted to the drying chamber and the mass of the pellet during drying was continuously recorded throughout the experimental period at regular intervals. Each drying experiment continued till the recorded mass reached equilibrium, i.e. when the mass change over time was ≤ 0.0001 g. The change in mass of the pellet over the drying time was plotted to determine the equilibrium point. The drying characteristic curves were developed from each experimental data. The average of 15 to 20 data points (moisture content) of the drying characteristic where the curve plateaued was used as the equilibrium moisture content. The experiments were repeated in triplicate for different temperatures (120, 150, 180°C) and superficial SS velocities (0.5, 1.0, 1.5 m/s) calculated at the cross-section where the sample was located. Each experiment took about 1 to 2 hours depending on the time required for the pellets to reach equilibrium moisture content.

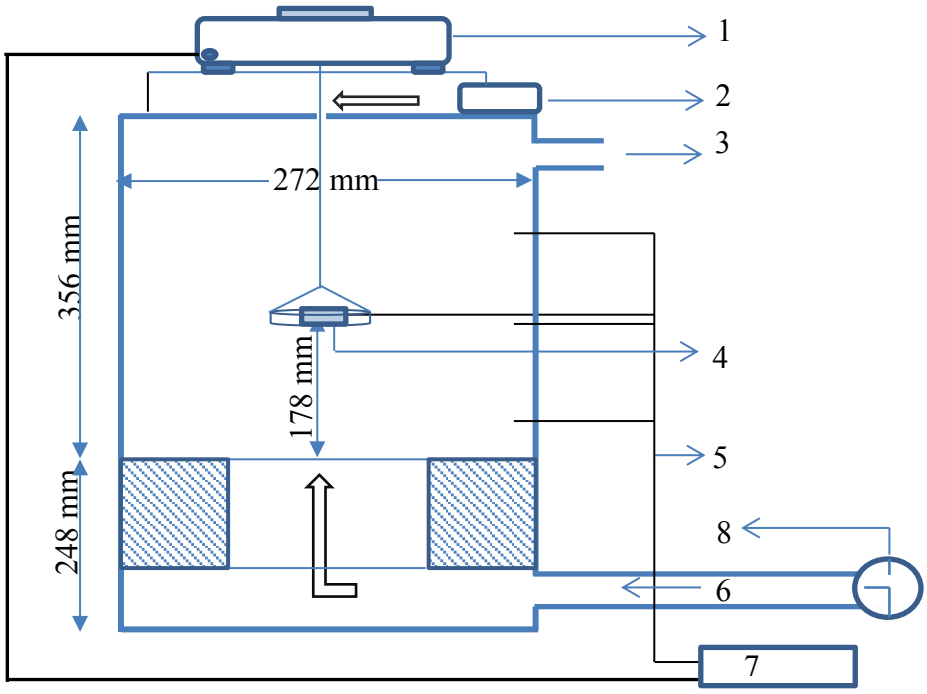

Figure 6.1 Schematic diagram of experimental setup for superheated drying of a single DSG pellet. 1- Weighing balance, 2- Heater-fan assembly, 3- Steam outlet, 4- Sample tray with DSG pellet, 5- thermocouples, 6- Steam inlet, 7- Data acquisition unit, 8- Flow diversion valve

The effective diffusivity of the pellets during drying was determined using Fick's law of diffusion (Pabis et al., 1998). The concept of using the geometric ratio (length to radius ≥ 10) for a cylinder to consider it as infinite is not always correct since it depends on the Biot number (Erdogdu and Turhan, 2006). Hence, the finite cylinder model (Pabis et al., 1998; Bourassa et al., 2015) was used for calculating the effective diffusivity of the pellets from the experimental values of moisture ratios (Equation 6.1 and Equation 6.2). Iyota et al. (2001) found that the simulation results of SS drying show better agreement in the initial stages than in the later stages of drying. They reported that the assumption of constant moisture diffusion coefficient regardless of temperature might be the reason for the divergence of the simulation result at the later stages of drying. Therefore the dependency

of effective diffusivity on the temperature of the sample can be represented by the Arrhenius type equation (Gely and Santalla, 2007) (Equation 6.2a):

$$MR(t) = \frac{M_{(t)} - M_e}{M_{(0)} - M_e} = \sum_{n=1}^{\infty}\sum_{m=1}^{\infty} \beta_n \beta_m \exp\left[-\left(\mu_n{}^2 + \mu_m{}^2 k_t{}^2\right) Fo_m\right] \quad (6.1)$$

Where, *MR(t)* is the instantaneous moisture ratio and $M_{(t)}$, $M_{(0)}$, M_e are the instantaneous, initial, and equilibrium moisture content (wb).

$$\beta_n = \frac{4}{\mu_n{}^2},\ \beta_m = \frac{2}{\mu_m{}^2},\ J_0(\mu_n) = 0, \text{ and } \mu_m = (2m-1)\frac{\pi}{2}$$

Where, μ_n are the roots of the Bessel function of first kind of the order zero, and the values of μ_n defined in Equation 6.1 for n=1 to 10 are 2.4048, 5.5201, 8.6537, 11.7915, 14.4309, 18.0711, 21.2116, 24.3525, 27.4935, and 30.6346, respectively.

$k_t = \frac{r_t}{L_t}$ (r_t is the radius of DSG pellet, and L_t is the length of the DSG pellet).

$$D_{eff} = \frac{Fo_m r_t{}^2}{t} \quad (6.2)$$

Also, $D_{eff} = D_o \exp\left(-\frac{Ea}{RT}\right)$ (6.2a)

The D_o is the pre-exponential factor, which is determined from the experimental value of diffusivity. The value of *Ea* and D_o were determined using the slope and intercept of a semi-log plot of the experimental values of diffusivity and inverse of corresponding temperature (Mirzaee et al., 2009; Afolabi et al., 2014).

6.3.5 Temperature changes while drying

The temperature profile of the pellets during drying was measured separately from the drying experiments using the same SS operating parameters. Pellets of approximately the

same length (35.5 ±2 mm) and diameter 12.7 ±1 mm with an initial temperature of about 22 ± 3^{o}C were used for this study. All samples with dimensions outside these limits were discarded. A T-type thermocouple was inserted through the longitudinal axis of the DSG pellet. To measure the change in surface temperature, the thermocouple was positioned approximately 2-3 mm from the other end of the pellet. This method also prevented the conductive heating of thermocouple wire, which could have led to the error in temperature measurement (Pronyk et al., 2010). A data acquisition system recorded temperature from the thermocouple every second for 1 hour until the thermocouple reading was equal to the SS temperature. These experiments were conducted in triplicate and the temperature values were averaged.

6.3.6 Mathematical modelling

The modelling methodology was divided into two components: (i) modelling of the fluid domain, which is SS flow around the drying element (i.e. the pellet) and (ii) modelling of the solid domain, represented by the DSG pellet.

6.3.6.1 RANS and energy equations for the fluid domain

The flow of SS as the drying medium was considered here as the external flow (fluid domain) surrounding the pellet and was modelled by solving the RANS and energy equations for the conservation of mass, momentum, and energy (Defraeye et al., 2012a; De-Bonis and Ruocco, 2008; Akbarzadeh et al., 2012). Therefore, the solution to Navier-Stokes equations in the fluid domain gives information on the boundary conditions for the transport equation in the solid domain represented by the pellet (Errigiuble et al., 2005). As the methodology of obtaining the governing equation for mass, momentum and heat transfer during drying have been already detailed by previous researchers (Perre and Moyne, 1991), only the relevant set of partial

differential equations are discussed here. Superheated steam medium surrounding the pellet consists of only pure vapour (which is assumed to be a Newtonian fluid), and the conservation of mass, momentum (given by the RANS equations (Equations 6.3, 6.6) and energy equation (Equation 6.7) (Bernard and Wallace, 2002).

$$\frac{\partial \rho_{ss}}{\partial t} + \vec{\nabla} \cdot \left(\rho_{ss} \vec{V}\right) \tag{6.3}$$

The aforementioned model equation is valid under the assumption that SS is incompressible (Erriguible et al., 2005; 2006). For an incompressible fluid, the density is constant; therefore, the differential mass balance becomes:

$$\vec{\nabla} \cdot \vec{V} = 0 \tag{6.3a}$$

Where, ∇ is the Laplace operator, which denotes derivatives with respect to position, also commutes with time-averaging. The differential equation for motion is given by (Bernard and Wallace, 2002):

$$\rho_{ss} \frac{\partial \vec{V}}{\partial t} + \rho_{ss}\left(\vec{V} \cdot \nabla \vec{V}\right) = -\vec{\nabla} P + \vartheta \nabla^2 \vec{V} + \rho_{ss} \vec{g} \tag{6.4}$$

The fluid is assumed to be Newtonian and of constant viscosity. By substituting $\left|\vec{V}\right| = \bar{V} + V'$ and $\left|\vec{P}\right| = \bar{P} + P'$, time averaging yields:

$$\rho_{ss}\left(\overrightarrow{\frac{\partial \vec{V}}{\partial t} + (\bar{V} \cdot \bar{\nabla} \bar{V}) + (V' \cdot \nabla V')}\right) = -\bar{\nabla}\left(\overrightarrow{\bar{P} + P'}\right) + \overrightarrow{\vartheta \nabla^2 \left(\bar{V} + V'\right)} + \rho_{ss} \vec{g} \tag{6.5}$$

Where, $\bar{V}$ and $\bar{P}$ are the average values of velocity and pressure, and V' and P' are the random fluctuations of the same variables. By applying the continuity equation for incompressible fluid ($\nabla \cdot V = 0$) and Equation 6.3a, Equation 6.5 can be simplified to

$$\rho_{ss}\left(\overrightarrow{\frac{\partial \vec{V}}{\partial t} + (\bar{V} \cdot \bar{\nabla} \bar{V})}\right) = -\bar{\nabla} \vec{\bar{P}} + \vartheta \nabla^2 \vec{\bar{V}} + \rho_{ss} \vec{g} - \overrightarrow{\nabla \cdot \rho_{ss} V' \cdot V'} \tag{6.6}$$

Where, the quantity ($\rho_{ss} V' \cdot V'$) in the last term of the Equation 6.6 is called Reynolds stress. ϑ_t is the eddy (turbulent) viscosity given by:

$$\vartheta_t = \frac{C_\mu k^2}{\varepsilon} \tag{6.6a}$$

Where, C_μ is the constant of proportionality (equal to 0.09), and k and ε are the turbulence kinetic energy and dissipation rate, respectively (Akbarzadeh et al., 2012), which can be obtained from the following equations:

$$\frac{\partial k}{\partial t} = \vec{\nabla} \cdot \left(\vec{V} k - \vartheta \vec{V} k\right) = P_k - \varepsilon \tag{6.6b}$$

$$\frac{\partial \varepsilon}{\partial t} = \vec{\nabla} \cdot \left(\vec{V} \varepsilon - \vartheta \vec{V} \varepsilon\right) = P_k + \frac{\varepsilon}{k}(C_1 P_k - C_2 \varepsilon) \tag{6.6c}$$

where, P_k is the production rate of k, and C_1 and C_2 are equation constants (ANSYS CFX theory guide, 2009). Details of the turbulence model equations and coefficients can be found in the literature (Akbarzadeh et al., 2012).

The differential equation for energy balance is given by:

$$\frac{\partial \rho_{SS}\, H}{\partial t} + \nabla \cdot (\rho_{SS}\, V\, h + k t_{SS}\, \nabla T) = 0 \tag{6.7}$$

$$H = \lambda_v^{ref} + Cp_s (T - T_{ref}) \tag{6.8}$$

Where, H is the enthalpy in the control volume of the fluid domain with respect to the reference temperature (kJ/kg[1]), λ_v^{ref} is the latent heat of vaporization at a reference temperature (kJ/kg[1]) of steam T_{ref}. The reference temperature of steam is the operating temperature of the SS unit for each experiment. The Reynolds number for the SS flow was calculated using Equation 6.9 (Olsson et al., 2004; Olsson et al., 2005; Akbarzadeh et al., 2012):

$$\mathrm{Re} = \frac{\rho_{SS}\, V\, d}{\vartheta} \tag{6.9}$$

6.3.6.2 Mathematical model for the solid domain

In developing the mathematical model for the solid domain represented by the pellet, the following assumptions were considered: (i) the sample was considered to be isotropic and homogeneous and (ii) the longitudinal expansion of the pellets due to the relaxation of stress during drying was negligible (Tzempelikos et al., 2015). In SS drying, mass transfer cannot be considered as the primary drying force for the drying process. But certainly, a heat and mass balance is generated at the interface of the pellet and SS. Hence, the drying phenomenon is measured in terms of the flux of moisture in the form of vapor leaving the interface of the pellet into SS (Pakowski and Adamski, 2011). Mass transfer in the solid domain can be caused by a pressure gradient, and diffusion of moisture either in vapour or liquid phase, which is governed by the moisture gradient (Pakowski et al., 2011). The heat transfer inside the pellet is governed by the conduction in all directions. The governing equations for energy and mass balance within the solid domain (the pellet) are as follows (Wang and Brennan, 1995; Ruiz-López et al., 2004; Chandramohan and Talukdar, 2010):

$$\frac{\partial T_p}{\partial \mathrm{t}} = \frac{1}{\rho_{p_i}\left(Cp_{p_i}\right)}\left[\frac{\partial}{\partial x}\left(kt_{p_i}\frac{\partial T_p}{\partial x}\right)+\frac{\partial}{\partial y}\left(kt_{p_i}\frac{\partial T_p}{\partial y}\right)+\frac{\partial}{\partial z}\left(kt_{p_i}\frac{\partial T_p}{\partial z}\right)\right] \tag{6.10}$$

$$\frac{\partial M}{\partial t} = \left[\frac{\partial}{\partial x}\left(D_{eff\,i}\frac{\partial M}{\partial x}\right)+\frac{\partial}{\partial y}\left(D_{eff\,i}\frac{\partial M}{\partial y}\right)+\frac{\partial}{\partial z}\left(D_{eff\,i}\frac{\partial M}{\partial z}\right)\right] \tag{6.11}$$

The values of kt_{p_i} and Cp_{p_i} were defined as a function of moisture content and temperature in the thermo-physical properties of DSG pellet in the model.

Unlike air drying, SS drying typically has three stages. These are initial condensation of steam on a sample, the evaporation of condensed steam, and the drying phase period (Hamawand 2011). Hence, the heat and mass balance equations have to be defined for three

different conditions depending on the surface temperature of the pellet. The governing transport equations for each section are described as follows:

(i) Initial condensation occurs when the sample (being initially at a lower temperature) comes in contact with the SS leading to a local condensation of steam on its surface (Hamawand, 2011; Johnson et al., 2013; Hamawand et al., 2014; Jamradleodluk, 2007). The moisture either evaporates or is adsorbed by the sample depending on the sample's sorption behaviour (Pakowski and Adamski, 2011). The boundary conditions for heat (Kittiworrawatt and Devahastin, 2009) and mass (Xiao et al., 2013) transfer for this case are given by Equations 6.12 and 6.14, respectively.

If $T_p < T_{sat}$, $-kt_p(\nabla T \cdot n) = \lambda_v \dot{m}_{ic}$ (6.12)

The film condensation heat transfer plays a major role in the heat flux occurring during initial condensation period as the latent heat generated during the initial condensation is much higher than the heat flux due to convection (Iyota et al., 2007; Ramachandran et al., 2017). The film condensation heat transfer coefficient of superheated steam, where water vapour condenses on the cylindrical pellet surface, is given by the Equation 6.13 (Holman, 2001):

$$\mathrm{h}_{film} = 0.725\left(\frac{\rho_{film}(\rho_{film-}\rho_{ss})g\lambda_v(kt_{film})^3}{2r\eta_{film}(T_{sat}-T_P)}\right)^{\frac{1}{4}} \quad (6.13)$$

$$\dot{m}_{ic} = \frac{h_{film}(T_{sat}-T_{p)}}{\lambda_v} \quad (6.14)$$

(ii) When the sample surface temperature reaches the saturation temperature of steam, evaporation of free water from the surface of the pellet begins. This evaporation continues at a constant pellet temperature and is dominated by the heat transfer coefficient between the water on the surface and SS (Iyota et al., 2007; Suvarnakuta et al., 2007; Kittiworrawatt and

Devahastin, 2009; Hamawand et al., 2014). Hence, the heat and mass transfer boundary conditions for the constant drying rate period are given by Equations 6.15 and 6.16:

If $T_p = T_{sat}$, $-kt_p(\nabla T \cdot n) = h(T_{sat} - T_{ss}) = \lambda_v \dot{m}_{cr}$ (6.15)

$$\dot{m}_{cr} = \frac{h(T_{sat} - T_p)}{\lambda_v} \quad (6.16)$$

Where, h near wall is the automatic heat transfer coefficient obtained from the solution of RANS equation in (SS) region.

(iii) After the pellet reaches the critical moisture content, the temperature of the pellet rises and the evaporation inside the pellet is dominated by moisture diffusion (i.e. liquid or vapour or both). But, as the temperature rises above the boiling temperature of water, an internal pressure builds up due to vapour formation which may cause the capillary/Darcy's flow. In that case, drying rate can be predicted by basing it on the sensible heat transfer rate between the pellet and the SS divided by the latent heat of vaporization of moisture (Beeby and Potter, 1985; Pakowski and Adamski, 2011). The heat balance at the interface in this case (Pakowski and Adamski, 2011) is given by Equation 6.17:

If $T_p > T_{sat}$, $-kt_p(\nabla T \cdot n) = (\lambda_v + C_{pv}T_p)\dot{m}_{fr} + q_p = h(T_{ss} - T_p)$ (6.17)

where, q_p is the net heat flux penetrating the pellet and T_p is the temperature of pellet at a given moisture content and vapour partial pressure which in this case is atmospheric pressure (Pakowski et al., 2011). The conservation of mass was solved by balancing the mass flux at the interface. Hence, the mass transfer boundary condition is:

$$\dot{m}_{cr} = D_{eff_i}(\nabla M \cdot n) = \frac{h(T_p - T_{ss}) - q_p}{\lambda_v + C_{pv}T_p} \quad (6.18)$$

The equilibrium condition at the interface is given by

$$P_v = F(M, T_p)P_{sat}(T_p) \quad (6.19)$$

Where, the saturation vapour pressure of water vapour at different solid surface temperature is given by (Messai et al., 2015):

$$ln\left(P_{sat}(T_p)\right) = 25.506 - \frac{5204.9}{T_p} \quad (6.19a)$$

6.3.7 Implementation of the model

To predict the heat and mass transfer in the DSG pellet during SS drying, a 3D mathematical model was developed using the CFD software ANSYS-CFX 16.2 package (ANSYS Inc., Canonsburg, PA). A quarter section of the geometry, including both the DSG pellet and the SS drying chamber was used as the computational domain for the 3D model (Figure 6.2). The selected pellet was 12.7 mm in diameter and 35.5 mm long. The drying chamber had 272 mm internal diameter and 356 mm length. The schematic illustration of the DSG pellet placed at the geometric center of the drying chamber and the meshing of the corresponding computational domain using the CFX is shown in Figure 6.2. The thermo-physical properties of the DSG pellets were defined as a function of their moisture content and temperature in CFX. In order to capture the changes in the variables, the resolution of the mesh near the walls was increased by adding on inflation layer with structured meshes (Figure 6.2). The mesh sensitivity was also tested using three different computational meshes with different grid resolutions of 0.98, 1.11, and 2.30 million nodes. The convergence of the experimental data with the predicted values was used to check the sensitivity of the mesh. An interface was created between the solid and liquid domain where the transport equations for condensation were applied as a source term. The model equations for the solid domain represented by the pellet were also defined in the CFX. In order to consider evaporation of moisture, a subdomain was created for the solid and the heat transfer boundary conditions were applied as a source term. When the surface temperature of the coating reaches the

saturation temperature, the film condensation heat transfer coefficient is replaced by the flow field heat transfer coefficient which was automatically taken care of by the CFD solver. The code for solving the flow equations and the equations for the solid were then coupled by executing both codes in the same time step (Erriguible et al., 2005). At first, the conservation equations were defined for both domains, and then boundary conditions were substituted for the conservation equations (Erriguible et al., 2006). Additional source terms were considered at the pellet/steam interface to model the initial condensation on the DSG pellet. The operating SS temperature and velocity were set as the initial conditions at the chamber inlet. A zero velocity boundary condition was assumed for the interface between the SS and the pellet. All flow variables (i.e. temperature, pressure, and velocity) were derived for the outlet of the chamber from the fluid domain (Akbarzadeh et al., 2012). A moisture content of 25% and the temperature (25°C) was assigned as initial conditions for the DSG pellet.

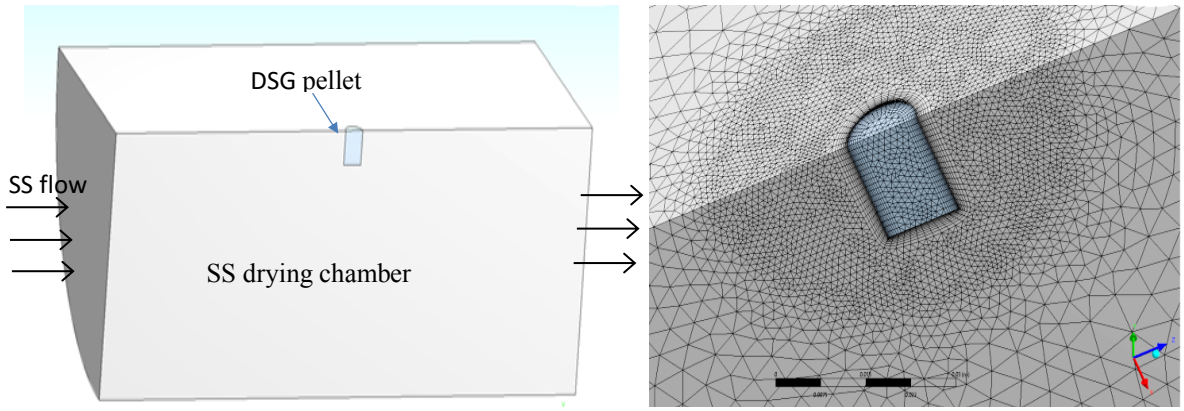

Figure 6.2 (a) Schematic diagram of the SS drying chamber and the DSG pellet (b) The enlarged view of the unstructured mesh near and inside the half pellet.

For the fluid domain, the shear stress transport (SST) k-ω turbulence model was applied (Menter, 1994; Ljung et al., 2011a; Ljung et al., 2011b; Tzempelikos et al., 2015). The SST

k-ω model uses a two-equation k-ω model formulation to solve the transport phenomena in the near-wall region and a k-ε model formulation to solve the turbulent central region of the fluid flow (Menter, 2009). The Reynolds number obtained for different SS operating conditions was in the range of 3650-7500, which falls in the transition to the turbulent flow region (Karabelas et al., 2012). The SST k-ω turbulence model performs well with low Reynolds numbers, especially near the walls (Defraeye et al., 2012b) and also when adverse pressure gradient boundary layer flows are simulated (Ljung et al., 2011a). Also, the SST k-ω turbulence model was found to be sufficiently accurate for predicting the convective heat transfer coefficient (Dixon et al., 2011). In the beginning of the simulation, the steady-state and isothermal analysis of flow equations (i.e., without drying) were performed to obtain a fully developed steam flow around the pellet. In case of transient simulations, variable time step size with the increase in simulation (drying) time was chosen and each time step had 10 iterations. The time step size varies as 0.05, 1, 1.5, 5, 10, 20, 50, and 100, respectively for 1, 5, 10, 20, 40, 60, 90, 120 min. Each time step had ten iteration as it is recommended for the multiphase problems. The smaller time step size during the initial stages of drying was chosen to capture the initial condensation and the relatively fast changing transport phenomena when compared to the later stages of drying. The steady-state simulation results were used as the initial conditions for the transient-state analysis of the drying simulation. The convergence criteria for the root mean square (RMS) values of the residuals were set to 1×10^{-4} and 1×10^{-6} for the steady-state and transient-state analysis, respectively. A non-slip wall boundary condition was assumed for the interface between the SS and the pellet (Kaya et al., 2007).

6.3.8 Validation of the model

The experimental and simulation trials were conducted for three different SS temperatures (120, 150, and 180°C) and three different SS velocities (0.5, 1.0, and 1.5 m/s). The overall moisture content and the surface temperature of the DSG pellets obtained from SS drying experiments at each of the operating conditions were compared with the average moisture content and surface temperature values obtained from the simulation using the mean relative percentage error (Kaleemullah and Kailappan, 2006; Sabarez, 2012). The mean relative percentage error of the simulation results was calculated using the following equation:

$$MRP = \frac{1}{n}\sum_{i=1}^{n}\frac{|Pv_i - Ev_i|}{Ev_i}\times 100 \qquad (6.20)$$

where, MRP is the mean relative percentage error, Pv_i and Ev_i are the instantaneous predicted and experimental values of the variable, respectively, and n is the number of data points compared.

6.4 Results and discussion

6.4.1 Thermo-physical properties

The particle density of the DSG pellets at a moisture content of 25% wb was 873.7±2.7 kg/m^3. The particle density of the DSG pellet decreased with a decrease in moisture content following an empirical relation (Equation 6.21). The value of thermal conductivity and specific heat capacity of DSG pellets within a temperature range of 0 to 80°C were 0.17-0.22 W/(m K) and 4.13- 5.28 kJ/(kg K), respectively. Both, thermal conductivity and specific heat values increased with increasing moisture content of the DSG pellet. A similar trend was reported by Yu et al., (2015). The experimental results show that thermal conductivity

and specific heat of DSG pellets were empirically related to temperature and moisture content of the pellet (Figure 6.3a and 6.3b) as given by Equations 6.22 and 6.23, respectively (Ramachandran et al., 2016).

$$\rho_p = 1011 - 46M \tag{6.21}$$

$$kt_p = 0.001\,T + 0.006\,M - 0.002 \tag{6.22}$$

$$C_p = 0.02\,T + 0.02\,M + 0.27 \tag{6.23}$$

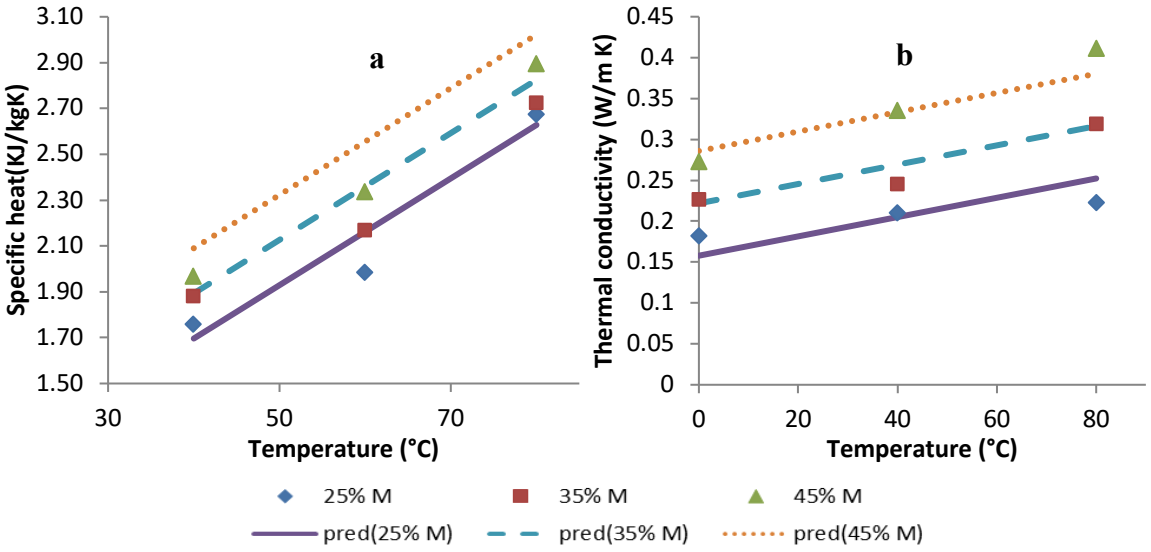

Figure 6.3 Effect of temperature on the a) specific heat and b) thermal conductivity of DSG pellets at different moisture content (25, 35, and 45% wb), where, exp- experimental values and pred- predicted values.

6.4.2 Effective moisture diffusivity

The effective moisture diffusivity of the DSG pellets at different operating conditions of the SS drying unit was in the range of 3.06 $\times 10^{-9}$ to 13.5$\times 10^{-9}$ m^2/s. The value of the effective moisture diffusivity increased with an increase in temperature and velocity of the SS (Azzouz et al., 2002; Babalis and Belessiotis, 2004). These results are in agreement with the results

reported by Zielinska et al. (2009). The change in the effective diffusivity as affected by temperature (120,150, and 180°C) and velocities of SS (0.5, 1.0, and 1.5 m/s) are shown in Figure 6.4a. As per the Arrhenius type equation (Equation 6.2a), the effective moisture diffusivity is dependent on the material temperature. But in the current study, it is considered as a function of a reciprocal of SS temperature. This approach is adopted based on the assumption that during the falling drying rate period, the average material temperature is the same as that of the SS temperature (Zielinska et al., 2009). Therefore, the values of the activation energy for each SS velocity were determined from the relationship between the natural log of effective diffusivity and the inverse of SS temperature as shown in Figure 6.4b. The activation energy of the DSG pellet for the SS velocity of 0.5, 1.0, and 1.5 m/s was found to be 15.64, 20.53, and 24.61 kJ/mol, respectively. A similar trend of an increase in activation energy and moisture diffusivity with an increase in velocity of drying medium was reported by Aghbashlo et al. (2008) and Motevali et al. (2012), who also related activation energy to the temperature of the drying medium. There was an increase in activation energy when the velocity of SS increased above 1 m/s irrespective of the SS temperature, which supports the findings of Chayjan et al. (2011). This effect of the velocity of SS on activation energy is due to the higher rates of heat transfer than the mass transfer. It may cause the internal temperature of the pellet to rise above the boiling point resulting in an internal pressure build-up forcing the moisture to the surface. This increase in vapour pressure might cause a liquid flow (Darcy's flow) inside the pellet. In that case, the effective diffusivity values of the falling drying rate curve as per the Arrhenius equation will not be sufficient for predicting the complete drying process (Pakowski and Adamski, 2011). Hence, the diffusion equation with moisture diffusivity as a function of SS temperature was used to define the transport

phenomena within the pellet until the local temperature of the pellet is less than boiling temperature (Hamawand et al., 2014). But once the local temperature of the pellet rises above the boiling point, the approach of sensible heat transfer rate between the steam and the pellet divided by the latent heat of vaporization of moisture was used to describe the drying rate as shown in Equation 6.18 (Pakowski and Adamski, 2011).

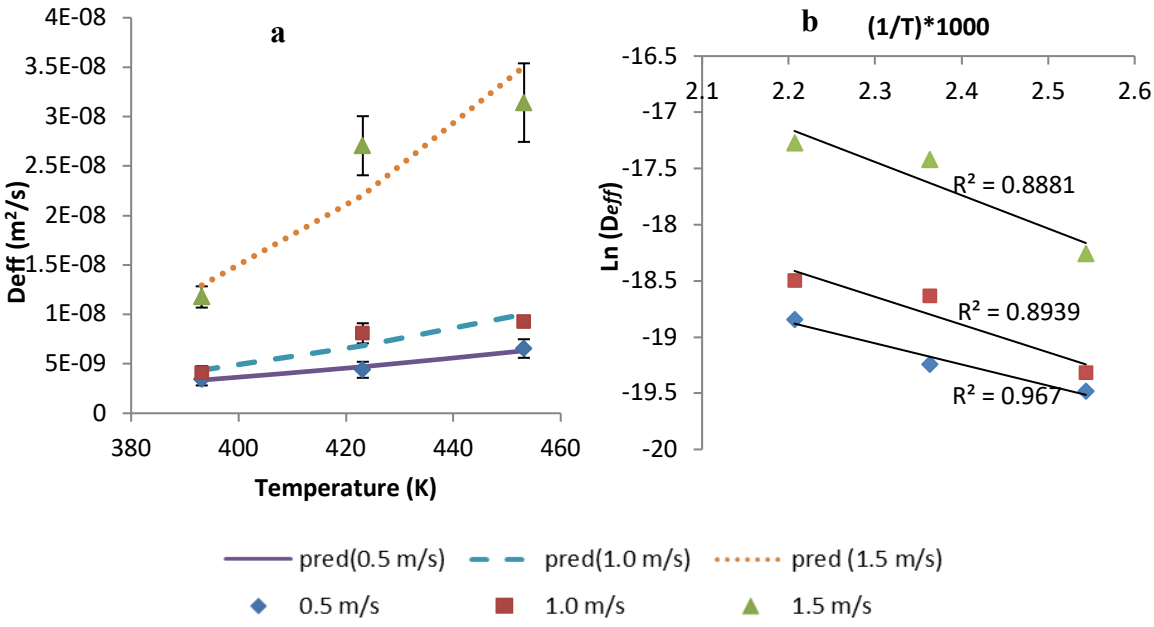

Figure 6.4a) Effect of SS temperature on the effective moisture diffusivity of DSG pellet at different SS velocities, b) Arrhenius plot of ln(D_{eff}) verses (1/T) at different SS velocities. * R^2 is the coefficient of determination.

6.4.3 Validation of SS drying model

The multi-configuration approach in which the transient state simulation is automatically started with the solution of an initial steady state simulation, used for the simulation of SS drying of DSG pellet improved the total simulation time when compared to the single configuration. The average simulation time for the simulation with multi-configuration was

found to be 6h, 27min which was 15% less than that of the single configuration simulation (7h, 22min), where the steady- and transient-state configurations are run separately. The maximum turbulence residual values of the simulation with the SST k-ω model (1×10^{-5} - 1×10^{-6}) were less than the residuals for the simulation with k-ε model (1×10^{-2} -1×10^{-5}). Among the three meshes tested (0.98, 1.11, and 2.3 million nodes), the meshes with 1.11 and 2.3 million nodes showed minimum deviation from the experimental results when tested at the lowest SS temperature for all the test velocities. The details of the $y_{Auto}+$ values of nodes closest to the solid-fluid interface and the comparison of RMS and maximum percentage deviation of moisture content and temperature at the interface are given in Appendix (Table A.3 and A.4). The difference in maximum MRP error for the moisture prediction of the DSG pellet from the simulations with 1.11 and 2.3 million nodes were less than 2.4%. The simulation time for the meshes with 2.3 million nodes were relatively high (13.1 h) compared that required for the mesh with 1.11 million nodes (6.45 h). Hence, the mesh with 1.11 million nodes was used for the rest of the simulations.

Experimental results show that there was a negligibly short constant drying rate period for the pellet (Figures 6.5, 6.6, and 6.7), which supports the findings of Zielinska and Cenkowski (2012) and Kittiworrawatt and Devahastin (2009). But a relatively constant temperature period with a gradual increase in temperature in the later phase was observed for the tested SS temperatures and velocities (Figures 6.5, 6.6, and 6.7). The short constant temperature period might be due to the evaporation of the condensed steam from the surface of the pellet (Zielinska et al., 2009). A gradual increase in temperature afterward indicates the removal of moisture from the pellet and steam penetration in the expanded pellet. It could also be due to the release of the stored mechanical energy due to the pellet expansion during SS drying

(Bourassa et al., 2015). This increase in temperature in the proposed constant temperature period might be also attributed to the exothermal processes that occur during the denaturation of protein (Fitzsimons et al., 2007).

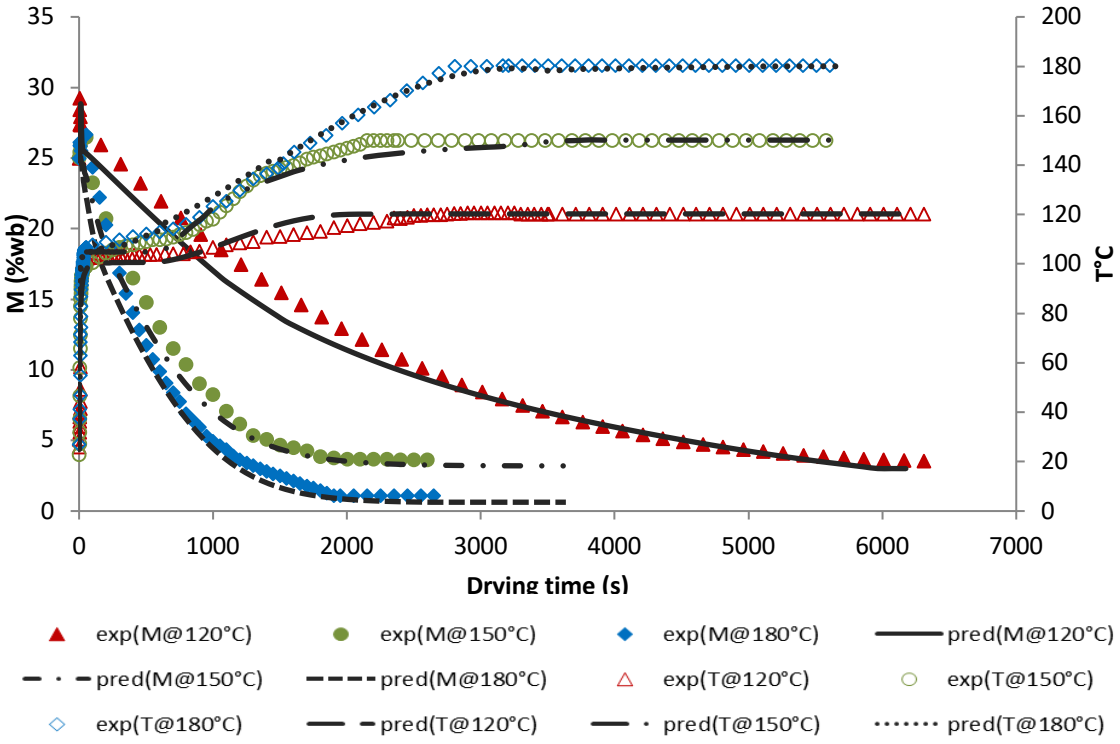

Figure 6.5 Comparison of experimental and predicted values of moisture (M) and surface temperature (T) history of DSG pellet at SS velocity of 0.5 m/s, where, exp- experimental values and pred- predicted values

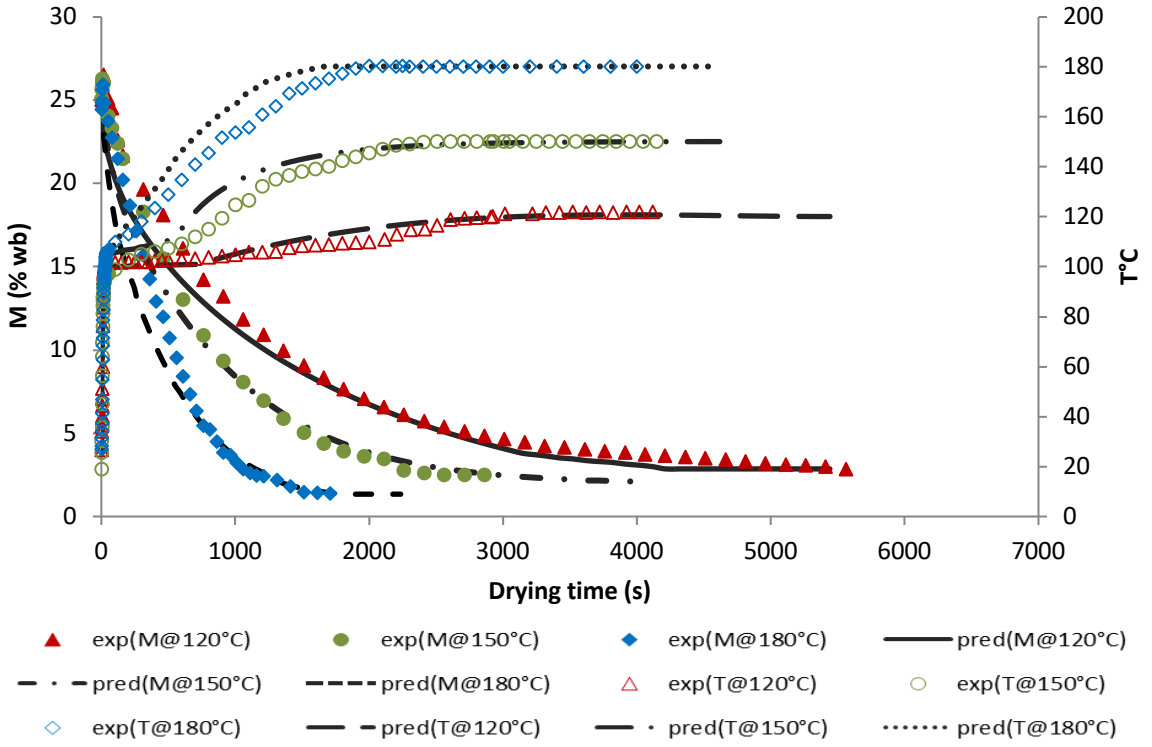

Figure 6.6 Comparison of experimental and predicted values of moisture (M) and surface temperature (T) history of DSG pellet at SS velocity of 1.0 m/s, where, exp-experimental values and pred-predicted values

The mean relative percentage error was in the range of 3.1–7.8% and 8.8–9.5% for the surface temperature values and average moisture values of the pellet dried at different operating conditions, respectively. The lower percentage error (≤ 10%) shows that the experimental data are well predicted by the model (Kaymak-Ertekin and Gedik, 2005). The initial condensation period was slightly under predicted by the model when compared to the experimental results (Figure 6.8). This is in concurrence with the findings of Hamawand et al. (2014) and can be attributed to the absorption of moisture by the pellet. The pellets' ability to absorb a part of condensed water has previously been reported by Johnson et al. (2013).

This absorbed moisture is no longer available as free water on the surface of the pellet during the initial evaporation phase (Taechapairoj et al., 2006).

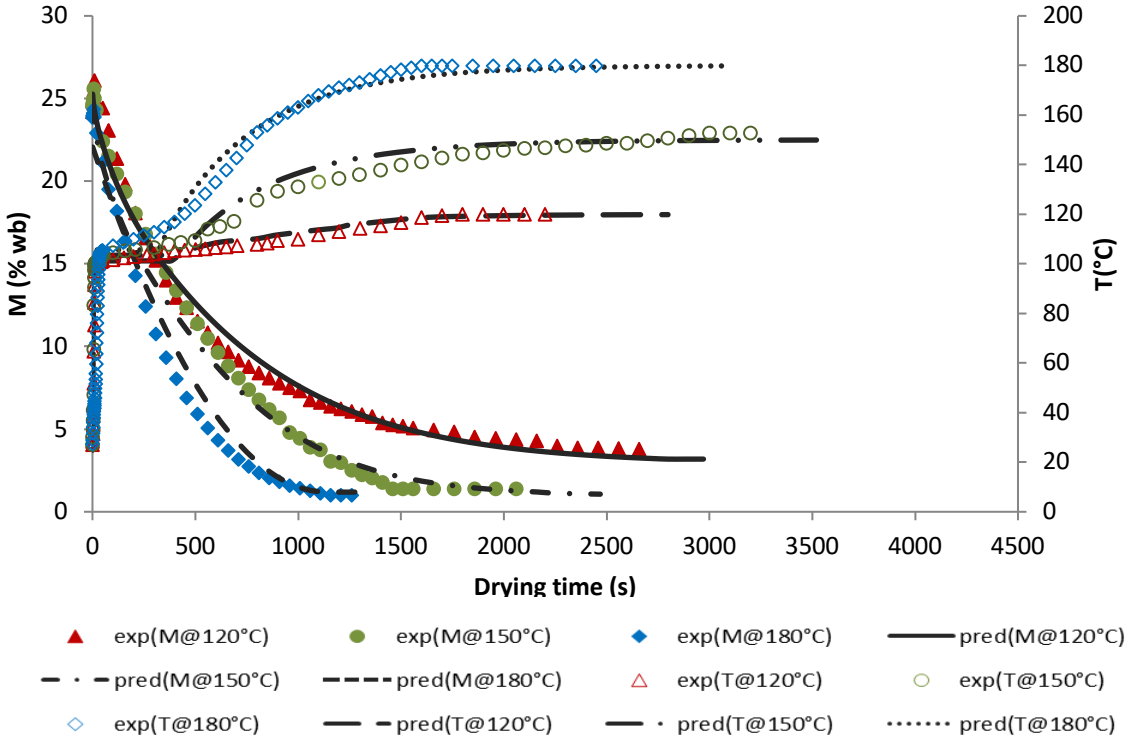

Figure 6.7 Comparison of experimental and predicted values of moisture (M) and surface temperature (T) history of DSG pellet at SS velocity of 1.5 m/s, where, exp- experimental values and pred- predicted values

The agreement of the simulation results with the experimental values of moisture content during the initial phase of drying was lower (Figures 6.5 and 6.6) when compared to the later stages of drying, especially for the lower SS temperature (120°C) and lower SS velocities (0.5 and 1 m/s). The poor agreement (MRP is 22.2 ± 2%) of simulation and experimental moisture content in the early drying period can be explained by the limitations of the simulation in accommodating the internal movement of condensed moisture occurring during the initial condensation (Parkowski and Adamski, 2011). Therefore, the experimental

drying curve was found to give higher results than the predicted drying curve during the early 'so-called' constant drying rate period.

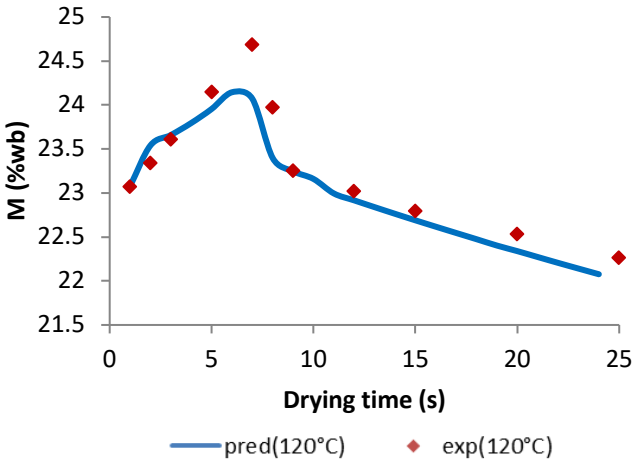

Figure 6.8 Comparison of experimental and predicted values of initial condensation on DSG pellet at SS velocity of 1.0 m/s, where, exp- experimental values, pred- predicted values, and M- moisture content.

The predicted change in the local moisture content and temperature at the center of the DSG pellet is also given in Figures 9a and 9b. The moisture in the center of the pellet remains intact during the initial stages of SS drying (Figure 6.9a). Once the free water available on the outer layers of the pellet evaporated during drying, the moisture from the center began to diffuse towards the periphery of the pellet. The temperature at the center of the pellet reached the saturation temperature of the steam around 500-550 s of drying while the local moisture content at the center of the pellet remained constant during that time, especially for lower SS temperature drying (Figure 6.9a and 6.9b). This might be due to the latent heat energy build-up from evaporation either on the surface or inside the pellet, which we cannot precisely distinguish. Also, in actual drying experiments, there might be chances that the condensed steam on the surface of the pellet migrated into its interior. This moisture migration towards

the center of the pellet would be dominated by the receding evaporation front from the surface to center at later stages of drying. Even though the exact time of start of these phenomena cannot be precisely determined, the study of spatial variation of moisture content could give an insight into the instantaneous changes in the moisture profile during SS drying. Hence, the local moisture content and temperature profile of DSG pellet at any instant of SS drying were also studied.

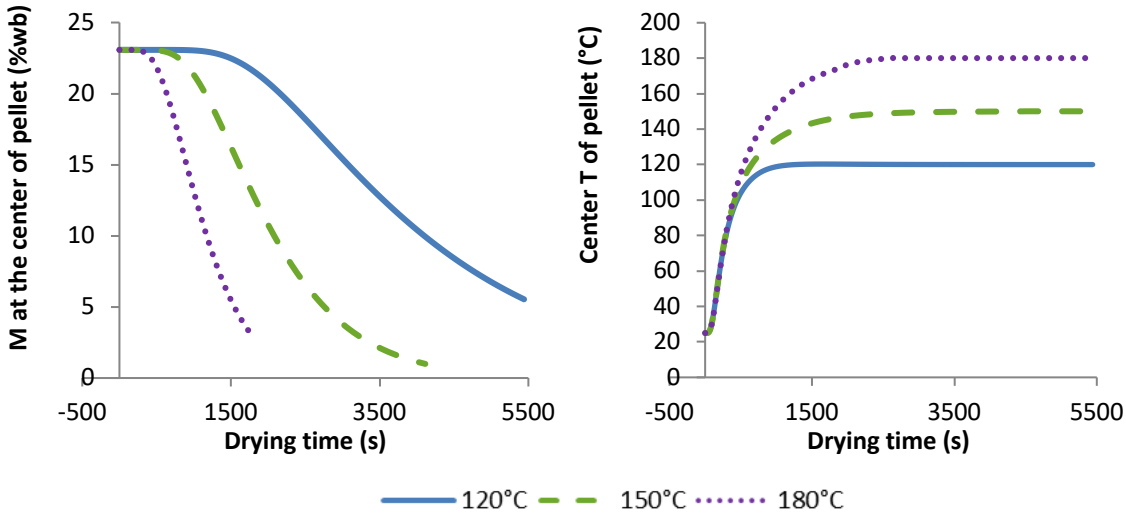

Figure 6.9 Predicted values of a) moisture history b) temperature history at the center of the DSG pellet at SS velocity of 1 m/s; where, M and T are the moisture content and temperature of the pellet, respectively.

The simulation results of the instantaneous moisture profile of DSG pellet at various operating conditions (SS temperature of 120, 150, 180°C, and SS velocity of 0.5, 1.0, and 1.5 m/s) showed that the mechanism of drying was supported by surface evaporation (Hamawand, 2013) right after the initial condensation (Figure 6.10a) when the surface temperature of the pellet was 100°C (Figure 6.10b). The drying front moves from the surface to centre as drying proceeds (Figure 6.10a and 6.10b) supporting the receding core

model reported by Looi et al. (2001). During the later stages of drying (i.e. when the surface temperature of the pellet increases) the diffusion of moisture (liquid or vapour or both) to the surface of the pellet and evaporation from the surface facilitates drying (Figure 6.10a and 6.10b). The values of local moisture and temperature within the sample decreased with an increase in distance from the centre of the pellet at a given drying time. The temperature of SS has a more significant effect on the decay rate of the moisture content of the pellet than the velocity of the SS (Figure 6.11a and 6.11b).

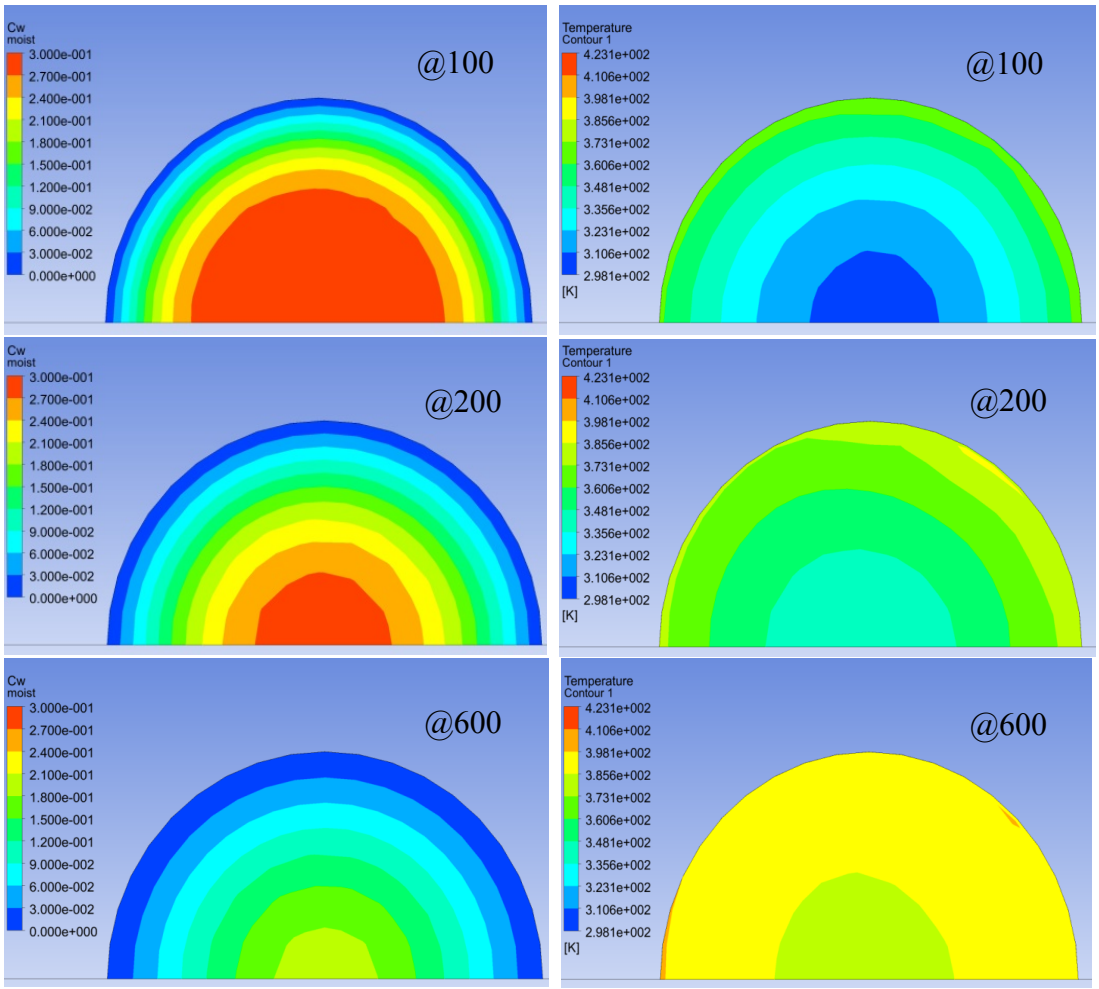

Figure 6.10 Predicted a) moisture distribution (left side) b) temperature distribution (right side) of the DSG pellet at 100, 200, 600s of drying, respectively (SS at 150°C and 1 m/s).

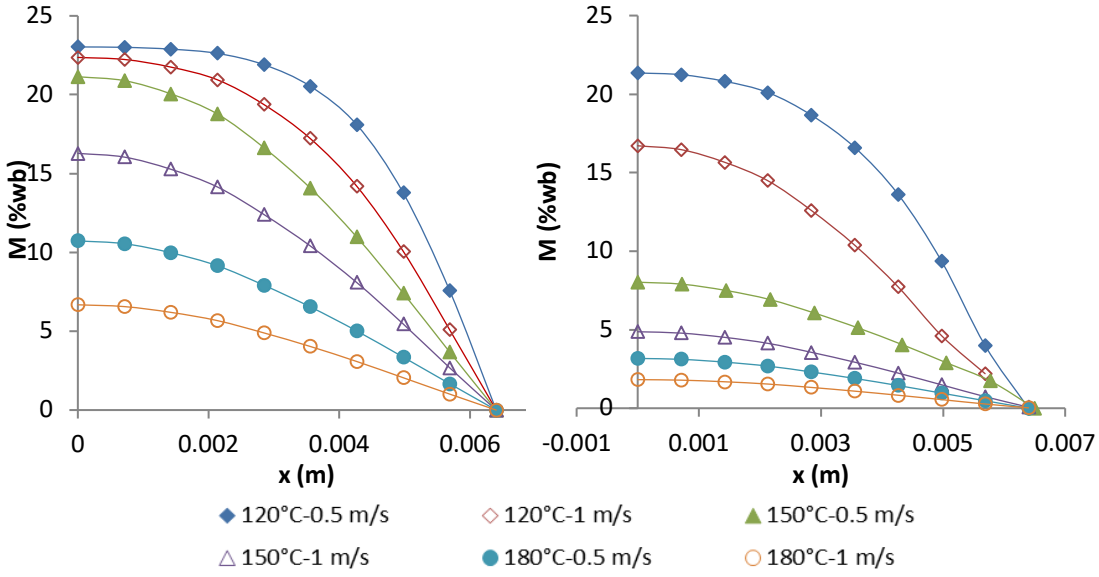

Figure 6.11 Moisture (M) profile of DSG pellet as a function of distance (x) from its center after (a) 1000 s and (b) 1500 s of SS drying at different SS conditions.

6.5 Conclusions

The multi-configuration approach featured with the ability to run a string of simulations in a given sequence reduced the simulation time significantly (about 15%) for tested range of SS temperature (120-180°C) and SS velocity (0.5-1.5 m/s) when compared to the single configuration approach where an initial steady state and transient state configurations have to be done separately. The SST k-ω turbulence model with the robust and accurate near-wall formulation can fairly predict the transport phenomena occurring at the solid-fluid (pellet-SS) interface with maximum turbulence residual value in the range of 1×10^{-5}-1×10^{-6}. By defining the appropriate boundary condition for each stage of SS drying (i.e. initial condensation, constant and falling drying rate periods) and by setting accurate thermo-physical properties for both the DSG pellet and SS, we can obtain a more accurate prediction of the drying process with the simulation residual for moisture concentration ranging

between 1×10^{-4}-1×10^{-7} kg of water per kg of dry matter. As the mass transfer coefficient is not available for this method of drying, the presented model is mainly dependent on the boundary conditions between the domains and on the resolution of conservation equations in the environment. Even though there are stages (e.g.: constant vs falling drying rate periods) of less convergence with the experimental results in the model, the overall mean relative percentage errors for the temperature and moisture curves were less than 10%. A comparison of the decay rate of moisture content during drying at different operating conditions showed that the effect of SS temperature (in the range of 120-180°C) is more prominent than the effect of SS velocity (in the range of 0.5-1.5 m/s). There was more than 50% decrease in drying time with increasing SS temperature as opposed to about 20% decrease with increase in SS velocity. The same trend in the effect of SS temperature and velocity was noticed in the simulation results too. The results of the study show that the coupling of solid (moist cylinder) medium drying models and CFD codes for fluid domain models with an explicit treatment of boundary condition is a fairly successful approach for numerical modelling of SS drying. The simulation by using this coupling method helped us to obtain the complete distribution of mass fluxes in the pellet and at the interface without defining a mass boundary layer. Hence, the proposed model can be used as a preliminary tool for the design and optimization of large-scale SS drying systems.

Acknowledgements

The authors acknowledge the Natural Sciences and Engineering Research Council of Canada, Graduate Enhancement of Tri-Council Stipends, and University of Manitoba Graduate Fellowship for their financial support. The authors also thank Dr. Scott J. Ormiston for his guidance on CFD software.

Nomenclature

Cp	Specific heat capacity (kJ/(kg K))
CFD	Computational fluid dynamics
D	Moisture diffusivity (m^2/s)
d	Equivalent diameter of the pellet (m)
DSG	Distillers' spent grain
Ev	Experimental value
F	Sorption isotherm-isobar
Fo_m	Fourier number
g	Acceleration due to gravity m/s
H	Enthalpy of the control volume (kJ/kg)
h	Heat transfer coefficient ($W/(m^2 K)$
k	Turbulence kinetic energy
kt	Thermal conductivity (W/(m K)
L	Length of DSG pellet
M	Moisture content
$\dot{m}$	Mass flux ($kg/(m^2 s)$)
MR	Moisture ratio
MRP	Mean relative percentage error
P	Pressure (Pa)
p_k	Production rate of k
Pv	Predicted value
R	Universal gas constant (8.314 J/(mol K)
r	Radius of DSG pellet
Re	Reynolds number
SS	Superheated steam
SST	Shear stress transport
T	Temperature (K)
t	Time (s)
V	Velocity m/s
WDS	Wet distillers spent grain
wb	Wet basis moisture content
x, y, z	Distance along x, y, and z axis

Symbols

ε	Dissipation rate
ρ	Density of the pellet (kg/m^3)
λ	Latent heat (J/kg)
ϑ	Eddy viscosity (kg/(m s)
η	Viscosity (kg/(s m))
∇	Laplace gradient function

Subscripts and Superscripts

t	Instantaneous time
e	Equilibrium
eff	Effective value
ref	Reference value
p	Pellet interface
sat	Saturation
ic	Initial condensation
$film$	Condensed film (water)
ss	Superheated steam
cr	Constant rate drying
fr	Falling rate drying
i	Instantaneous time
v	Water vapour

References

1. AACC (2000), AACC Method 44-15A- Moisture-air-oven methods. In: Approved Methods of the American Association of Cereal Chemists. St. Paul, MN.
2. Afolabi, T. J., Toyosi Y., Tunde-Akintunde, & Oyelade, O. J. (2014). Influence of drying conditions on the effective moisture diffusivity and energy requirements of ginger slices. Journal of Food Research 3(5), 103-112.
3. Aghbashlo, M., kianmehr, M. H., & Samimi-Akhijahani, H. (2008). Influence of drying conditions on the effective moisture diffusivity, energy of activation and energy consumption during the thin-layer drying of berberis fruit (Berberidaceae). *Energy Conversion and Management* 49, 2865–2871.
4. Akbarzadeh, M., Birouk, M., & Sarh, B. (2012). Numerical simulation of a turbulent free jet issuing from a rectangular nozzle. *Computational Thermal Sciences* 4 (1), 1–22.
5. Awolu, O. O. & Ibileke, I. O. (2011). Bioethanol production from brewer's spent grain, bread wastes, and corn fiber. *African Journal of Food Science* 5(3), 148-155.
6. Azzouz, S., Guizani, A., Jomaa, W., & Belghith, A. (2002). Moisture diffusivity and drying kinetic equation of convective drying of grapes. *Journal of Food Engineering* 55, 323–330.
7. Babalis, S. J. & Belessiotis, V. G. (2004). Influence of the drying conditions on the drying constants and moisture diffusivity during the thin-layer drying of figs. *Journal of Food Engineering* 65, 449–458.
8. Baini, R. & Langrish, T.A.G., (2008). An assessment of the mechanisms for diffusion in the drying of bananas. *Journal of Food Engineering* 85 (2), 201–214.
9. Beeby, C. & Potter, O.E. (1985). Steam drying. Drying ’85, Selection of papers from the 4th international drying symposium, Kyoto, Japan, 1985.
10. Bernard, P. S. & Wallace, J. M. (2002). Turbulent Flow: Analysis, Measurement and Prediction, John Wiley and Sons Inc.
11. Bourassa, J., Ramachandran, R. P., Paliwal, J., & Cenkowski, S. (2015). Drying characteristics and moisture diffusivity of distillers’ spent grains dried in superheated steam. *Drying Technology* 33, 2012-2018.

12. Canadian renewable fuels association, (2011) Ethanol Key Issues *http://ricanada.org/wp-content/uploads/2014/11/ethanol-fact-sheet-august102011.pdf*, accessed on 16 September 2016
13. Cenkowski, S., Pronyk, C., Zmidzinska, D., & Muir, W.E. (2007). Decontamination of food products with superheated steam. *Journal of Food Engineering* 83, 68–75.
14. Chandramohan, V. P. & P. Talukdar. (2010). Three dimensional numerical modeling of simultaneous heat and moisture transfer in a moist object subjected to convective drying. *International Journal of Heat and Mass Transfer* 53(21–22), 4638–4650.
15. Chayjan, R. A, Parian, J. A., & Esna-Ashari, M. (2011). Modeling of moisture diffusivity, activation energy and specific energy consumption of high moisture corn in a fixed and fluidized bed convective dryer. *Spanish Journal of Agricultural Research* 9(1), 28-40.
16. Chen, Z., Wu, W., & Agarwal, P. K. (2000). Steam drying of coal part 1. Modeling the behavior of a single particle. *Fuel* 79(8): 961-974.
17. Da-Silva, W. P., Silva, C. M. D. P. S.e, & Gomes, J. P. (2013). Drying description of cylindrical pieces of bananas in different temperatures using diffusion models. *Journal of Food Engineering* 117, 417–424.
18. Daurelle, J. V., Topin, F., & Occelli, R. (1998). Modeling of coupled heat and Mass transfers with phase change in a porous medium: application to superheated steam drying, Numerical Heat Transfer, Part A: Applications. *An International Journal of Computation and Methodology* 33(1), 39-63.
19. De Bonis, M. V. & Ruocco, G. (2008). A generalized conjugate model for forced convection drying based on an evaporative kinetics. *Journal of Food Engineering* 89, 232-240.
20. Defraeye, T. (2014). Advanced computational modelling for drying processes – A review. *Applied Energy* 131, 323–344.
21. Defraeye, T., Blocken, B., & Carmeliet, J. (2012a). Analysis of convective heat and mass transfer coefficients for convective drying of a porous flat plate by conjugate modelling. *International Journal of Heat Mass Transfer* 55,112–124.

22. Defraeye, T., Herremans, E., Verboven, P., Carmeliet J., & Nicolai, B. (2012b). Convective heat and mass exchange at surfaces of horticultural products: A microscale CFD modelling approach. *Agricultural and Forest Meteorology* 162– 163, 71– 84.
23. Dixon, A.G., Taskin, M.E., Nijemeisland, M., & Stitt, E.H., (2011). Systematic mesh development for 3D CFD simulation of fixed beds: single sphere study. *Computer and Chemical Engineering* 35(7), 1171–1185.
24. Ducept, F., Sionneau, M., & Vasseur, J. (2002). Superheated steam dryer: simulations and experiments on product drying. *Chemical Engineering Journal* 86, 75–83.
25. Elgamal, R., Ronsse, F., Radwan, S. M., & Pieters, J. G. (2014). Coupling CFD and Diffusion Models for Analyzing the Convective Drying Behavior of a Single Rice Kerne. *Drying Technology* 32(3), 311-320.
26. Erdogdu, F. & Turhan, M. (2006). Analysis of dimensional ratios of regular geometries for infinite geometry assumptions in conduction heat transfer problems. *Journal of Food Engineering* 77(4), 818–824.
27. Erickson G. E., Klopfenstein, T. J., Adams, D. C., & Rasby, R. J. (2005). General overview of feeding corn milling co-products to beef cattle. In: Corn Processing Co-Products Manual. University of Nebraska. Lincoln, NE, USA.
28. Erriguible, A., Bernada, P., Couture, F., & Roques, M. (2005). Modeling of heat and mass transfer at the boundary between a porous medium and its surroundings. *Drying Technology* 23(3), 455-472.
29. Erriguible, A., Bernada, P., Couture, F., & Roques, M. (2006). Simulation of Superheated Steam Drying from Coupling Models. *Drying Technology* 24, 941–951.
30. Fitch, A. L. (1935). A new thermal conductivity apparatus. *American Physics Teacher* 3(3), 135-136.
31. Fitzsimons, S. M., Mulvihill, D. M., & Morris E. R. (2007). Denaturation and aggregation processes in thermal gelation of whey proteins resolved by differential scanning calorimetry. *Food Hydrocolloids* 21(4), 638–644.
32. Ganesan,V., Rosentrater, K. A., & Muthukumarappan, K. (2008). Flowability and handling characteristics of bulk solids and powders – a review with implications for DDGS. *Biosystems Engineering* 101(4), 425–435.

33. Gely, M. C. & Santalla, E. M. (2007). Moisture diffusivity in quinoa (Chenopodium quinoa Wild.) seeds: Effect of air temperature and initial moisture content of seeds. *Journal of Food Engineering* 78, 1029–1033
34. Hamawand, I. (2011). Effect of colloidal particles associated with the liquid bridge in sticking during drying in superheated steam. *International Journal of Engineering* 24(2), 119-126.
35. Hamawand, I. (2013). Drying Steps under Superheated Steam: A Review and Modeling. *Energy and Environment Research* 3(2), 569-577.
36. Hamawand, I., Yusaf, T., & Bennett, J. (2014). Study and modelling drying of banana slices under superheated steam. *Asia-Pacific Journal of Chemical Engineering* 9, 591–603.
37. Holman, J. P., (2001). Heat Transfer. eighth ed. McGraw-Hill, New York
38. Iyota, H., Nishimura, N., Yoshida, M., & Nomura, T. (2007). Simulation of superheated steam drying considering initial steam condensation. *Drying Technology* 19(7), 1425-1440.
39. Jamaleddine T. J. & Ray, M. B. (2010). Application of Computational Fluid Dynamics for Simulation of Drying Processes: A Review. *Drying Technology* 28, 120–154.
40. Jamradleodluk, J. (2007).Influences of drying medium and temperature on drying kinetics and quality attributes of durian chip. *Journal of Food Engineering* 78, 198–205.
41. Johansson, A., Fyhr, C., & Rasmuson, A. (1997). High temperature convective drying of wood chips with air and superheated steam. *International Journal of Heat and Mass Transfer* 40 (12), 2843–2858.
42. Johnson, P., Paliwal, J., & Cenkowski, S. (2014). Analysis of the Disintegration of Distiller's Spent Grain Compacts as Affected by Drying in Superheated Steam. *Drying Technology* 32, 1060–1070.
43. Johnson, P., Paliwal, J., & Cenkowski, S. (2011). Current and Potential Applications of Distiller's Spent Grain. The Canadian Society for Bioengineering Paper No. CSBE11-316. Written for presentation at CSBE 2011 annual conference, Winnipeg, Manitoba, 10-13 July 2011.
44. Johnson, P., Paliwal, J., & Cenkowski, S. (2013). Compaction and relaxation characteristics of single compacts produced from distillers' spent grain. *Journal of Food Engineering* 116, 260-266.

45. Kaleemullah, S. & Kailappan, R. (2006). Modelling of thin-layer drying kinetics of red chillies. *Journal of Food Engineering* 76, 531–537.
46. Karabelas, S. J., Koumroglou, B. C., Argyropoulos, C. D., & Markatos, N. C. (2012). High Reynolds number turbulent flow past a rotating cylinder. *Applied Mathematical Modelling* 36, 379–398.
47. Kaya, A., Aydın, O., & Dincher, I. (2007). Numerical modeling of forced convection drying of cylindrical moist objects. *Numerical Heat Transfer* 51, 843–854.
48. Kaymak-Ertekin, F. & Gedik, A. (2005). Kinetic modelling of quality deterioration in onions during drying and storage. *Journal of Food Engineering* 68, 443–453.
49. Khan, J. A., Beasley, D. E., & Alatas, B. (1991). Evaporation from a packed bed of porous particles into superheated vapor. *International Journal of Heat and Mass Transfer* 34 (1), 267–280.
50. Kittiworrawatt, S., & Devhastin, S. (2009). Improvement of a mathematical model for low-pressure superheated steam drying of a biomaterial. *Chemical Engineering Science* 64(11), 2644 – 2650.
51. Ljung, A. L., Lundström, T. S., & Tano, K. (2011a). Simulation of convective drying of a cylindricaliron ore pellet. *International Journal of Numerical Methods for Heat & Fluid Flow* 21 (6), 703 -716.
52. Ljung, A. L., Lundstrom,T. S., Marjavaara, B. D., & Tano, K. (2011b). Convective drying of an individual iron ore pellet – Analysis with CFD. *International Journal of Heat and Mass Transfer* 54, 3882–3890.
53. Looi, A. Y., Golonka, K., & Rhodes, M. (2002). Drying kinetics of single porous particles in superheated steam under pressure. *Chemical Engineering Journal* 87, 329-338.
54. Menter, F. R. (1994). Two-equation eddy-viscosity turbulence models for engineering applications. *The American Institute of Aeronautics and Astronautics Journal* 32 (8), 1598-1605.
55. Menter, F. R. (2009). Review of the shear-stress transport turbulence model experience from an industrial perspective. *International Journal of Computational Fluid Dynamics* 23(4), 305-316

56. Messai, S., Sghaier, J., El Ganaoui, M., Chrusciel, L., & Gabsi, S. (2015). Low-Pressure Superheated Steam Drying of a Porous Media, *Drying Technology: An International Journal* 33(1), 103-110.
57. Mirzaee, E., Rafiee, S., Keyhani, A., & Emam-Djomeh, Z. (2009). Determining of moisture diffusivity and activation energy in drying of apricots. *Research in Agricultural Engineering* 55 (3), 114–120.
58. Mohsenin, N. N. (1980). Thermal Properties of Foods and Agricultural Materials. New York, N.Y.: Gordon and Breach Science Publishers.
59. Moreira, G. R. (2001). Impingement drying of foods using hot air and superheated steam. *Journal of Food Engineering* 49, 759-778.
60. Motevali,A., Abbaszadeh, A., Minaei, S., Khoshtaghaza, M. H., & Ghobadian, B. (2012). Effective moisture diffusivity, activation energy and energy consumption in thin-layer drying of jujube (*Zizyphus jujube Mill*). *Journal of Agricultural science and Technology* 14, 523-532.
61. Olsson, E.E.M., Ahrne, L.M., & Tragardh, A.C. (2004). Heat transfer from a slot air jet impinging on a circular cylinder. *Journal of Food Engineering* 63, 393–401.
62. Olsson, E.E.M., Ahrne, L.M., & Tragardh, A.C. (2005). Flow and heat transfer from multiple slot air jets impinging on circular cylinders. *Journal of Food Engineering* 67, 273–280.
63. Pabis, S. & Henderson, M. (1962). Grain drying theory II. A critical analysis of the drying curve for shelled maize. *Journal of Agricultural Engineering Research* 6, 272-277.
64. Pabis, S., Jayas, D.S., & Cenkowksi, S. (1998). Grain Drying: Theory and Practice. John Wiley & Sons, Inc., New York, NY.
65. Pakowski, Z. & Adamski, R. (2011). Onprediction of the drying rate in superheated steam drying process. *Drying Technology* 29, 1492-1498.
66. Pakowski, Z., Adamski, R., & Kwapisz, S. (2011). Effective diffusivity of moisture in low rank coal during superheated steam drying at atmospheric pressure. *Chemical and Process Engineering* 33(1), 43-51.
67. Pang, S. (1997). Some considerations in simulation of superheated steam drying of softwood lumber. *Drying Technology* 15(2), 651-670.

68. Perre, P. & Moyne, C. (1991), Processes related to drying: Part II, use of the same model to solve transfers both in saturated and unsaturated porous media. *Drying Technology* 9 (5), 1153–1179.
69. Pronyk, C., Cenkowski, S., & Muir, W.E. (2004). Drying foodstuffs with superheated steam. *Drying Technology* 22(5), 899-916.
70. Pronyk, C., Cenkowski, S., & Muir, W.E. (2010). Drying kinetics of instant Asian noodles processed in superheated steam. *Drying Technology* 28(2), 304 – 314.
71. Rahman, S. (1991). Evaluation of precision of the modified Fitch method for thermal conductivity measurement of foods. *Journal of Food Engineering* 14, 71-82.
72. Ramachandran R. P., Paliwal, J., & Cenkowski, S. (2017) Thermo-physical properties of distillers' spent grain pellets at different moisture content and condensed distillers' soluble concentrations. *Food and Bioprocess Technology* 10: 175-185.
73. Ramachandran, R. P., Bourassa J., Paliwal, J., & Cenkowski, S. (2017b). Effect of temperature and velocity of superheated steam on initial condensation of distillers' spent grain pellets during drying. *Drying Technology* 35(2), 182-192.
74. Ruiz-López, I. I., Córdova, A. V., Rodríguez-Jimenes, G. C., & García-Alvarado, M. A. (2004). Moisture and temperature evolution during food drying: effect of variable properties. *Journal of Food Engineering* 63 (1), 117–124.
75. Sabarez, H. T., (2012). Computational modelling of the transport phenomena occurring during convective drying of prunes. *Journal of Food Engineering* 111, 279–288.Stroem, L. K., Desai, D. K., & Hoadley, A. F. A. 2009. Superheated steam drying of brewer's spent grain in a rotary drum. *Advanced Powder Technology* 20, 240–244.
76. Stroem, L. K., Desai, D. K., & Hoadley, A. F. A. (2009). Superheated steam drying of brewer's spent grain in a rotary drum. *Advanced Powder Technology*, 20, 240–244. doi: 10.1016/j.apt.2009.03.009
77. Suvarnakuta, P., Devahastin, S., & Mujumdar, A. S. (2007). A mathematical model for low pressure superheated steam drying of biomaterial. *Chemical Engineering and Processing* 46(7), 675-683.
78. Taechapairoj, C., Prachayawarakorn, S., & Soponronnarit, S. (2006). Modelling of parboiled rice in superheated-steam fluidized bed. *Journal of Food Engineering* 76(3), 411–419.

79. Taechapairoj, C., Prachayawarakorn, S., & Soponronnarit, S. (2003). Superheated steam fluidized bed paddy drying. *Journal of Food Engineering* 58, 67–73.
80. Tang, Z., S. Cenkowski, & M. Izydorczyk. (2005). Thin-layer drying of spent grains in superheated steam. *Journal of Food Engineering* 67, 457-465.
81. Tumuluru, J. S., Tabil, L., Opoku, A., Mosqueda, M. R., & Fadeyi, O. (2010). Effect of process variables on the quality characteristics of pelleted wheat distiller's dried grains with solubles. *Biosystems Engineering* 105 (4), 466–475.
82. Tzempelikos, D. A., Mitrakos, D., Vouros, A. P., Bardakas, A. V., Filios, A.E., & Margaris D. P. (2015). Numerical modelling of heat and mass transfer during convective drying of cylindrical quince slices. *Journal of Food Engineering* 156, 10-21.
83. Wang, N. & Brennan, J.G. (1995). A mathematical model of simultaneous heat and moisture transfer during drying of potato. *Journal of Food Engineering* 24, 47–60.
84. Xiao, H. W., Bai, J-W., Sun, D-W., & Gao, Z. J. (2014). The application of superheated steam impingement blanching (SSIB) in agricultural products processing- A review. *Journal of Food Engineering* 132, 39-47.
85. Xiao, Z. F., Zhang, F., Wu, N. X., & Liu, X. D. (2013). CFD Modeling and simulation of superheated steam fluidized bed drying process. CCTA 2012, Part I, IFIP (International Federation for Information Processing) AICT 392:141–149.
86. Xiros, C., Topakas, E., Katapodis, P., and Christakopoulos, P. 2008. Hydrolysis and fermentation of brewer's spent grain by *Neurospora crassa*. *Bioresource Technology* 99, 5427-5435.
87. Yu, D. U., Shrestha, B. L., & Baik, O. D. (2015). Thermal conductivity, specific heat, thermal diffusivity, and emissivity of stored canola seeds with their temperature and moisture content. *Journal of Food Engineering* 165, 156–165
88. Zielinska, M., & Cenkowski, S. (2012). Superheated steam drying characteristic and moisture diffusivity of distillers' wet grains and condensed distillers' solubles. *Journal of Food Engineering* 109, 627–634.
89. Zielinska, M., Cenkowski, S., & Markowski, M. (2009). Superheated Steam Drying of Distillers' Spent Grains on a Single Inert Particle. *Drying Technology 27*, 1279–1285.

CHAPTER 7. MODELLING OF SS DRYING OF A DSG PELLET COATED WITH SOLUBLES

This chapter is based on the research paper submitted to *Journal of Food Engineering* and is under second round of review. The manuscript is entitled 'Three-dimensional modelling of superheated steam drying of a single distillers' spent grain pellet coated with condensed solubles', Ref: JFOODENG-D-18-00481R2.

7.1 Abstract

The method of using a dried core as a nucleus for drying a wet paste-like material is proven to be one of the most suitable methods for drying sticky wet materials. The current study focuses on the superheated steam drying of distillers' spent grain (DSG) pellets and then utilizing those dried pellets as a core material to dry the slurry of wet distillers' solubles. The drying experiments were conducted with cylindrical DSG pellets at 25% (wet basis) moisture content coated with a thin layer (3±0.3mm) of solubles at different superheated steam temperatures (120, 150, 180°C) and velocities (0.5, 1.0, 1.5 m/s). The average effective moisture diffusivity of the solubles (100% w/w) and DSG pellets with or without solubles (0, 10, 30% w/w) was found to be in the range of $3.3 \times 10^{-10} - 3.7 \times 10^{-9}$ and $4.1 \times 10^{-9} - 4.2 \times 10^{-8}$ m^2/s, respectively. A computational fluid dynamics (CFD) model was developed using ANSYS CFX by combining the Reynolds-Average Navier-Stokes (RANS) equations for the superheated steam flow and the diffusion models (thin layer and finite cylinder models) for a DSG pellet coated with solubles. When compared with experimental drying curves, the developed CFD model showed good agreement (mean relative percentage error ≤10%). Such models that are immensely helpful in predicting the superheated steam drying

characteristics of liquid materials dried over a porous dry nucleus, can provide valuable information for the design or optimization steps of an appropriate SS drying unit

Keywords: *Distillers' spent grain, Distillers' solubles, Computational Fluid Dynamics, Superheated steam, Numerical modelling*

7.2 Introduction

Bioethanol production has been increasing worldwide for the past decade reaching about 26.6 million gallon production in 2016 (Renewable-Fuels-Association, 2016). The biofuel industry primarily uses corn for bioethanol production but other cereal grains such as wheat, barley, rice, and sorghum are also being used. A coproduct of biofuels is known as distillers' spent grain (DSG) and due to its high protein (27-35%) and dietary fiber content (27-55%), it has been used as a valuable raw material for animal feed (Awoyale et al., 2016). The generated additional income to the ethanol industry from selling DSG can be as high as 10-20% (Ramachandran et al., 2017b). However, a short shelf life of wet DSG is a major challenge for the industry. The distillers' spent grain generally has high moisture content of about 80% wb (wet basis) irrespective of the milling method (Bourassa et al., 2015). To make it marketable, DSG is generally dried to a safe storage moisture content of 8-12% into a product called dried distillers' spent grain with solubles (DDGS) (Zentek et al., 2014). The dried product ensures convenient handling and safe storage with greater application potential as a feed material for cattle (Penner et al., 2009), poultry (Salim et al., 2010), fish (Li et al., 2011), and swine (Lyberg et al., 2012); human food (Brochetti et al., 1991; Fiasco et al., 1990; Liu et al., 2011); and in nutritional supplements for the simultaneous saccharification and ethanol fermentation (Bi et al., 2011).

The wet material left after fermentation of starch is called by the ethanol producers whole stillage which in the next step is centrifuged to remove excess water from it (Ramachandran et al., 2017a). During centrifugation fine particles (Distillers' solubles) are separated from the coarse fraction of spent grain. As solubles have smaller particle size they have more micro-porosity and water holding capacity than the coarse grain fraction of DSG (Ramachandran et al., 2017c). The solubles contain more protein and unfermented starch than the coarse fraction and hence are mixed with the coarse fraction to yield custom feed products (Johnson et al., 2013a). The industrial drying of this slurry like material faces some practical challenges. Currently, the dewatered/centrifuged wet spent grain is dried using rotary drum dryers at internal dryer temperatures ranging between 250-600°C (Stein and Shurson, 2009). The slurry form of wet solubles requires the presence of inert core material that increases the surface area enabling faster drying. Also, the thick paste of solubles which behaves like a thixotropic fluid (Broniarz-Press et al., 2014) sticks on the dryer surface and leaves darkened deposits decreasing the efficiency of the dryer (Stroem et al., 2009). Wet DSG is then mixed with previously dried/dewatered spent grain granules at the feeding section of the dryer. This approach generates a large surface area for drying slurry that coats the dried DSG granules. As the dried granules pass twice through the dryer, the double passage of the product at high temperatures causes charring of the product and in some cases even fire inside the drum dryer resulting in high monetary losses and safety issues. Hence, for slurry products or combustible materials such as lignite, an alternative drying method is under research. Superheated steam (SS) as a drying medium can eliminate the risk of fire as it creates an anaerobic environment (Cenkowski et al., 2007b; Sehrawat et al., 2016). Industries are now looking at the possibility of using spouted bed SS drying systems for

drying coated DSG. In order to realize this goal, there is a need for scientifically valid data describing the heat and mass transfer phenomena of SS drying of coated DSG pellets. To this end, the present study focuses on simulation and modelling of SS drying of coated DSG pellets. The superheated steam drying has a better drying efficiency if it is a closed system where the exiting steam is recovered and reused (Ducept et al., 2002; Moreira, 2001). Research has already established that steam drying reduces mycotoxins that can be present in biological products (Cenkowski et al., 2007b; Granby et al., 2012; Hu et al., 2016) and preserves their colour and nutritional quality (Pimpaporn et al., 2007; Rordprapat et al., 2005).

The current paper is a part of our ongoing research done by Ramachandran et al. (2017a) and deals with the simulation and modelling of the SS drying of the dried core of DSG pellet coated with a thin layer of distillers' solubles. Ramachandran et al. (2017a) studied the heat and mass transfer phenomena occurring in a DSG pellet during SS drying where the industrial method of drying a core material (first stage of drying) was simulated. The presented study covers the transport phenomena occurring in coated pellets during SS drying (i.e. a dried DSG pellet coated wet distillers' solubles). This method mimics the second stage of industrial drying of the wet solubles poured over previously dried DSG granules. Industrial drying of this multilayer product at high temperature is challenging because of the bidirectional moisture movement in the coated materials. If the drying process is not optimized, moisture movement from the relatively wet coating into the dry core and from the whole coated pellet to the drying medium causes non-uniform drying. Also, the bidirectional mass diffusions in multi-layered materials are difficult to estimate using a general empirical model. Hence, in this study simulation of the transport phenomena occurring in both, wet

coating and dried core are done using the CFD software. Computational modelling and drying simulation of such materials enable complete characterization of temperature and moisture changes occurring in an element during SS drying with high spatial and temporal resolution (Ramachandran et al., 2018). Such simulations reduce capital investment in product development and scaling up of laboratory models to industrial scale systems (Gharsallaoui et al., 2007). As the material of interest for this study is a multilayer product with complex geometry, a single element modelling approach was adopted (Ramachandran et al., 2018). The drying kinetic of the bulk material is affected by its local temperature and moisture content of individual elements. Thus, the heat and mass transfer phenomena occurring inside a single element are of considerable interest for developing a drying model (Baini and Langrish, 2007; Da Silva et al., 2013; Ljung et al., 2011; Malafronte et al., 2015). Abbott et al.,(2011) identified different modes of drying involved in a coated material dried over a core solid such as the models limited to only heat transfer, to diffusion, and to mass transfer. They concluded that such drying models for defining coated materials could provide insight into the drying process and could be used to minimize energy consumption in industrial coating and drying.

The present study uses a combination of Reynolds-Average Navier-Stokes (RANS) equations for defining the SS flow around the coated pellet, and drying models defining the transport phenomena in the coated pellet. Two interfaces; one connecting the SS and the coating and the other connecting the coating and the core DSG pellet link the different problem domains. The main objective of the present paper is to develop a three-dimensional model for describing the SS drying of a single multi-layered cylindrical pellet at selected operating conditions of SS drying and validate the model with experimental results.

7.3 Materials and method

7.3.1 Sample preparation

The raw material used in this study was whole stillage (mashed corn and wheat in the ratio of 9:1). The whole stillage with 84 ± 2% wet basis (wb) moisture content was centrifuged to remove excess water and separate coarse grain fraction and distillers' solubles. The separated fraction was stored in sealed plastic bags in a freezer at -15°C until further experimentation. Samples for producing the core material for drying experiments were made with a mixture of coarse grain fraction and distillers' solubles. The mixing was done to minimize volumetric expansion of the samples/pellets during superheated steam drying (Johnson et al., 2015; Ramachandran et al., 2017a). As thermo-physical properties and stability of the pellets were determined in previous experiments for 10 and 30% soluble concentrations (Johnson et al., 2015; Ramachandran et al., 2017c), the same two concentrations were selected for the present study. A known mass of wet coarse grain and calculated amount of distillers' solubles (corresponding to 10 and 30% solubles) were mixed for 2 minutes using a spatula. The mixture was then dried in a laboratory oven at 60±5°C until the moisture content reached 25% wb. This dried mixture was then stored in sealed plastic bags until pelleting.

7.3.2 Compaction

The compaction of the aforementioned sample mixture was done using a universal testing machine (Model 3366, Universal Testing Systems, Instron Corp., Norwood, MA). About 4.3 ± 0.2 g of sample (coarse grain fraction with 10 and 30% solubles) was used for each compact. The sample was placed in a cylindrical mold of 12.2 ± 0.01 mm diameter and 80 mm height. It was then placed on the fixed platform of the universal testing machine and

compressed using a cylindrical die of 12.08 ± 0.01 mm diameter and 84 mm length attached to a 10 kN load cell and compacted with an endpoint pressure of 60.3 MPa at a speed of 50 mm/min (Bourassa et al., 2015). The formed pellet was then held at that pressure for 5 minutes to minimize the spring back effect of the pellet (Tumuluru et al., 2010; Wongsiriamnuay and Tippayawong, 2015). After compaction and the hold, the pellet was ejected out of the mold by removing the mold frame and pushing the pellet using the die attached to the testing machine.

7.3.3 Coating

Wet solubles (3±0.5 g) were spread and leveled using a long metal spatula to form a uniform layer of 3 ± 0.3 mm depth on a 5 cm × 8 cm sized thin polyester mesh cloth of 1.5 mm × 1.5 mm mesh size. The thin metal spatula was slid straight on the soluble layer and was leveled again with a flat metal plate. The depth of the soluble layer was measured at 6 different points using a Vernier caliper with an accuracy of 0.01 mm. The layer had a width slightly greater than the height of the pellet (30 ± 0.5 mm) and length equal to the circumference of the cylinder. A single spent grain pellet of known dimension (diameter 12.35 ± 0.5 mm and length 25.5 ± 0.5 mm) was placed at the center of the solubles layer. It was wrapped by folding the mesh cloth from both, the ends so that the solubles formed a uniform thin layer around the pellet. The additional width of the thin layer at the two ends was folded to cover the two side faces of the pellet. The ends of the mesh cloth were then sutured using a thin copper wire.

7.3.4 Superheated steam drying experiments

The individual coated pellets were dried in a SS system described by Pronyk et al. (2010) and Ramachandran et al. (2017a). A single coated pellet was placed on a perforated

aluminum tray suspended from the under-weighing hook of a precision weighing balance (Sartorius ENTRIS 423-1S, Sartorius, Germany) placed above the SS drying chamber. The aluminum tray was positioned in such a way that the pellet was suspended at the center of the chamber with steam passing symmetrically around the pellet. The pellet was placed horizontal with its longitudinal axis perpendicular to the direction of steam flow. The pellet holding tray and the inner walls of the drying chamber were pre-heated to operating conditions prior to each drying test to avoid steam condensation (Ramachandran et al., 2017a). Thin guiding pins attached to the tray ensured that the coated pellet had its horizontal axis aligned perpendicular to the SS flow direction during drying. The mass of the pellets over the entire period of drying was recorded at regular intervals (5 s) using a data-logger. Drying was carried out until the mass of the pellet reached equilibrium. The data was used to generate drying characteristics and to determine moisture diffusivity. The same procedure was repeated in triplicates for different operating conditions of the SS drying unit (SS temperature of 120, 150, and 180°C and velocity of 0.5, 1, and 1.5 m/s). The lifting force of SS on the holding tray and the pellet was determined by diverting the SS from the drying chamber for approximately 15-20 s at time intervals of 2, 5, 15, 30, 45, and 60 min, and measuring the mass of the sample without the lifting force. These values were then used to determine the true mass of the pellet during drying experiments for developing the drying characteristics (Bourassa et al., 2015; Pronyk et al., 2008).

7.3.5 Volumetric change

To determine the dimensional changes in the pellets when subjected to SS, a separate set of experiments was conducted with DSG pellets of the same two levels of solubles (10, and 30% w/w) and their initial moisture content of 25% (wb). The operating conditions of

the SS drying unit were kept the same as in the drying experiments. The tests were conducted with single pellets of known dimensions and approximately the same mass and dimensions as that of the pellets used for the drying experiments coated with solubles (i.e. 3 ± 0.3 mm depth). Individual coated pellets were subjected to SS drying for 0.5, 1, 2.5, 5, 10, 30, and 60 min. Pellets that disintegrated during drying were not used in calculations of the volumetric change. For each aforementioned drying time a fresh pellet was used. This prevented from the alternative cooling and heating of the pellet when the same pellet is used over and over again (Bourassa et al., 2015). The dimensions of the coated pellet after treatment were measured using Vernier calipers with an accuracy of 0.01 mm. Based in the data gathered, a polynomial relationship between the percentage dimensional change and the drying time was developed.

7.3.6 Drying characteristics and effective moisture diffusivity

In order to study the drying characteristics of distillers' solubles and the DSG core pellet, a separate set of drying experiments was conducted with the same SS operating conditions as discussed above. A thin layer (approximately 3 ± 0.3 mm thickness) of wet solubles with a moisture content of 82.4 ± 1% was placed on a perforated sample tray to conduct the moisture diffusivity experiments. The effective moisture diffusivity of the solubles was determined using the drying characteristics of these thin-layer drying experiments. Fick's law of diffusion for an infinite slab was used to determine the moisture diffusivity of the soluble coating (Taheri-Garavand et al., 2011). The drying experiments with DSG pellets containing 10 and 30% solubles were conducted with the same operating conditions (section 7.3.4) to determine the effective diffusivity of the core pellet. The moisture diffusivity of the core pellet was computed using Fick's law of diffusion for a finite cylinder (Ramachandran et al.,

2017a). The effect of volumetric changes occurring during SS drying was considered for calculating the effective moisture of the coated pellet. The dependency of pellet temperature and moisture content on the effective moisture diffusivity was also determined separately and compared with the experimental diffusivity obtained from Fick's law. Initially, the correlation between the pellet temperature and the effective moisture diffusivity was expressed by using Arrhenius type equation with an assumption that the average pellet temperature is the same as that of the SS during drying. Coefficients of Arrhenius equation (i.e. activation energy and pre-exponential factor) were then used as a first approximation for the Levenberg-Marquardt optimization (Rahman and Kumar, 2011). The coefficients of the model equation for effective moisture diffusivity (D_{eff}) as a function of temperature and moisture content (Equation 7.1) were then obtained from the preset limits (based on Arrhenius equation) using MatLab (R2014b, Mathworks, USA).

$$D_{eff} = a\, exp\left(\left(\frac{-E_a}{RT}\right) + cM_t\right) \tag{7.1}$$

Where, a and c are the model constants and E_a is the corrected activation energy using Levenberg-Marquardt optimization. T and M_t are the temperature and instantaneous moisture content of the pellet.

7.3.7 Temperature changes while drying

The temperature profile of the coated pellet during SS drying was measured by conducting a separate set of experiments using the same SS operating parameters as that of the drying experiments discussed in section 2.4. Pellets were of the same dimensions as in the previous experiments with initial temperature of 22 ± 3°C. To measure the pellet's temperature during SS drying, a T-type thermocouple was inserted through the longitudinal axis of the pellet to its geometric center. Inserting the thermocouple halfway through the

axis prevented the conductive heating of the thermocouple wire, which could have led to an error in temperature measurement (Pronyk et al., 2010). The center temperature of the coated pellet was recorded every second for 1 – 1.5 hour using a data acquisition system until the thermocouple reading was equal to the SS temperature. These experiments were conducted in triplicate and the temperature values were averaged.

7.3.8 Simulation and modelling

Numerical modelling of the SS drying of coated DSG pellets has three components: (i) modelling of the fluid domain, (SS flow around the coated pellet); (ii) modelling of the high moisture solid domain (solubles coating around the pellet), and (iii) modelling of the solid domain (the spent grain core pellet).

7.3.8.1 Simulation of fluid domain

The external fluid flow (SS) surrounding the coated pellet at varying operating conditions was simulated by solving the RANS (Reynolds-Averaged Navier-Stokes) equations for conservation of mass and momentum and the energy balance equation (Defraeye et al., 2012a; Pulat et al., 2011). The solution to the RANS equations for a defined set of initial conditions of the SS flow corresponding to the operating condition generates the information on the boundary conditions for the transport equation for the coated pellet (Erriguible et al., 2006, 2005). The details of the governing transport equations for fluid domain, assuming SS as an incompressible fluid, have been discussed in a previous paper (Ramachandran et al., 2017a). Among the RANS models, the shear stress transport (SST) k-ω model is an advanced model with the combined features of the standard and transformed k-ω models. The SST k-ω model includes a cross-diffusion term in the specific dissipation rate 'ω'. The transport equations for

the SST k-ω model are given in equation 7.2 and 7.3 (Goldberg and Batten, 2015; Menter, 1994; Musa et al., 2016; Pulat et al., 2011).

$$\rho\frac{\partial k}{\partial t} = \tilde{P}_k - \beta^*\rho k\omega + \nabla\cdot[(\mu + \sigma_k\mu_k)\nabla k] \tag{7.2}$$

$$\rho\frac{\partial \omega}{\partial t} = \frac{\gamma}{\hat{\vartheta}_t}\tilde{P}_k - \beta\rho\omega^2 + \nabla\cdot[(\mu + \sigma_k\mu_k)\nabla\omega] + 2(1-F_1)\rho\sigma_{\omega_2}\frac{1}{\omega}\nabla k\cdot\nabla\omega \tag{7.3}$$

Where, the eddy viscosity υ_t and the specific dissipation rate ω are given by:

$$\hat{\vartheta}_t = \frac{\mu_t}{\rho} = \frac{a_1 k}{max\{a_1\omega_2 SF_2\}} \tag{7.3a}$$

And maximum value of eddy viscosity $\hat{\vartheta}_t = max\{\vartheta_i, 10^{-8}\}$

$$\omega = \frac{\varepsilon}{C_\mu k} \tag{7.3b}$$

And, P_k is the production rate of k and $\widetilde{P}_k = \min\{P_k, 10\beta^*\omega\rho k\}$, F_1 and F_2 are the blending functions which vary with wall distances (Goldberg and Batten, 2015; Musa et al., 2016) and model constants σ_k = 1.176, σ_{ω_2} = 1.168, k = 0.41, γ =0.55, β = 0.075, β^* = 0.09. In SST k-ω model, the two-equation k-ω model formulation solves the transport phenomena in the near-wall region and a k-ε model formulation solves the turbulent central region of the fluid flow (Pulat et al., 2011). Defraeye et al. (2012b) and Ljung et al. (2011) reported that the SST k-ω turbulence model performs well with flows of low Reynolds numbers, especially near the walls and also when adverse pressure gradient boundary layer flows are simulated. Hence, the model was used for the simulation of SS flow around the coated DSG pellet.

7.3.8.2 Numerical model for the solid domain

In developing the mathematical model for the solid domain represented by the coated pellet, both, the coating and the core pellet were considered to be isotropic and homogeneous. The

solid domain in this problem has two layers; the solubles as coating and the core pellet. The external interface of the coated pellet shared between the SS and the coating forms the first interface, which uses the solutions for the transport equations of the fluid medium as its initial guess for its boundary condition for the heat transfer. As there is no distinguishable mass transfer boundary layer for the SS drying, the heat transfer acts as the driving force for drying. In this case, the drying phenomenon was described in terms of the flux of moisture in the form of vapor leaving the interface of the coating into SS (Johansson et al., 1997; Pang, 1997; Pakowski and Adamski, 2011). The energy and mass balance at the fluid-solid interface in SS drying has three stages (Figure 7.1): the initial condensation, the evaporation of condensed steam and constant rate drying, and the drying phase period. The heat and mass balance equations for the three different stages of SS drying depend on the surface temperature of the pellet. The governing transport equations for each stage are described as follows:

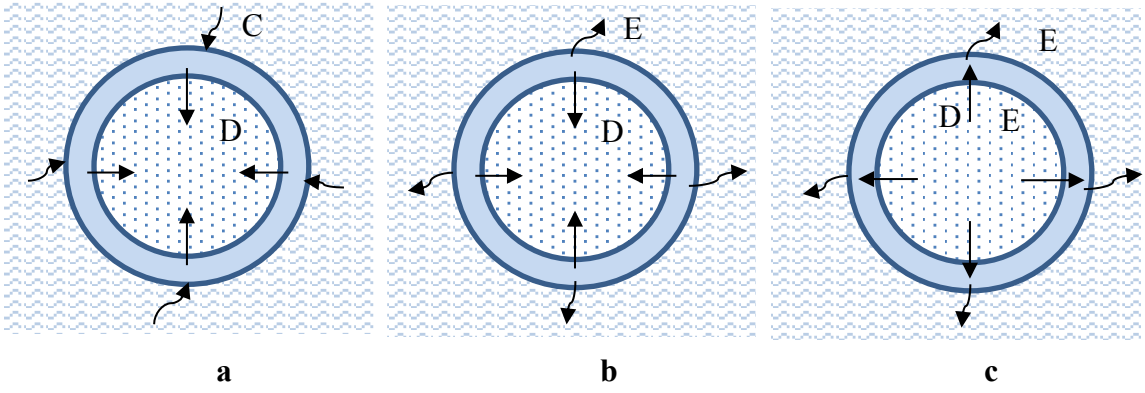

Figure 7.1 Schematic diagram of cross section of the coated DSG pellet with the direction of moisture migration during different stages of SS drying, where: C is the initial condensation, D is the diffusion, and E is the evaporation.

The initial condensation stage occurs when the sample at a lower temperature comes in contact with the SS leading to a local condensation of steam on its surface (Hamawand, 2013; Le et al., 2017; Ramachandran et al., 2017b). Depending on its sorption behavior, the condensed steam either evaporates or is adsorbed by the coating (or eventually the core pellet) (Figure 7.1a) (Adamski and Pakowski, 2013). The boundary conditions for heat (Kittiworrawatt and Devahastin, 2009; Le et al., 2017) and mass (Erriguible et al., 2006; Messai et al., 2015; Xiao et al., 2013) transfer for this case are given by Equations 7.4 and 7.5, respectively.

If $T_c < T_{sat}$, $-kt_c(\nabla T \cdot n) = \lambda_v \dot{m}_{ic}$ (7.4)

$$\dot{m}_{ic} = \frac{h_{film}(T_{sat} - T_c)}{\lambda_v} \quad (7.5)$$

Where, the film condensation heat transfer coefficient of superheated steam (Iyota et al., 2008; Ramachandran et al., 2017b; Sa-adchom et al., 2011) is:

$$\mathrm{h}_{film} = 0.725\left(\frac{\rho_{film}(\rho_{film-}\rho_v)g\lambda_v(kt_{film})^3}{2r\mu_{film}(\mathrm{T_{sat}} - \mathrm{T_p})}\right)^{\frac{1}{4}} \quad (7.5a)$$

The evaporation of the condensed steam on the coating starts once the surface temperature of the coating reaches the saturation temperature of steam (Figure 7.1b). This evaporation continues at a constant temperature of the coating layer and is dominated by the heat transfer coefficient between the water on the surface and SS (Suvarnakuta et al., 2007). The energy and mass transfer boundary conditions for the constant drying rate period are given by equations 7.6 and 7.7:

If $T_c = T_{sat}$, $-kt_c(\nabla T \cdot n) = h(T_{sat} - T_{ss}) = \lambda_v \dot{m}_{cr}$ (7.6)

$$\dot{m}_{cr} = \frac{h(T_{sat} - T_c)}{\lambda_v} \quad (7.7)$$

In the falling rate drying period, the temperature of the coating layer and the pellet rises and the moisture movement inside the coating and in the pellet is dominated by moisture diffusion (i.e. liquid or vapour, or both). As the temperature rises above the boiling temperature of water, an internal pressure increase occurs due to vapour formation (Figure 7.1c), which may cause the capillary/Darcy's flow. In that case, drying rate can be predicted based on the sensible heat transfer rate between the coating and the SS divided by the latent heat of vaporization of moisture (Pakowski and Adamski, 2011). The heat balance at the interface in this case is given by equation 7.8:

If $T_c > T_{sat}$, $-kt_c(\nabla T \cdot n) = (\lambda_v + C_{pv}T_c)\dot{m}_{fr} + q_c = h(T_{ss} - T_c)$ (7.8)

Where, T_c is the temperature of coating at a given moisture content and vapour partial pressure (in this case, atmospheric pressure) and q_c is the net heat flux penetrating the coating (Pakowski et al., 2011). The mass transfer rate was obtained by balancing the mass flux at the interface and the mass transfer boundary condition is:

$$\dot{m}_{fr} = D_{eff,c_i}(\nabla M \cdot n) = \frac{h(T_c - T_{ss}) - q_c}{C_{pv}T_c + \lambda_v} \quad (7.9)$$

The equilibrium condition at the interface is given by:

$$P_v = f(M, T_c)P_{sat}(T_c) \quad (7.10)$$

Where, the saturation vapour pressure of water vapour at different solid surface temperature is given by (Messai et al., 2015):

$$ln(P_{sat}(T_c)) = 25.506 - \frac{5204.9}{T_c} \quad (7.10a)$$

Mass transfer inside the solid domain (coating and core pellet) can be caused by a pressure gradient, and diffusion of moisture either in vapour or liquid phase, which is governed by the moisture gradient (Adamski and Pakowski, 2013; Pakowski et al., 2011). Since, the moisture

content of the core pellet and the coating are significantly different, moisture diffusion is considered to be the major driving force for moisture migration inside the core pellet (Braud et al., 2001; Taechapairoj et al., 2006). Initially, the moisture of the coating migrates to the drier core until the evaporation front expands to the depth of the coating. Then the reverse diffusion of moisture from the core pellet to the exterior coating begins, which is assumed to be governed by moisture diffusion. The heat transfer inside the pellet is governed by the principles of conduction in all directions. The governing equations for energy and mass balance within the coating and the core pellet are as follows:

$$\frac{\partial T_{c/p}}{\partial \mathrm{t}} = \frac{1}{\rho_{c/p_i}\left(Cp_{c/p_i}\right)}\left[\frac{\partial}{\partial x}\left(kt_{c/p_i}\frac{\partial T_{c/p}}{\partial x}\right)+\frac{\partial}{\partial y}\left(kt_{c/p_i}\frac{\partial T_{c/p}}{\partial y}\right)+\frac{\partial}{\partial z}\left(kt_{c/p_i}\frac{\partial T_{c/p}}{\partial z}\right)\right] \quad (7.11)$$

$$\frac{\partial M_{c/p}}{\partial t} = \left[\frac{\partial}{\partial x}\left(D_{eff\,c/p_i}\frac{\partial M_{c/p}}{\partial x}\right)+\frac{\partial}{\partial y}\left(D_{eff\,c/p_i}\frac{\partial M_{c/p}}{\partial y}\right)+\frac{\partial}{\partial z}\left(D_{eff\,c/p_i}\frac{\partial M_{c/p}}{\partial z}\right)\right] \quad (7.12)$$

Where, $Cp_{c/p}$, $kt_{c/p}$, and $D_{eff\,c/p}$ were defined as a function of moisture content and temperature. The subscript *c/p* denotes that, the equation applies for both coating and core.

7.3.8.3 Configuration

A 3D mathematical model of the SS drying problem of a single DSG core pellet coated with a thin layer of solubles coated over it was developed using the commercial CFD software 'ANSYS-CFX 16.2 package' (ANSYS Inc., Canonsburg, PA). The geometry of the entire problem domain with all these components was created in ANSYS-workbench and then meshed using ANSYS-mesh. A quarter section of the geometry, including the DSG core pellet, coating, and the SS drying chamber was used as the computational domain for the 3D model (Figure 7.2). The core pellet was 12.35 mm in diameter and 25.5 mm long and the coating had a thickness of 3.0 mm. The equivalent diameter of the drying chamber and the

internal height of the chamber were used as the diameter (272 mm) and length (356 mm) of the fluid (SS) domain, respectively. The illustration of the coated DSG pellet placed at the geometric center of the fluid domain of the chamber and the meshing of the corresponding computational domain using the CFX is shown in Figure 7.2. The thermo-physical properties of the DSG pellets (Ramachandran et al., 2017c) and the effective moisture diffusivity at the solubles concentration (10 and 30%) of the core pellet as well as the coating were defined in CFX separately as a function of their moisture content and temperature. The resolution of the mesh near the walls was increased by adding inflation layer with structured meshes for capturing the changes in the variables (Figure 7.2).

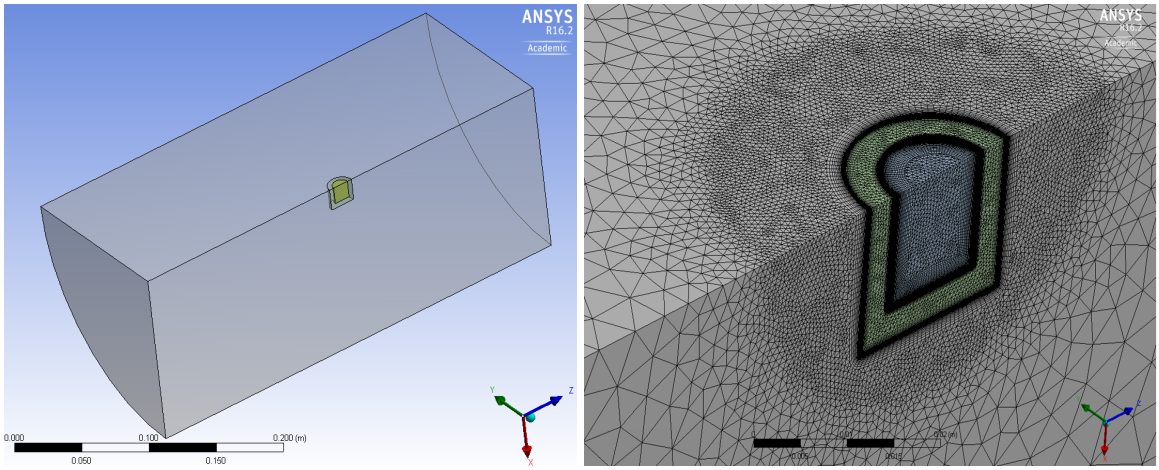

Figure 7.2 a) Geometry of the problem domain with SS and the coated pellet, b) closer view of the unstructured mesh generated within the coated pellet and the SS domain.

The mesh sensitivity was also tested using three different computational meshes with different grid resolutions of 1.5, 2.3, and 4.8 million nodes. The convergence of the experimental data with the predicted values was used to check the sensitivity of the mesh (Capone et al., 2016; Yang and Zhang, 2017). The number of inflation layers for each of the interfaces was also optimized after the mesh sensitivity analysis was done. A denser

inflation layer was given to the interface for the core pellet to capture the inward and outward diffusion, followed by the coating and the solid-fluid interface.

7.3.9 Implementation of the model

The solid and fluid domains were connected by two defined interfaces. They were defined in the CFX itself as: interface 1, between the coating and fluid domain, and interface 2, between the core pellet and the coating. The initial and boundary conditions for both, the coating and core pellet were also defined in CFX. The SS temperature and velocity used in the SS drying experiments were set as the initial conditions at the chamber inlet. The initial moisture of the core DSG pellet (25% wb) and the solubles coating (82.5 % wb) used in the SS drying experiments, and a temperature of 25°C (room temperature) for both core pellet and coating were set as the initial conditions for the solid domain. The transport equations for initial condensation were applied as a source term to the interface 1 (Figure 7.2). Once the surface temperature of the coating reaches the saturation temperature, the film condensation heat transfer coefficient is replaced by the flow field heat transfer coefficient i.e. the source term will be zero. By doing this, the wall heat transfer coefficient of the solid does not rely on any empirical equation once the initial condensation is completed; instead, the wall heat transfer coefficient obtained from the solutions of the RANS equation is automatically chosen. The mass flux over both, the interfaces during the evaporation and drying stages were defined by the diffusion equation to the interfaces until the local temperature was less than or equal to the boiling point of water. To account for the evaporation of moisture in both, the coating and the core pellet when the temperature is above the boiling temperatures, a subdomain was created for the coating and the core pellet and separate heat and mass transfer boundary conditions were applied as source terms. In this

way, the inward and outward diffusion of the moisture in the core pellet as well as the effective diffusion and evaporation of both, the coating and the core pellet were captured. The code for solving the flow equations and the equations for the coating and the core pellet were then coupled by executing both codes in the same time step (Erriguible et al., 2006, 2005; Ramachandran et al., 2017a). A zero-velocity boundary condition was assumed for the interface 1 between the SS and coating.

The Reynolds number obtained for different SS operating conditions for the geometry used in the study was in the range of 3495 - 7480, which was in the transient to turbulent flow region (Karabelas et al., 2012). Hence, the SST k-ω turbulence model was used for the fluid domain (Defraeye et al., 2012b; Ljung et al., 2011). The SST k-ω turbulence model was reported to be sufficiently accurate for predicting the convective heat transfer coefficient near the wall (Trujillo et al., 2003). The steady-state and isothermal analysis of flow equations (i.e. without drying) were performed initially to obtain a fully developed SS flow around the coated pellet. These simulation results were used as the initial conditions for the transient-state analysis of the transient state drying simulation by utilizing the multi-configuration feature of CFX (Ramachandran et al., 2018). For transient simulations, variable time step size with the increase in drying time was chosen and each time step had 10 iterations each. The time step sizes were 0.05, 1, 1.5, 5, 10, 20, 50, and 100, respectively for 1, 5, 10, 20, 40, 60, 90, 120 min with 10 iteration per each time step. The smaller time step size during the initial stages of drying was chosen to capture the initial condensation and the relatively fast changing transport phenomena when compared to the later stages of drying. The convergence criteria for the root mean square (RMS) values of the residuals were set to 1×10^{-4} and 1×10^{-6} for the steady-state and transient-state analysis, respectively.

7.3.10 Validation of the model

The experimental as well as the simulation based drying characteristics for the coated DSG pellet (with two levels of solubles concentration (10 and 30% w/w) in the core pellet) were conducted for three different SS temperatures (120, 150, and 180°C) and three different SS velocities (0.5, 1.0, and 1.5 m/s). The simulation results were validated with the experimental results by comparing the overall moisture content and the surface temperature of the coated DSG pellets obtained from the SS drying experiments with the average moisture content and surface temperature values obtained from the simulation. The validation of simulation was done for each operating condition of SS drying and each level of solubles concentration in the core DSG pellet using the mean relative percentage (MRP) error (Fabbri and Cevoli, 2015; Kaleemullah and Kailappan, 2006; Sabarez, 2012). The mean relative percentage error of the simulation results was calculated using the following equation:

$$MRP = \frac{1}{n}\sum_{i=1}^{n}\frac{|Pv_i - Ev_i|}{Ev_i} \times 100 \quad (7.13)$$

Where, MRP is the mean relative percentage error, $Pv_i$and Ev_i are the instantaneous predicted and experimental values of the variable, respectively, and *n* is the number of data points compared.

7.4 Results and discussion

7.4.1 Volumetric change

During SS drying under selected operating conditions (SS temperatures 120, 150, and 180°C, and SS velocities 0.5, 1.0, 1.5 m/s) the coated DSG pellets showed longitudinal as well as lateral expansion. This is in agreement with a previous study by Johnson et al. (2014) who reported similar behaviour of compacted pellets during SS drying. Johnson et al. (2015)

reported that the increase in solubles concentration in the DSG pellet decreased the volumetric expansion during SS drying (Figure 7.3). The lateral expansion, however, is comparatively smaller than that of the longitudinal expansion (Bourassa et al., 2015). The volumetric expansion of a pellet (Figure 7.3) due to SS drying is attributed to the relaxation of stored stress energy in the pellet as well as due to initial condensation (Johnson et al., 2015; Ramachandran et al., 2017a). The coated pellets showed volumetric expansion during the initial stages of drying and then started to shrink as drying proceeded (Figure 7.3). As the core pellet was the responsible element for the volumetric expansion during the initial stages of drying and the coating played minimum role in it, the reported volumetric expansion was considered for computing the effective diffusivity of the core pellet. This assumption was confirmed by comparing the percentage volumetric expansion of the DSG pellet with the same solubles concentration with that of the coated pellet.

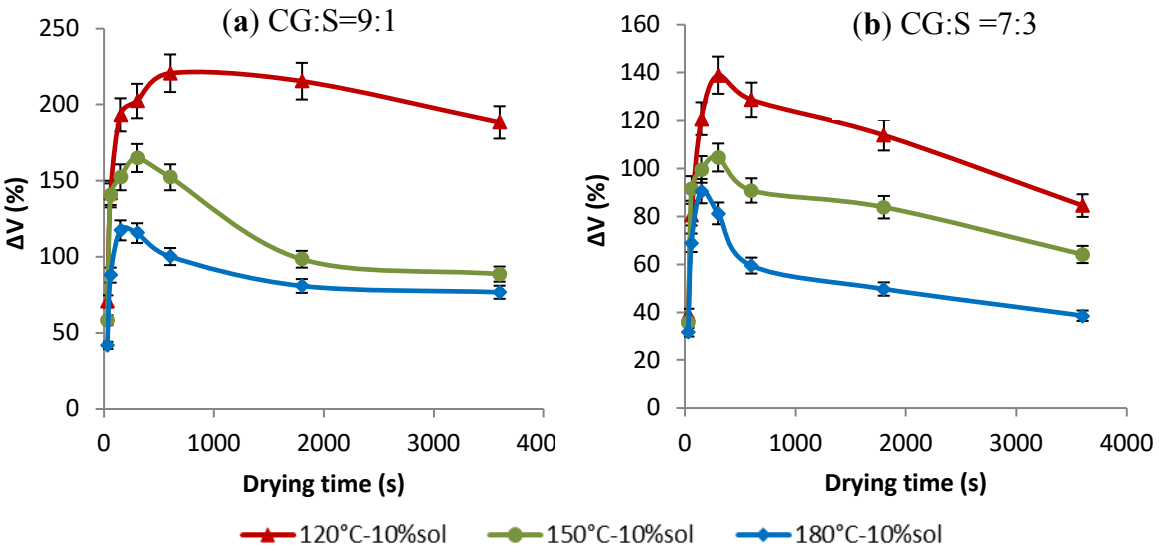

Figure 7.3 Volumetric change (expansion) of coated DSG pellet during SS drying at a velocity of 1 m/s; where, CG: S is the coarse grain fraction: solubles in the core pellet.

7.4.2 Effective moisture diffusivity

The experiment based effective moisture diffusivity of the coated DSG pellet was calculated from the SS drying data obtained for each operating condition and solubles concentration in the core pellet. The volumetric expansion had a significant effect on effective moisture diffusivity (Zielinska and Cenkowski, 2012) hence, it was considered for computing the effective moisture diffusivity of the coated pellet. The effective diffusivity of the coating and the core pellet was computed separately by using Fick's law of diffusion. The average effective moisture diffusivity based on drying curves of the distillers' solubles and DSG pellets was found to be in the range of $0.33 \times 10^{-9} - 3.7 \times 10^{-9}$ and $0.41 \times 10^{-8} - 4.2 \times 10^{-8}$ m^2/s, respectively. The effective moisture diffusivity was expressed as a function of temperature and moisture content using equation 7.1. The diffusivity decreased with moisture content and increased with SS temperature irrespective of the solubles concentration (Figure 7.4).

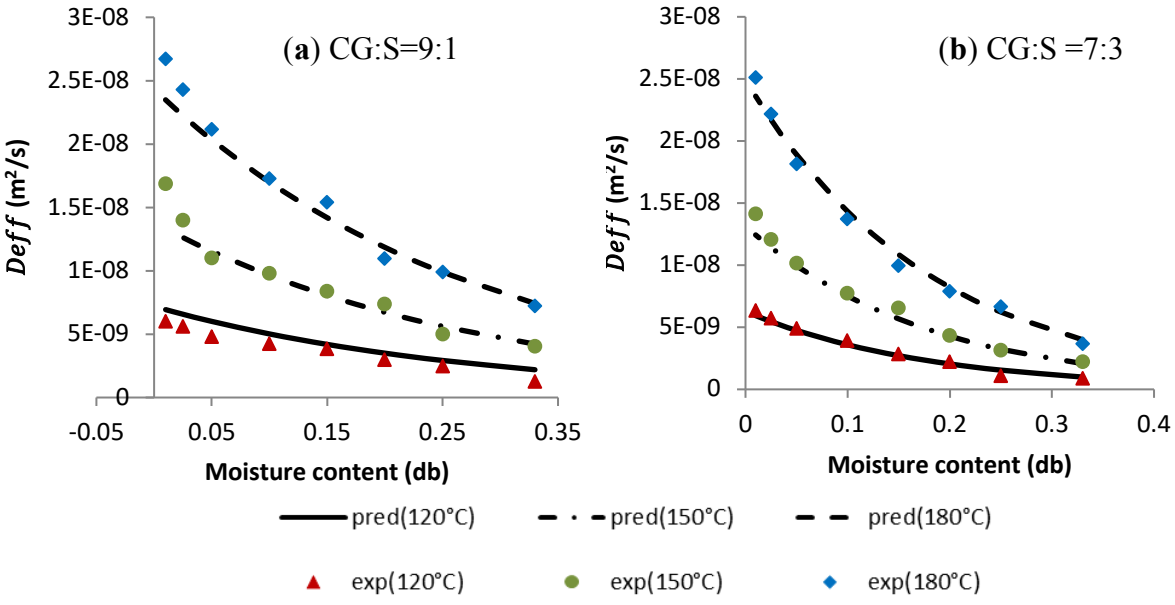

Figure 7.4 Predicted and experimental effective moisture diffusivity of coated DSG pellet at 0.5 m/s SS velocity; where, CG: S is the coarse grain fraction: solubles in the core pellet.

The model constants and activation energy of the core pellet and solubles were estimated and validated using respective drying characteristics (Table 7.1). The predicted effective moisture diffusivities were in good agreement with the experimental values with R^2 value ≥0.78 and error ≤10% (Figure 7.4). The effective moisture diffusivity was found to increase with temperature and decrease with moisture content.

Table 7.1 Model constants and activation energy of DSG pellet and solubles derived for effective diffusivity function

%Solubles w/w	SS Velocity ±0.1 (m/s)	M±0.1 (% wb)	Ea* ±0.6 (kJ/mol)	a	*c*	R^2
10	0.5	25	30.00	3.12×10^{-5}	-3.60	0.82
10	1.0	25	32.00	9.60×10^{-5}	-5.20	0.78
10	1.5	25	33.40	2.11×10^{-4}	-5.80	0.86
30	0.5	25	33.50	1.21×10^{-4}	-5.60	0.96
30	1.0	25	35.02	3.43×10^{-4}	-7.20	0.90
30	1.5	25	37.30	8.20×10^{-4}	-8.13	0.80
100	0.5	83	43.01	1.10×10^{-3}	-1.39	0.82
100	1.0	83	43.40	9.21×10^{-3}	-1.70	0.9
100	1.5	83	44.10	5.80×10^{-2}	-1.90	0.90

-SS is the superheated steam, M is the moisture content, Ea is the activated energy, a and c are the model coefficients, R^2 is coefficient of determination, and * percentage deviation obtained from 3 experimental trials.

7.4.3 Validation of the model

Among the three tested meshes (1.5, 2.3, and 4.8 million nodes), the meshes with 2.3 and 4.8 million nodes showed minimum deviation from the experimental results. Mesh sensitivity was tested at the lowest SS temperature for all the test velocities. The details of the $y_{Auto}+$ values of nodes closest to the solid-fluid interface and the comparison of RMS and maximum percentage deviation of moisture content and temperature at the interface are given in Appendix (Table A.3 and A.4). The maximum MRP error for the moisture prediction of the coated pellet from the simulations with 2.3 and 4.8 million nodes were 9.0 and 8.5%, respectively. But, simulation time for the meshes with 4.8 million nodes (43 h) was approximately double of that required for the mesh with 2.3 million nodes (25.2 h). Hence, the mesh with 2.3 million nodes was used for the rest of the simulations (for the selected operating conditions of SS drying system as discussed in section 7.3.4). A micro-level analysis of the moisture and temperature changes in a coated pellet with different moisture content in each layer was possible with the help of advanced features of the ANSYS package. The presented CFD model developed enabled the study of the temporal and spatial variation of the heat and mass transfer of such a multilayer pellet.

The temporal changes of average moisture and temperature of the coated DSG pellet were obtained from the drying experiments under selected operating condition (as discussed in section 7.3.4 and 7.3.7, respectively). The predicted values of temporal changes in moisture and temperature of the coated pellet were obtained from simulation results obtained from the ANSYS-CFX solver. The predicted values of the average moisture content of the coated pellet and the experimental values of the average moisture content over the drying period for the corresponding operating conditions were comparable with the experimental

values as reflected in the MRP (Table 7.2). The maximum MRP error value obtained for the moisture and temperature curves were 9.1 and 8.0%, respectively. A larger error in the prediction of change in average moisture content of the coated pellet was attributed to the relatively higher deviation in the predicted and the experimental moisture curves during the initial condensation and restoration period. A similar trend was reported by Ramachandran et al. (2017a) in which the diffusion of moisture from the condensation layer to the interior of the pellet was pointed as the possible reason for the under-prediction of moisture change during initial condensation (Adamski and Pakowski, 2013). The presented model successfully accounted for the effect of condensation on the pellet, as reflected in the moisture profile analysis (Figure 7.5). The adsorption of condensed water by the coating was negligible as the coating itself was at high moisture content. Hence the condensation film disappeared after a few seconds (Sa-Adchom et al., 2011b) depending on the evaporation rate (Figure 7.6). But the initial condensation periods reported in the drying experiments were longer than the simulated values as the steam flow experienced a time lag in equilibrating inside the drying chamber with the set operating condition after the steam diversion valve was turned on. This delay caused prolongation of the condensation period (up to 5.3%) in the experimental drying curve when compared to the simulation results (Figure 7.6).

Table 7.2 Predicted and experimental drying time for the coated pellet to reach 10% wb (safe storage) moisture content

%Solubles (w/w)	SS Temperature ±2°C	SS Velocity ±0.1 (m/s)	Drying time ±6.2% *(s)	Drying time (s)	MRP %
10	120	0.5	6200	5700	9.06
10	120	1	4360	4040	8.34
10	120	1.5	3300	3050	7.58
10	150	0.5	3150	2950	7.35
10	150	1	2530	2050	6.93
10	150	1.5	1860	1600	6.45
10	180	0.5	1800	1650	7.33
10	180	1	1450	1280	6.83
10	180	1.5	880	650	7.61
30	120	0.5	9950	9700	9.03
30	120	1	8050	7890	6.23
30	120	1.5	6500	6150	7.38
30	150	0.5	6150	5760	8.34
30	150	1	5650	5005	7.88
30	150	1.5	4050	3850	4.94
30	180	0.5	3340	2850	8.33
30	180	1	1640	1450	7.93
30	180	1.5	1050	840	6.09

- SS is the superheated steam, * percentage deviation obtained from 3 experimental trials, MRP is the mean relative percentage error.

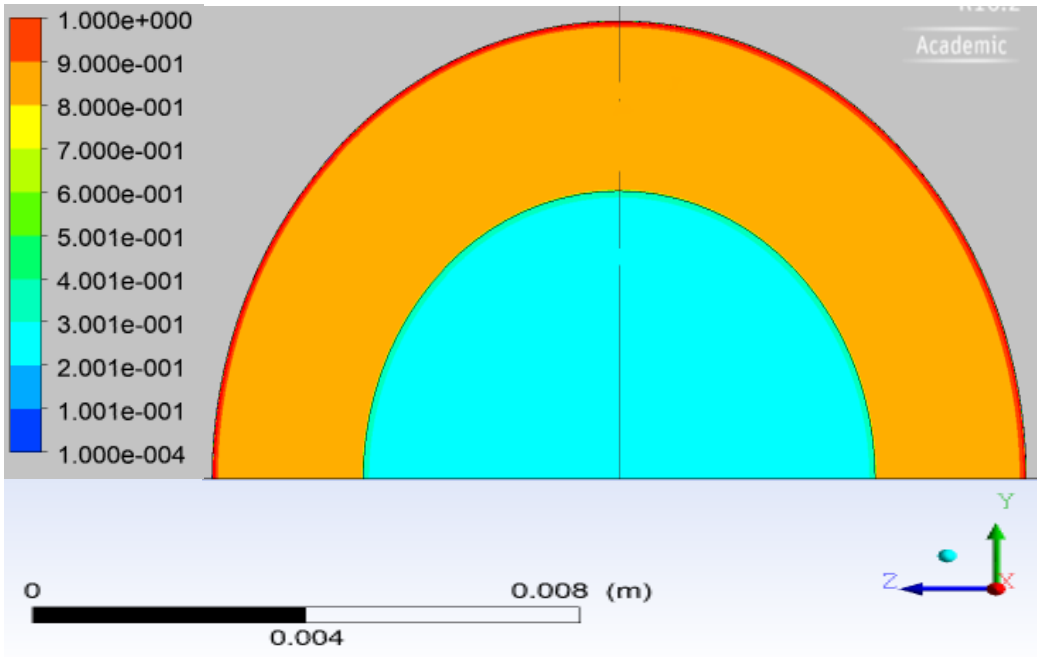

Figure 7.5 Moisture profile of coated DSG pellet with initial condensation layer when treated with SS for 25 s, at 120°C temperature and 0.5 m/s velocity; where the moisture content varies from 0.0001 to 1.0 wb from the bottom to top in the colour scale shown at the left.

The effect of solubles concentration in the core pellet on drying was also captured by the simulation. The moisture diffusion from the coating to the core pellet was governed by the diffusion equations of the coating and the core pellet (Figure 7.7). The higher solubles concentration in the core pellet decreased the drying rate, especially during the falling rate drying period. A decrease in drying rate with increased solubles concentration in the core pellet could be due to the increased micro-porosity of the core pellet. The closed lattice packaging of small particles of solubles during compaction causes a decrease in large pores and increase in density of the pellet (Johnson et al., 2015). This could cause increased resistance to moisture diffusion during drying (Figures 7.6 and 7.7). A comparison of simulated moisture and temperature profiles of coated DSG pellet with 10% and 30%

solubles in their core pellet after a specific period of drying is given in Figures 7.7 and 7.8. Both the moisture and temperature profiles (Figure 7.7 and 7.8) showed a shift in the symmetry of the contour lines as a result of the direction of SS flow. The increase in solubles concentration increased the thermal conductivity of the pellet (Figure 7.8), as the solubles act as a binder and minimize the porosity, especially open porosity (Johnson et al., 2015; Ramachandran et al., 2017c). Moisture migration from the coating to SS was governed by heat transfer rather than mass transfer (Iyota et al., 2008) due to the moisture gradient; whereas the moisture movement inside the pellet and the coating were governed by the moisture gradient. Hence, the effective diffusivity of the core pellet and the coating influences the drying process, especially in the early falling drying rate period (Ramachandran et al., 2017a; Zielinska et al., 2009; Zielinska and Cenkowski, 2012). Since it was impractical to incorporate the physical change in dimensions (local coordinates of the coated pellet) in the simulation, a deviation in the prediction of instantaneous moisture and temperature profile is suspected. This deviation can be corrected to some extent by defining the thermo-physical properties such as density and thermal conductivity as a function of the moisture content of the coating and the core pellet.

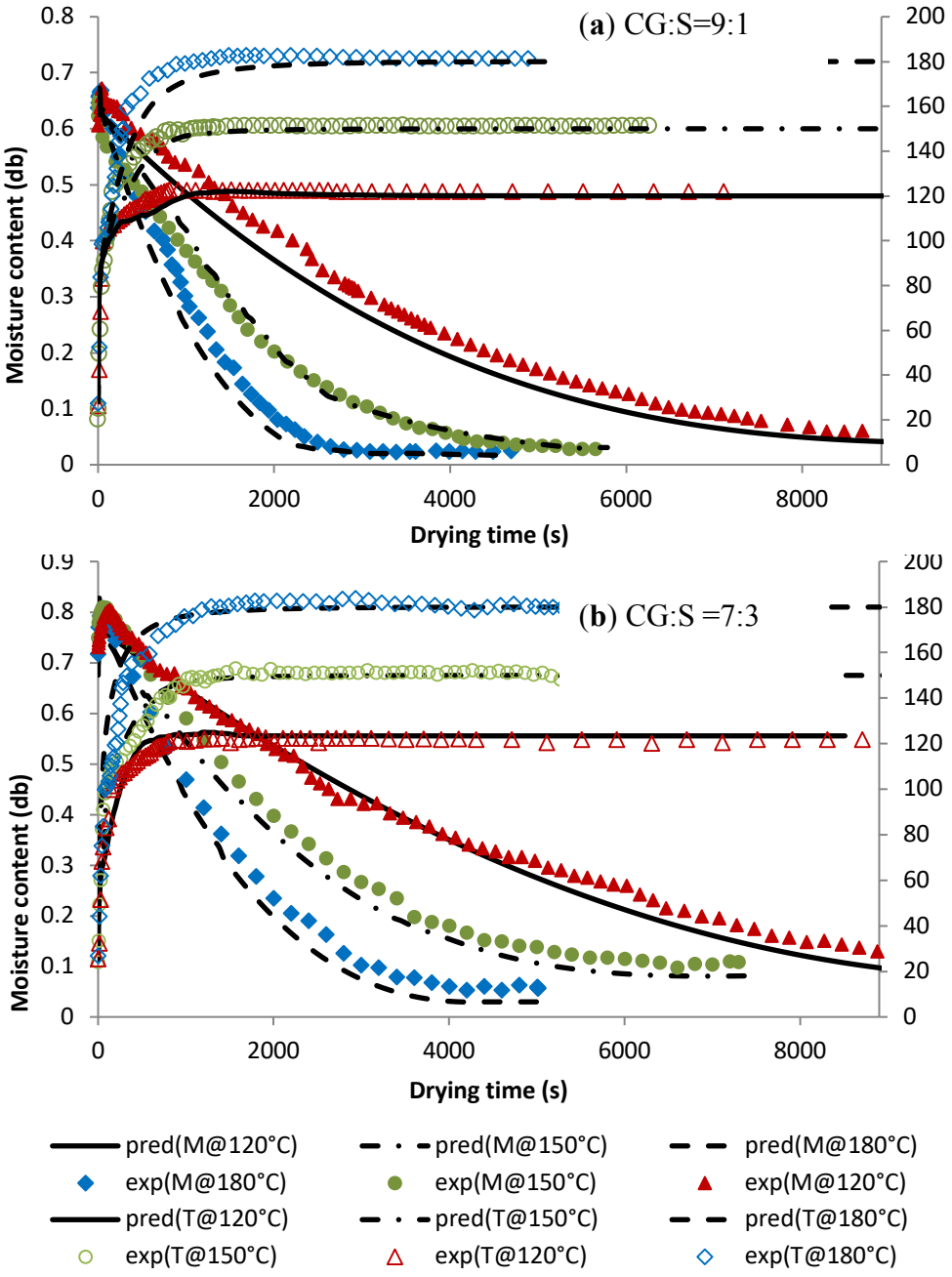

Figure 7.6 Experimental and predicted moisture and surface temperature of coated DSG pellet at SS velocity of 0.5 m/s; where, CG:S is the coarse grain fraction:distillers' solubles in the core pellet, exp- experimental values, and pred- predicted values

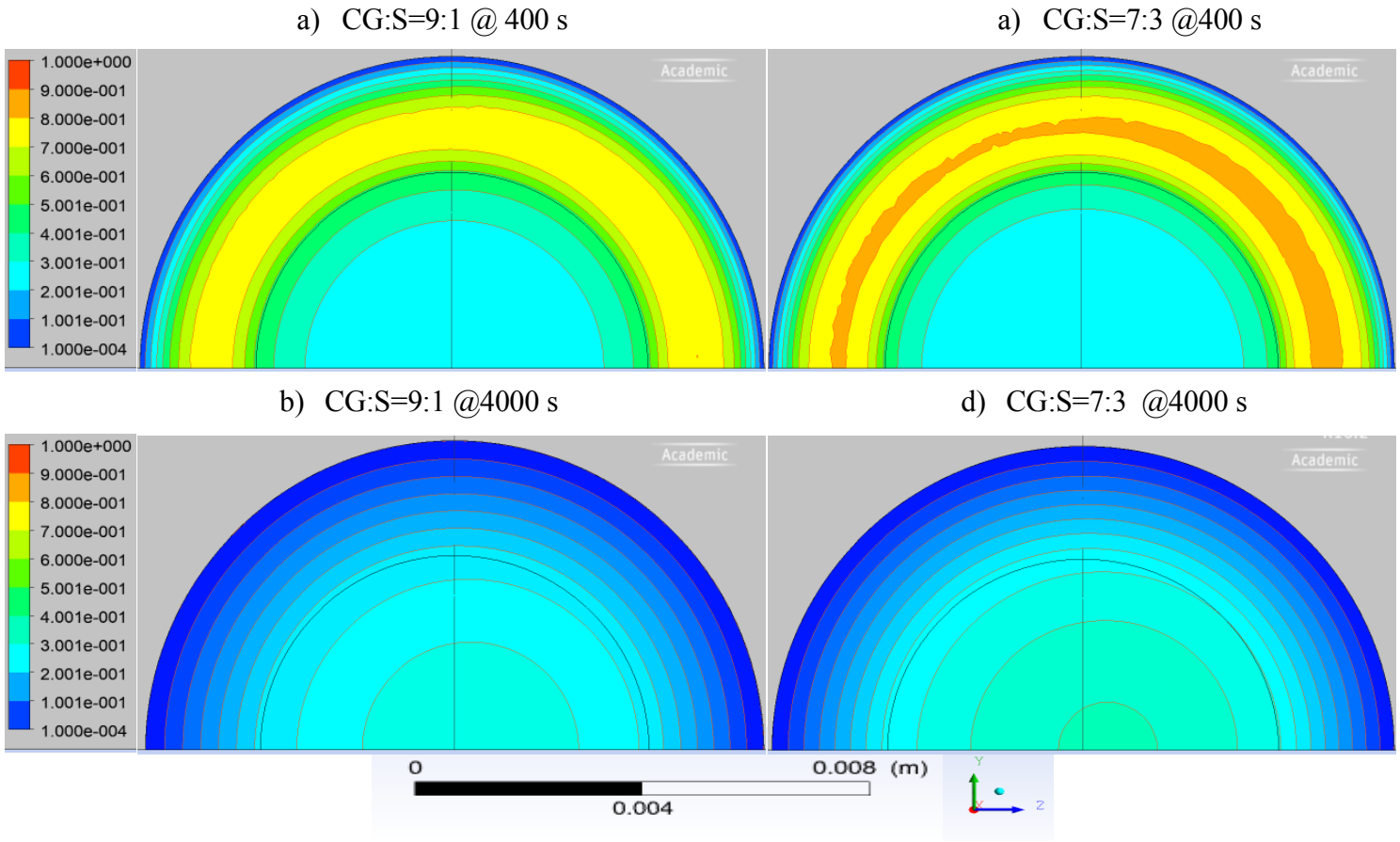

Figure 7.7 Moisture profile of coated DSG pellet after of drying in SS for about 400 s, at 120°C temperature and 0.5 m/s velocity; where, CG:S is the coarse grain fraction:distillers' solubles in the core pellet; and the moisture content varies from 0.0 to 1.0 wb from the bottom to top in the colour scale shown at the left

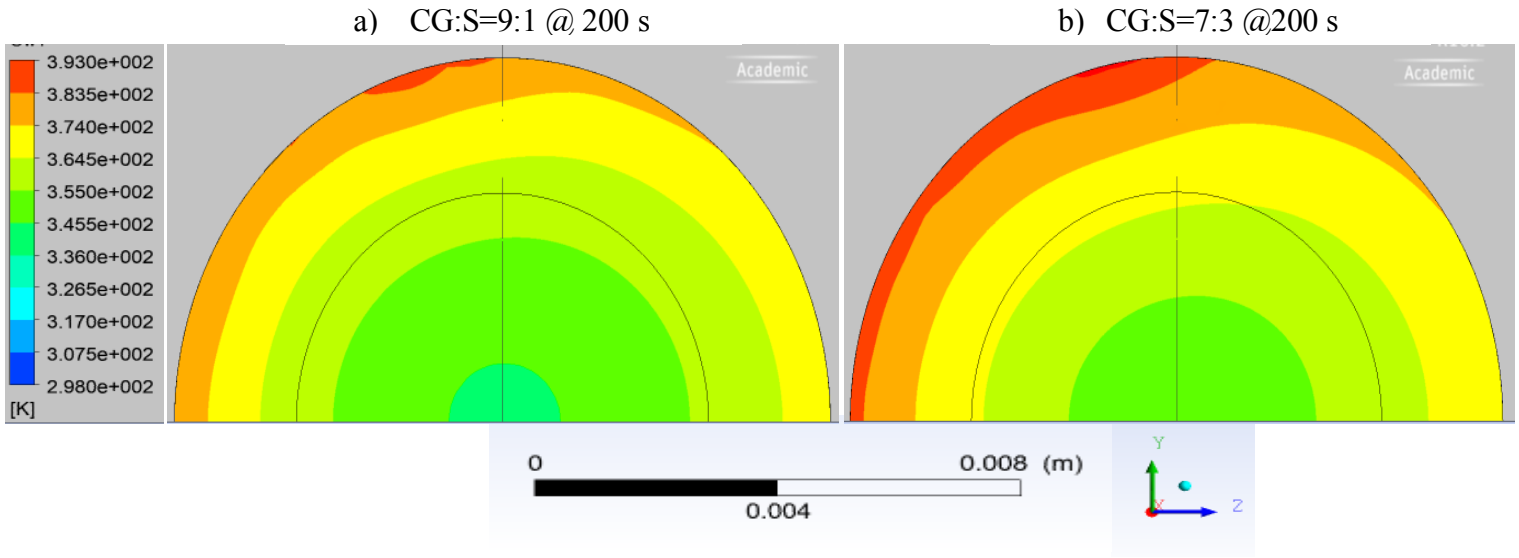

Figure 7.8 Temperature profile of coated DSG pellet after of drying in SS for about 200 s, at 120°C temperature and 0.5 m/s velocity; where, CG:S is the coarse grain fraction: distillers' solubles in the core pellet; and the temperature varies from 298 to 393 K from the bottom to top in the colour scale shown at the left.

The sensitivity of the model for the different operating conditions such as SS temperature and velocity and the relative errors were also studied as shown in Table 7.2. The model predicted the effect of SS temperature and velocity on the moisture migration of the coated pellet (Figure 7.9). The temporal change in moisture at the geometric center of the coated pellet with 10 and 30% solubles concentration in the core pellet at various operating conditions of SS drying system are shown in Figure 7.9. The predicted moisture content at the center of the coated pellet increased initially due to the inward diffusion of moisture from the coating to the core pellet governed by the moisture gradient. The rate of this moisture diffusion was influenced by the SS velocity and temperature (Figure 7.9). The inward moisture diffusion to the center of the core pellet was counter-acted by the outward moisture diffusion from core to the SS. As drying time elapses, the inward moisture diffusion diminishes and the moisture content at the center of the pellet starts to decrease (Figure 7.7). The change in moisture profile of the coated pellet as a function of the radial distance from the center of the pellet at different drying times (500 s and 2500 s) is shown in Figure 7.10. During the early stages of drying, the moisture content of the core pellet (0.0064 mm diameter) gains moisture from the outer coating, while the outermost layer of the coating loses moisture to the SS. With the progress in drying, the entire pellet starts losing moisture to the SS (Figure 7.10). This trend was visible in drying simulations at all operating conditions of the SS drying unit.

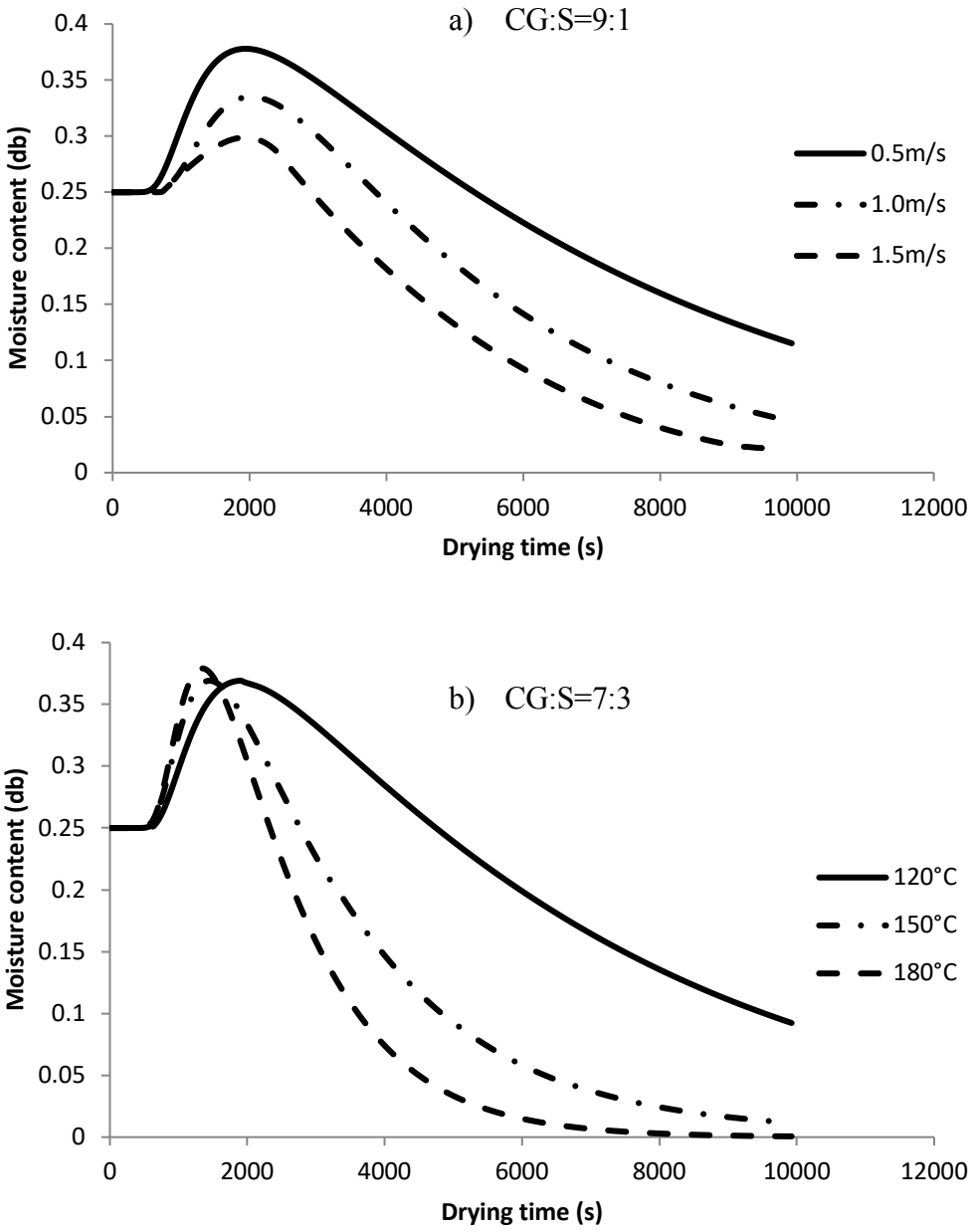

Figure 7.9 Temporal changes of moisture content at the center of the coated DSG pellet (with 30% solubles in its core pellet) when dried under SS at different temperatures and velocities; where, CG:S is the coarse grain fraction:distillers' solubles in the core pellet.

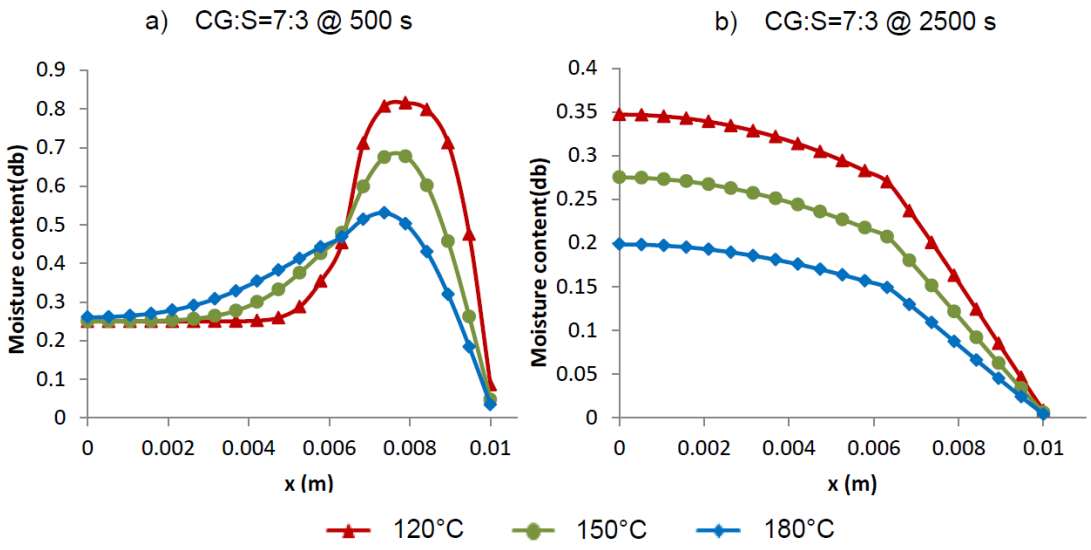

Figure 7.10 Moisture profile of coated DSG pellet as a function of the distance (x) from its center after (a) 500 s and (b) 2500 **s** of SS drying at different SS temperatures; where, CG:S is the coarse grain fraction: distillers' solubles in the core pellet.

7.5 Conclusions

A three-dimensional CFD model has been developed in the realm of this research study. The model elucidates the temporal and spatial variation of the heat and mass transfer during the SS drying of multilayer DSG pellets. Since the determination of the mass transfer coefficient is impractical for the SS drying, the presented model is solely dependent on the boundary conditions between the domains and on the resolution of conservation equations in the environment. By defining separate interfaces for each domain (SS, coating, and the core pellet), the transport phenomena occurring in each domain can be simulated with the mean square (RMS) values of the residuals of moisture content and temperature equal to 1×10^{-6}. The heat and mass transfer phenomena occurring in both the coating and core pellet can be fairly predicted (with maximum MRP error $\leq$ 10%) by defining the separate initial and boundary

condition, thermo-physical properties for each domain. The assigned diffusivity equation and the thermo-physical properties of the coating and the core pellet influence the accuracy of prediction of the temperature and moisture migration inside the coated pellet. Even though the effect of the overall volumetric change of the coated pellet during SS drying was accounted for the effective diffusivity function, the change in physical dimensions (local coordinates of the coated pellet) was not captured by the simulation. This may cause deviation in the prediction of instantaneous moisture and temperature profile, as volumetric change itself affects the local moisture and temperature computations. But this deviation can be neglected, when the thermo-physical properties such as density and thermal conductivity are defined as a function of moisture content and temperature. As both the simulation and experimental results showed higher change in drying time with change in SS temperature (up to 71.4%) when compared to that of the change in SS velocity (up to 36.6%), it can be concluded that for the tested range of SS operating conditions the effect of SS temperature is more prominent than the effect of SS velocity.

The validation results of the study show that the coupling of solid core pellet and wet solid coating diffusion models and SST k-ω turbulence model for fluid domain models with explicitly defined interfaces and boundary condition can be successfully applied for the numerical modelling of SS drying. This coupling method aids to predict the spatial and temporal variations in moisture and temperature of multi-layer moist objects without defining a mass boundary layer and hence, suitable for modelling SS drying. Also, the proposed model can be used as a reliable tool for the optimization and design of large-scale SS drying units for such wet products.

Acknowledgements

The authors acknowledge the Natural Sciences and Engineering Research Council of Canada, Graduate Enhancement of Tri-Council Stipends, and University of Manitoba Graduate Fellowship for their financial support. The authors are also thanking the NSERC-funded summer research assistants, Jennifer Pienuita and Alain Jeffrey Lagasse and the post-doctoral fellow Mohsen Akbarzadeh for their technical support.

Nomenclature

A	model constant (pre-exponential factor)
a_1	Bradshaw constant (0.31)
Cp	Specific heat capacity (kJ/(kg K))
CFD	Computational fluid dynamics
c	model constant for moisture content
db	dry basis moisture content
D	Moisture diffusivity (m^2/s)
DSG	Distillers' spent grain
Ev	Experimental value
f	Sorption isotherm-isobar
F_1, F_2	Blending functions
g	Acceleration due to gravity m/s^2
H	Enthalpy of the control volume (kJ/kg)
h	Heat transfer coefficient ($W/(m^2 K)$)
k	Turbulence kinetic energy
kt	Thermal conductivity (W/(m K))
L	Length of DSG pellet
M	Moisture content (kg of water/kg of dry mass)
$\dot{m}$	Mass flux ($kg/(m^2 s)$)

Nomenclature

MR	Moisture ratio
MRP	Mean relative percentage error
P	Pressure (Pa)
p_k	Production rate of k
Pv	Predicted value
R	Universal gas constant (8.314 J/(mol K))
r	Radius of DSG pellet
Re	Reynolds number
S	mean strain (1/s)
SS	Superheated steam
SST	Shear stress transport
T	Temperature (K)
t	Time (s)
V	Velocity m/s
wb	Wet basis moisture content
WDS	Wet distillers spent grain
x, y, z	`Distance along x, y, and z axis

Subscripts and Superscripts

c	Coating
t	Instantaneous time
e	Equilibrium
eff	Effective value
ref	Reference value
p	Pellet interface
sat	Saturation
ic	Initial condensation
film	Condensed film (water)
ss	Superheated steam
cr	Constant rate drying
fr	Falling rate drying
i	Instantaneous time
v	Water vapour

Symbols

β^*	Eddy viscosity coefficient (0.09)
ε	Dissipation rate
ρ	Density of the pellet (kg/m)
λ	Latent heat (J/kg)
ϑ	Eddy viscosity (kg/(m s))
μ	dynamic viscosity (kg/(m s))
σ_k	Prandtl number in k-equation
σ_ω	Prandtl number in ω-equation
∇	Laplace gradient function

References

1. Abbott, S.J., Kapur, N., Sleigh, P.A., Summers, J.L., Thompson, H.M., 2011. Industrial film drying. Fundam. Coat. Res. Convert. e-Print 1, 47–51.
2. Adamski, R., Pakowski, Z., 2013. Identification of Effective Diffusivities in Anisotropic Material of Pine Wood during Drying with Superheated Steam. *Drying Technology* 31, 264–268. doi.org/10.1080/07373937.2012.717152
3. Awoyale, W., Maziya-Dixon, B., Sanni, L.O., Shittu, T.A., 2016. Effect of water yam (Dioscoreaalata) flour fortified with distiller's spent grain on nutritional, chemical, and functional properties. *Food Science and Nutrition* 4, 24–33. doi.org/10.1002/fsn3.254
4. Baini, R., Langrish, T.A.G., 2007. Choosing an appropriate drying model for intermittent and continuous drying of bananas. *Journal of Food Engineering* 79, 330–343. doi.org/10.1016/j.jfoodeng.2006.01.068.

5. Bi, D., Chu, D., Zhu, P., Lu, C., Fan, C., Zhang, J., Bao, J., 2011. Utilization of dry distiller ' s grain and solubles as nutrient supplement in the simultaneous saccharification and ethanol fermentation at high solids loading of corn stover. *Biotechnology Letters* 33, 273–276. doi.org/10.1007/s10529-010-0429-z
6. Bourassa, J., Ramachandran, R.P., Paliwal, J., Cenkowski, S., 2015. Drying characteristics and moisture diffusivity of distillers' spent grains dried in superheated steam. *Drying Technology* 33. doi.org/10.1080/07373937.2015.1040883
7. Braud, L.M., Moreira, R.G., Castell-Perez, M.E., 2001. Mathematical modeling of impingement drying of corn tortillas. *Journal of Food Engineering* 50, 121–128.
8. Brochetti, D., Penfield, M.P., Heim-edelman, M.F., 1991. Yeast bread containing distillers' dried grain dough development and bread quality. *Journal of Food Quality* 14, 331–344.
9. Broniarz-Press, L., Różański, J., Różańska, S., 2014. Rheological properties of condensed corn distillers solubles. Zywnosc.Nauka.Technologia.Jakosc/ *Food Science and Technology*. Quality 5, 195–205. https://doi.org/10.15193/zntj/2014/96/195-205
10. Capone, L., Benhamadouche, S., Hassan, Y.A., 2016. Source terms modeling for spacer grids with mixing vanes for CFD simulations in nuclear reactors. *Computers and Fluids* 126, 141–152. doi.org/10.1016/j.compfluid.2015.11.011
11. Cenkowski, S., Pronyk, C., Zmidzinska, D., Muir, W.E., 2007. Decontamination of food products with superheated steam. *Journal of Food Engineering* 83, 68–75.
12. Da Silva, W.P., e Silva, C.M.D.P.S., Gomes, J.P., 2013. Drying description of cylindrical pieces of bananas in different temperatures using diffusion models. *Journal of Food Engineering* 117, 417–424. doi.org/10.1016/j.jfoodeng.2013.03.030
13. Defraeye, T., Blocken, B., Carmeliet, J., 2012a. Analysis of convective heat and mass transfer coefficients for convective drying of a porous flat plate by conjugate modelling. *International Journal of Heat and Mass Transfer* 55, 112–124.
14. Defraeye, T., Blocken, B., Derome, D., Nicolai, B., Carmeliet, J., 2012b. Convective heat and mass transfer modelling at air-porous material interfaces: Overview of existing methods and relevance. *Chemical Engineering Science* 74, 49–58.

15. Defraeye, T., Herremans, E., Verboven, P., Carmeliet, J., Nicolai, B., 2012c. Convective heat and mass exchange at surfaces of horticultural products: A microscale CFD modelling approach. Agric. For. Meteorol. 162–163, 71–84.
16. Ducept, F., Sionneau, M., Vasseur, J., 2002. Superheated steam dryer: Simulations and experiments on product drying. *Chemical Engineering Journal* 86, 75–83.
17. Erriguible, A., Bernada, P., Couture, F., Roques, M., 2006. Simulation of Superheated Steam Drying from Coupling Models. *Drying Technology* 24, 941–951.
18. Erriguible, A., Bernada, P., Couture, F., Roques, M. -a., 2005. Modeling of Heat and Mass Transfer at the Boundary Between A Porous Medium and Its Surroundings. *Drying Technology* 23, 455–472. doi.org/10.1081/DRT-200054119
19. Fabbri, A., Cevoli, C., 2015. 2D water transfer finite elements model of salami drying, based on real slice image and simplified geometry. *Journal of Food Engineering* 158, 73–79.
20. Faghani, E., Maddahian, R., Faghani, P., Farhanieh, B., 2010. Numerical investigation of turbulent free jet flows issuing from rectangular nozzles: The influence of small aspect ratio. *Archive of Applied Mechanics* 80, 727–745.
21. Fiasco, B.A., Rubenthaler, G., Borhan, M., Dong, F.M., 1990. Baking properties of bread and cookies incorporating distillers ' or brewer ' s grain from wheat or barley. *Journal of Food Science* 55, 424–429.
22. Gharsallaoui, A., Roudaut, G., Chambin, O., Voilley, A., Saurel, R., 2007. Applications of spray-drying in microencapsulation of food ingredients: An overview. *Food Research International* 40, 1107–1121. doi.org/10.1016/j.foodres.2007.07.004
23. Goldberg, U.C., Batten, P., 2015. A wall-distance-free version of the SST turbulence model. Eng. Appl. Comput. Fluid Mech. 9, 33–40.
24. Granby, K., Mortensen, A., Broesboel-Jensen, B., 2012. Potential contamination issues arising from the use of biofuel and food industry by-products in animal feed. *Animal Feed Contamination* 514–539. doi.org/10.1533/9780857093615.5.514
25. Hamawand, I., 2013. Drying Steps under Superheated Steam: A Review and Modeling. *Energy and Environment Research* 3(2), 107-125.
26. Hu, Y., Nie, W., Hu, X., Li, Z., 2016. Microbial decontamination of wheat grain with superheated steam. Food Control 62, 264–269.

27. Iyota, H., Inoue, T., Yamagata, J., Nishimura, N., 2008. Effect of time-dependent humidity profiles from air to superheated steam on drying of a wetted starch sphere. *Drying Technology* 26, 211–221. doi.org/10.1080/07373930701831598
28. Johansson, A., Fyhr, C., Rasmuson, A., 1997. High temperature convective drying of wood chips with air and superheated steam. International Journal of Heat and MassTransfer 40, 2843–2858. doi.org/10.1016/S0017-9310(96)00341-9
29. Johnson, P., Cenkowski, S., Paliwal, J., 2014. Analysis of the disintegration of distiller's spent grain compacts as affected by drying in superheated steam. *Drying Technology* 32, 1060–1070. doi.org/10.1080/07373937.2014.881849
30. Johnson, P., Cenkowski, S., Paliwal, J., 2013. Compaction and relaxation characteristics of single compacts produced from distiller's spent grain. *Journal of Food Engineering* 116, 260–266. doi.org/10.1016/j.jfoodeng.2012.11.025
31. Johnson, P., Paliwal, J., Cenkowski, S., 2015. Effect of solubles on disintegration of distiller's spent grain compacts during superheated steam drying. *Drying Technology* 33, 1–13. doi.org/10.1080/07373937.2014.967403
32. Kaleemullah, S., Kailappan, R., 2006. Modelling of thin-layer drying kinetics of red chillies. *Journal of Food Engineering* 76, 531–537.
33. Karabelas, S.J., Koumroglou, B.C., Argyropoulos, C.D., Markatos, N.C., 2012. High Reynolds number turbulent flow past a rotating cylinder. *Applied Mathematical Modelling* 36, 379–398. doi.org/10.1016/j.apm.2011.07.032
34. Kittiworrawatt, S., Devahastin, S., 2009. Improvement of a mathematical model for low-pressure superheated steam drying of a biomaterial. *Chemical Engineering Science* 64, 2644–2650. doi.org/10.1016/j.ces.2009.02.036
35. Le, K.H., Kharaghani, A., Kirsch, C., Tsotsas, E., 2017. Discrete pore network modeling of superheated steam drying. *Drying Technology* 35, 1584–1601.
36. Li, E., Lim, C., Cai, C., Klesius, P.H., 2011. Growth response and resistance to streptococcus iniae of Nile Tilapia , Oreochromis niloticus , Fed Diets containing distiller ' s dried grains with solubles. *Animal Feed Science and Technology* 170, 246–255. doi.org/10.1111/j.1749-7345.2007.00093.x

37. Liu, S.X., Singh, M., Inglett, G., 2011. Effect of incorporation of distillers' dried grain with solubles (DDGS) on quality of cornbread. LWT - *Food Science and Technology* 44, 713–718. doi.org/10.1016/j.lwt.2010.10.001
38. Ljung, A.-L., Lundström, T.S., Tano, K., 2011. Simulation of convective drying of a cylindrical iron ore pellet. *International Journal of Numerical Methods for Heat & Fluid Flow* 21, 703–716. doi.org/10.1108/09615531111148464
39. Lyberg, K., Borling, J., Lindberg, J.E., 2012. Ileal and total tract digestibility of wet and dried wheat distillers grain products in growing pigs. *Journal of Animal Science* 90, 131–133. doi: 10.2527/jas.53797.
40. Malafronte, L., Ahrné, L., Kaunisto, E., Innings, F., Rasmuson, A., 2015. Estimation of the effective diffusion coefficient of water in skim milk during single-drop drying. *Journal of Food Engineering* 147, 111–119. doi.org/10.1016/jjfoodeng.2014.09.032
41. Menter, F.R., 1994. Two-equation eddy-viscosity turbulence models for engineering applications. Am. Inst. Aeronaut. Astronaut. J. 32, 1598–1605.
42. Messai, S., Sghaier, J., Ganaoui, M. El, Chrusciel, L., Gabsi, S., 2015. Low Pressure Superheated Steam Drying of a Porous Media-Part I. *Drying Technology* 33, 103–110. doi.org/10.1080/07373937.2014.933843
43. Moreira, R.G., 2001. Impingement drying of foods using hot air and superheated steam. *Journal of Food Engineering* 49, 291–295. doi.org/10.1016/S0260-8774(00)00225-9.
44. Musa, O., Changsheng, Z., Xiong, C., Lunkun, G., 2016. Prediction of swirling cold flow in a solid-fuel ramjet engine with a modified rotation/curvature correction SST turbulence model. *Applied Thermal Engineering* 105, 737–754.
45. Pakowski, Z., Adamski, R., 2011. On prediction of the drying rate in superheated steam drying process. *Drying Technology* 29, 1492–1498.
46. Pakowski, Z., Adamski, R., Kwapisz, S., 2011. Effective diffusivity of moisture in low rank coal during superheated steam drying at atmospheric pressure. *Chemical and Process Engineering* 33, 43–51. doi.org/10.2478/v10176-012-0004-3
47. Pang, S., 1997. Some Considerations In Simulation Of Superheated Steam Drying Of Softwood Lumber. *Drying Technology* 15, 651–670.

48. Penner, G.B., Yu, P., Christensen, D.A., 2009. Effect of replacing forage or concentrate with wet or dry distillers ' grains on the productivity and chewing activity of dairy cattle. *Animal Feed Science and Technology* 153, 1–10.
49. Pimpaporn, P., Devahastin, S., Chiewchan, N., 2007. Effects of combined pretreatments on drying kinetics and quality of potato chips undergoing low-pressure superheated steam drying. *Journal of Food Engineering* 81, 318–329.
50. Pronyk, C., Cenkowski, S., Muir, W.E., 2010. Drying Kinetics of Instant Asian Noodles Processed in Superheated Steam. *Drying Technology* 37–41.
51. Pronyk, C., Cenkowski, S., Muir, W.E., Lukow, O.M., 2008. Effects of superheated steam processing on the textural and physical properties of Asian noodles. *Drying Technology* 26, 192–203. doi.org/10.1080/07373930701831382
52. Pulat, E., Isman, M.K., Etemoglu, A.B., Can, M., 2011. Effect of Turbulence Models and Near-Wall Modeling Approaches on Numerical Results in Impingement Heat *Numerical Heat Transfer Part B-Fundamentals* 60, 486–519.
53. Rahman, N., Kumar, S., 2011. Evaluation of moisture diffusion coefficient of cylindrical bodies considering shrinkage during natural convection drying. *International Journal of Food Engineering* 7, 1–18. doi.org/10.2202/1556-3758.1352
54. Ramachandran, R.P., Akbarzadeh, M., Paliwal, J., Cenkowski, S., 2018. Computational Fluid Dynamics in Drying Process Modelling — a Technical Review. *Food and Bioprocess Technology* 11, 271–292. doi.org/10.1007/s11947-017-2040-y
55. Ramachandran, R.P., Akbarzadeh, M., Paliwal, J., Cenkowski, S., 2017a. Three-dimensional CFD modelling of superheated steam drying of a single distillers ' spent grain pellet. *Journal of Food Engineering* 212, 121–135.
56. Ramachandran, R.P., Bourassa, J., Paliwal, J., Cenkowski, S., 2017b. Effect of temperature and velocity of superheated steam on initial condensation of distillers ' spent grain pellets during drying. *Drying Technology* 35, 182–192.
57. Ramachandran, R.P., Paliwal, J., Cenkowski, S., 2017c. Thermo-physical properties of distillers' spent grain pellets at different moisture contents and condensed distillers' soluble concentrations. *Food and Bioprocess Technology* 10, 175–185.
58. Renewable-Fuels-Association, 2016. World Fuel Ethanol Production. URL http://ethanolrfa.org/resources/industry/statistics/#1454098996479-8715d404-e546

59. Rordprapat, W., Nathakaranakule, A., Tia, W., Soponronnarit, S., 2005. Comparative study of fluidized bed paddy drying using hot air and superheated steam. *Journal of Food Engineering* 71, 28–36. doi.org/10.1016/j.jfoodeng.2004.10.014
60. Sa-adchom, P., Swasdisevi, T., Nathakaranakule, A., Soponronnarit, S., 2011. Mathematical model of pork slice drying using superheated steam. *Journal of Food Engineering* 104, 499–507. doi.org/10.1016/j.jfoodeng.2010.12.025
61. Sa-Adchom, P., Swasdisevi, T., Nathakaranakule, A., Soponronnarit, S., 2011. Drying kinetics using superheated steam and quality attributes of dried pork slices for different thickness, seasoning and fibers distribution. *Journal of Food Engineering* 104, 105–113. doi.org/10.1016/j.jfoodeng.2010.12.002
62. Sabarez, H.T., 2012. Computational modelling of the transport phenomena occurring during convective drying of prunes. *Journal of Food Engineering* 111, 279–288.
63. Salim, H.M., Kruk, Z.A., Lee, B.D., 2010. Nutritive value of corn distillers dried grains with solubles as an ingredient of poultry diets : A review. *World's Poultry Science Journal* 66, 411–433. doi.org/10.1017/S0043933910000504
64. Sehrawat, R., Nema, P.K., Kaur, B.P., 2016. Effect of superheated steam drying on properties of foodstuffs and kinetic modeling. *Innovative Food Science and Emerging Technologies* 34, 285–301. doi.org/10.1016/j.ifset.2016.02.003
65. Stein, H.H., Shurson, G.C., 2009. Board- Invited Review : The use and application of distillers dried grains with solubles in swine diet. *Journal of Animal Science* 87, 1292–1303. doi.org/10.2527/jas.2008-1290
66. Suvarnakuta, P., Devahastin, S., Mujumdar, A.S., 2007. A mathematical model for low-pressure superheated steam drying of a biomaterial. *Chemical Engineering and Processing* 46, 675–683. doi.org/10.1016/j.cep.2006.09.002
67. Taechapairoj, C., Prachayawarakorn, S., Soponronnarit, S., 2006. Modelling of parboiled rice in superheated-steam fluidized bed. *Journal of Food Engineering* 76, 411–419. doi.org/10.1016/j.jfoodeng.2005.05.040
68. Taheri-Garavand, A., Rafiee, S., Keyhani, A., 2011. Study on effective moisture diffusivity, activation energy and mathematical modeling of thin layer drying kinetics of bell pepper. *Australian Journal of Crop Science* 5, 128–131.

69. Trujillo, F.J., Lovatt, S.J., Harris, M.B., Willix, J., Pham, Q.T., 2003. CFD modelling of the heat and mass transfer process during the evaporation of water from a circular cylinder. 3rd Internaltional Conference on CFD in the Minerals and Processing Inustries 99–104.
70. Tumuluru, J.S., Tabil, L., Opoku, A., Mosqueda, M.R., Fadeyi, O., 2010. Effect of process variables on the quality characteristics of pelleted wheat distiller's dried grains with solubles. *Biosystems Engineering* 105, 466–475.
71. Wongsiriamnuay, T., Tippayawong, N., 2015. Effect of densification parameters on the properties of maize residue pellets. *Biosystems Engineering* 139, 111–120. doi.org/10.1016/j.biosystemseng.2015.08.009
72. Xiao, Z., Zhang, F., Wu, N., Liu, X., 2013. CFD Modeling and Simulation of Superheated Steam Fluidized Bed Drying Process. IFIP Int. Fed. Inf. Process. 141–149.
73. Yang, B., Zhang, K.M., 2017. CFD-based turbulent reactive flow simulations of power plant plumes. *Atmospheric Environment* 150, 77–86.
74. Zentek, J., Knorr, F., Mader, A., 2014. Reducing waste in fresh produce processing and households through use of waste as animal feed Abstract : *Global Safety of Fresh Produce*. 104–152. doi.org/doi.org/10.1533/9781782420279.2.140
75. Zielinska, M., Cenkowski, S., 2012. Superheated steam drying characteristic and moisture diffusivity of distillers' wet grains and condensed distillers' solubles. *Journal of Food Engineering* 109, 627–634. doi.org/10.1016/j.jfoodeng.2011.06.017
76. Zielinska, M., Cenkowski, S., Markowski, M., 2009. Superheated Steam Drying of Distillers' Spent Grains on a Single Inert Particle. *Drying Technology* 27(12), 37–41.

THESIS SUMMARY AND CONCLUSIONS

The research covers the numerical modelling of SS drying of high moisture materials such as DSG. The method of drying this slurry was developed after a series of experimental and computational studies. As the wet DSG constitutes of a coarse grain fraction and thin solubles (small cohesive particles), the drying studies on each fraction were done separately and then combined at the later stages of the research. In this thesis, the concept of drying wet materials on the dried core was adopted for drying wet solubles. The core used in this study was a compacted DSG pellet with or without solubles at an initial moisture content of 25% wb. This method generates a larger surface area for drying wet solubles than drying the solubles alone. It also prevents wet solubles from sticking to the dryer surface during drying and therefore, can improve effectiveness of drying.

The input parameters for numerical modelling of SS drying such as thermo-physical properties of DSG with different solubles concentrations (0, 10, 30, and 50% w/w), and their effective moisture diffusivity were studied separately for different operating conditions. The analysis of the effect of temperature and moisture content on the thermal properties of DSG showed that both, thermal conductivity and specific heat had a positive correlation with the moisture content, solubles concentration, and SS temperature. The particle density of the individual DSG pellets compacted to 60.3±0.1 MPa increased from 898.8 to 1136.7 kg/m^3 with the increase in solubles concentration. But an increase in moisture of the pellet above 25% tends to decrease its particle density by 10-18% with respect to control (i.e. no solubles in the pellet). The study of effective moisture diffusivity of the DSG pellet with variable solubles concentration (0, 10, 30, and 100% w/w) when dried in SS at different operating conditions (SS temperature 120, 135, 150, 165, 180°C,

and velocities 0.5, 1.0, 1.5 m/s) showed that the effective moisture diffusivity increased with SS temperature and its velocity. Even though the addition of distillers' solubles to the DSG reduced the volumetric expansion (up to 32%) irrespective of the SS temperature and velocity, it is not recommended to add solubles in excess of 30% as it increases the drying time by more than 25%.

The operating parameters affected the amount and duration of initial condensation on DSG pellets during SS drying. An increase in SS temperature from 120 to 180°C resulted in a 60–64% decrease in the initial condensation irrespective of SS velocity. The initial condensation on DSG pellets can be minimized by increasing the SS temperature (≥180°C) and velocity (≥1 m/s) assuming adiabatic conditions are maintained. As there is no distinguishable mass transfer boundary in the case of SS drying, the initial condensation was predicted (mean square error 0.2) using equations and analogy for heat balance and film condensation.

The determined input parameters and their respective functions with variable operating conditions were used to define the solid and fluid domain in the computational model. The capabilities of commercial CFD software (ANSYS CFX) were utilized for configuration, meshing, and solution of the SS drying simulations. A coupled model with Reynolds-Averaged Navier-Stokes equation for solving the fluid (SS) domain and a drying model for the solid (DSG pellet) was found to be a suitable (mean relative percentage error ≤10%) approach for modelling the SS drying of DSG pellets. The SST k-ω turbulence model with the robust and accurate near-wall formulation can fairly predict the transport phenomena occurring at the solid-fluid (pellet-SS) interface with turbulence residual value in the range of 1×10^{-5}-1×10^{-6}. A similar approach with a multi-layer cylinder representing the DSG core

pellet and wet solubles coating was adopted for simulating the SS drying of coated pellets. The effect of volumetric changes (expansion) in the DSG pellet (coated or uncoated), its changes in thermo-physical properties, and initial condensation played a significant role in the predictability of the model. The sensitivity analysis of the model with variable operating conditions showed that the effect of SS temperature (120-180°C) on drying characteristics and drying time was higher (up to 35%) than that of the effect of SS velocity (0.5-1.5 m/s) for the same SS temperature range. The developed model could serve as a tool to design and optimize SS drying systems for multilayer materials.

RECOMMENDATIONS FOR FUTURE RESEARCH

In the realm of this study, the numerical modelling of superheated steam (SS) drying of distillers' spent grain (DSG) pellet with or without solubles coating are dependent on the input parameters for the computer simulations such as the thermo-physical properties of both the pellet and SS, effective moisture diffusivity of the pellet etc. These parameters are influenced by the volumetric changes occurring in the pellet during SS drying. Therefore, the following issues need to be addressed:

- The change in physical dimensions of the sample during drying should be incorporated in the modelling and simulation. One possible avenue could be to use a different aspect ratio (length/radius) of the sample (cylindrical pellets).
- Since, the effect of initial condensation is minimized for a SS temperature of 180°C and velocities above 1 m/s, the study of drying characteristics of multilayer moist objects at higher levels of operating conditions would minimize the volumetric expansion and therefore, could be of value to practical application such as improved sample mechanical stability.
- The study could also expand into the fluidized conditions, by having more durable pellets over the period of SS drying.
- Expansion of experimentation and simulations for bulk materials at various operating conditions are also needed.
- A comparative study on different turbulence models such as k-ε and SST k-ω with standard and enhanced wall functions for variable Reynold number would help to identify the suitability of the turbulence model for different flow velocities.

APPENDICES

Appendix A: Permissions for the reuse of the publication in the thesis/dissertation.

SPRINGER NATURE LICENSE TERMS AND CONDITIONS

Feb 06, 2018

This Agreement between University of Manitoba -- Rani Ramachandran ("You") and Springer Nature ("Springer Nature") consists of your license details and the terms and conditions provided by Springer Nature and Copyright Clearance Center.

License Number	4283071349516
License date	Feb 06, 2018
Licensed Content Publisher	Springer Nature
Licensed Content Publication	Food and Bioprocess Technology
Licensed Content Title	Computational Fluid Dynamics in Drying Process Modelling—a Technical Review
Licensed Content Author	Rani Puthukulangara Ramachandran, Mohsen Akbarzadeh, Jitendra Paliwal et al
Licensed Content Date	Jan 1, 2017
Licensed Content Volume	11
Licensed Content Issue	2
Type of Use	Thesis/Dissertation
Requestor type	academic/university or research institute
Format	print and electronic
Portion	full article/chapter
Will you be translating?	no
Circulation/distribution	10,001 to 20,000
Author of this Springer Nature content	yes
Title	Computational fluid dynamics in drying process modeling - a technical review
Instructor name	Dr. Jitendra Paliwal; Dr. Stefan Cenkowski
Institution name	University of Manitoba
Expected presentation date	Jun 2018
Requestor Location	University of Manitoba

For Adaptations/Translations:
Adapted/Translated by permission from [**the Licensor**]: [**Journal Publisher** (e.g. Nature/Springer/Palgrave)] [**JOURNAL NAME**] [**REFERENCE CITATION** (Article name, Author(s) Name), [**COPYRIGHT**] (year of publication)

Note: For any republication from the British Journal of Cancer, the following credit line style applies:

Reprinted/adapted/translated by permission from [**the Licensor**]: on behalf of Cancer Research UK: : [**Journal Publisher** (e.g. Nature/Springer/Palgrave)] [**JOURNAL NAME**] [**REFERENCE CITATION** (Article name, Author(s) Name), [**COPYRIGHT**] (year of publication)

For **Advance Online Publication** papers:
Reprinted by permission from The [**the Licensor**]: on behalf of Cancer Research UK: [**Journal Publisher** (e.g. Nature/Springer/Palgrave)] [**JOURNAL NAME**] [**REFERENCE CITATION** (Article name, Author(s) Name), [**COPYRIGHT**] (year of publication), advance online publication, day month year (doi: 10.1038/sj. [JOURNAL ACRONYM])

For Book content:
Reprinted/adapted by permission from [**the Licensor**]: [**Book Publisher** (e.g. Palgrave Macmillan, Springer etc) [**Book Title**] by [**Book author**(s)] [**COPYRIGHT**] (year of publication)

Other Conditions:

Version 1.0

Taylor & Francis
Taylor & Francis Group

Our Ref: P020718-06/LDRT

07 February 2018

Dear Rani Puthukulangara on Behalf of the University of Manitoba,

Material requested: Rani Puthukulangara Ramachandran, Justin Bourassa, Jitendra Paliwal & Stefan Cenkowski (2017)
Effect of temperature and velocity of superheated steam on initial condensation of distillers' spent grain pellets during drying
Drying Technology **35 (2): 182-192.**
https://doi.org/10.1080/07373937.2016.1166123

Thank you for your correspondence requesting permission to post your above mentioned 'Accepted Manuscript' on your departmental website for your dissertation.

As you are the author of the above article, we will be pleased to grant entirely free permission on the condition that you make the following acknowledgement:

This is an **Accepted Manuscript** of an article published by Taylor & Francis in [*JOURNAL TITLE*] on [date of publication], available online: http://www.tandfonline.com/ [Article DOI]."

Thank you very much for your interest in Taylor & Francis publications. Should you have any questions or require further assistance, please feel free to contact me directly.

Sincerely,

Mary Ann Muller

Permissions Coordinator

E-mail: maryann.muller@taylorandfrancis.com

Telephone: 215.606.4334

530 Walnut Street, Suite 850, Philadelphia, PA 19106 • Phone: 215-625-8900 •
Fax: 215-207-0050
Web: www.tandfonline.com

an informa business

Appendix B: Data on SS drying of DSG

Table A.1 Thermo-physical properties of DSG pellet at different operating conditions of SS drying unit.

SS T (°C)	M (% wb)	Solubles (% w/w)	Cp (kJ/kgK)	Tk (W/m K)	Density (kg/m^3)
120	25	0	3.56	0.54	1071.15
150	25	0	4.26	0.58	946.88
180	25	0	4.96	0.61	1122.32
120	35	0	3.76	0.70	983.33
150	35	0	4.46	0.74	1152.28
180	35	0	5.16	0.77	1040.76
120	25	10	3.67	0.61	1071.15
150	25	10	4.37	0.64	946.88
180	25	10	5.07	0.68	1122.32
120	35	10	3.87	0.77	983.33
150	35	10	4.57	0.80	1152.28
180	35	10	5.27	0.84	1040.76
120	25	30	3.90	0.73	1071.15
150	25	30	4.60	0.77	946.88
180	25	30	5.29	0.81	1122.32
120	35	30	4.09	0.89	983.33
150	35	30	4.79	0.93	1152.28
180	35	30	5.49	0.97	1040.76

- SS is the superheated steam, T is the temperature, M is the moisture content, Cp and Tk is the specific heat, and thermal conductivity, respectively.

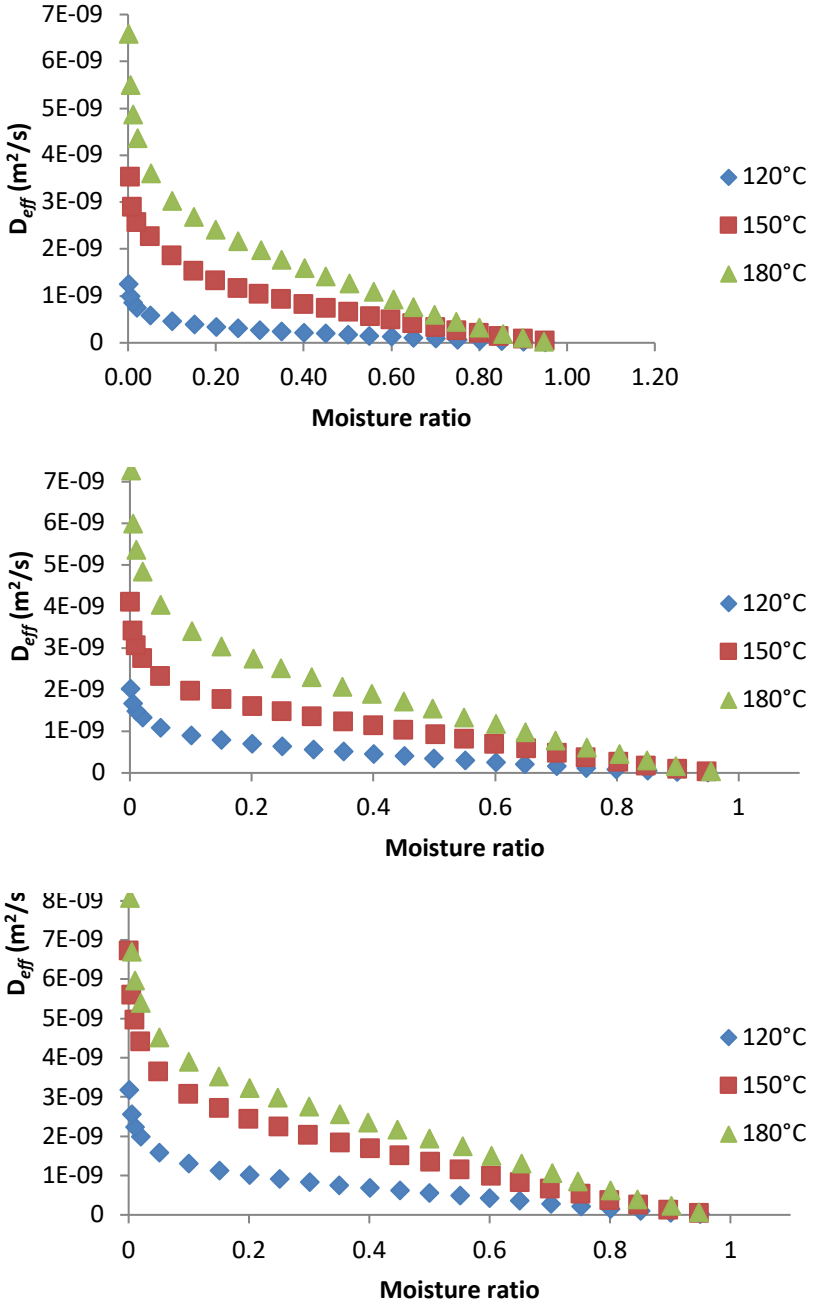

Figure A. 1 Effective moisture diffusivity of distillers' solubles at 0.5, 1.0, and 1.5 m/s SS velocities; where, D_{eff} is the effective moisture diffusivity.

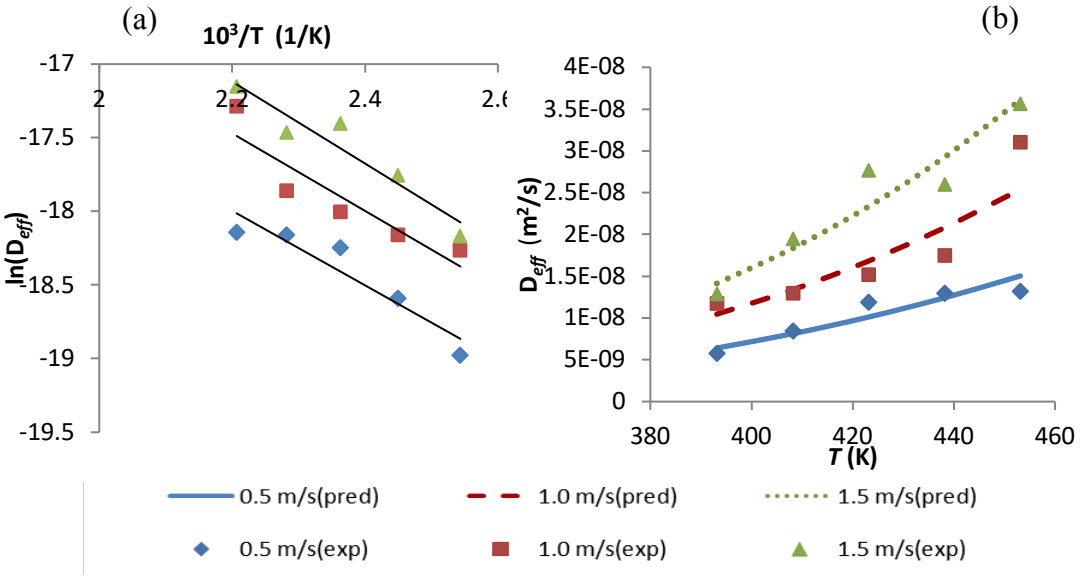

Figure A. 2 Arrhenius plot of ln (D_{eff}) versus inverse of SS temperature in K, (b) predicted and experimental effective diffusivity (D_{eff}) of DSG pellets with of 0% solubles and initial moisture content of 25% wb at different SS temperature (T).

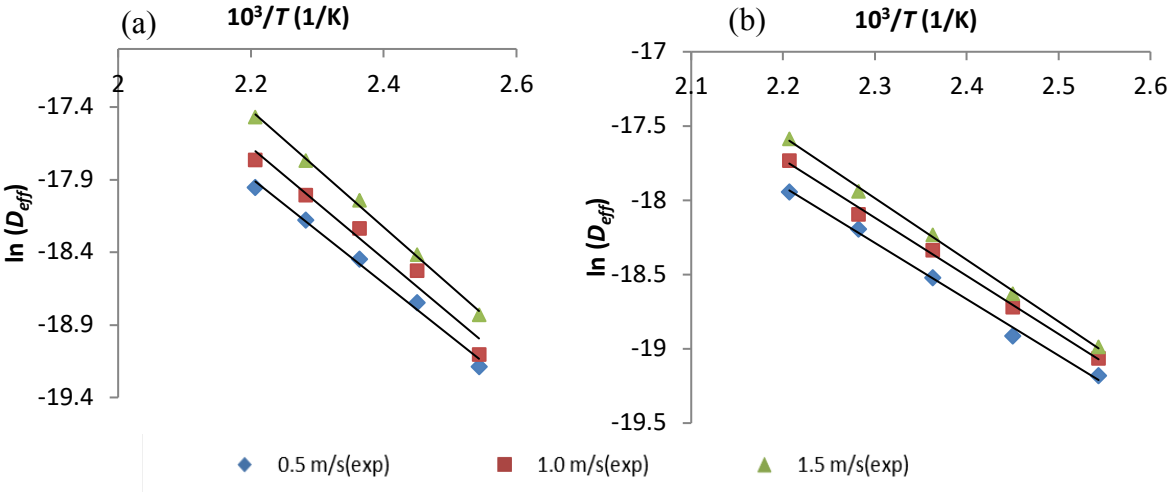

Figure A. 3 Arrhenius plot of ln (D_{eff}) versus inverse of SS temperature in K of DSG pellets with 10% solubles and initial moisture contents of (a) 25% and (b) 35% wb, respectively, at different SS temperature (T); where, D_{eff} - effective moisture diffusivity.

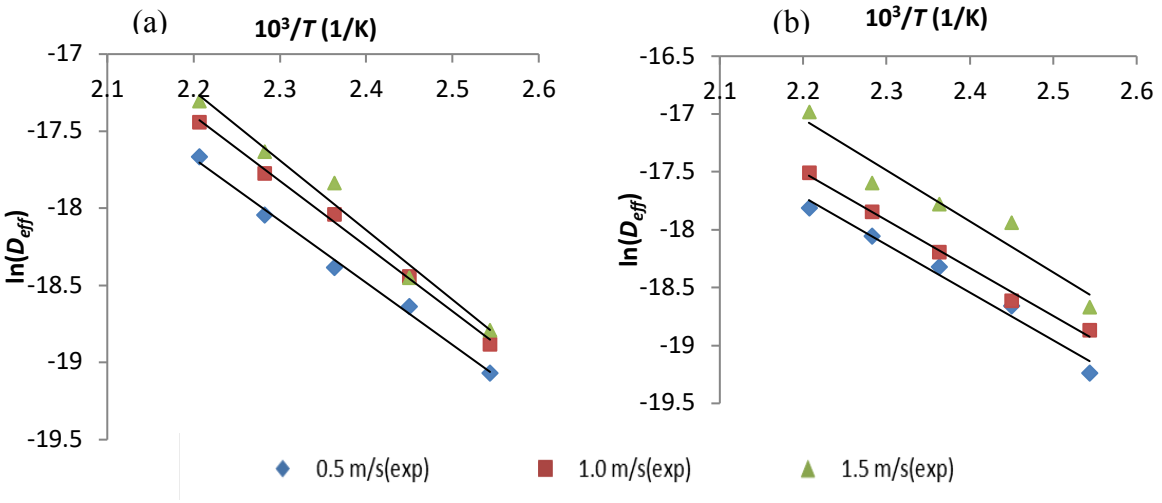

Figure A. 4 Arrhenius plot of ln(D_{eff}) versus inverse of SS temperature in K of DSG pellets with 30% solubles and initial moisture contents of (a) 25% and (b) 35% wb, respectively, at different SS temperature(T); where, D_{eff} - effective moisture diffusivity.

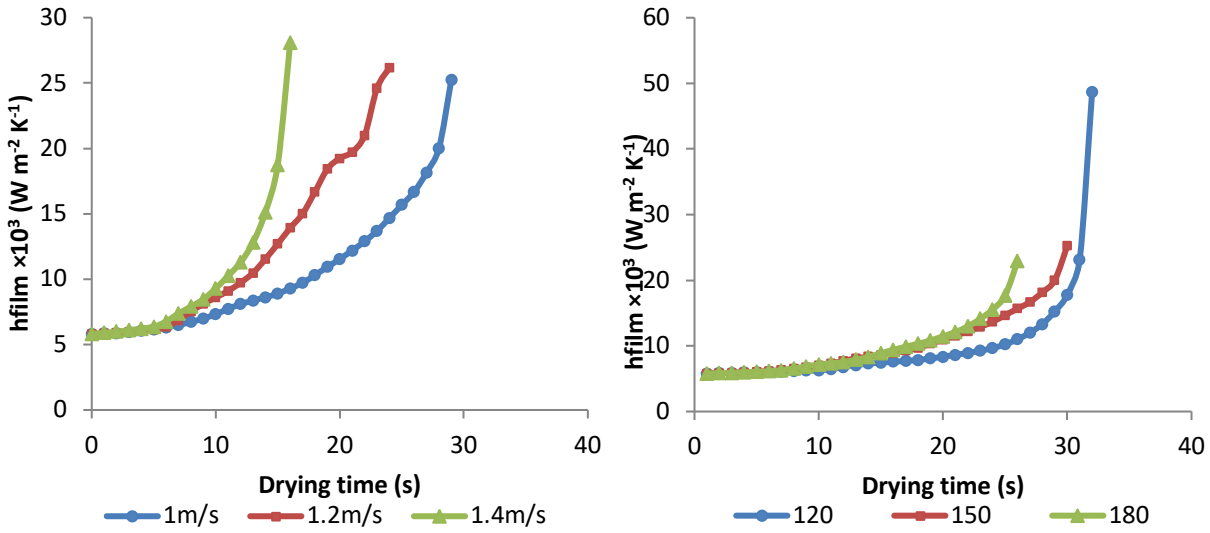

Figure A. 5 Film condensation heat transfer coefficient at different a) velocities of SS at 150 °C and b) temperatures of SS at 1.0 m/s

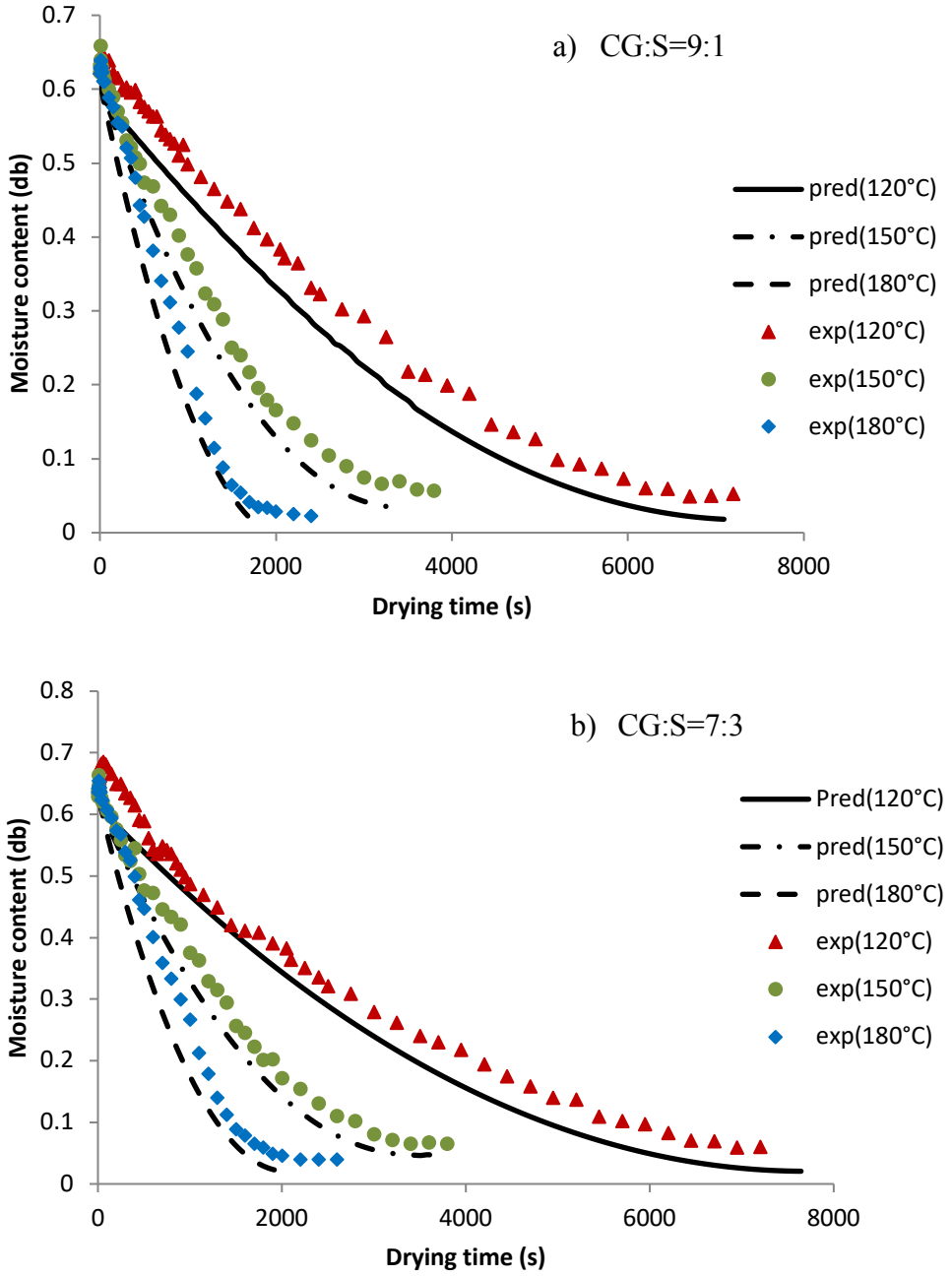

Figure A. 6 Experimental and predicted moisture content of coated DSG pellet at SS velocity of 1.0 m/s; where, CG:S is the coarse grain fraction: distillers' solubles in the core pellet, exp - experimental values, and pred - predicted values

Appendix C: CFD modelling

C.1 Geometry for CFD modelling

The problem geometry for the CFD modelling of SS drying of single DSG pellet (case A) and SS drying of DSG pellet with solubles coating were done using 'Geometry' feature of Fluid Flow CFX in ANSYS. The details of the geometries are given below:

Table A.2 Details of CFD geometry

	Domain	**Shape**	**Dimension of full geometry**
SS drying of a single DSG pellet (Case A)	Fluid (SS)	Quarter section of Cylinder	272 mm diameter and 356 mm length (both dimensions are equivalent to the actual drying Chamber
	Solid (DSG pellet)	Quarter section of Cylinder	12.7 mm in diameter and 35.5 mm length
SS drying of a single DSG pellet with solubles coating (Case B)	Fluid (SS)	Quarter section of Cylinder	272 mm diameter and 356 mm length (both dimensions are equivalent to the actual drying Chamber
	Solid 1 (DSG pellet)	Quarter section of Cylinder	12.35 mm in diameter and 25.5 mm length
	Solid 2 Solubles caoting	Thin layer over DSG cylinder	3.0 mm depth

C.2 Meshing

Meshing of the problem geometry was done with the auto mesh feature of the FluidFlow (CFX). Tetrahedral mesh CFD mesh option was chosen for both cases (A and B as defined in Table A.2). The SST turbulence model with automatic wall treatment was used in CFX to perform the grid independence study. In order to form fine grids near the interface and wall, inflation layer was added. This enables the capturing of boundary layer gradients.

The spacing of the nodes directly in contact with the solid walls were reduced to certain values so that the non-dimensional wall distance, $y_{Auto}+$, was less than 1, for all meshes. The maximum and minimum values of $y_{Auto}+$ obtained for the different meshes as shown in Table A.3

Table A.3 Maximum and minimum $y_{Auto}+$ values of nodes closest to the solid-fluid interface

Case	Mesh Million nodes	pellet-SS Inflation layer (first layer thickness/growth rate)	Maximum $y_{Auto}+$	Minimum $y_{Auto}+$
A1	0.98	0.005 mm/1.2	1.011	0.0164
A2	1.11	0.001 mm/1.2	0.956	0.0151
A3	2.3	0.0005 mm/1.2	0.8871	0.0144
Case	Mesh Million nodes	coating-SS Inflation layer (first layer thickness/growth rate)	Maximum $y_{Auto}+$	Minimum $y_{Auto}+$
B1	1.5	0.0005 mm/1.2	1.042	0.0234
B2	2.3	0.00014 mm/1.2	0.928	0.186
B3	4.8	0.00005 mm/1.2	0.854	0.141

Table A.4 RMS and maximum percentage deviation of moisture content and temperature at the solid-fluid interface

Grids compared	Moisture content at interface		Temperature at interface	
	RMS difference (kg/kg)	Max deviation (%)	RMS difference (K)	Max deviation (%)
A1-A2	8×10^{-6}	1.6	6.3	5.2
A2-A3	4×10^{-6}	0.7	1.7	1.3
B1-B2	9×10^{-3}	1.8	12.8	8.6
B2-B3	2×10^{-3}	0.9	4.7	3.1

C. 3 **CFX Setup**

Table A.5 Details of CFX setup

Domain	Material chosen	Conditions	Model
Superheated steam (fluid)	IAPWS-IF97 from Library	373.15-500 K, and 0.611-100 kPa	Shear stress transport -automatic wall function, Turbulence Prandtl Number -0.9
DSG pellet (Solid)	User defined (density, thermal conductivity, specific heat)	298.15 K and 25% initial moisture and temperature	Diffusion model, Initial condensation
Solubles	User defined (density, thermal conductivity, specific heat)	298.15 K and 82.5% initial moisture and temperature	Diffusion model, Initial condensation